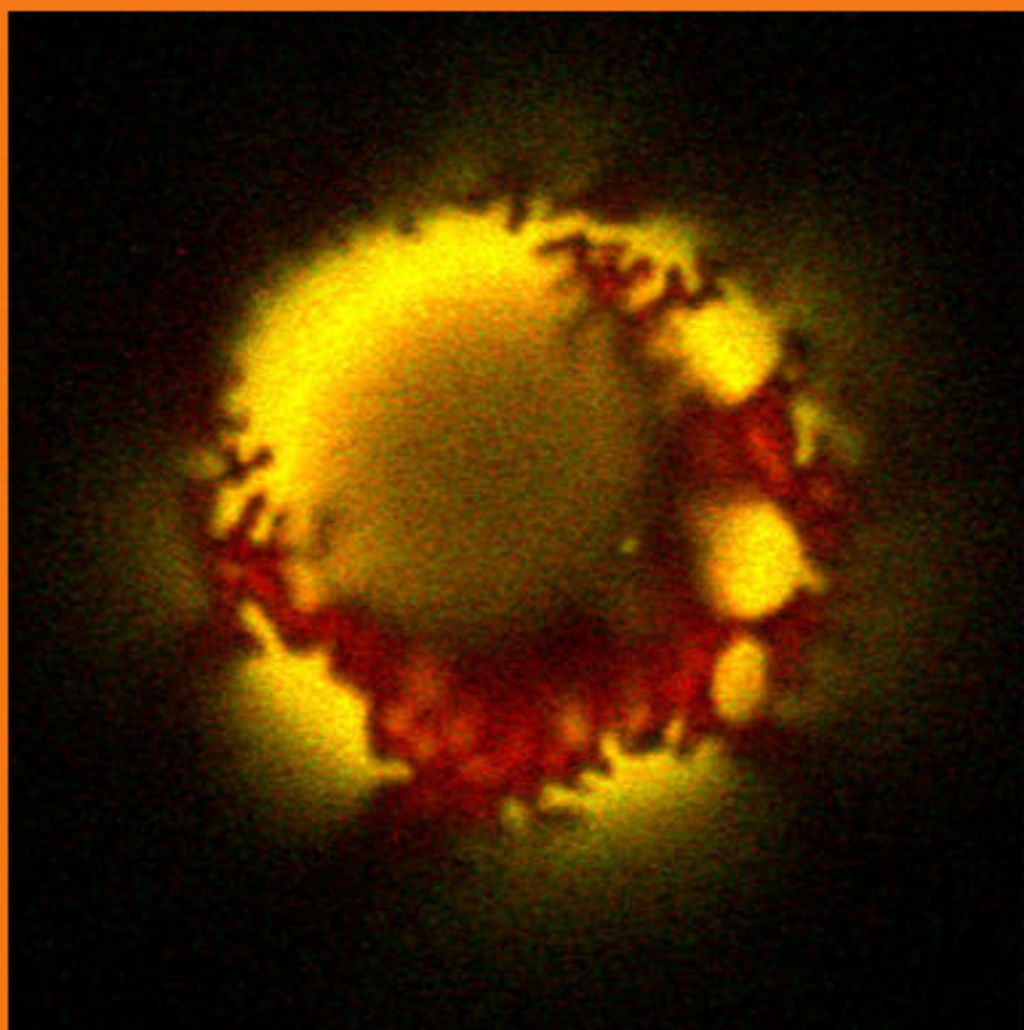# Propiedades Fisicoquímicas de Complejos Mesoscópicos Formados por Fosfolípidos y Macroiones Multivalentes

César Rodríguez Beas

Tesis Doctoral 2012

Caracterización Fisicoquímica de Complejos Mesoscópicos Formados por Fosfolípidos y Macroiones Multivalentes

Memoria para optar al grado de Doctor en Ciencias Físicas

Doctorado Internacional presentada por:

César Rodríguez Beas

Tesis Doctoral

Universidad de Granada

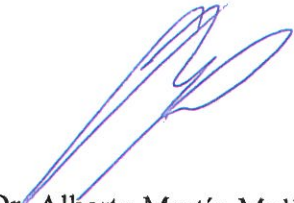Facultad de Ciencias

Departamento de Física Aplicada
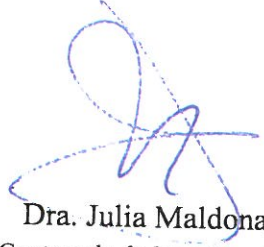
Granada, Junio de 2012

Caracterización Fisicoquímica de Complejos Mesoscópicos Formados por Fosfolípidos y Macroiones Multivalentes

por: César Rodríguez Beas

Lic. en Física

Directores

Dr. Alberto Martín Molina
Prof. Contratado Doctor
Departamento de Física Aplicada
Facultad de Ciencias
Universidad de Granada

Dra. Julia Maldonado Valderrama
Contratada de Investigación
Juan de la Cierva
Departamento de Física Aplicada
Facultad de Ciencias
Universidad de Granada

Grupo de Física de Fluidos y Biocoloides
Departamento de Física Aplicada
Universidad de Granada

Granada, Junio de 2012

A mis Padres y Hermanos,

especialmente en memoria de mi hermano Jorge Arturo

AGRADECIMIENTOS

Esta tesis doctoral refleja gran parte del trabajo que he realizado durante los últimos cuatro años y medio en el grupo de "Física de Fluidos y Biocoloides", perteneciente al Departamento de Física Aplicada de la Universidad de Granada. Es por ello que quiero agradecer a todas aquellas personas que de alguna manera u otra me apoyaron y enseñaron a elaborar este trabajo de investigación.

En primer lugar quisiera agradecer a mi director de tesis Alberto Martín Molina, por haberme dirigido está tesis doctoral sin ni siquiera conocerme. Durante la realización de este trabajo nos enfrentamos a muchos problemas, ya que este trabajo de tesis aborda un tema un poco complicado, pero aún así, con los conocimientos e ingenió de Alberto salimos de todos los problemas que se presentaron durante este tiempo, con algunos tirones de oreja pero que fueron muy necesarios. Y mi otra directora Julia Maldonado Valderrama por la dirección de esta tesis que fue de manera más relajada pero no menos importante ya que con su tranquilidad y conocimientos nos llevaba a pensar mejor antes de actuar.

Agradezco a Todos los miembros el grupo de Física de Fluidos y Biocoloides por las cuantiosas ayudas y consejos que recibí gracias a sus experiencias en el tema de Biocoloides. Especialmente quiero agradecer a Roque, Cabrerizo, María José, Miguel Ángel y María,

Delfi, Juan Luis que bastante aprendí de ellos en el tema de la investigación.

Y por supuesto, es imposible olvidar agradecer a mis compañeros/amigos de estudios de la "sala de becarios" con los que compartí momentos maravillosos e inolvidables. Empezando por los que me acogieron cuando llegue al grupo: Juan Carlos, Miguel Peláez (que no sé porque se ponía mal cada fin de mes), Manuel Santander, Sándalo, Roberto, el Moro, Fernando Vereda, Fernando Martínez, Carlos y Pablo (que por fin nos deshicimos de él, ¿pero ahora quien contestará el teléfono?). Después, con los que he convivido y aprendido más, los de mi generación; Amelia (la ganadora de trofeos en las carreras de San Alberto…y eso que yo llegaba primero que ella y nunca gané nada), Miguel, José (y no Jóse, por las charlas de desahogo que tanto bien me hicieron) y Efrén. Continúo con los que llegaron después; Carmen y Felipe (y aparte, gracias por su invitación en las noches de navidades confortables que pase con ustedes), Juan Pablo, Paola (que arte tiene esta mujer, me encanta), Azahara (para ser sincero, mi ignorancia me condenaba en el tema de los lipoplejos, hasta que ella y me enseño mucho de lo que ahora se, aparte de los consejos y actividades fuera del ámbito profesional y/o por simplemente escuchar ¿cómo podré pagarte todo esto?). Finalmente a la más reciente generación; Germán (que fue como mi discípulo, espero haberle enseñado bien lo que intenté enseñarle, además de que también aprendí de él), Jóse (que alegría tiene este tío), Miguel Ángel y Leonor, Luis-ma (que aunque estuvo sólo de estancia, fue muy grata

su presencia en el grupo). Espero no haber olvidado a alguien, y si así lo fue, no te preocupes, siente incluido.

Quiero también dar mis más preciados agradecimientos a la Dra. Dominique Langevin y el Dr. Gabriel Espinosa del *Laboratoire de Physique des Solides de l'Université Paris Sud XI,* Orsay (Francia) por su maravillosa acogida, ayuda y en señanza durante en mi estancia de investigación en esa institución. De la misma forma agradezco al Dr. Federico Bordi y la Dra. Simona Sennato del grupo *"PhoBia" del Dipartimento di Fisica della Università degli Studi di Roma "La Sapienza"*, Roma (Italia) durante mi estancia de investigación en su grupo.

Fuera del ámbito profesional me gustaría agradecer a todos los integrantes de mi familia: a mis padres Florentina Beas F. y Salvador Rodríguez H., a mis hermanas y hemanos; Héctor, Rosa, Paty, Chavo, Lurdes, Vero, Flor, Mery y a la memoria de Jorge, por todo el apoyo y amor incondicional que he recibido de todos ellos (destacando aquellos que me brindaron su ayuda instantánea cuando más la necesitaba). En gran parte, gracias a esto puede seguir adelante ya que es difícil estar lejos de casa.

ÍNDICE

RESUMEN

La *terapia génica* es considerada uno de los métodos científicos estratégicos para introducir material genético en células dañadas (células diana), con el fin de reparar o sustituir un gen dañado y así poder aliviar los síntomas de las muchas enfermedades heredadas o adquiridas que presenta el ser humano. Los vectores de transfección de genes no víricos representan una de las estrategias de la terapia génica de mayor éxito en la actualidad, por tratarse de un sistema biocompatible que presenta baja citotoxicidad. Los *lipoplejos* (liposomas/ADN) son los vectores no víricos más usados en transfección por sus propiedades para proteger al gen e introducirlo en la célula diana. Sin embargo, a pesar de los recientes avances en relación al uso de lipoplejos en la terapia génica, el uso de estos vehículos genéticos aún se encuentra en una etapa muy temprana pues presentan una baja transfección en relación a los vectores víricos. No obstante, tal y como predijo Danilo D. Lasic (1952−2000), pionero de la aplicación de liposomas a la medicina, un buen conocimiento de las propiedades fisicoquímicas de los lipoplejos contribuye de manera significativa al aumento de sus índices de transfección [1]. En consecuencia, el presente trabajo de tesis doctoral tiene como principal objetivo contribuir a la caracterización fisicoquímica de lipoplejos tanto catiónicos (liposomas catiónicos/ADN) como aniónicos (liposomas aniónicos/cationes divalentes/ADN.

La memoria de esta tesis doctoral se presenta en el denominado formato de publicaciones de artículos de investigación en donde los artículos que la componen deben estar bien integrados como capítulos de la tesis según las directrices establecidas por la Universidad de Granada.

En consecuencia, la memoria ha sido organizada en cinco capítulos y se incluye además un apartado de apéndices. El primer capítulo consta de una introducción en la que se presentan los antecedentes sobre estudios de lipoplejos en terapia génica y que han servido de motivación para la presente tesis doctoral. También en este capítulo se hace una descripción general de los liposomas y de sus componentes: los *fosfolípidos*. El segundo capítulo consta de una parte de justificación que nos llevó a la realización de este trabajo de tesis y otra parte donde se plantean los principales objetivos a desarrollar. El tercer capítulo consiste en la discusión de manera conjunta de los resultados obtenidos en los distintos trabajos. El capítulo 3 se divide a su vez en tres partes. La primera parte consiste en la caracterización experimental y teórica de nuevos lipoplejos catiónicos. La segunda parte abarca el estudio de la interacción de cationes multivalentes con sistemas coloidales modelo y liposomas aniónicos. Por último, en la tercera parte se caracteriza la interacción de lípidos aniónicos y ADN en presencia de cationes divalentes. En el cuarto capítulo se exponen las principales conclusiones obtenidas a partir de los resultados presentados en el capítulo 3. En este capítulo se incluyen además las perspectivas a desarrollar en el futuro en relación con el tema de estudio. El quinto capítulo está formado por los cuatro artículos

publicados hasta la fecha, en formato de artículos de investigación. Además se incluye un quinto manuscrito que recientemente se ha enviado para su publicación.

SUMMARY

Gene therapy is considered one of the most reliable strategic scientific methods to introduce genetic material in damaged cells (target cells), to repair or replace a damaged gene and thus to relieve symptoms of many inherited or acquired human diseases. The non−viral gene delivery vectors represent one of the strategies most successful in gene therapy at present, because they constitute a biocompatible system that has low cytotoxicity. The *lipoplexes* (liposomes/DNA) are the non−viral vectors most used in transfection owing to their protective action on the gene and ability to introduce it into the target cell. However, despite recent progress in relation to the use of lipoplexes in gene therapy, the use of these genetic vehicles is still in an early stage because they have a low transfection capacity with regard to the viral vectors. Nonetheless, as predicted Danilo D. Lasic (1952−2000), pioneer of the application of liposomes in medicine, a good understanding of the physicochemical properties of the lipoplexes would contribute significantly to the increase in their rates of transfection [1]. Accordingly, the main objective of this doctoral thesis is to carry out a physicochemical characterization of both cationic lipoplexes (cationic liposomes/DNA) and anionic (anionic liposomes/divalent cations/ DNA.

The memory of this thesis is presented in the recognized format of publications of research articles where the articles that compose it must be well integrated as chapters of the thesis according to

4

guidelines established by the University of Granada.

Accordingly, the memory is organized in five chapters and also includes a section of appendices. The first chapter contains an introduction that provides the background about the studies of lipoplexes in gene therapy which serves as motivation for this doctoral thesis. Chapter 1 also provides an overview of the liposomes and their components: the *phospholipids*. The second chapter consists of one part of justification of this thesis and another part which establishes the main objectives which have been established. The third chapter is a joint discussion of the results obtained in the different studies. Chapter 3 is divided into three parts. The first part consists of an experimental and theoretical characterization of new cationic lipoplexes. The second part involves the study of the interaction of multivalent cations with model colloidal systems and anionic liposomes. Finally, the third part characterizes the interaction of anionic lipids and DNA in the presence of divalent cations. The fourth chapter presents the main conclusions from the results presented in the chapter 3. Chapter 4 also includes prospects to develop in the future regarding the subject matter. The fifth chapter displays the four manuscripts published to date in the format of research articles. It also includes a fifth manuscript that was recently submitted for publication.

CAPÍTULO 1

INTRODUCCIÓN

En este capítulo se presentan los antecedentes esenciales de la temática principal, y que sirven de base a la idea final de esta tesis doctoral. Para este fin, primero se describen los "vectores de transfección de genes", como los son los vectores víricos y no víricos, en los que destacan los tipos de vectores no víricos, y dentro de los cuales se hace énfasis en los lipoplejos catiónicos y aniónicos. Asimismo, se describen las características y estructuras generales de los materiales utilizados en este trabajo.

1.1. Terapia Génica

En el transcurso de su vida, el ser humano ha adquirido, desarrollado y heredado enfermedades que durante siglos han reducido su tiempo de vida. El estudio y la compresión de estas enfermedades han permitido el desarrollo de muchas curas que controlen o reparen los síntomas que estas enfermedades presentan, aumentando así su esperanza de vida. Investigaciones realizadas a lo largo de los años han llevado a desarrollar métodos estratégicos, como la *terapia génica*, la cual consiste en introducir medicamento en el interior de las células dañadas para curar los síntomas de muchas enfermedades que presenta el ser humano. A lo largo del siglo pasado se han ido desarrollando numerosas técnicas de transfección[1] de genes tanto *in vitro* como *in*

vivo, con el objetivo de introducir ADN externo en el núcleo de células y que éste repare o reemplace el ADN dañado. Conceptualmente, la terapia génica envuelve la identificación de una enfermedad y su potencial está relacionado con la introducción de un nuevo material genético en las células enfermas. Los pasos subsecuentes son la identificación de los tipos apropiados de células a tratar y el desarrollo de una forma conveniente de introducir suficiente material genético terapéutico en esas células. Los sistemas de transfección de genes – también llamados *vectores* – tienen la habilidad de introducir material genético en las células, por lo cual, en el transcurso de los años han sido llamados *vectores de transfección de genes*.

Con la ayuda de los principios de la biología, la química y la física, un vector de transfección de genes ideal debería tener las siguientes características (ordenadas por importancia) [2]:

1. La habilidad de transferir material genético con una alta eficacia.
2. La capacidad de llegar a un tipo de célula deseada (diana).
3. La habilidad localizar un sitio específico en el cromosoma anfitrión y mantenerse estable.
4. La habilidad de llegar a células no divididas.
5. No contener componentes que evoquen una respuesta inmune.
6. Tener un tamaño de empaquetamiento de material genético no limitado.

_____

[1]La transfección consiste en la introducción de material genético en células eucariotas mediante vectores u otras herramientas de transferencia.

7. Ser convenientemente reproducible y bioseguro.

8. Ser altamente concentrado, permitiendo que muchas células sean afectadas.

9. Contener una unidad transcribible inducida para regular la expresión genética.

10. No causar efectos secundarios.

Estos estándares ideales permitirán el desarrollo de tratamientos clínicos más seguros y específicos. A pesar de que las nuevas tecnologías tienen sus limitaciones técnicas, el éxito de la terapia génica es cada vez mayor.

1.2. Ácido Desoxirribonucleico (ADN)

La molécula de ADN no sólo es importante por su papel en las bases fundamentales de la vida humana, sino también por el desarrollo de modelos terapéuticos [3]. Por tanto, en esta sección se hace una descripción de sus propiedades fisicoquímicas más importantes así como de su papel en los vectores de transfección de genes.

El ácido desoxirribonucleico es un polielectrolito que está compuesto por dos cadenas de nucleótidos entrelazadas que forman una doble hélice. El esqueleto de cada cadena es un polímero formado por una molécula de azúcar, la desoxirribosa, con un grupo fosfato en el carbono 3´ y una base de purina (adenina y guanina) o pirimidina (citosina o timina) en el carbono 1´. Se considera que el esqueleto azúcar−fosfato tiene una polaridad 5´ a 3´, como se puede ver en la

Fig. 1.1. El ADN se puede caracterizar en función de su nivel estructural. La estructura primaria denota la secuencia específica de las bases, responsable de la información genética. Tres bases consecutivas forman un gen. Por su parte, la estructura secundaria describe la estructura global de las dos cadenas de ADN. Las bases del ADN interaccionan mediante una regla que consiste en que sólo existen dos tipos de pares de bases: A-T y G-C. Se dice que las bases de estas parejas son complementarias, lo que significa que en cualquier peldaño de la escalera en doble hélice, las únicas asociaciones base–base que pueden existir entre las cadenas, sin distorsionar sustancialmente la doble hélice, son A-T y G-C [4].
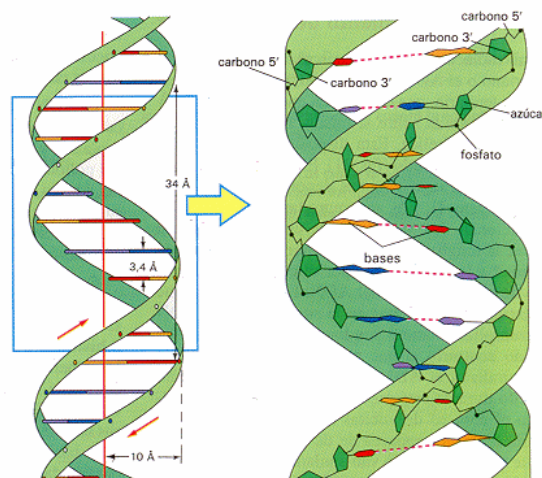
Fig. 1.1. Estructura de la doble hélice del ADN.
[Fuente:http://secundaria.us.es/josromrom/an/an_archivos/adn25.gif]

La cadena del ADN presenta una cierta flexibilidad cuando contiene menos de 1000 pares de bases (pb), sin embargo, en la mayoría de los casos las hebras de ADN son más largas de tal manera que se parece

más a un polímero semirrígido con forma de rodillo. Esta estructura le permite minimizar las repulsiones estéricas y electrostáticas debidas a su completa ionización a pH fisiológico. Finalmente, la estructura terciaria refleja los distintos modos que tiene el ADN para agruparse: lineal, circular, circular sesgado o superenrollado.

A continuación se presentan los tipos de ADN que normalmente se usan en terapia génica.

1.2.1. Tipos de ADN Utilizados en Terapia Génica

Una de las ventajas más significativas de los medicamentos basados en ADN y usados en la actualidad, es el reconocimiento selectivo de células diana, las cuales imparten una poderosa acción específica. Estos medicamentos pueden ser usados para tratar enfermedades así como prevenirlas. Por ejemplo, la terapia génica típica implica correcciones del mal funcionamiento del gen mediante la introducción de una copia de gen, que da como resultado un sólo producto. Aun así, muchas de las componentes de los vectores basados en ADN son nuevos candidatos para medicamentos farmacéuticos y cuyo efecto en el ser humano aún no ha sido completamente investigado. En los últimos años, la investigación de sistemas de portadores de ADN ha dado resultados muy prometedores en transfección, por lo que a continuación se describen dos de los tipos de ADN más usados en terapia génica.

ADN plasmídico: El plásmido es un ADN de doble cadena circular y de alto peso molecular que codifican proteínas especificas [5]. La

terapia génica implica el uso de ADN plasmídico para introducir transgenes (material genético) en células diana las cuales carecen esencialmente de habilidades para producir proteínas y que el mismo transgén está programado para generar. El mecanismo de acción del ADN requiere que éste gane acceso al núcleo de la célula diana después de entrar en el citoplasma. Además del interés transgénico, el ADN plasmídico contiene varias señales reguladoras tales como promover y mejorar la regulación del gen[2] expresivo (gen que posee la información), características que juegan un papel muy importante [6]. En los vectores víricos, tales señales pueden estar presentes endógenamente (generadas dentro del virus) o diseñadas artificialmente en el genoma del virus.

Oligonucleótidos: Son pequeños segmentos de ADN (≤ 50 pb) de una sola cadena que en la internalización celular pueden inhibir selectivamente la expresión de una sola proteína [7]. Los oligonucleótidos pueden entrar en el núcleo de la célula diana, formando un doblete con un ADN plasmídico, y exhibir la traducción y el proceso de transcripción de la proteína [8]. Para propósitos terapéuticos, los oligonucleótidos pueden ser usados para seleccionar el bloc de expresión de la proteína que está implicado en las enfermedades.

_____

[2]Un gen es una secuencia ordenada de nucleótidos (moléculas orgánicas) en una molécula de ADN que contiene la información necesaria para la síntesis de una macromolécula (habitualmente proteínas) con función celular específica.

Como ya se ha mencionado, normalmente estos tipos de ADN se utilizan directamente en transfecciones génicas y poseen propiedades específicas. Debido a que nuestro principal objetivo en esta tesis es la caracterización fisicoquímica de lipoplejos, hemos escogido un ADN genómico comercial proveniente de timo de ternera y que ha sido habitualmente utilizado en este tipo de estudios. Por ejemplo, se ha utilizado en la caracterización de lipoplejos catiónicos con sistemas: CTAB/ADN [9], DSTAP−DOPE/ADN [10], BGTC−DMPC/ADN [11]. Mientras que en lipoplejos aniónicos la utilización de este tipo de ADN ha sido más escasa: por ejemplo el sistema DOPG−DOPC/ADN [12]. Sin embargo, estudios interfaciales con monocapas de lípidos aniónicos y/o zwitteriónicos con ADN de timo de ternera son más comunes, con sistemas como: PS:2POPC/Ca^{2+}/ADN [13-14], DMPE/Mg^{2+}/ADN [15], DMPE/(Ca^{2+} o Mg^{2+})/ADN [16]. En cualquier caso, la justificación de los sistemas experimentales escogidos se detallará en el capítulo siguiente.

1.3. Vectores de Transferencia de Genes

Como ya se ha dicho anteriormente, la terapia génica consiste en la corrección de un defecto genético introduciendo genes normales en las células dañadas para desempeñar las funciones que el gen defectuoso no puede llevar a cabo. En consecuencia, una modalidad posterior de la terapia génica consiste en introducir en las células de los pacientes un gen específicamente designado para proveer de una nueva propiedad (Fig. 1.2). Es decir, el objetivo principal de la terapia génica

es el desarrollo eficiente de genes portadores no tóxicos que puedan transferir material genético externo al interior de células diana.

Los vectores de transferencia génica basados en ADN son por tanto candidatos sumamente prometedores en la terapia génica dentro de un amplio intervalo de enfermedades. Este tipo de vectores han sido clasificados en tres formas generales de transferencia: mecánica, eléctrica y mediante un sistema de transferencia asistida.
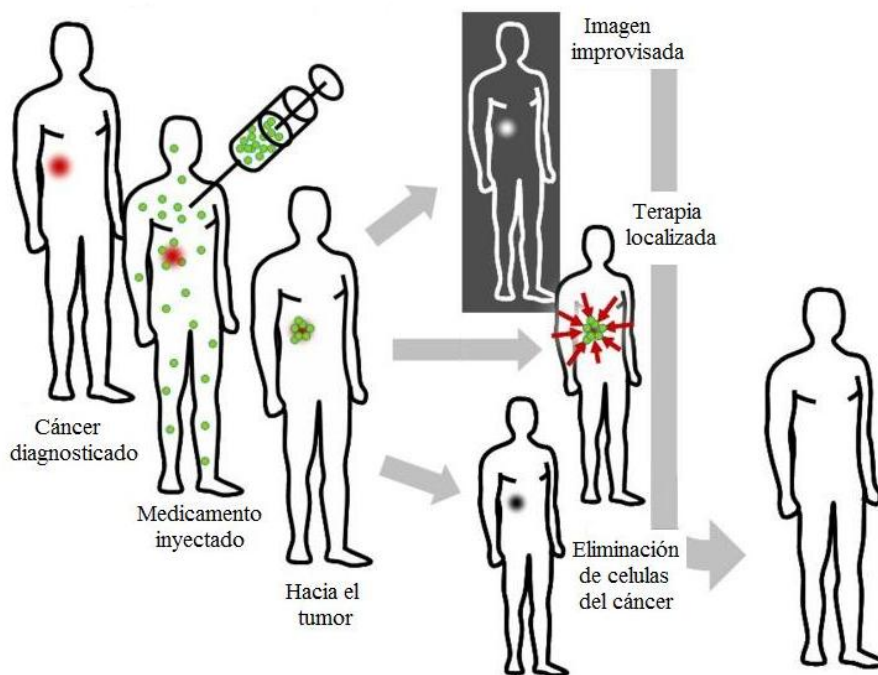
Fig. 1.2. Evolución de la terapia génica.
[Fuente: http://en.wikipedia.org/wiki/Molecular_imaging]

Las técnicas mecánicas y eléctricas tratan de introducir ADN desnudo en las células, mediante técnicas como: la microinyección, el bombardeo con partículas, el uso de la presión, la electroporación, etc. La microinyección consiste en la introducción directa, usando un micromanipulador, de material genético dentro del núcleo de la célula y es altamente eficiente [17]. Por ejemplo, la transferencia de macropartículas compuestas de ADN/oro puede llevarse a cabo bombardeando las partículas con una pistola genética. Este método ha sido probado y es muy efectivo para transferir genes tanto *in-vitro* como *in-vivo* [18]. Usando un sistema de propulsor de aire, varios inyectores que contienen ADN pueden ser usados para transferir genes en músculos, piel, grasa y tejidos. La electroporación usa corriente eléctrica de alto voltaje para transferir genes a las células, a través de poros en las membranas celulares facilitando así la transferencia del ADN [19].

Sin embargo, a pesar de la alta eficacia transfección que se ha adquirido usando las técnicas mecánicas y eléctricas, éstas han sido extremadamente difíciles de estandarizar en el entorno clínico y han sido consideradas tediosas, poco prácticas y agresivas [20]. Por lo cual, el método más exitoso para transferir ADN ha sido el uso de un sistema de transfección asistida, el cual consiste en la manipulación de un gen externo para ser transferido a una célula recesiva. Este método contempla propiedades ideales de vectores para la transfección de ADN terapéutico y las de mayor criterio son:

1. Alta eficacia para transferir.

2. Alto grado para llegar a células diana.
3. Baja toxicidad e inmunogenicidad (de respuesta inmunitaria).
4. Altamente biodegradables.
5. Alta estabilidad en las formulaciones farmacéuticas.

Además, el sistema de transferencia de ADN debe de ser simple para permitir una fácil versión modificada, transferir y expresar el ADN.

El inicio de la creación del método de la transfección de genes asistida fue en 1963, cuando Joshua Lederberg escribió: *"Podemos anticipar el cultivo in-vitro de células germinales y manipularlas con el intercambio de cromosomas y segmentos. Las aplicaciones finales de la biología molecular serían el control directo de las secuencias de los nucleótidos en los cromosomas humanos, junto con el reconocimiento, selección e integración de los genes deseados"* [21]. 26 años después, en 1989, Rosenberg y col. llevaron a cabo el primer ensayo humano de terapia génica cuando usaron retrovirus para inducir el gen de codificación para la resistencia a la neomicina en tumores humanos infiltrando linfocitos antes de implantarlos en cinco pacientes con melanoma avanzada [22]. Este estudio mostró la viabilidad del uso de retrovirus en la transducción de genes en humanos, proporcionando así las bases para futuros estudios en transfecciones génicas. Desde entonces, cientos de ensayos clínicos se han llevado a cabo, están en progreso o han sido aprobados por todo el mundo.

Actualmente, este sistema de transfección asistida tiene dos enfoques principales para transferir ADN en las células, los cuales están

basados en el uso de vectores víricos y no víricos. Cada uno de estos métodos presenta distintas ventajas y debilidades en términos de eficacia, producción, seguridad, etc.

1.3.1. Vectores Víricos

A través de los millones de años de la evolución de los virus como agentes infectantes, éstos han desarrollado la habilidad de transferir moléculas de ADN en las células con relativa facilidad [23]. Para fines terapéuticos, el gen de interés es integrado en el genoma del virus y éste usa su mecanismo de infección para entrar a la célula y liberar el gen expresivo. Es decir, *"los vectores víricos son virus modificados que no pueden replicarse y no pueden causar daño mientras que siguen siendo capaces de transferir ADN exógeno en las células"*. Los virus son modificados en el laboratorio para eliminar su patología y retener su alta eficacia para transferir genes (Fig. 1.3) [24]. Estos vectores han sido los más usados frecuentemente para transferir genes a las células humanas, siendo los *retrovirus* y *adenovirus* la gran mayoría [25-26].

Los retrovirus son virus con un genoma compuesto de aproximadamente 9.7 kilo−bases, constituidos por una sola molécula de ARN (ácido ribonucleico, ácido nucléico formado por una cadena de ribonucleótidos). Este tipo de virus tiene la habilidad de reemplazar el gen viral vital por el gen terapéutico [27]. Los adenovirus son virus con ADN de doble cadena que pueden infectar a las células divididas y no divididas [28]. Las transfecciones con los adenovirus son

transitorias debido a que su genoma de ADN no se integra permanentemente en el material genético de la célula huésped.
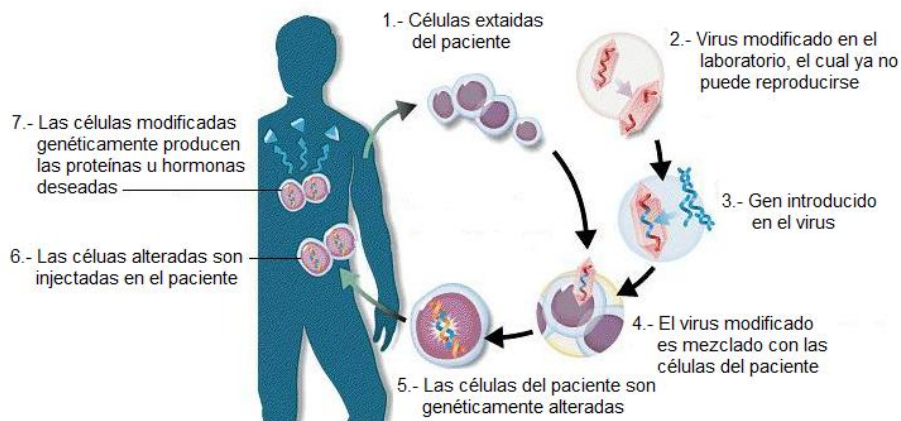
Fig. 1.3. Vectores víricos genéticamente modificados para terapia génica.
[Fuente:http://sgugenetics.pbworks.com/w/page/38371765/Gene%20Therapy]

Una ventaja significativa de los vectores víricos basados en ADN es su extremadamente alta eficacia para la transfección en una gran variedad de tejidos humanos. En el caso de los retrovirus, éstos son capaces de transferir altas cantidades (45−95%) de genes a células humanas primarias endoteliales y musculares lisas, una clase de células que son generalmente difíciles para lograr la transfección [29]. Por otro lado, los adenovirus han sido usados con alta eficacia en tejidos del corazón, músculos [30], ojos [31], etc. Éste tipo de virus son actualmente usados en más del 65% de los ensayos clínicos en todo el mundo [32].

A pesar de las impresionantes estadísticas de los vectores víricos, hay varias preocupaciones sobre el uso de los virus para transferir ADN

terapéutico en humanos. Las principales preocupaciones son la toxicidad, la inmunogenicidad, los efectos secundarios, la patogenicidad, la especificidad de la meta restringida de células, su alto coste, la dificultad de producción [33]. Debido a los problemas que presentan los vectores víricos, en los últimos años se ha incrementado sustancialmente la búsqueda de técnicas, como es el caso de los vectores no víricos, que se describen a continuación.

1.3.2. Vectores no Víricos

El éxito de la terapia génica depende fundamentalmente del desarrollo de un vector o vehículo que pueda transferir selectiva y eficazmente a un gen en una célula específica con toxicidad mínima (Fig. 1.4).

El uso de los vectores no víricos se ha expandido debido a su relativa seguridad, su amplia y fácil producción, su habilidad para transferir grandes cantidades de genes, que tienen objetivos específicos, que no son inflamatorios y que presentan bajas propiedades tóxicas e infecciosas. Además, su biocompatibilidad y su potencial de producción en grandes cantidades hacen que estos vectores sean muy atractivos para la terapia génica [34]. Los vectores no víricos terapéuticos basados en ADN pueden ser clasificados según la naturaleza del material sintético: *i)* sistemas de transferencia polimérica (polímero/ADN) y *ii)* sistema de transferencia liposómica (liposoma/ADN – donde el ADN puede ser encapsulado o formar un complejo con el liposoma) [35-36]. El complejo polímero/ADN, también conocido como *poliplejo*, puede ser utilizado para introducir

al ADN en las células [20]. Los polímeros catiónicos forman fácilmente un complejo con la molécula de ADN y su mecanismo de interacción se basa en las interacciones electrostáticas entre las cargas positiva del polímero y la negativa del ADN.
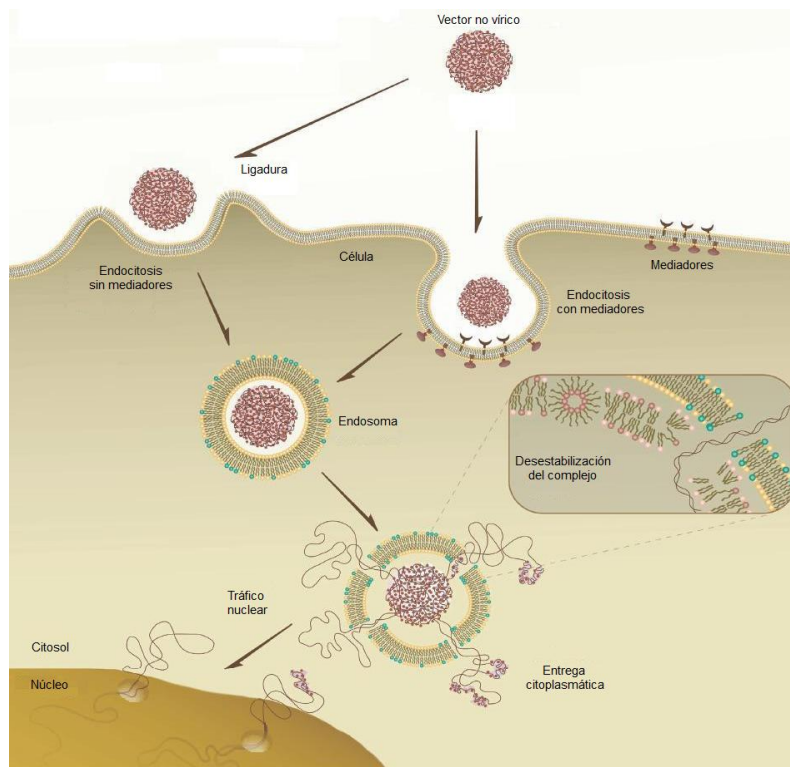
Fig. 1.4. Vectores no víricos usados para transferir genes en células diana.
[Fuente: http://www.jle.com/en/revues/medecine/bdc/e-docs/00/04/2D/03/article .phtml?fichier=images.htm]

El poliplejo catiónico puede interaccionar con la carga superficial negativa de la célula para mejorar la absorción del ADN. Las propiedades fisicoquímicas y su fácil manipulación son algunas de las propiedades más importantes de los poliplejos como portadores de genes [35]. Algunos polímeros que comúnmente se utilizan para la

formación de poliplejos son: la PLL (*poli(lisina)*) [37], el PEI (*poli(éter-imida)*) [38], el *quitosano* [39], el PANAM (*poli(amido-amina)*) [40]. Sin embargo, la transfección con poliplejos presenta los siguientes inconvenientes: baja capacidad de transfección, problemas en la distribución del peso molecular y en algunos casos, los poliplejos pueden presentar propiedades farmacéuticas inertes que los hacen desfavorables para el uso humano [41].

En paralelo al desarrollo de los poliplejos, los sistemas liposomas/ADN (*lipoplejos*) forman en otro tipo de vectores no víricos de transfección más importantes en la actualidad. Precisamente este ha sido el sistema elegido como objeto de estudio en la presente tesis doctoral. En consecuencia, a continuación detallaremos con mayor profundidad este tipo de sistemas, empezando por la descripción de los liposomas como sistemas modelo de membranas biológicas así como de sus principales aplicaciones en biotecnología. Una vez presentados estos sistemas, los diferentes tipos de lipoplejos serán descritos en las siguientes secciones.

Los liposomas han sido investigados desde el inicio de los años 70 como portadores de genes para enriquecer los agentes terapéuticos [42-43]. Los liposomas ofrecen la posibilidad de transferir medicamentos en tejidos y células diana, facilitando su transferencia citoplasmática. Así pues, estos sistemas son utilizados como portadores de medicamentos y ser administrados transdérmica y parenteralmente (es decir, por una vía distinta a la digestiva).

Los liposomas fueron descubiertos por A. D. Bangham y R. W. Horne en 1961, cuando estudiaban el comportamiento de la lecitina y otros fosfolípidos con colesterol [44]. En su estudio encontraron que los fosfolípidos eran capaces de formar esferas en soluciones acuosas diluidas, y los definieron como: *"Pequeñas vesículas artificiales de forma esféricas que pueden ser producidas de fosfolípidos naturales no tóxicos y colesterol"*. Actualmente, el concepto de liposoma ha evolucionado según las propiedades fisicoquímicas de sus componentes mayoritarios, los fosfolípidos y según su proceso de formación a partir de las micelas.

Los *fosfolípidos* (a los que por abreviar nos referiremos en adelante como *lípidos*), son moléculas anfifílicas que están formados por dos partes químicamente diferentes: una cabeza polar hidrófila y una o dos cadenas hidrocarbonadas hidrófobas (Fig. 1.5).
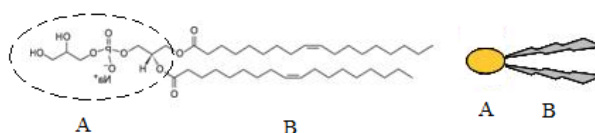
Fig. 1.5. Molécula anfifílica formada por (A) una cabeza polar hidrófila y (B) una o dos cadenas hidrocarbonadas hidrófobas.

De acuerdo con la naturaleza de la cabeza polar de los lípidos, éstos se clasifican en: iónicos (catiónicos y aniónicos) y no–iónicos (zwitteriónicos). Los lípidos iónicos normalmente son sales orgánicas (e inorgánicas) que poseen grupos que al disolverse en el agua se disocian adquiriendo una carga neta en la cabeza polar (positiva o

negativa) liberando un contraión. Por otro lado, los lípidos zwitteriónicos tienen grupos que pueden adquirir carga en función del pH de la solución en que se encuentren y se comportan de dos maneras, ya sea como lípidos iónicos o no−iónicos. Por tanto, según el pH, pueden estar cargados positivamente (pH > 7), negativamente (pH < 7) y tener una carga neta nula (pH = 7).

Al dispersar una concentración pequeña de un lípido en un disolvente (como el agua), la naturaleza anfifílica de las moléculas hace que formen una monocapa en la interfase aire−agua, donde la parte hidrófila del lípido está en contacto con el agua, mientras la parte hidrófoba se orienta hacia la fase no polar (aire) (Fig. 1.6).
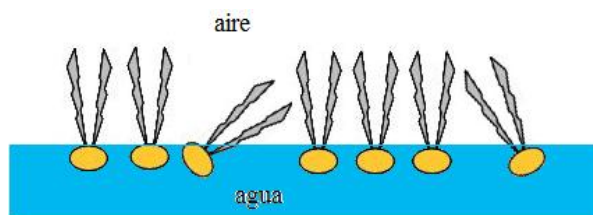
Fig. 1.6. Monocapa de lípidos en la interfase aire−agua.

Si la concentración de lípidos se incrementa, además de la formación de la monocapa en la interfase aire−agua, se produce la formación de *micelas* (estructuras mediante las cuales los lípidos evitan el contacto de su parte hidrófoba con el agua). En general dependiendo del lípido, las micelas pueden ser esféricas o cilíndricas, las cuales a su vez pueden estructurarse de manera hexagonal o cilindros interconectados, como se puede ver en la Fig. 1.7.
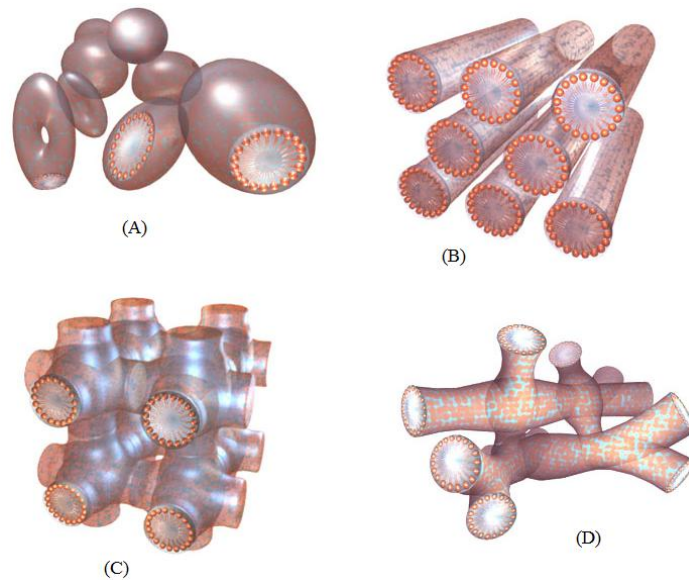
Fig. 1.7. Representación estructural micelar: esféricas (A), cilíndricas (B), hexagonal (C) y cilindros interconectados (D). [Fuente: http://simscience.org/membranes/advanced/page5.html]

Otra posible manera de que los lípidos se organicen es la forma de bicapas (o membranas). Las bicapas consisten en dos monocapas de lípidos orientados paralelamente, de la misma forma que las membranas celulares biológicas, Fig. 1.8.
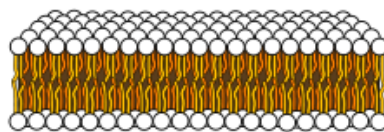
Fig. 1.8. Representación estructural de una bicapa de lípidos.
[Fuente: http://www.isrn.com/journals/pharmaceutics/2012/738432/fig1/]

Las bicapas pueden dar lugar también a diferentes estructuras en la escala mesoscópica. La más frecuente es la llamada fase lamelar, que

es un conjunto de bicapas orientadas paralelamente con una distribución periódica y caracterizada por una distancia de repetición.

Otra estructura es la llamada vesícula o liposoma, que son estructuras esféricas que encierran un volumen de disolvente y que pueden estar formadas por una sola bicapa (Fig. 1.9) o por varias capas lipídicas (multilamelares).
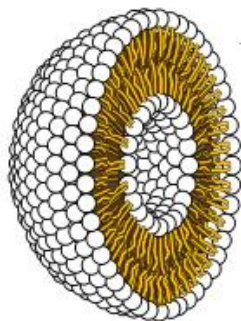
Fig. 1.9. Representación estructural de un liposoma unilamelar.
[Fuente: http://www.isrn.com/journals/pharmaceutics/2012/738432/fig1/]

Al igual que con el ADN, en este trabajo se han utilizado diferentes lípidos cuyas características y justificación se describirán en el capítulo siguiente.

Como se mencionó anteriormente, una de las propiedades de los liposomas es su estabilidad, la cual puede verse afectada por factores químicos, físicos o biológicos. La estabilidad química de los liposomas está relacionada con la presencia de ácidos grasos insaturados que sufren reacciones oxidantes, cambiando la permeabilidad de su bicapa lipídica [45]. La estabilidad física, está

relacionada con el tamaño, polidispersidad, morfología, composición, etc., de los liposomas [46]. Por último, la estabilidad biológica depende de la capacidad de penetración y difusión en órganos o tejidos, así como de la presencia de agentes que pueden interactuar con los liposomas durante la ruta de administración [45].

En las últimas décadas, los liposomas se han usado extensamente como sistemas portadores de medicamentos muy eficaces, debido a sus características únicas tales como: la capacidad de incorporar medicamentos hidrófilos e hidrófobos, enorme variedad de estructuras y composiciones, alta biocompatibilidad, baja toxicidad, falta de activación del sistema inmune, etc. [47-48]. Los medicamentos se disponen de manera diferente en el liposoma y dependiendo de sus características de solubilidad y partición, exhiben diferentes propiedades de encapsulamiento y liberación [49]. Los medicamentos lipofílicos son generalmente atrapados casi completamente en la bicapa lipídica de los liposomas, y como son muy poco solubles en agua, presentan una escasa pérdida de medicamentos en suero sanguíneo. Los medicamentos hidrófilos pueden ser encapsulados dentro o sobre la parte externa de los liposomas. El porcentaje de encapsulación de medicamentos hidrófilos en los liposomas depende de la composición y del procedimiento de su preparación [50].

Recientemente se han desarrollado nuevos tipos de liposomas para incrementar la transferencia de moléculas activas dentro del citoplasma [47]. Un tipo de estos liposomas es el que es sensible a los estímulos, es decir, que generalmente depende de los diferentes factores de su entorno con el fin de activar los medicamentos [51]. La

estrategia de uso de estos liposomas se basa en la modificación de su superficie (bicapa) con polímeros hidrófilos, los cuales les confieren propiedades ventajosas como la biocompatibilidad, baja toxicidad, y baja inmunogenicidad y antigenicidad (mediante una sustancia que desencadena la formación de anticuerpos y puede causar una respuesta inmunitaria) [49]. Los liposomas utilizados para transportar medicamentos suelen ser funcionalizados con diferentes tipos de anticuerpos, péptidos, glicoproteínas, oligopéptidos, etc. [52-54]. Los anticuerpos, los péptidos y las proteínas han sido los más extensamente estudiados como un ligando directo con los liposomas debido a sus estructuras moleculares, las cuales están esencialmente compuestas por secuencias conocidas de aminoácidos. En cuanto a los liposomas como portadores de ADN, están formados de lípidos con cabezas hidrófilas de tipo de aminas. Estos tipos de liposomas son capaces de almacenar y transferir ADN en las células, y como ya se ha comentado anteriormente, según su carga superficial, pueden clasificarse como liposomas catiónicos, aniónicos o zwitteriónicos.

Los liposomas catiónicos pueden estar formados por uno o varios tipos de lípidos catiónicos los cuales que estarán compuestos a su vez por una o dos cadenas de ácidos grasos, uno o varios ligandos y un grupo hidrofílico basado en amina. Algunos de los lípidos catiónicos más conocidos son: el DOTAP (*propano de dioctadecil-trimetilamonio*), el DODAB (*bromuro de dioctadecildimetilamonio*), el CTAB (*bromuro de cetiltrimetilamonio*), el DSTAP (*propano de distearoiltrimetilamonio*). Por otro lado, los liposomas aniónicos presentan la ventaja de ser más eficientes en la endocitosis que los

liposomas catiónicos debido al hecho de que son reconocidos por la fuente eliminadora de la célula, que es la responsable de la absorción de estos liposomas [55]. Por ejemplo, los liposomas aniónicos mezclados con PAA (ácido poliacrílico), muestran una rápida endocitosis por los macrófagos (células mononucleadas que se caracterizan por capacidad de incorporar y degradar material particulado) y su alta afinidad se debe al reconocimiento de las cargas negativas por los receptores superficiales de las células. Algunos de los lípidos aniónicos más conocidos son: el DOPG (*dioleoilfosfatidilglicerol*), el POPG (*palmitoilfosfatidilglicerol*), el DMPG (*dimistiroilfosfatidilglicerol*), el DPPG (*dipalmitoilfosfatidilglicerol*), el DPPA (*ácido dipalmitoilfosfatidico*) y el DOPS (*dioleoilfosfatidilserina*), comúnmente estudiado debido a que es el lípido iónico más abundante en las membranas celulares bilógicas.

Además de los lípidos catiónicos y aniónicos están los lípidos que bajo determinadas condiciones pueden presentar una carga neta neutra, y se les denomina lípidos zwitteriónicos. Usualmente son llamados lípidos auxiliares, ya que generalmente son mezclados con los lípidos catiónicos y/o aniónicos para formar liposomas con el objetivo de: *i)* incrementar la eficacia de transfección, *ii)* reducir la toxicidad, *iii)* incrementar la elasticidad de la bicapa liposómica y *iv)* promover la fusión con la membrana de la célula. [10]. Algunos de los lípidos zwitteriónicos más conocidos son: el DLPC (*dilauroilfosfatidilcolina*), DOPE (*dioleoilfosfatidiletanolamina*), el DOPC (*dioleoilfosfatidilcolina*), que al igual que el PS, es el lípido zwitteriónico más abundante en las membranas celulares biológicas.

A la formación de complejos formados por liposomas catiónicos o aniónicos con ADN, se le denomina *lipoplejo*, el cual ofrece numerosas ventajas como vectores no víricos en la terapia génica. Contrario a los vectores víricos, los lipoplejos ofrecen biocompatibilidad, biodegrabilidad y no inmunogenicidad en el momento de transferir el ADN [1].

A continuación se describen los tipos de lipoplejos usados en la terapia génica.

1.3.2.1. Lipoplejos Catiónicos

El estudio de los lipoplejos catiónicos como sistema de portadores de genes fue implantado a finales de los años 80 por Felgner y col. [56]. En su trabajo original se refirieron a los lipoplejos como: *"Pequeños liposomas unilamelares compuestos de DOTMA (dioctadeceniltri-metilamonio) que interactúan espontáneamente con ADN para formar complejos lípido–ADN, atrapando el ADN al 100%. El DOTMA facilita la fusión de los complejos con la membrana plasmática de las células cultivadas, dando como resultado la captación y la expresión del ADN. La técnica es simple, altamente reproducible y efectiva para la expresión transitoria y estable del ADN transferido"*. Desde entonces un gran número de científicos utilizan este tipo de vectores no víricos en terapia génica [13, 57-59].

El mecanismo de interacción del ADN con los liposomas catiónicos condiciona sus aplicaciones clínicas y biológicas. Este proceso de

formación de complejos, formados por liposomas catiónicos y ADN, se debe esencialmente a la atracción electrostática entre las cargas opuestas de ambas componentes [60]. La morfología óptima de los lipoplejos catiónicos depende de la elasticidad y de la carga superficial de la membrana o bicapa del liposoma, la cual está relacionada a su vez con la naturaleza de su carga, concentración y composición lipídica (mezcla de lípidos catiónicos y zwitteriónicos), el pH, la temperatura, y la fuerza iónica del medio [1, 61].

Dentro de los lipoplejos catiónicos se pueden mencionar los lipoplejos de oligonucleótidos. Éstos están formados con elementos como una conformación secundaria (secuencias especificas que le permiten tener una conformación preferida, como la presencia de guaninas continuas que hacen resistente al oligonucleótido a la degradación debido a su habilidad de configurarse en hiperestructuras) que los ayudan a transferirse a células humanas [62-63]. También se ha llevado a cabo otra formación de lipoplejos con liposomas catiónicos y péptidos (protamina), conocidos como LPA (Liposomas/Protamina/ADN). El péptido puede interactuar con la carga negativa del ADN antes de formar complejos con los liposomas catiónicos, resultando una restructuración de los lípidos, formando un complejo compacto de liposoma/ADN [64]. El pequeño tamaño del LPA facilita la endocitosis e incrementa el tiempo medio de circulación *in-vivo*. Además, después de las inyecciones intravenosas, el LPA tiende a acumularse en los pulmones y otros órganos como el riñón, bazo e hígado [65].

A pesar de las ventajas que poseen los lipoplejos catiónicos, éstos tienen limitaciones; estudios recientes han mostrado que éstos causan citotoxicidad y una baja eficacia de transfección tanto *in vitro* como *in vivo* [66-69]. En estudios *in vitro*, esta baja eficacia en el proceso de transfección, es atribuida a su heterogeneidad [70]. En estudios *in-vivo*, la baja eficacia de transfección se debe a que los lipoplejos catiónicos son susceptibles de ser alterados por las proteínas del suero fisiológico[3], es decir, a una rápida liberación del ADN del complejo y en consecuencia una degradación debido a las nucleasas[4] del suero.

1.3.2.2. Lipoplejos Aniónicos

Recientemente se ha demostrado que el proceso de formación de complejos entre los liposomas aniónicos y el ADN surge como una alternativa a los lipoplejos catiónicos, principalmente por su baja toxicidad y porque los lípidos aniónicos son componentes naturales de la membrana de las células eucariotas [12, 71-72]. Sin embargo, el uso de lipoplejos aniónicos es aún muy escaso pese a presentar una alta eficacia de transfección y baja toxicidad [73-74]. La mayor parte de los lipoplejos aniónicos están formados por lípidos como: DOPG/DOPE [71], DPPG [75], DOPG/DOPC [12], DPPG/DOPE, DPPA/DOPE [73] y EDOPC/DOPS [74].

---

[3]El suero fisiológico es una disolución acuosa de sustancias (agua, electrolitos, glucosa) compatible con los organismos vivos debido a sus características definidas de osmoticidad, pH y fuerza iónica.

[4]Las nucleasas son enzimas (proteínas complejas que producen un cambio químico especifico en todas las partes del cuerpo) que degradan ácidos nucleicos.

Por ejemplo, lipoplejos compuestos de lípidos DOPC/DOPG y oligonucleótidos han sido utilizados como vectores génicos *in-vivo*, expuestos a neuronas de hipocampos incrementando la expresión de las proteínas y aumentando la supervivencia de las neuronas alrededor de un 75% [72]. Lipoplejos de composición similar, DPPC/DMPG /oligonucleótidos, han sido capaces de introducir al oligonucleótido marcado fluorescentemente en células de bacterias [76]. También, se han hecho estudios sobre la liberación del ADN de lipoplejos aniónicos de EDOPC/DOPS, cuando éstos son fusionados con liposomas catiónicos [74].

No obstante, estos vectores aniónicos tienen aplicaciones limitadas, principalmente por las dificultades derivadas de formar complejos entre el ADN y los liposomas aniónicos [72, 76]. La repulsión electrostática entre los liposomas aniónicos y el ADN requiere de agentes intermediarios para que puedan atraerse y formar complejos [77]. En particular los cationes multivalentes son usados para la formación de complejos de lipoplejos aniónicos, entre los cuales los cationes divalentes como el Ca^{2+} suelen ser los más comunes [71, 73, 78]. El Ca^{2+} es capaz de encapsular ADN lineal y plasmídico mediante el auto ensamblado, y es considerado como un mediador en las actividades esenciales de las células [79-80]. Además el Ca^{2+} presenta baja toxicidad en las transfecciones de los lipoplejos aniónicos [71, 81-82].

En resumen, aunque en general la utilidad de los lipoplejos (tanto catiónicos como aniónicos) ha sido limitada hasta el momento en gran medida por su baja eficacia de transfección y su relativa baja expresión transgénica, la baja toxicidad junto con los resultados favorables en ensayos clínicos recientes, hacen de estos vectores no víricos la mejor promesa para la evolución de la terapia génica a corto y medio plazo.

Por consiguiente, en este trabajo de tesis doctoral nos proponemos aportar mayor información sobre las propiedades fisicoquímicas de lipoplejos tanto catiónicos como aniónicos. En el caso de lipoplejos catiónicos, se aportará información sobre el proceso de formación de complejos así como de sus propiedades de estabilidad (propiedad importante en el proceso de transfección) mediante la utilización de lípidos auxiliares. En el caso de lipoplejos aniónicos, nuestro objetivo principal es la caracterización fisicoquímica de algunos de estos complejos formados por lípidos más comunes. Para ello, se estudian los efectos de iones multivalentes como agentes intermediarios entre los lípidos aniónicos y el ADN.

CAPÍTULO 2

JUSTIFICACIÓN Y OBJETIVOS

El objetivo fundamental de esta tesis doctoral es la caracterización fisicoquímica de complejos de liposomas (catiónicos y aniónicos) con ADN, denominados *lipoplejos*. Como se comentó en el capítulo anterior, estos complejos poseen un gran potencial en terapia génica como vectores no víricos de transfección.

2.1. Justificación

A través de la terapia génica se han desarrollado métodos estratégicos para introducir medicamentos (o ADN) en el interior de células diana para tratar enfermedades de tipo genético. Uno de los métodos de la terapia génica es la utilización de vectores no víricos, dentro de los cuales se encuentran los lipoplejos. Éstos se han clasificado en lipoplejos catiónicos (liposomas catiónicos y ADN) y aniónicos (liposomas aniónicos, cationes y ADN).

Los lipoplejos catiónicos han resultado eficaces como transporte de material genético (ADN) en el organismo con objeto de transferirlo a las células diana. Esta propiedad de transporte genético se debe principalmente a que la doble capa lipídica de los liposomas presenta una gran similitud estructural con la membrana celular. Sin embargo,

estudios recientes han mostrado que los lipoplejos catiónicos pueden causar citotoxicidad tanto *in vitro* como *in vivo* y que además son susceptibles de ser alterados por las proteínas del suero fisiológico.

En la primera parte del presente trabajo de tesis se estudian lipoplejos catiónicos compuestos por liposomas de DODAB−DOPE/ADN y DODAB−DLPC/ADN. Este trabajo es fruto de la colaboración con el grupo "Química Coloidal y Supramolecular", liderado por la Dra. Elena Junquera y perteneciente al Departamento de Química Física I de la Universidad Complutense de Madrid. Este grupo ha realizado diversos estudios de caracterización fisicoquímica de lipoplejos catiónicos formados por diferentes lípidos siendo pioneros en España de la realización de este tipo de trabajos [10, 83]. En nuestro trabajo de colaboración se hace una caracterización experimental y teórica de lipoplejos catiónicos utilizando nuevos lípidos tanto catiónicos como zwitteriónicos, con el sentido de mejorar este tipo de vectores no víricos.

La justificación de los lípidos constituyentes de los liposomas catiónicos que se estudian se describe a continuación:

- ✓ El DODAB (Bromuro de dioctadecildimetilamonio) es un lípido catiónico de dos cadenas saturadas de 18 carbonos cada una de ellas. Este lípido pertenece a la familia de sales de dialquil-dimetil amonio, la cual es muy utilizada en la industria cosmética y farmacéutica debido a su estabilidad.
- ✓ El DOPE (1,2-dioleoil-sn-glicero-3-fosfatidiletanolamina) es

un lípido zwitteriónico (auxiliar) de dos cadenas de 18 carbonos y una insaturación en cada una de ellas. Este lípido pertenece a la familia de las fosfatidiletanolaminas, las cuales son ampliamente utilizadas por su eficacia en transfección.

✓ El DLPC (1,2-dilauroil-sn-glicero-3-fosfatidilcolina) es un lípido zwitteriónico de dos cadenas saturadas de 12 carbonos cada una de ellas. Este lípido pertenece a la familia de la fosfatidilcolina que, al igual que el DOPE, es frecuentemente utilizado por su eficacia de transfección.

La importancia de los lípidos auxiliares se debe a que incrementan la elasticidad de la bicapa de los liposomas y favorecen la fusión de los lipoplejos en la membrana de la célula, incrementando la eficacia de la transfección del ADN en la célula [1, 84-85].

El ADN utilizado es de tipo genómico y proviene de timo de ternera. Se trata por tanto de un ADN comercial comúnmente utilizado para la caracterización fisicoquímica de lipoplejos [9-10, 12-13, 83].

La preparación de liposomas y lipoplejos se hizo en un medio tamponado. El tampón de *HEPES* (*Sulfónato de 4-(2-Hidroxietil)-1-Piperacina*) en sus dos presentaciones, ácido (HEPES−H) y sódico (HEPES−Na), se ha utilizado para preparar las disoluciones reguladoras a pH ≈ 7.4 para mantener a los lípidos zwitteriónicos con su carga neutra y también para evitar la disociación del ADN.

La estructura química e información sobre la temperatura de transición

(T_m) de todos los lípidos citados anteriormente, así como la estructura del tampón, se detallan en el apéndice A.

Cabe señalar que el estudio de los lipoplejos catiónicos no es el objetivo principal de esta tesis doctoral. Sin embargo, este primer estudio con lipoplejos catiónicos se realizó en virtud de la colaboración con el grupo de la Dra. Elena Junquera con objeto de adquirir experiencia en los procesos de formación y caracterización de lipoplejos. Nuestra aportación a este trabajo fue la aplicación de un modelo teórico sobre la formación de complejos de polielectrolitos con partículas esféricas de signo opuesto. Mediante la aplicación del citado modelo, se construyó un diagrama de fases que describe la agregación y desagregación de los lipoplejos (ver artículo 1 para más detalles sobre el modelo utilizado).

Una vez adquirida la suficiente destreza con lipoplejos catiónicos, abordamos el objetivo principal planteado en esta tesis es el estudio de los lipoplejos aniónicos. La justificación de tal interés reside en el hecho de que recientemente los lipoplejos aniónicos se han postulado como una alternativa a los lipoplejos catiónicos como vehículos no víricos de transfección dada su baja toxicidad. Esta propiedad se debe en gran medida a que en este caso, los lípidos aniónicos usados son componentes naturales de las membranas celulares. Sin embargo, su utilización en la terapia génica aún es muy escasa. Esto último se debe principalmente a que los lipoplejos aniónicos presentan mayor dificultad en su formación, ya que requieren de cationes multivalentes que actúen como puente entre los liposomas y el ADN.

Es por eso, de que antes de abordar estudio de complejos formados por liposomas aniónicos, cationes multivalentes y ADN, se comenzó estudiando la interacción entre coloides aniónicos con cationes multivalentes. Con este fin se eligió un sistema experimental modelo formado por partículas de poliestireno (*látex*) en presencia de cationes trivalentes. La caracterización de este tipo de sistemas fue el objetivo principal de la tesis doctoral de uno de los directores de la presente tesis [86]. En particular, los sistemas escogidos para este trabajo fueron partículas de látex de tipo sulfonato con diferentes densidades superficiales de carga y como catión trivalente se usó el lantano (La^{3+}). Una vez caracterizado el efecto de este catión sobre un sistema coloidal modelo cargado negativamente, se pasó al estudió del efecto del mismo catión sobre liposomas aniónicos formados por lípidos de fosfatidilserina (PS) y fosfatidilcolina (PC). Finalmente, se extendió el estudió al caso de interacción de liposomas aniónicos de PS con cationes divalentes, usados comúnmente en la formación de lipoplejos aniónicos, como son el calcio (Ca^{2+}) y magnesio (Mg^{2+}).

A continuación los lípidos constituyentes de los liposomas aniónicos que se estudiaron en estos trabajos se describen:

- ✓ PS (fosfatidilserina), lípido aniónico de dos cadenas de 18 carbonos y con una insaturación en cada una de ellas. Este lípido pertenece a la familia de la fosfatidilserina.
- ✓ PC (fosfatidilcolina), lípido zwitteriónico de dos cadenas de 18 carbonos y una insaturación en cada una. Este lípido pertenece

a la misma familia que el lípido DLPC.

La importancia de los lípidos PS y PC se debe principalmente a que son los principales componentes naturales de las membranas celulares, por lo que son reconocidos fácilmente en los procesos de transfección [87]. Además, estos lípidos son comúnmente utilizados en aplicaciones industriales y estudios biofísicos [88].

Los cationes utilizados, para los estudios de interacción de los sistemas aniónicos, presentan características importantes que se describen a continuación:

- ✓ El catión trivalente de *lantano* es un ion comúnmente utilizado en los estudios de interacción de sistemas aniónicos por su habilidad de invertir la carga de las macromoléculas.
- ✓ El catión divalente de calcio es un ion que aparece como un mensajero intracelular y que favorece a la transfección del ADN a la célula.
- ✓ El catión divalente de magnesio es esencial para todas las células vivas ya que tiene una función estabilizadora de la estructura de las cadenas del ADN y ARN.

Finalmente, una vez caracterizada la compleja interacción entre liposomas aniónicos y cationes multivalentes, se procedió a caracterizar lipoplejos aniónicos. Con este fin se utilizó el sistema formado por liposomas aniónicos DOPS–DOPC, cationes divalentes de Ca^{2+} y ADN (DOPS–DOPC/Ca^{2+}/ADN). Las principales

40

características de estos lípidos son:

- ✓ El DOPS (1,2-dioleoil-sn-glicero-3-fosfatidilserina) es un lípido aniónico de dos cadenas de 18 carbonos y una insaturación en cada una de ellas. Este lípido pertenece a la misma familia del PS.

- ✓ El DOPC (1,2-dioleoil-sn-glycero-3-fosfatidilcolina) es un lípido zwitteriónico de dos cadenas de 18 carbonos y una insaturación en cada una de ellas. Este lípido pertenece a la misma familia del PC y DLPC.

La razón por la que se usaron estos lípidos en lugar de PS y PC, respectivamente se debe a que tanto los lípidos de DOPS como los de DOPC poseen mayor grado de pureza y tienen cadenas hidrocarbonadas similares. Las características estructurales y las propiedades fisicoquímicas de los lípidos y los cationes multivalentes, así como los procesos de formación de los liposomas y lipoplejos que se utilizaron para este estudio, se encuentran descritos en el apéndice A.

2.2. Objetivos

De acuerdo con el análisis anterior sobre la importancia de los lipoplejos y de los materiales que los constituyen, a continuación se enumeran los objetivos específicos de este trabajo:

1. Caracterización fisicoquímica de nuevos complejos formados por

liposomas catiónicos y ADN.

2. Estudio de la interacción entre un catión trivalente (La^{3+}) y sistemas coloidales modelo.

3. Estudio de la interacción entre lantano y liposomas aniónicos.

4. Estudio de la interacción específica entre liposomas aniónicos y cationes divalentes (Ca^{2+} y Mg^{2+}).

5. Caracterización fisicoquímica del sistema compuesto por lípidos aniónicos, calcio y ADN (DOPS–DOPC/Ca^{2+}/ADN).

CAPÍTULO 3

DISCUSIÓN CONJUNTA DE LOS RESULTADOS OBTENIDOS EN LOS DISTINTOS TRABAJOS

En este capítulo del trabajo de tesis se presenta una discusión conjunta de todos los resultados obtenidos en los distintos trabajos realizados. El capítulo se distribuye en tres secciones, de acuerdo a la temática estudiada. La primera sección (3.1) corresponde al estudio de sistemas formados con liposomas catiónicos y ADN, la segunda sección (3.2) trata sobre sistemas aniónicos y cationes multivalentes, y finalmente la tercera sección (3.3) está dedicada al sistema formado por liposomas aniónicos, cationes divalentes y ADN. En cada sección se resume y comenta tanto la temática principal como los principales resultados de los artículos de investigación publicados (o enviados para su publicación). A continuación se presenta un breve esquema de cada sección.

En la sección 3.1 se hace un análisis de la formación de complejos de ADN con liposomas catiónicos dando lugar a lipoplejos catiónicos. Con este fin se realizó una caracterización tanto experimental como teórica de la formación y estabilidad de los lipoplejos resultantes. Esta sección está constituida por el siguiente trabajo:

ARTÍCULO 1: A Theoretical and Experimental Approach to the Compactation Process of DNA by Dioctadecy-

*ldimethylammonium Bromide/Zwitterionic Mixed Liposomes. (J. Phys. Chem. B **2009**, 113, 15648-15661)*

En la sección 3.2 se analiza la interacción de sistemas aniónicos con cationes multivalentes. Este análisis se considera como un estudio previo y necesario antes del estudio de los lipoplejos aniónicos y está constituida por los siguientes trabajos:

*ARTÍCULO 2: Effect of the Surface Charge on Colloidal Charge Reversal. (J. Phys. Chem. B **2009**, 113, 6834-6839)*

*ARTÍCULO 3: Charge Reversal of Anionic Liposomes: Experimental Demostration and Molecular Oringin. (Phys. Rev. Lett. **104**, 168103 (2010))*

ARTÍCULO 4: Effect of Calcium and Magnesium on Phosphatidyl-serine Membranes: Experimental and all−Atomic Simulations.(Biophys. J. 102 (9) 2012, 2095-2103)

Una vez caracterizada la interacción liposoma aniónico−catión, en la sección 3.3 se caracteriza un sistema representativo de lipoplejos aniónicos formado por liposomas aniónicos, calcio y ADN. La sección está constituida por el siguiente trabajo:

ARTÍCULO 5: Interaction between DNA and Mixtures of Anionic/ Zwitterionic Phospholipids Mediated by Calcium. (J.

A continuación se presentan los resultados y discusión de cada sección.

3.1. Liposomas Catiónicos y ADN

Como ya se ha comentado en el capítulo de introducción, los lipoplejos catiónicos presentan en la actualidad algunas deficiencias, entre las que se encuentran su baja estabilidad y baja eficacia de transfección. Ambos factores dependen en gran medida del tipo y proporción de lípidos utilizados. Además, la presencia del lípido auxiliar (zwitteriónico) en la composición de los liposomas es muy importante ya que de ellos pueden depender en gran medida las propiedades mecánicas de los liposomas [89].

Basándonos en estudios previos del proceso de formación de lipoplejos catiónicos [10, 83] llevados a cabo por el grupo colaborador de la Universidad de Complutense de Madrid (detalles sobre el grupo se encuentran en el capítulo 2: Justificación y Objetivos), en este primer trabajo nos proponemos caracterizar dos tipos de lipoplejos catiónicos compuestos por DODAB−DOPE/ADN y DODAB−DLPC/ADN. El objetivo es aportar más información sobre nuevos lipoplejos catiónicos en función de su composición lipídica. En concreto, uno de los objetivos principales de esta parte del trabajo consiste en hacer un análisis de la influencia de los lípidos auxiliares

(DOPE y DLPC) en el proceso de formación y estabilidad de lipoplejos formados por lípidos DODAB y ADN.

Además de la caracterización experimental, este trabajo presenta como novedad la aplicación de un modelo teórico que describe la formación de complejos entre polielectrolitos y coloides de carga opuesta (ver artículo 1).

Así pues, el trabajo consta de una parte experimental donde se hace uso de diversas técnicas experimentales con las que se caracteriza la formación de complejos de ADN y liposomas. Por otro lado, la aplicación del modelo teórico al que se acaba de hacer referencia, nos permite construir un diagrama de fases que describe el fenómeno de agregación y desagregación de los lipoplejos.

A continuación, se presenta una breve descripción de las técnicas experimentales y de los resultados más significativos obtenidos con de dichas técnicas.

3.1.1. Sistemas Experimentales

Entre las técnicas experimentales que se usaron para analizar las interacciones entre el ADN y los liposomas catiónicos se encuentran: la *electroforesis*, la *conductimetría*, la *microscopía de fluorescencia* y la *crio−microscopía*. Con la electroforesis, se estudió el movimiento en la disolución de los liposomas y lipoplejos por el efecto de sus cargas, al aplicarles un campo eléctrico externo ($\vec{E}$). El parámetro que

se obtiene a partir de esta técnica es la movilidad electroforética (μ_e), que se define como la constante de proporcionalidad entre el campo externo aplicado y la velocidad con la que se mueven las partículas ($\vec{v}_e$): $\vec{v}_e = \mu_e \vec{E}$. Las medidas se hicieron con una concentración fija ADN mientras que la concentración total de lípidos se fue variando hasta cubrir un intervalo de proporción (*L/D*):

$$\frac{L}{D} = \frac{L^+ + L^0}{D} \qquad (3.1)$$

donde *L* es la masa total de lípidos, L^+ es la masa del lípido catiónico, L^0 es masa del lípido zwitteriónico y *D* es la masa del ADN [90]. La otra técnica para estudiar las propiedades eléctricas de los liposomas y lipoplejos que se utilizó fue la conductimetría, de la que se obtuvo la conductividad específica (*k*). Esta magnitud está relacionada con la inversa de la resistencia (R_k) de la disolución al movimiento de partículas cargadas por el efecto de campo eléctrico externo. Ésta última puede determinarse a partir de la ley de Ohm como: $R_k = \Delta V / \Theta$, donde ΔV es el voltaje aplicado y Θ es el flujo de corriente a través del medio. La resistencia de la disolución se mide en una célula de dimensiones determinadas por el área (A_e) de cada electrodo y la separación entre ellos. A la relación $1/A_e$ se le denomina constante de la célula y a la inversa de la resistencia ($1/R_k$) se le denomina conductancia o conductividad especifica: $k = 1/A_e R_k$. Al igual que la electroforesis, esta técnica permite cuantificar la carga superficial de los liposomas y lipoplejos. En particular, ambas técnicas

electroquímicas permitieron calcular la proporción de isoneutralidad $(L/D)_\phi$, de los lipoplejos estudiados. Es decir, la proporción L/D tal que la carga neta de los lipoplejos es nula.

Además de las técnicas anteriormente descritas, la espectroscopía de fluorescencia también se usó para estudiar estos sistemas [91-92]. Para ello, se llevaron a cabo ensayos de intercalación de fluorescencia con bromuro de etidio (EtBr). Este fluoróforo tiene la propiedad de emitir intensidad de luz cuando está en contacto con el ADN. Sin embargo, cuando el ADN interacciona con los liposomas, el fluoróforo se desliga del ADN y por tanto la intensidad de emisión del fluoróforo decae. Con la espectroscopía se hicieron medidas intensidad de emisión de fluorescencia de los liposomas en presencia de ADN y en función de L/D. Para este fin, se fijaron las concentraciones de EtBr y ADN.

Finalmente, se obtuvieron imágenes mediante la técnica de crio−microscopía de transmisión [93-94], con las que se determinaron el tamaño, la estructura y la morfología de los liposomas compuestos por los lípidos DODAB/DOPE y DODAB/DLPC en ausencia y presencia de ADN. En particular, se realizaron experimentos para dos valores de L/D por encima y por debajo de $(L/D)_\phi$. Las muestras se prepararon mediante congelaciones ultrarrápidas para conseguir que el agua permanezca en forma vítrea y así evitar la aparición de cristales de hielo que dañen la muestra.

Además de la caracterización experimental, el proceso de formación

de los complejos liposomas/ADN se analizó desde un punto de vista teórico mediante un modelo que se presenta a continuación y que está descrito en detalle en el artículo 1.

3.1.2. Modelo de Agregación y Desagregación de Lipoplejos

En el caso de lipoplejos catiónicos, la interacción responsable de la formación de los complejos es la interacción electrostática por la que ADN y liposomas son atraídos como consecuencia de sus cargas de signo opuesto. Sin embargo, este proceso electrostático no culmina cuando el complejo adquiere una carga neta nula sino que puede ocurrir que dada una molécula de ADN, la cantidad de liposomas atraídos por el polielectrolito sea tal que la carga neta del complejo se invierta y sea de signo positivo. A este proceso se le denomina comúnmente en ciencia coloidal como *fenómeno de sobrecarga*, o como *inversión de carga* (IC). Estudios recientes de IC ponen de manifiesto la naturaleza de tal fenómeno así como las múltiples aplicaciones que pueden tener en biotecnología [86, 95-97]. Sirva como ejemplo la condensación de ADN por efecto de electrolitos trivalentes y tetravalentes.

En relación al fenómeno de sobrecarga, Shklovskii y col. han desarrollado una teoría fenomenológica que describe la IC de diferentes coloides cargados en presencia de iones multivalentes [98-99]. En particular, uno de los sistemas estudiados fue el constituido por polielectrolitos negativos y partículas esféricas cargadas positivamente. En este caso, el modelo analiza la IC de un

polielectrolito cuya longitud es tal que le permite formar complejos con diversas esferas positivas de tal forma que el complejo resultante adquiere una carga neta positiva.

A partir de este trabajo, Sennato y col. [100] han modificado la teoría para el caso opuesto; cuando varios polielectrolitos se adsorben en la superficie de una macropartícula de carga opuesta dando lugar a un complejo cuya carga neta es del mismo signo que la del polielectrolito.

Entre otras cosas, ambos modelos fenomenológicos permiten la construcción de un diagrama de fases de los complejos resultantes en función de la proporción polielectrolito/partícula. En nuestro caso, el desarrollo teórico realizado por Sennato y col. ha sido aplicado por primera vez al sistema formado por liposomas catiónicos y ADN. De acuerdo con el formalismo detallado en el apéndice B, dada una concentración fija de ADN (P) y variando la concentración de liposomas (S), el modelo proporciona un sistema de ecuaciones encaminado a determinar la concentración (S_a) en la que los lipoplejos empiezan a agregarse y son coloidalmente inestables. También permite calcular la concentración en la que el lipoplejo posee una carga neta nula (S_ϕ), a partir de la cual se produce un fenómeno de IC. Finalmente el modelo predice un fenómeno de *reestabilización* según el cual, para concentraciones mayores a un determinado valor (S_d), los lipoplejos vuelven a ser estables (pero con signo opuesto al que tenía para concentraciones $S < S_a$).

Así pues, si se tiene acceso a datos experimentales de $S_a(P)$ y $S_d(P)$ para una concentración de ADN, como es nuestro caso, la teoría permite predecir estas magnitudes para cualquier valor de

concentración de ADN. En nuestro caso, la teoría se aplicó a los sistemas DODAB−DOPE/ADN y DODAB−DLPC/ADN partiendo de los valores de S_a y S_d obtenidos de los experimentos de movilidad electroforética. Los diagramas resultantes se compararon con el construido para un lipoplejo de DSTAB−DOPE/ADN que fue caracterizado en un trabajo anterior por el grupo de la Profesora Elena Junquera [10]. De esta forma, se pudo ampliar el análisis comparativo del efecto del lípido catiónico en el comportamiento del lipoplejo resultante.

3.1.3. Discusión de Resultados

La eficacia de los lipoplejos catiónicos depende de muchos factores que modulan el proceso de transfección. Uno de esos factores es la proporción de lípidos/ADN necesaria para alcanzar la isoneutralidad, $(L/D)_\phi$, es decir, el momento en el que estos sistemas poseen una carga neta nula y por tanto el sistema es inestable. Esta información puede ser obtenida experimentalmente a partir de la movilidad electroforética y estudiando cuando ésta se hace cero (*punto isoeléctrico*). En ocasiones, los experimentos de electroforesis se expresan en términos del potencial ζ[5] (en lugar de μ_e).

_____

[5]Cuando un macroión cargado se mueve en el seno de una disolución electrolítica por efecto de un campo eléctrico externo, parte de los iones y moléculas que hay en el disolvente se mueven de manera solidaria con el macroión de forma que se pueden distinguir dos regiones de partículas, una próxima a la superficie del macroión y otra (seguida de la primera) que disminuye gradualmente con la distancia. De acuerdo con esto, al plano que separa las dos regiones se le denomina potencial electrocinético o potencial ζ.

La conversión de una magnitud a la otra depende de las características del sistema. En particular, para el caso en el que se tengan partículas con radios electrocinéticos elevados, se puede usar la aproximación de Helmholtz−Smoluchowski $\mu_e = \varepsilon_0 \varepsilon_r \zeta / \eta$, donde ε_0 y ε_r son la permitividad en el vacío y relativa, respectivamente y η es la viscosidad del medio. Así pues, los resultados de electroforesis en función de la proporción *L/D* nos permiten distinguir tres regiones (Fig. 3.1): *(i)* una región donde los lipoplejos muestran un potencial ζ negativo y casi constante, similar al valor de movilidad de las moléculas de ADN en ausencia de liposomas; *(ii)* una región donde se alcanza el punto isoeléctrico a partir del cual se produce un proceso de inversión del signo de la movilidad y *(iii)* una región en la que se muestra un potencial ζ positivo que tiende al valor de potencial ζ de los liposomas en ausencia de ADN.

Las medidas de conductividad específica (*k*) e incluidas también en la Fig. 3.1 muestran como *k* de los lipoplejos de DODAB/DOPE aumenta con la concentración de liposomas debido a que cuando se forma el lipoplejo, se liberan iones de sodio (Na^+) del ADN y de bromo (Br^-) de los liposomas, incrementando así la conductividad del medio.

Con el fin de obtener más información acerca de la formación de los complejos liposoma/ADN, se hicieron medidas de la intensidad de emisión fluorescencia de los lipoplejos DODAB−DOPE/ADN y

DODAB−DLPC/ADN en función de la concentración de liposomas (Fig.3.2).
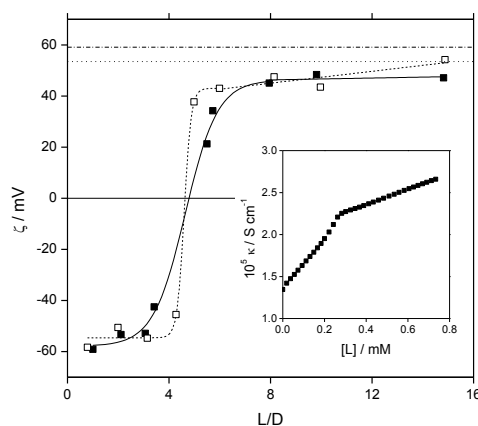
Fig. 3.1. Valores de potencial ζ de los sistemas DODAB−DOPE/ADN (cuadros sólidos) y DODAB−DLPC/ADN (cuadros vacíos) en función de *L/D*. La línea punteada indica el valor absoluto del potencial ζ de los liposomas DODAB/DOPE en ausencia de ADN y la línea discontinua el correspondiente a los liposomas DODAB/DLPC en ausencia de ADN. La gráfica insertada muestra la conductividad específica k del sistema DODAB/DOPE en presencia de ADN y en función de la concentración de liposomas (*L*).

Con el fin de obtener más información acerca de la formación de los complejos liposoma/ADN, se hicieron medidas de la intensidad de emisión fluorescencia de los lipoplejos DODAB−DOPE/ADN y DODAB−DLPC/ADN en función de la concentración de liposomas (Fig.3.2). En concreto, la Fig. 3.2A muestra claramente cómo la intensidad de emisión del fluoróforo disminuye gradualmente cuando *L/D* aumenta. De acuerdo con lo explicado en secciones anteriores, este comportamiento de la intensidad del fluoróforo confirma la interacción del ADN con los liposomas.
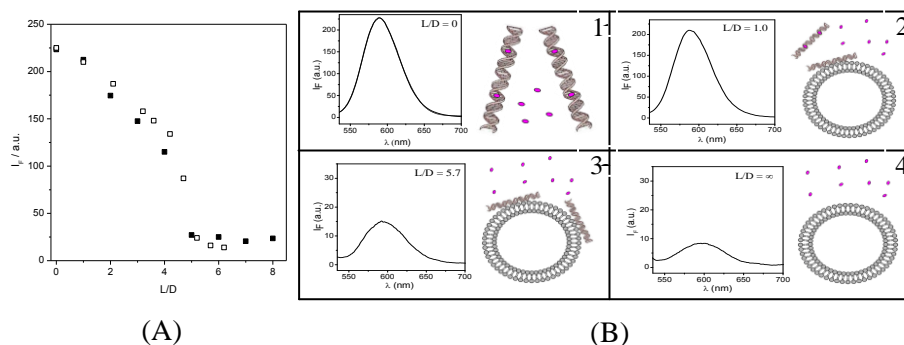
Fig. 3.2. (A) Intensidad de emisión de fluorescencia de los lipoplejos DODAB-DOPE/ADN (cuadros sólidos) y DODAB-DLPC/ADN (cuadros vacíos) en función de *L/D*. (B) espectros de emisión de fluorescencia de EtBr en presencia de lipoplejos de DODAB-DLPC/ADN para una L/D seleccionada. Adjunto un bosquejo ilustrativo para: *L/D* = 0 (1), *L/D* = 1.0 (2), *L/D* = 5.7 (3) y *L/D* = ∞ (4).

La intensidad permanece constante hasta una *L/D* ≈ 5, siendo muy similar para los dos sistemas estudiados. En este valor de *L/D* se alcanza la proporción de isoneutralidad, siendo éstos muy similares a aquellos obtenidos por electroforesis para ambos sistemas.

Un análisis muy interesante es el proceso sucesivo de la emisión de la intensidad de fluorescencia que se puede ver en la Fig. 3.2B. Esta figura muestra los espectros de la intensidad de emisión del fluoróforo en su intercalación con el ADN, junto a un bosquejo ilustrativo de la disociación del fluoróforo del ADN. Los espectros pertenecen a los liposomas y los lipoplejos para diferentes *L/D* para el sistema DODAB/DLPC y ADN. En la Fig. 3.2B se observa que para cuando sólo hay ADN (**1**), la intensidad del fluoróforo es alta debido a su intercalación con el ADN. Una pequeña concentración de liposomas (**2**) reduce la intensidad de emisión, es decir, el fluoróforo que se

desliga del ADN deja de emitir debido a que el éste interacciona con los liposomas dejando libre al fluoróforo. Una concentración mayor de liposomas (**3**), hace que más ADN interaccione con éstos y la intensidad de emisión del fluoróforo decae más, indicando que muy poco ADN queda libre. Finalmente, en ausencia de ADN (**4**), el fluoróforo no interacciona con los liposomas y la intensidad de emisión del fluoróforo tiende a cero.

Las micrografías de crio−microscopía muestran liposomas esféricos en ausencia de ADN ($L/D = \infty$) y prácticamente unilamelares, de tamaños de (70 ± 5) nm para el DODAB/DOPE y (61 ± 10) nm para el DODAB/DLPC (Fig 3.3). Para los liposomas en presencia de ADN, se estudiaron valores de *L/D*, tanto mayores como menores, que *(L/D)$_\phi$* observando claramente diferencias entre los lipoplejos con exceso de ADN de carga neta negativa (*L/D < (L/D)$_\phi$*) y con exceso de liposomas de carga neta positiva (*L/D > (L/D)$_\phi$*).
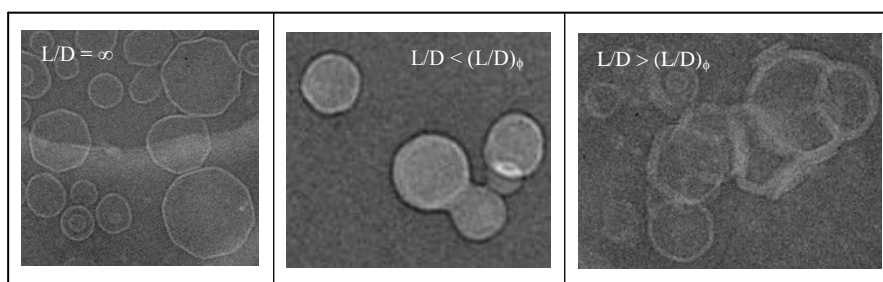
Fig. 3.3. Micrografías de los liposomas en ausencia (L/D = ∞) y presencia (*L/D < (L/D)$_\phi$*) − (*L/D > (L/D)$_\phi$*) de ADN para diferentes *L/D*. Agregación (*L/D < (L/D)$_\phi$*) y desagregación (*L/D > (L/D)$_\phi$*) de los lipoplejos.

Para *L/D < (L/D)$_\phi$*, los lipoplejos resultaron casi esféricos, como los

liposomas, pero con diámetros menores y similares para los dos sistemas. Lo anterior indica que los liposomas se reestructuran en presencia de ADN formando estructuras más pequeñas. Para $L/D > (L/D)_\phi$ hay una rica distribución de lipoplejos. Las micrografías muestran lipoplejos multilamelares y agregados de lipoplejos. Para los dos casos, la estructura, el tamaño y la morfología de los liposomas cambiaron en presencia de ADN. Comparando el comportamiento de los liposomas del lípido catiónico DODAB en ausencia y presencia de ADN, con liposomas compuestos con otro lípido catiónico (DSTAP) [10], se observó que los lipoplejos en ambos casos eran muy similares tanto en tamaño, estructura y morfología. En el artículo 1 (capítulo 5, sección 5.1) se presenta una completa caracterización de los lipoplejos con esta técnica, así como con otras técnicas no comentadas.

Una vez determinados experimentalmente los valores de L/D que dan lugar a las diferentes regiones de estabilidad de los lipoplejos, se aplicó el modelo fenomenológico anteriormente descrito. Para ello, se usaron los datos experimentales obtenidos de electroforesis para así poder calcular los parámetros libres P_0 (relacionado con una concentración de ADN que está en equilibrio con los lipoplejos) y E_0 (relacionada con la energía de enlace entre el ADN y los liposomas) (ver ecuaciones 3 y 4 del artículo 1). Así pues, conocidos los valores límites de $S_a(P)$ y $S_d(P)$ para la concentración de ADN experimental (P), la teoría permite predecir los valores de $S_a(P)$ y $S_d(P)$ para cualquier valor de P. De esta forma, se pueden construir diagramas de fase como el mostrado en la Fig. 3.4 en donde se muestra como para $S < S_a(P)$ (Fig. 3.4-1), los lipoplejos son estables y poseen una carga

neta negativa.
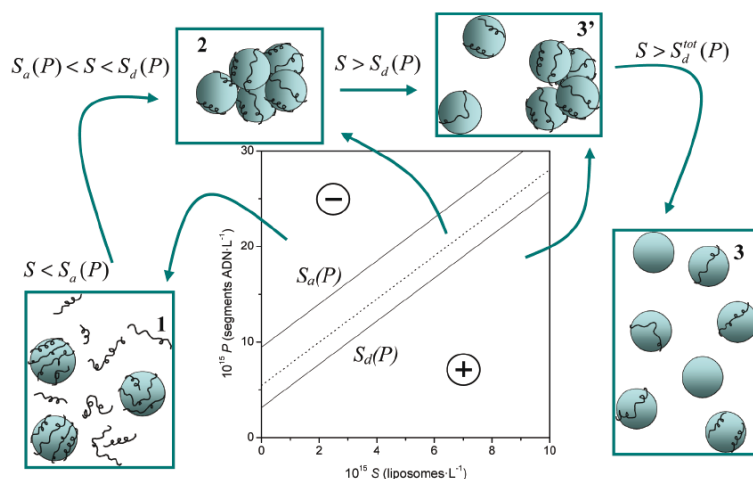
Fig. 3.4. Diagrama de fase de los lipoplejos formados por DODAB−DOPE/ADN, de acuerdo con el modelo teórico. Las líneas solidas indican a $S_a(P)$ y $S_d(P)$, mientras que la línea punteada indica a $S_\phi(P)$. Las figuras de los cuadros bosquejan a: (1) lipoplejos con carga neta negativa, (2) agregados de lipoplejos con carga alrededor o igual a cero (isoneutralidad), (3') coexistencia de lipoplejos y agregados con carga neta positiva y (3) lipoplejos con carga neta positiva.

Cuando S aumenta, los lipoplejos comienzan a agregarse y en esta región (entre $S_a(P)$ y $S_d(P)$) (Fig. 3.4-2), se llega al punto isoeléctrico de los agregados de forma que si se sigue aumentando S, la carga de los lipoplejos se invierte (Fig. 3.4-3'). Finalmente, para $S > S_d(P)$ los agregados tienden a desagregarse dando lugar a un sistema estable formado por lipoplejos de carga neta positiva (Fig. 3.4-3).

Al comparar los resultados de los sistemas formados con los lípidos catiónicos DODAB, con aquellos obtenidos previamente de liposomas catiónicos DSTAP, se observa que las líneas límites (dadas por S_a y S_d) se desplazan hacia concentraciones mayores de liposomas en el

orden DODAB/DLPC > DSTAP/DOPE > DODAB/DOPE (ver figura 14 del artículo 1). Como consecuencia, los lipoplejos formados por liposomas que contienen lípidos auxiliares de DOPE, requieren un número menor de liposomas para inducir la IC. Esto podría ser muy importante en el proceso de transfección porque así podrían formarse lipoplejos catiónicos con menos citotoxicidad.

En resumen, la tendencia observada de los resultados experimentales de movilidad electroforética, conductimetría e intensidad de fluorescencia de los liposomas de DODAB/DOPE, DODAB/DLPC en ausencia y presencia de ADN, coincidieron con las micrografías de crio−microscopía obtenidas. Todos lo resultados apuntan en la misma dirección; indican una clara interacción electrostática entre el ADN y los liposomas catiónicos. También se hizo una evaluación del efecto que causan los diferentes tipos de lípidos zwitteriónicos, DOPE y DLPC, en el proceso de formación de complejos, concluyendo que ambos lípidos influyen de manera diferente en los lipoplejos resultantes. Por otro lado, el desarrollo del diagrama teórico proporciona información sobre las concentraciones límites de liposomas en las cuales se forman agregados de liposomas aniónicos y después se desagregan dando paso a lipoplejos estables de carga opuesta.

Una vez adquirida experiencia en la caracterización de lipoplejos catiónicos, nuestro próximo objetivo es estudiar lipoplejos aniónicos (liposomas aniónicos/cationes multivalentes/ADN). Sin embargo, antes de abordar dicha tarea, es necesario analizar la interacción entre

sistemas aniónicos y cationes multivalentes.

3.2. Sistemas Aniónicos y Cationes Multivalentes

Como ya se ha dicho en la introducción, el estudio de los lipoplejos aniónicos presenta muchas dificultades, principalmente debido a que los liposomas y el ADN poseen cargas del mismo signo, por lo que se requiere de cationes para inducir a su formación. Es por ello que primero estudiaremos la interacción entre coloides aniónicos y cationes multivalentes, en ausencia de ADN.

Para empezar, en esta sección vamos a analizar nuevamente el fenómeno de la IC, pero ahora con sistemas aniónicos donde los cationes multivalentes actúan como contraiones inductores de la IC. Con este fin, estudiaremos la IC producida por iones trivalentes en un sistema coloidal modelo, compuesto por partículas de látex con diferentes valores de densidad superficial de carga (σ_0) (apartado 3.2.1). Después estudiaremos la IC que causan los mismos cationes trivalentes en liposomas aniónicos (apartado 3.2.2). Finalmente, esta sección concluye con un estudio similar al anterior pero con cationes divalentes ya que con iones trivalentes no fue posible formar lipoplejos aniónicos (apartado 3.2.3). Finalmente se discuten de manera conjunta los resultados obtenidos de los tres apartados (apartado 3.2.4).

3.2.1. Inversión de Carga en Sistemas Coloidales Modelo

De acuerdo con los trabajos previos realizados por uno de los directores de esta tesis y colaboradores, la IC producida en sistemas coloidales modelos está íntimamente relacionada con las correlaciones entre iones, especialmente en el caso de iones multivalentes [86, 96, 101]. En estos trabajos se usó la técnica de electroforesis para poner de manifiesto la IC como una inversión en el signo de la movilidad electroforética. Además, se usaron modelos teóricos de doble capa eléctrica de acuerdo con los cuales, además de iones multivalentes, la IC se ve favorecida por un aumento de la densidad de carga superficial (σ_0) de los coloides. Aunque estos modelos predecían también una IC para iones divalentes, experimentalmente se demostró que los electrolitos divalentes (incluso a grandes concentraciones) eran incapaces de invertir el signo de la μ_e. Por este motivo, en el trabajo correspondiente al artículo 2 se estudió experimentalmente el efecto de la σ_0 en la IC de partículas de látex inducida por iones de trivalentes (lantano). Además, para este trabajo se contó con la colaboración del Dr. M. Quesada Pérez de la Universidad de Jaén quien contribuyó con el desarrollo de simulaciones Monte Carlo (MC). De acuerdo con estas simulaciones, las partículas de látex se modelaron como superficies planas homogéneamente cargadas inmersas en un modelo primitivo (MP) de electrolito en donde el tamaño iónico está considerado implícitamente y el disolvente se considera como un continuo caracterizado por ε. Así pues, el objetivo de este trabajo es, usando experimentos de electroforesis y simulaciones MC, encontrar las condiciones experimentales

adecuadas para producir una IC en un sistema coloidal modelo. En particular se determinaron los valores críticos de σ_0 y de concentración de electrolito trivalente requeridos para producir la IC.

Experimentalmente se usaron cuatro suspensiones de látex de poliestireno (L1-L4) con el mismo grupo funcional superficial de ácido fuerte (sulfonato), pero de diferente σ_0 (ver tabla 3.1). Para cada sistema se midió la μ_e en función de la concentración de lantano

Tabla 3.1 Densidad superficial de carga superficial de los látex.

Látex	σ_0 (Cm^{-2})
L1	−0.04
L2	−0.08
L3	−0.12
L4	−0.46

Como se mostrará más adelante en la discusión de resultados, sólo se observó IC para los dos sistemas más cargados y para una elevada concentración de lantano (superior a 20 mM). Esta dependencia de IC con la concentración de catión y de la carga de las partículas se vio corroborada con las simulaciones MC.

Mediante estas simulaciones se determinó potencial difuso[6] (ψ_d), el

---

[6]De acuerdo con la definición del potencial ζ (apartado 3.1.3), a la segunda región de iones o moléculas que disminuye gradualmente con la distancia de la superficie del macroión, se le conoce como capa difusa.

cual puede aproximarse a ζ cuando para el caso de sistemas coloidales modelo [86]. Los cálculos de ψ_d se hicieron considerando iones de La^{3+} de diámetro de 0.90 nm según valores experimentales obtenidos en la bibliografía [102-103]. Los detalles y especificaciones de las simulaciones MC se pueden ver en el artículo 2 del capítulo 5, sección 5.2.

3.2.2. Inversión de Carga de Liposomas Aniónicos

Una vez caracterizada la IC de sistemas coloidales modelo, el siguiente objetivo fue caracterizar este fenómeno para el caso de liposomas aniónicos. Las interacciones superficiales de biocoloides con iones multivalentes son muy importantes en la determinación de sus propiedades fisicoquímicas y aplicaciones. El estudio anterior demuestra que bajo determinadas condiciones, los iones trivalentes son capaces de inducir una IC en sistemas coloidales modelo. En estos sistemas modelo, los iones se acumulan en la superficie de los coloides pero siempre están restringidos a permanecer en la fase acuosa, es decir, no son capaces de penetrar en la superficie solida de las macromoléculas [104-106]. Sin embargo, en coloides no rígidos como es el caso de los liposomas, la situación es bien diferente. Por tanto la pregunta es ¿cómo influye la rigidez de una superficie coloidal en la interacción de dicha superficie con iones multivalentes? Con el fin de responder a esta pregunta se realizó un trabajo (artículo 3) en donde nuevamente se usó la electroforesis para estudiar la IC de los liposomas por efecto del lantano.

En concreto los sistemas experimentales que se utilizaron en este trabajo son los formados por liposomas de PS y de PC. Además de las medidas de μ_e de los liposomas en función de la concentración de La^{3+}, también se midió en ausencia y presencia del ión monovalente de nitrato de sodio (Na$^+$). Las medidas se realizaron a pH = 5.4 donde las moléculas de PS tienen su carga total negativa y las de PC es neutra.

Además de los experimentos de movilidad, y al igual que en el caso anterior, se realizaron simulaciones por ordenador. Sin embargo en este caso, el MP no es el mejor modelo para simular los liposomas ya que de acuerdo con este modelo, la superficie del coloide es rígida e impenetrable. Así pues, para poder llevar a cabo nuevas simulaciones que modelen una superficie blanda como la de las membranas lipídicas se colaboró con el Dr. Faraudo del ICMAB-CSIC de Barcelona. Estas simulaciones se realizaron mediante dinámica molecular (DM) a nivel atómico. El modelo utilizado fueron las bicapas de los liposomas de PS completamente hidratadas y las cuales estaban en contacto con cationes de La^{3+}. Los algoritmos de los cálculos y las especificaciones de simulación están dados en el artículo 3 del capítulo 5, sección 5.3, y otros detalles técnicos respecto a los modelos moleculares han sido previamente presentados en [107].

Como consecuentica de los resultados experimentales y de simulación, en este trabajo se propuso un nuevo mecanismo de IC para sistemas blandos basado en la absorción preferencial de los

contraiones multivalentes por las moléculas anfifílicas (lípidos). De acuerdo con este mecanismo y como se verá en la sección de discusión, la concentración de lantano requerida para producir IC es dos órdenes de magnitud inferior al caso de partículas de látex.

3.2.3. Interacción Específica entre Liposomas Aniónicos y Cationes Divalentes

Además de la interacción entre los cationes trivalentes de La^{3+} y liposomas aniónicos, en la bibliografía se puede encontrar cómo la condensación del ADN puede ser inducida mediante iones trivalentes [108] y poliaminas [58, 109]. Por tanto, llegado a este punto nuestro objetivo era formar lipoplejos aniónicos formados por liposomas aniónicos (PS), cationes trivalentes (La^{3+}) y ADN. Sin embargo, experimentalmente esto no fue posible ya que al añadir el ADN en la disolución de PS/La^{3+}, se observó que el sistema gelificaba.

Así pues, se decidió usar cationes divalentes para formar los lipoplejos aniónicos de acuerdo con otros trabajos publicados en la bibliografía en donde se usaron cationes como el Ca^{2+}, Mg^{2+}, Co^{2+}, Cd^{2+}, Mn^{2+} y Zn^{2+} [12, 78, 81]. En nuestro caso, elegimos estudiar los cationes divalentes de Ca^{2+} y Mg^{2+} en la formación de complejos con liposomas de PS. Estos iones fueron estudiados previamente para analizar la agregación de liposomas de PS [110-112].

Sin embargo, antes de formar los lipoplejos, se realizó un estudio previo encaminado a la caracterización de la interacción de estos dos iones con liposomas y membranas lipídicas de PS (artículo 4). Con

este fin, se usaron diversas técnicas experimentales con las se determinó tanto la movilidad electroforética de los liposomas de PS como su estabilidad en función de la concentración de Ca^{2+} y Mg^{2+}. Para estudiar la estabilidad coloidal se usaron técnicas de dispersión de luz con objeto de poder calcular el *factor de estabilidad (W)*. Esta magnitud se define a su vez como el cociente: $W = K_r/K_l$, donde K_r y K_l son las constantes de agregación en condiciones agregación rápida y lenta, respectivamente. De acuerdo con esta definición W, puede tomar valores entre 1 y ∞. Cuando $W = 1$ ($K_l = K_r$) el sistema es completamente inestable y agrega, por lo que se dice que se está en el régimen de agregación rápida. Ahora bien, cuanto mayor es W, mayor es la estabilidad de la disolución. La inversa de W se puede interpretar como una medida de la efectividad de las interacciones entre los liposomas y los cationes que da lugar a la agregación. A partir de las medidas de estabilidad se determinó la concentración mínimo de electrolito para que el sistema pase de un régimen lento de agregación a uno rápido. A ese valor de concentración de sal se le denomina concentración crítica de coagulación (CCC). Estas medidas de agregación se complementaron con medidas de turbidez de la suspensión de liposomas en función de la concentración de Ca^{2+} y Mg^{2+}. En concreto, se midió la *absorbancia* (ΔA) de la suspensión en función de la concentración de los cationes. De esta forma, además de medir la agregación de liposomas, también se pudo obtener información de la evolución de los agregados en cada caso.

Nuevamente, el contenido del trabajo se estructura en dos partes, una parte experimental que se acaba de detallar y otra parte de simulación

65

de dinámica molecular realizada por el Dr. Faraudo similar a la realizada en el trabajo anterior.

3.2.4. Discusión Conjunta de los Resultados

En esta última parte de la sección 3.2 se discuten de manera conjunta los resultados obtenidos de los tres apartados anteriores (3.2.1, 3.2.2 y 3.2.3) que conforman la sección de sistemas aniónicos y cationes multivalentes.

En el caso de las medidas de μ_e de partículas de látex en función de la concentración de La^{3+}, se observó cómo la IC depende fundamentalmente de la σ_0 y de la concentración de electrolito (Fig. 3.5). En concreto, se observaron los siguientes resultados: *(i)* para la concentración de La^{3+} < 0.02 M el valor absoluto de la μ_e disminuye (en todos los casos) conforme La^{3+} aumenta, *(ii)* para la concentración de La^{3+} > 0.02 M, los látex de mayor densidad (L3 y L4) presentan una IC, mientras que la μ_e de los látex de menor densidad (L1 y L2) tiende a cero y no invierten su carga, *(iii)* el látex de mayor densidad de carga (L4) tiene un comportamiento similar al del látex L3, es decir, una vez alcanzada la IC la μ_e invertida parece alcanzar un valor de saturación. Estos resultados fueron confirmados por las simulaciones MC (ver gráfica 2 del artículo 2) donde el ψ_d calculado en cada caso tiene un comportamiento similar al de los valores de μ_e.

Así pues, los resultados experimentales y de simulación muestran

como el La^{3+} es capaz de invertir el signo de μ_e si la carga superficial del coloide es lo suficientemente alta ($\sigma_0 > 0.12$C m^{-2}).
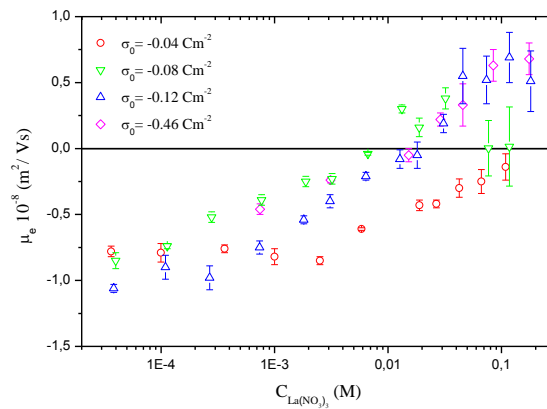
Fig. 3.5. Movilidad electroforética de partículas de látex con diferentes σ_0 en función de la concentración de La^{3+}.

En cuanto al estudio de la IC de liposomas de PS y PC, los experimentos de electroforesis mostraron cómo la μ_e de los liposomas de PS alcanza una inversión a bajas concentraciones de La^{3+} ($\approx 10^{-4}$ M) (Fig. 3.6). Es más, en el caso de liposomas de PC, se observa una clara inversión de la movilidad pese a ser un sistema eléctricamente neutro. Además, en el caso del PS, los resultados no se ven afectados por la presencia de sal monovalente añadida. Estos resultados muestran claras diferencias con los observados experimentalmente y por simulación para coloides modelo en presencia de mezclas de electrolito [113-114]. La cantidad de La^{3+} requerida para invertir el signo de la movilidad de partículas de látex aniónicas es de dos órdenes de magnitud superior al observado para el caso de los liposomas (3.5x10^{-6} M). Además, este proceso de inversión resulta ser

muy dependiente de la presencia de sal monovalente añadida y de la densidad de carga de las partículas.
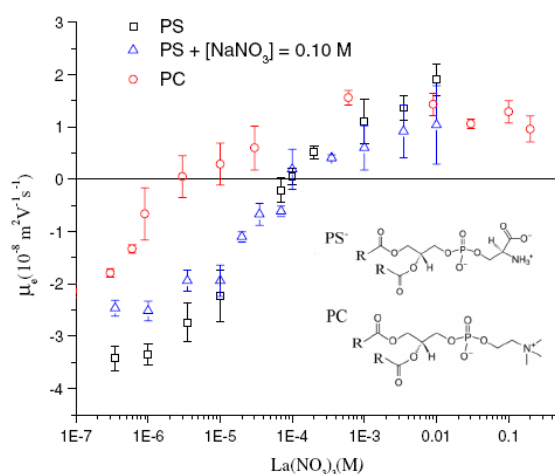
Fig. 3.6. Movilidad electroforética de liposomas de PS (en ausencia y presencia de Na^+) y de liposomas de PC, en función de la concentración de La^{3+}.

Estas diferencias entre los experimentos de electroforesis con partículas de látex y liposomas ponen de manifiesto que en este último caso, la IC no puede ser explicada en términos de las correlaciones iónicas. Con objeto de profundizar en las causas de la IC en el caso de las partículas blandas, los resultados de simulación de DM demostraron que a diferencia del Na^+, los iones de La^{3+} tienen la capacidad de penetrar en la región hidrófila de membranas de los lípidos de PS y de PC. En el artículo 3 se muestran diferentes figuras en donde se muestra la distribución de iones de La^{3+} en relación al centro de la membrana lipídica. Además, las simulaciones nos permitieron constatar la deshidratación parcial que experimentan estos

cationes al ser absorbidos por la membrana así como el cálculo de la energía libre de interacción lípido−ion en cada caso (Tabla 3.2). Como se puede ver en la tabla, la energía de interacción de PS/La^{3+} es mayor que la de PS/Na$^+$. Sin embargo, es considerablemente menor que en el caso de PC/La^{3+}, lo cual es consistente con los resultados de electroforesis.

Tabla 3.2. Energías libre de interacción de los sistemas estudiados

Sistema	Energía aproximada ($k_B T$)
PS/La^{3+}	−9
[‡]PC/La^{3+}	−12
[‡]PC/Ca^{2+}	−6.5
[*]PS/Na$^+$	−3.5

[*]Referencias 27 y 33, y [‡]referencia 34 del artículo 3 del capítulo 5, sección 5.3.

En resumen, la interacción de iones trivalentes con liposomas es muy diferente a la observada para el caso de sistemas coloidales modelo. En consecuencia, los mecanismos tradicionales de IC basados en correlaciones entre iones no pueden explicar lo observado con liposomas. Por tanto, las simulaciones atomísticas nos permiten proponer un nuevo mecanismo de IC para materia blanda basado en la absorción de iones multivalentes por la membrana fosfolipídica.

Recordando que nuestro objetivo principal es la caracterización de los lipoplejos aniónicos, el La^{3+}, por su capacidad de invertir la carga de los liposomas aniónicos, aparecía como un candidato idóneo para ser usado como puente entre los liposomas y el ADN. Sin embargo, como ya se ha explica con anterioridad, cuando se añade ADN a una

suspensión de PS y La^{3+}, la disolución gelifica. Así pues, se optó por usar cationes divalentes y por ello, se procedió a la caracterización de la interacción lípido–ion como paso previo a la adición del ADN. En concreto se escogieron los cationes de Ca^{2+} y Mg^{2+} los cuales intervienen en la fusión y agregación de lípidos de carga negativa con la membrana biológica [115-116]. Dichas funciones parecen estar relacionadas con la capacidad que tienen los cationes de enlazar a las cabezas polares de los lípidos y formar complejos deshidratados. Estudios recientes [110-112] han mostrado un efecto más pronunciado de las interacciones y agregaciones del Ca^{2+} y el Mg^{2+} con los liposomas de PS, en los que la estructura de los agregados depende del catión utilizado; agregados de PS/Ca^{2+} forman estructuras ramificadas mientras que agregados de PS/Mg^{2+} forman grandes muchos más densos.

Con objeto de ahondar más en este aspecto, se procedió a los experimentos de electroforesis y estabilidad coloidal (Fig. 3.7). Según los primeros, el valor absoluto de μ_e decrece de manera similar con la concentración de Ca^{2+} y Mg^{2+} observando en ambos casos una muy débil inversión de movilidad (Fig. 3.7A).
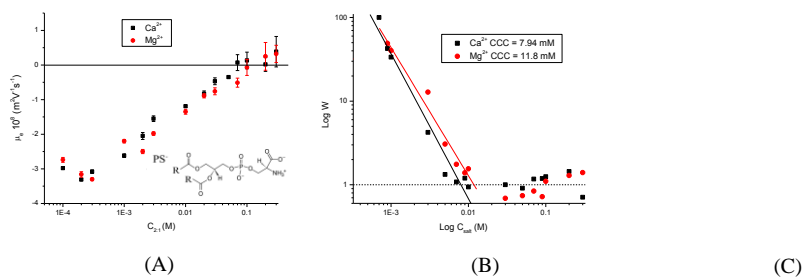

(A)   (B)   (C)

Fig. 3.7. (A) Movilidad electroforética, (B) estabilidad y (C) absorbancia de los liposomas de PS en función de Ca^{2+} y Mg^{2+}.

70

Las medidas de estabilidad de los liposomas (Fig. 3.7B) resultaron también ser muy similares para ambos iones. Las concentraciones de coagulación crítica (*CCC*) fueron de 0.008 M para el Ca^{2+} y de 0.01 M para el Mg^{2+}. Es decir, se requiere de una ligera concentración mayor de Mg^{2+} para inducir la agregación rápida de los liposomas. Finalmente, con el propósito de extender el análisis experimental sobre la afinidad de los cationes sobre los liposomas, se hicieron las medidas de turbidez (Fig. 3.7C). En ambos casos, el comportamiento general es el mismo, es decir, *A* aumenta con el incremento de la concentración de cationes. Sin embargo el valor de saturación de *A* alcanza un valor significativamente mayor con el Ca^{2+} que con el Mg^{2+}. Por tanto, con excepción de este último resultado, todos los resultados experimentales obtenidos ponen en evidencia que el comportamiento del PS con los cationes de Ca^{2+} y Mg^{2+} es muy similar. Sin embargo, en estudios previos se ha observado que ambos cationes provocan diferentes estructuras de agregación de los liposomas. Para explicar esta aparente contradicción, se hicieron simulaciones de DM similares a la realizada en el caso del La^{3+}. A partir de éstas, se pudieron construir diagramas de distribución iónica en relación a una membrana de PS (ver figura 4 del artículo 4). De acuerdo con estos perfiles de distribución, se observó que ambos cationes tienen una tendencia similar a ser absorbidos por la membrana. Además, se calcularon las áreas por lípido en la bicapa de PS cuando interacciona con los cationes (Tabla 3.3) obteniendo áreas similares para el Ca^{2+} y el Mg^{2+}.

Tabla 3.3. Áreas por lípido de PS alcanzadas cuando interacciona con diferentes cationes multivalentes.

Sistema	Área por lípido ($\mathring{A}^2$)
PS/La^{3+}	55.41
PS/Ca^{2+}	55.55 ± 0.01
PS/Mg^{2+}	55.30 ± 0.01
*PS/Na$^+$	53.75 ± 0.10

*Pandit, S.A. and Berkowitz, M.L. *Biophys. J.* 82, (2002) 1818-1827.

Sin embargo, las simulaciones muestran claras diferencias en cuanto a la posición que el Ca^{2+} y del Mg^{2+} tienden a adoptar en la región hidrofílica de los lípidos. La organización más probable de los cationes de Ca^{2+} dentro de la región hidrofílica de lípidos corresponde a dos átomos de oxígeno del grupo fosfato de los lípidos y dos del carboxilo (ver estructura química del lípido PS del apéndice A y Fig. 6B del artículo 4). Por el contrario, en el caso del Mg^{2+} se aprecian dos formas probables en las que se organiza el catión dentro de la región hidrofílica de los lípidos, involucrando a dos átomos de oxígeno, perteneciente ya sea al grupo fosfato o carboxilo de dos lípidos distintos. Cuando el modo de enlace del Mg^{2+} en los lípidos involucra a dos átomos de oxígeno del grupo fosfato, implica una profunda penetración del Mg^{2+} dentro de la bicapa de lípidos, mientras que si el enlace involucra a dos átomos de oxígeno del grupo carboxilo, implica una localización de los cationes más superficial en la bicapa.

Así pues, estos resultados moleculares podrían explicar las diferencias observadas en las estructuras de los agregados de liposomas de PS

según el catión que induzca la agregación. Además, nuestros resultados concuerdan con los observados en la literatura según la cual estas diferencias sugerían la posibilidad de diferentes modos de enlace de los cationes con el PS, es decir, diferentes sitios en los que se enlazan el Ca^{2+} y el Mg^{2+} en la bicapa de los liposomas de PS. Aunque ambos cationes penetran profundamente en la bicapa de PS [117], el Ca^{2+} enlaza al grupo carboxilo de la PS induciendo al lípido una geometría *trans*[7], mientras que el Mg^{2+} una geometría *cis*[7] [118]. En resumen, todas las evidencias anteriores muestran que el Ca^{2+} y el Mg^{2+} tienen diferentes afinidades por el lípido de PS, induciendo a diferentes morfologías.

3.3. Liposomas Aniónicos, Cationes Divalentes y ADN

Una vez analizada la interacción de coloides modelo y liposomas aniónicos con cationes multivalentes, en esta sección vamos a presentar los resultados de caracterización de lipoplejos aniónicos.

Como ya se comentado anteriormente, los lipoplejos aniónicos suponen en la actualidad una alternativa a los lipoplejos catiónicos, como portadores de genes en el proceso de transfección. Esto se debe principalmente a que presentan menos toxicidad [71, 73] y porque los componentes con los que están formados son reconocidos fácilmente por el organismo por tratarse de componentes naturales de las

_____

[7]*Cis–Trans* son dos estructuras distintas que presentan las moléculas isómeras, las cuales poseen la misma fórmula molecular (fórmula química).

membranas biológicas. Sin embargo, el número de estudios de lipoplejos aniónicos es muy escaso en comparación con el número de trabajos sobre lipoplejos catiónicos. Este hecho se explica en gran medida por la dificultad que conlleva la formación de complejos entre lípidos aniónicos y el ADN, la cual requiere de la mediación de cationes multivalentes que actúen de puente.

Como consecuencia, además de los estudios de liposomas aniónicos y su interacción con ADN en presencia de iones divalentes, se ha incluido un trabajo de caracterización interfacial de monocapas de lípidos en la interfase aire/disolución acuosa. De esta forma, se ha podido estudiar los cambios conformacionales de monocapas compuestas por mezclas de lípidos aniónicos/zwiteriónicos (DOPS/DOPC) según la presencia de ADN y/o calcio en la fase acuosa. Cabe señalar que este tipo de estudios que combinan liposomas y monocapas con este tipo de lípidos constituyen una importante novedad del trabajo realizado en esta tesis doctoral ya que no se han encontrado previamente en la bibliografía. A continuación se describen las técnicas experimentales utilizadas.

3.3.1. Sistemas Experimentales

Una vez más, la técnica que se utilizó para caracterizar el comportamiento electrocinético de los liposomas aniónicos en ausencia y presencia de Ca^{2+} y/o ADN fue la electroforesis. Por otro lado, la caracterización interfacial se realizó con la balanza de Langmuir. Con esta última técnica se analizó la morfología superficial

de las monocapas de lípidos en ausencia y presencia de Ca^{2+} y/o ADN, en la fase acuosa. De esta forma, se pretende evaluar los posibles cambios debido a la presencia de Ca, ADN y evaluar las interacciones moleculares que gobiernan la formación de complejos. Los lípidos, por su carácter anfifílico, tienden a situarse en la interfaz aire/agua, de modo que al dispersarlos sobre la superficie de la balanza se quedan en la misma. A continuación mediante la compresión controlada de esta superficie por las barreras de la de la balanza se obtiene información estructural acerca de las interacciones intermoleculares que tienen lugar en la superficie. Al disminuir el área superficial, disminuye la tensión superficial y aumenta la presión superficial ($\pi = \gamma_0 - \gamma$), siendo γ_0 la tensión superficie la de la subfase acuosa, e igual a la tensión del sistema antes de comenzar la compresión, y γ la tensión superficial de la superficie recubierta con lípidos. Conforme disminuye el área superficial de la balanza, disminuye el área molecular (A), aumentando así la presión superficial (π). A partir de esta compresión se obtiene una relación estructural entre la presión superficial y el área molecular que contiene información estructural de la monocapa: estados de compresión, transiciones de fase ye interacciones intermoleculares (la isoterma π–A). A partir de esta se puede calcular la elasticidad de Gibbs (ε) (a la que nos referiremos simplemente como elasticidad):

$$\varepsilon = -A(d\pi/dA) \qquad (3.2)$$

La variación de la elasticidad de la monocapa con el estado de

compresión se evalúa mediante la gráfica $\varepsilon-\pi$, y a través de esta representación se puede tener conocimiento acerca de rigidez de la monocapa, del estado de compresión y de las transiciones de fase, propiedades que juegan un papel muy importante en las propiedades mecánicas de la membrana. La otra técnica interfacial utilizada fue la *espectroscopía infrarroja de reflexión–absorción* (*IRRAS* – por sus siglas en inglés), que se realiza sobre monocapas obtenidas en la balanza de Langmuir. Con esta técnica se estudian las vibraciones moleculares de los lípidos en las monocapas, cuyas variaciones ofrecen información sobre la conformación, orientación y reorientación de las cadenas hidrocarbonadas de los lípidos. Con esta técnica se obtuvieron los espectros de (reflexión-absorción – número de onda) para dos presiones interfaciales determinadas, 5 y 30 mN/m. La reflexión–absorción se define como *–log(R/R$_0$)*, donde *R* es la reflectividad de la monocapa de lípidos y *R$_0$* es la reflectividad de superficie tamponada.

A continuación se discuten los resultados más sobresalientes obtenidos con las técnicas experimentales utilizadas.

3.3.2. Discusión de Resultados

En primer lugar se midieron las movilidades de los liposomas aniónicos y del ADN por separado, tanto en ausencia como en presencia de cationes de Ca^{2+}. En este estudio se usaron dos concentraciones de ADN: 0.0295 y 1.25 mg/ml. La presente discusión se centrará en la concentración más baja de ADN debido que las

conclusiones extraídas para las dos concentraciones son similares (ver Fig. 1B del artículo 5). La Fig. 3.8 muestra los resultados de electroforesis en los que se ve claramente que la tendencia observada del valor absoluto de la μ_e de los liposomas, ADN y mezclas de ambos, disminuye conforme aumenta la concentración de Ca^{2+}. Este comportamiento es el clásico apantallamiento de la carga coloidal, debida a la presencia de electrolito.
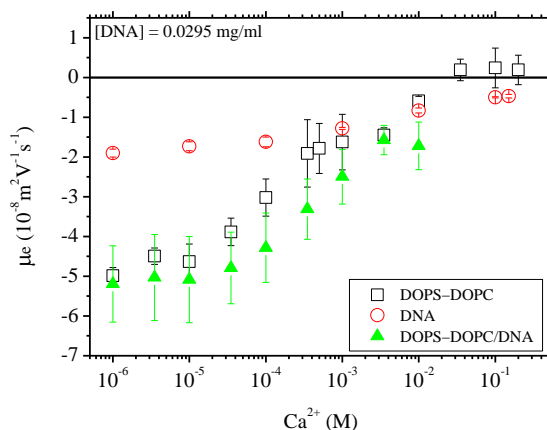
Fig. 3.8. μ_e de los liposomas en ausencia y presencia de ADN y μ_e del ADN solo, en función de la concentración de Ca^{2+} y para la concentración de ADN $= 0.0295$ mg/ml.

Sin embargo, si nos centramos en la curva de la μ_e de la mezcla de liposomas/Ca^{2+}/ADN, la gráfica muestra una movilidad (en valor absoluto) que en general es mayor que la de los liposomas y el ADN, por separado. Este hecho parece indicar que, en estas condiciones, la mezcla de liposomas y ADN podrían formar un complejo cuya carga neta, parece ser inferior a la de los liposomas y ADN por separado. De no ser así, es decir, si se estuviera en el caso de que los liposomas y el ADN no formaran complejos, el valor absoluto de la μ_e obtenida por

electroforesis debería ser un valor promedio de las movilidades de los liposomas y el ADN.

Por otro lado, se obtuvieron resultados muy interesantes al estudiar las interacciones interfaciales de los lípidos y el ADN. De las monocapas de Langmuir, al igual que la μ_e, se estudiaron las isotermas (π–A) y la elasticidad (ε) de la mezcla de lípidos DOPS/DOPC en ausencia y presencia de Ca^{2+} y/o ADN. Para ello, se eligieron dos concentraciones extremas de Ca^{2+} (10^{-4} y 10^{-2} M) de acuerdo con otros estudios en la bibliografía sobre lipoplejos aniónicos, que también sugieren este intervalo de concentraciones de iones [12]. En esta sección, nos centraremos en los resultados obtenidos para la concentración de Ca^{2+} más alta debido que en esta concentración los lipoplejos presentan mayor actividad. Se insta al lector a consultar el artículo 5 para un análisis completo. La Fig. 3.9 muestra las isotermas (Fig. 3.9A) y la elasticidad (Fig. 3.9B) de las monocapas de lípidos. En las isotermas se observa claramente una interacción nula entre los lípidos y el ADN en ausencia de Ca^{2+} es decir, las isotermas no se ven afectadas por la presencia de ADN en la fase acuosa. Este resultado está de acuerdo con otros trabajos encontrados en la bibliografía con sistemas similares [15]. La isoterma de lípidos en presencia de Ca^{2+} aparece desplazada hacia valores ligeramente superiores del área molecular. Es decir, la monocapa se encuentra ligeramente más extendida que en ausencia de Ca^{2+}. Esto podría ser debido a la formación de un complejo lípido/Ca^{2+}, como ocurre con el complejo PS/La^{3+} del apartado 3.2.2. No obstante, los resultados más llamativos son los de la isoterma del sistema lípidos/Ca^{2+}/ADN, que aparece

claramente desplazada áreas mayores. La monocapa se encuentra pues en un estado más expandido. Es decir, los lípidos presentan áreas moleculares mayores en presencia de Ca^{2+}/ADN (ver tabla 1 del artículo 5). Este incremento del área molecular del lípido puede ser provocado por la fuerte interacción que tiene lugar entre el grupo fosfato de los lípidos y del ADN mediada por el Ca^{2+}.
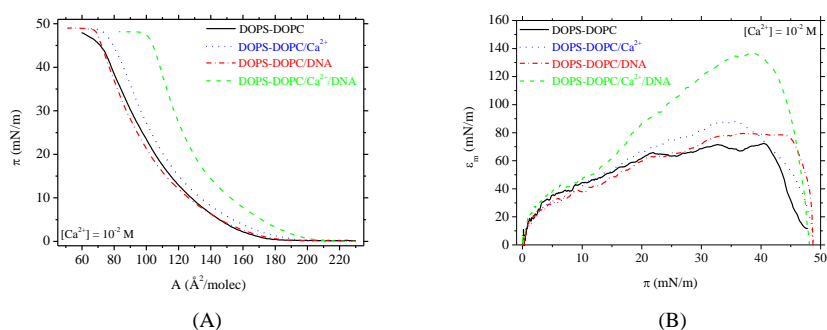
Fig. 3.9. Isotermas de compresión (A) y elasticidad (B) de las monocapas de Langmuir para la concentración de $Ca^{2+} = 10^{-2}$ M.

Los resultados de elasticidad muestran dos características generales: en principio, todas las curvas incrementan su valor conforme π aumenta. Este incremento se produce de manera muy pronunciada alcanzándose un valor de elasticidad de 20 mN/m para π cercanas a cero, como se observa en la Fig. 3.9B. La elasticidad sigue aumentando al aumentar la π, es decir, al aumentar la densidad superficial de lípidos hasta alcanzar un valor máximo en todos los casos. La monocapa de lípidos/Ca^{2+}, muestra un valor máximo de ε (ε_{max}) que es ligeramente mayor que la ε_{max} obtenida para los lípidos puros (tabla 3.4). Este hecho parece de nuevo apuntar a una fuerte interacción del Ca^{2+} con los lípidos, como ya se comprobó en el

artículo 4. El valor máximo de ε proporciona una idea de la rigidez de la monocapa. Nuevamente, los resultados más interesantes son para el sistema lípidos/Ca^{2+}/ADN en el que hay un incremento muy notable de la ε_{max} de las monocapas, comparadas con aquellas de los componentes por separado (ver Tabla 3.4). Esta característica sugiere que el ADN interacciona con los lípidos solo si el Ca^{2+} está presente. Estos resultados por tanto concuerdan con los obtenidos con las isotermas y la movilidad y demuestran el papel del Ca^{2+} como mediador de la interacción entre lípidos y ADN a nivel molecular.

Tabla 3.4. Valores de ε_{max} de las isotermas estudiadas en la Fig. 3.9.

Isoterma	ε_{max} (mN/m)
DOPS–DOPC	72 ± 4
DOPS–DOPC/$Ca^{2+}(10^{-4}M)$	90 ± 1
DOPS–DOPC/$Ca^{2+}(10^{-2}M)$	88 ± 4
DOPS–DOPC/ADN	79 ± 4
DOPS–DOPC/$Ca^{2+}(10^{-4}M)$/ADN	127 ± 3
DOPS–DOPC/$Ca^{2+}(10^{-2}M)$/ADN	137 ± 1

Un aspecto destacable en los resultados de elasticidad de todas las monocapas, es que la variación de ε con π es muy similar para todos los sistemas a baja densidad superficial (hasta un valor característico de 5 mN/m). A partir de este valor, solamente el sistema lípidos/Ca^{2+}/ADN, muestra un aumento considerable con respecto a los otros dos. Esto sugiere que la interacción del ADN con los lípidos no solo se debe a la presencia del Ca^{2+} sino que requiere de un mínimo recubrimiento superficial para mediar en la interacción entre lípidos y

ADN.

Por otra parte, en los espectros de IRRA se observan en general, diferencias de los distintos espectros, en la expansión de las bandas de los grupos fosfatos de los lípidos. La Fig. 3.10 muestra los espectros de IRRA de las monocapas de lípidos en ausencia y presencia de Ca^{2+} y/o ADN para una presión de 30 mN/m. De acuerdo con los resultados de ε discutidos previamente, el efecto del Ca^{2+} es solo apreciable a alto recubrimiento superficial. Las bandas de los grupos fosfatos de los lípidos presentan dos características importantes, una banda asimétrica de expansión ($v_{as}(PO_2^-)$), asociada a una vibración asimétrica de los átomos de oxigeno libres del grupo fosfato, y otra banda simétrica ($v(PO_2^-)$), asociada a una vibración simétrica de los átomos de oxigeno.
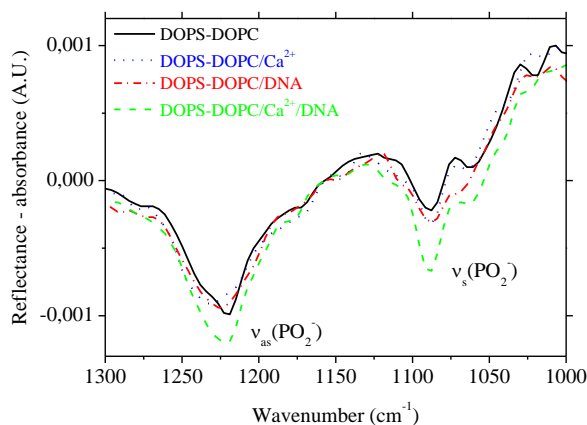

Fig. 3.10. Espectros de IRRA de las monocapas de lípidos en ausencia y presencia de Ca^{2+} y/o ADN para una presión de 30 mN/m.

La intensidad de las bandas $v_{as}(PO_2^-)$ y $v(PO_2^-)$ de los sistemas

lípidos/Ca^{2+} y lípidos/ ADN es prácticamente similar a la banda de los lípidos puros. La banda $v_{as}(PO_2^-)$ que contiene Ca^{2+} presenta un ligero desplazamiento a un número de onda más grande, indicando una deshidratación del grupo fosfato debido a su interacción con el Ca^{2+}. Las bandas $v_{as}(PO_2^-)$ y $v(PO_2^-)$ pertenecientes a la monocapa del sistema lípidos/Ca^{2+}/ADN mostraron un incremento en la intensidad, presentando una clara distinción de las bandas de las monocapas de los sistemas lípidos/Ca^{2+} y lípidos/ADN. Este incremento podría estar pues asociado con la interacción del ADN con los lípidos de la monocapa.

En resumen, todos los resultados presentados en este último trabajo proporcionan evidencias sobre la formación de complejos lípidos−ADN, sólo cuando el Ca^{2+} está presente. Por tanto, el sistema DOPS/DOPC podría suponer un sistema modelo de lipoplejos aniónico cuando interacciona con ADN en presencia de cationes divalentes de Ca^{2+}.

CAPÍTULO 4

CONCLUSIONES Y PERSPECTIVAS

A continuación se enumeran las conclusiones de los resultados más relevantes obtenidos de los distintos trabajos, en acuerdo con los objetivos planteados:

1. La caracterización fisicoquímica tanto experimental como teórica de liposomas catiónicos y ADN demuestra que **los liposomas de DODAB/DOPE y DODAB/DLPC forman complejos con el ADN de timo de ternera**, dando lugar a lipoplejos catiónicos. Este proceso está eléctricamente dirigido de forma que a partir de las medidas de movilidad electroforética, conductancia e intercalación de fluorescencia, se pudo determinar el punto de isoneutralidad de los lipoplejos, el cual es una característica importante en el proceso de transfección. Además, se aplicó un modelo teórico de interacción entre polielectrolitos y coloides de signo opuesto por primera vez a este tipo de sistemas. A partir del modelo, se realizó un diagrama de fases de los lipoplejos resultantes en concordancia con las micrografías de crio−microscopía. A partir de estas imágenes, se obtuvo además, información sobre el tamaño y morfología de los liposomas y lipoplejos.

2. A partir de los estudios experimentales y de simulación aplicados a

sistemas aniónicos en interacción con cationes multivalentes, se concluyó que:

✓ La inversión de carga (IC) de coloides aniónicos inducida por cationes multivalentes, es muy diferente según se trate de coloides modelo como las partículas de látex o sistemas blandos como los liposomas. Mientras un mecanismo basado en la correlación ion-ion es capaz de explicar la IC de los primeros, éste no es suficiente para justificar la IC observada en liposomas aniónicos por cationes trivalentes. En el caso de liposomas de PS y cationes de lantano, la IC se alcanza a bajas concentraciones de La^{3+} y es completamente indiferente a la presencia de iones monovalentes en la disolución. A partir de simulaciones de DM, se propuso como mecanismo de IC de estos sistemas, la penetración de los contraiones multivalentes en la región hidrófila de la membrana de lípidos.

✓ Las medidas electrocinéticas y de estabilidad coloidal probaron que los liposomas de PS interaccionan de la misma manera con cationes divalentes de Ca^{2+} y de Mg^{2+}. No obstante, las medidas de turbidez y la estructura de los agregados de PS inducida por estos cationes mostraron claras diferencias según el ion. Nuevamente, las simulaciones de DM mostraron que ambos cationes penetran en la región hidrófila de la membrana de lípidos. Sin embargo, la posición ocupada por cada catión así como su orientación, es diferente. Por un lado, el Ca^{2+} tiende a asociarse a dos átomos de oxígeno del grupo fosfato del lípido y a dos del carboxilo. Por otro lado, la organización del Mg^{2+} surgen dos formas posibles en la que

se organiza dentro de la región hidrófila involucrando a dos átomos de oxígeno: *(i)* cuando los oxígenos pertenecen al grupo fosfato, implica una profunda penetración del catión y *(ii)* cuando pertenecen al grupo carboxilo implica una localización más superficial de los cationes. Además, las propiedades de hidratación de los cationes absorbidos es también desigual según se trate de un catión o del otro.

3. Se ha caracterizado por primera vez el sistema formado por los **lípidos DOPS/DOPC, cationes divalentes de Ca^{2+} y ADN de timo de ternera**. Según nuestro conocimiento, este tipo de mezcla no ha sido estudiado previamente en la bibliografía. De acuerdo con las medidas experimentales realizadas tanto con liposomas (electroforesis) como con monocapas de lípidos (isotermas, elasticidad y espectros de IRRA), el ADN tiende a interaccionar con los lípidos de DOPS/DOPC sólo en presencia de Ca^{2+}.

Finalmente, las **perspectivas** planteadas de este trabajo de investigación se refieren principalmente al estudio de los lipoplejos aniónicos, en los cuales se ha puesto un gran interés. Se plantea utilizar diversas técnicas experimentales que nos permitan obtener imágenes estructurales y morfológicas de los lipoplejos. Por ejemplo, algunas de estas técnicas son la microscopía electrónica de crio–fractura, la microscopía electrónica de transmisión, la microscopía láser confocal y la microscopía de fuerza atómica.

Además, se plantea extender el estudio de lipoplejos aniónicos a

sistemas donde varíe tanto el catión que actúa de puente entre los lípidos y el ADN, como los propios lípidos así como el tipo de ADN. En concreto, la finalidad última será el estudio de lipoplejos aniónicos con un ADN de tipo plásmido, que es el que se usa principalmente en terapia génica.

CONCLUSIONS AND PERSPECTIVES

The main conclusions of the most relevant results obtained from the different studies are detailed next.

1. The physicochemical characterization of both experimental and theoretical cationic liposomes and DNA demonstrated that **liposomes of DODAB/DOPE and DODAB/DLPC form complexes with calf thymus DNA**, resulting in cationic lipoplexes. This process is electrically conducted so that from electrophoretic mobility measurements, conductance and fluorescence intercalation, we determined the point of isoneutrality of lipoplexes, which is an important feature in the transfection process. Additionally, we applied a theoretical model of interaction between polyelectrolytes and colloids of opposite sign for the first time in this type of systems. From the model, we constructed a phase diagram of the resulting lipoplexes in accordance with the micrographs of cryo−microscopy. From these images, we also obtained further information of the size and morphology of the liposomes and lipoplexes.

2. From the experimental and simulation studies applied to **anionic systems in interaction with multivalent cations**, it was concluded that:

✓ The charge reversal (CR) of anionic colloids induced by multivalent cations, varies widely from model colloids, such as

latex particles to soft systems, such as liposomes. Although a mechanism based on ion−ion correlation is able to explain the CR of the former system, this is not sufficient to justify the CR observed in anionic liposomes by trivalent cations. In the case of PS liposomes and lanthanum cations, the CR is reached at lower concentrations of La^{3+} and is completely indifferent to the presence of monovalent ions in the solution. Based on DM simulations, we proposed as CR mechanism of these systems, the penetration of multivalent counterions into the hydrophilic region of membrane lipids.

✓ The electrokinetic measurements and colloidal stability proved that PS liposomes interact in the same manner with divalent cations of Ca^{2+} and Mg^{2+}. However, turbidity measurements and the aggregate structure of PS induced by these cations showed clear differences depending on the ion. MD simulations again showed that both cations penetrate into the hydrophilic region of membrane lipids. However, the position occupied by each cation and its orientation is different. On one hand, the Ca^{2+} is associated to two oxygen atoms of the lipid phosphate group and two carboxyl. On the other hand, the organization of Mg^{2+} takes place in two possible ways depending on the localization of the oxygen atoms: *(i)* when the phosphate oxygens belong to the group this implies a deep penetration of the cation and *(ii)* when they belong to the carboxyl group it implies a more superficial location of the cations. Furthermore, the hydration properties of the cations absorbed is also uneven depending on whether a cation or another.

3. It has been characterized for the first time that the system formed by **lipids DOPS/DOPC, divalent cations Ca^{2+} and calf thymus DNA**. To our knowledge, this type of mixture has not been studied previously in the literature. According to experimental measurements performed either with liposomes (electrophoresis) and with lipid monolayers (π-A isotherms, elasticity and IRRA spectra), the DNA tends to interact with DOPS/DOPC lipids only in the presence of Ca^{2+}.

Finally, the **perspectives** arising from this research relate mainly to the study of anionic lipoplexes, where there has been great interest in the literature. We propose to use various experimental techniques that allow us to obtain structural and morphological information of lipoplexes. For example, some of these techniques are the cryo−fracture electron microscopy, transmission electron microscopy, confocal laser microscopy and atomic force microscopy.

In addition, we propose to extend the study of anionic lipoplexes to various systems where both the cation that acts as a bridge between lipids and DNA, the lipids themselves and the type of DNA are changed. Specifically, the ultimate goal is the study of anionic lipoplexes with a plasmid DNA type, which is mainly used in gene therapy.

REFERENCIAS

1. Lasic, D.D., *Liposomes in Gene Delivery*. 1997, Boca Raton. FL.: CRC Press.
2. Gao, X., et al., *Nonviral gene delivery: what we know and what is next.* AAPS J, **2007**. 9(1): p. E92-104.
3. Crooke, S.T., *An overview of progress in antisense therapeutics.* Antisense Nucleic Acid Drug Dev, **1998**. 8(2): p. 115-122.
4. Anthony J. F. Griffiths, et al., *Genética Moderna*, ed. M.G. Hill. 2000, Madrid.
5. Uherek, C., et al., *DNA-carrier proteins for targeted gene delivery.* Adv Drug Deliv Rev, **2000**. 44(2-3): p. 153-166.
6. Selkirk, S.M., *Gene therapy in clinical medicine.* Postgrad Med J, **2004**. 80(948): p. 560-570.
7. Crooke, S.T., *Molecular mechanisms of action of antisense drugs.* Biochim Biophys Acta, **1999**. 1489(1): p. 31-44.
8. Stull, R.A., et al., *Antigene, ribozyme and aptamer nucleic acid drugs: progress and prospects.* Pharm Res, **1995**. 12(4): p. 465-483.
9. Bonincontro, A., et al., *A biophysical investigation on the binding and controlled DNA release in a cetyltrimethylammonium bromide-sodium octyl sulfate cat-anionic vesicle system.* Biomacromolecules, **2007**. 8(6): p. 1824-1829.
10. Rodriguez-Pulido, A., et al., *Compaction process of calf thymus DNA by mixed cationic-zwitterionic liposomes: a physicochemical study.* J Phys Chem B, **2008**. 112(7): p. 2187-2197.
11. Castano, S., et al., *Asymmetric lipid bilayer formation stabilized by DNA at the air/water interface.* Biochimie, **2009**. 91(6): p. 765-773.
12. Liang, H., et al., *Polymorphism of DNA-anionic liposome complexes reveals hierarchy of ion-mediated interactions.* Proc Natl Acad Sci U S A, **2005**. 102(32): p. 11173-11178.
13. Frantescu, A., et al., *Interfacial ternary complex DNA/Ca/lipids at anionic vesicle surfaces.* Bioelectrochemistry, **2006**. 68(2): p. 158-170.
14. Frantescu, A., et al., *Adsorption of DNA and electric fields decrease the rigidity of lipid vesicle membranes.* Physical Chemistry Chemical Physics, **2005**. 7(24): p. 4126-4131.
15. Gromelski, S., et al., *Adsorption of DNA to zwitterionic DMPE monolayers mediated by magnesium ions.* Physical Chemistry Chemical Physics, **2004**. 6(24): p. 5551-5556.
16. Gromelski, S., et al., *DNA condensation and interaction with zwitterionic phospholipids mediated by divalent cations.* Langmuir, **2006**. 22(14): p. 6293-6301.
17. McAllister, D.V., et al., *Microfabricated microneedles for gene and drug delivery.* Annu Rev Biomed Eng, **2000**. 2: p. 289-313.
18. Gan, W.B., et al., *Multicolor "DiOlistic" labeling of the nervous system using lipophilic dye combinations.* Neuron, **2000**. 27(2): p. 219-225.

19. Regnier, V., et al., *Electroporation-mediated delivery of 3'-protected phosphodiester oligodeoxynucleotides to the skin.* J Control Release, **2000**. 67(2-3): p. 337-346.

20. Luo, D., et al., *Synthetic DNA delivery systems.* Nat Biotechnol, **2000**. 18(1): p. 33-37.

21. Lederberg, J., *Molecular biology, eugenics and euphenics.* Nature, **1963**. 198: p. 428-429.

22. Rosenberg, S.A., et al., *Gene transfer into humans--immunotherapy of patients with advanced melanoma, using tumor-infiltrating lymphocytes modified by retroviral gene transduction.* N Engl J Med, **1990**. 323(9): p. 570-578.

23. Walther, W., et al., *Viral vectors for gene transfer: a review of their use in the treatment of human diseases.* Drugs, **2000**. 60(2): p. 249-271.

24. McLachlin, J.R., et al., *Factors affecting retroviral vector function and structural integrity.* Virology, **1993**. 195(1): p. 1-5.

25. Khalighinejad, N., et al., *Adenoviral gene therapy in gastric cancer: a review.* World J Gastroenterol, **2008**. 14(2): p. 180-184.

26. Young, L.S., et al., *The promise and potential hazards of adenovirus gene therapy.* Gut, **2001**. 48(5): p. 733-736.

27. Wei, C.M., et al., *Construction and isolation of a transmissible retrovirus containing the src gene of Harvey murine sarcoma virus and the thymidine kinase gene of herpes simplex virus type 1.* J Virol, **1981**. 39(3): p. 935-944.

28. Quantin, B., et al., *Adenovirus as an expression vector in muscle cells in vivo.* Proc Natl Acad Sci U S A, **1992**. 89(7): p. 2581-2584.

29. Garton, K.J., et al., *Efficient expression of exogenous genes in primary vascular cells using IRES-based retroviral vectors.* Biotechniques, **2002**. 32(4): p. 830, 832, 834 passim.

30. Chamberlain, J.S., *Gene therapy of muscular dystrophy.* Hum Mol Genet, **2002**. 11(20): p. 2355-2362.

31. Martin, K.R., et al., *Gene delivery to the eye using adeno-associated viral vectors.* Methods, **2002**. 28(2): p. 267-275.

32. http://www.abedia.com/wiley/vectors.php.

33. Kay, M.A., et al., *Viral vectors for gene therapy: the art of turning infectious agents into vehicles of therapeutics.* Nat Med, **2001**. 7(1): p. 33-40.

34. Behr, J.P., *Synthetic Gene-Transfer Vectors.* Accounts of Chemical Research, **1993**. 26(5): p. 274-278.

35. Merdan, T., et al., *Prospects for cationic polymers in gene and oligonucleotide therapy against cancer.* Adv Drug Deliv Rev, **2002**. 54(5): p. 715-758.

36. Pedroso de Lima, M.C., et al., *Cationic lipid-DNA complexes in gene delivery: from biophysics to biological applications.* Adv Drug Deliv Rev, **2001**. 47(2-3): p. 277-294.

37. Lollo, C.P., et al., *Poly-L-lysine-based gene delivery systems. Synthesis, purification, and application.* Methods Mol Med, **2002**. 69: p. 1-13.

38. Lemkine, G.F., et al., *Polyethylenimines for in vivo gene delivery.* Curr Opin Mol Ther, **2001**. 3(2): p. 178-182.

39. Borchard, G., *Chitosans for gene delivery.* Adv Drug Deliv Rev, **2001**. 52(2): p. 145-150.

40.   Hughes, M.D., et al., *The cellular delivery of antisense oligonucleotides and ribozymes.* Drug Discov Today, **2001**. 6(6): p. 303-315.

41.   LeHoux, J.G., et al., *Some effects of chitosan on liver function in the rat.* Endocrinology, **1993**. 132(3): p. 1078-1084.

42.   Gregoriadis, G., et al., *Liposomes as carriers of enzymes or drugs: a new approach to the treatment of storage diseases.* Biochem J, **1971**. 124(5): p. 58P.

43.   Gregoriadis, G., *Liposomes in the therapy of lysosomal storage diseases.* Nature, **1978**. 275(5682): p. 695-696.

44.   Bangham, A.D., et al., *Negative Staining of Phospholipids and Their Structural Modification by Surface-Active Agents as Observed in the Electron Microscope.* J Mol Biol, **1964**. 8: p. 660-668.

45.   Lasic, D.D., *Novel applications of liposomes.* Trends Biotechnol, **1998**. 16(7): p. 307-321.

46.   Segota, S., et al., *Spontaneous formation of vesicles.* Adv Colloid Interface Sci, **2006**. 121(1-3): p. 51-75.

47.   Mastrobattista, E., et al., *Functional characterization of an endosome-disruptive peptide and its application in cytosolic delivery of immunoliposome-entrapped proteins.* J Biol Chem, **2002**. 277(30): p. 27135-27143.

48.   Immordino, M.L., et al., *Stealth liposomes: review of the basic science, rationale, and clinical applications, existing and potential.* Int J Nanomedicine, **2006**. 1(3): p. 297-315.

49.   Zucker, D., et al., *Liposome drugs' loading efficiency: a working model based on loading conditions and drug's physicochemical properties.* J Control Release, **2009**. 139(1): p. 73-80.

50.   Johnsson, M., et al., *Liposomes, disks, and spherical micelles: aggregate structure in mixtures of gel phase phosphatidylcholines and poly(ethylene glycol)-phospholipids.* Biophys J, **2003**. 85(6): p. 3839-3847.

51.   Kaneda, Y., *Virosomes: evolution of the liposome as a targeted drug delivery system.* Adv Drug Deliv Rev, **2000**. 43(2-3): p. 197-205.

52.   Ying, X., et al., *Dual-targeting daunorubicin liposomes improve the therapeutic efficacy of brain glioma in animals.* J Control Release, **2010**. 141(2): p. 183-192.

53.   Torchilin, V.P., *Tat peptide-mediated intracellular delivery of pharmaceutical nanocarriers.* Adv Drug Deliv Rev, **2008**. 60(4-5): p. 548-558.

54.   Shmeeda, H., et al., *Delivery of zoledronic acid encapsulated in folate-targeted liposome results in potent in vitro cytotoxic activity on tumor cells.* J Control Release, **2010**. 146(1): p. 76-83.

55.   Nishikawa, K., et al., *Scavenger receptor-mediated uptake and metabolism of lipid vesicles containing acidic phospholipids by mouse peritoneal macrophages.* J Biol Chem, **1990**. 265(9): p. 5226-5231.

56.   Felgner, P.L., et al., *Lipofection: a highly efficient, lipid-mediated DNA-transfection procedure.* Proc Natl Acad Sci U S A, **1987**. 84(21): p. 7413-7417.

57.   Safinya, C.R., *Structures of lipid-DNA complexes: supramolecular assembly and gene delivery.* Curr Opin Struct Biol, **2001**. 11(4): p. 440-448.

58. Vijayanathan, V., et al., *Formation of DNA nanoparticles in the presence of novel polyamine analogues: a laser light scattering and atomic force microscopic study.* Nucleic Acids Res, **2004**. 32(1): p. 127-134.

59. Rodriguez-Pulido, A., et al., *A theoretical and experimental approach to the compaction process of DNA by dioctadecyldimethylammonium bromide/zwitterionic mixed liposomes.* J Phys Chem B, **2009**. 113(47): p. 15648-15661.

60. de Lima, M.C.P., et al., *Cationic lipid-DNA complexes in gene delivery: from biophysics to biological applications.* Advanced Drug Delivery Reviews, **2001**. 47(2-3): p. 277-294.

61. Xu, Y.H., et al., *Physicochemical characterization and purification of cationic lipoplexes.* Biophysical Journal, **1999**. 77(1): p. 341-353.

62. Patil, S.D., et al., *Influence of divalent cations on the conformation of phosphorothioate oligodeoxynucleotides: a circular dichroism study.* Nucleic Acids Res, **2000**. 28(12): p. 2439-2445.

63. Agrawal, S., et al., *In vivo pharmacokinetics of phosphorothioate oligonucleotides containing contiguous guanosines.* Antisense Nucleic Acid Drug Dev, **1997**. 7(3): p. 245-249.

64. Sorgi, F.L., et al., *Protamine sulfate enhances lipid-mediated gene transfer.* Gene Ther, **1997**. 4(9): p. 961-968.

65. Li, S., et al., *In vivo gene transfer via intravenous administration of cationic lipid-protamine-DNA (LPD) complexes.* Gene Ther, **1997**. 4(9): p. 891-900.

66. Filion, M.C., et al., *Toxicity and immunomodulatory activity of liposomal vectors formulated with cationic lipids toward immune effector cells.* Biochim Biophys Acta, **1997**. 1329(2): p. 345-356.

67. Filion, M.C., et al., *Major limitations in the use of cationic liposomes for DNA delivery.* International Journal of Pharmaceutics, **1998**. 162(1-2): p. 159-170.

68. Lv, H., et al., *Toxicity of cationic lipids and cationic polymers in gene delivery.* J Control Release, **2006**. 114(1): p. 100-109.

69. Nguyen, L.T., et al., *Complex formation with plasmid DNA increases the cytotoxicity of cationic liposomes.* Biol Pharm Bull, **2007**. 30(4): p. 751-757.

70. Almofti, M.R., et al., *Cationic liposome-mediated gene delivery: biophysical study and mechanism of internalization.* Arch Biochem Biophys, **2003**. 410(2): p. 246-253.

71. Patil, S.D., et al., *Anionic liposomal delivery system for DNA transfection.* AAPS J, **2004**. 6(4): p. e29.

72. Lakkaraju, A., et al., *Neurons are protected from excitotoxic death by p53 antisense oligonucleotides delivered in anionic liposomes.* J Biol Chem, **2001**. 276(34): p. 32000-32007.

73. Khiati, S., et al., *Anionic nucleotide--lipids for in vitro DNA transfection.* Bioconjug Chem, **2009**. 20(9): p. 1765-1772.

74. Tarahovsky, Y.S., et al., *DNA release from lipoplexes by anionic lipids: correlation with lipid mesomorphism, interfacial curvature, and membrane fusion.* Biophys J, **2004**. 87(2): p. 1054-1064.

75. Patil, S.D., et al., *Conformation of oligodeoxynucleotides associated with anionic liposomes.* Nucleic Acids Res, **2000**. 28(21): p. 4125-4129.

76.   Fillion, P., et al., *Encapsulation of DNA in negatively charged liposomes and inhibition of bacterial gene expression with fluid liposome-encapsulated antisense oligonucleotides.* Biochim Biophys Acta, **2001**. 1515(1): p. 44-54.

77.   Gregoriadis, G., et al., *Entrapment of plasmid DNA vaccines into liposomes by dehydration/rehydration.* Methods Mol Med, **2000**. 29: p. 305-311.

78.   Patil, S.D., et al., *Biophysical characterization of anionic lipoplexes.* Biochim Biophys Acta, **2005**. 1711(1): p. 1-11.

79.   Carafoli, E., *Calcium signaling: a tale for all seasons.* Proc Natl Acad Sci U S A, **2002**. 99(3): p. 1115-1122.

80.   Neumann, E., et al., *Calcium-mediated DNA adsorption to yeast cells and kinetics of cell transformation by electroporation.* Biophys J, **1996**. 71(2): p. 868-877.

81.   Srinivasan, C., et al., *Optimization and characterization of anionic lipoplexes for gene delivery.* J Control Release, **2009**. 136(1): p. 62-70.

82.   Turek, J., et al., *Formulations which increase the size of lipoplexes prevent serum-associated inhibition of transfection.* J Gene Med, **2000**. 2(1): p. 32-40.

83.   Rodriguez-Pulido, A., et al., *A physicochemical characterization of the interaction between DC-Chol/DOPE cationic liposomes and DNA.* J Phys Chem B, **2008**. 112(39): p. 12555-12565.

84.   Lin, A.J., et al., *Three-dimensional imaging of lipid gene-carriers: membrane charge density controls universal transfection behavior in lamellar cationic liposome-DNA complexes.* Biophys J, **2003**. 84(5): p. 3307-3316.

85.   Barreleiro, P.C.A., et al., *Interaction of octaethylene glycol n-dodecyl monoether with dioctadecyldimethylammonium bromide and chloride vesicles.* Langmuir, **2002**. 18(4): p. 1024-1029.

86.   Martín-Molina, A., *Propiedades Electrocinéticas de Sistemas Coloidales Modelo: Efecto del Tamaño Iónico*, in *Departamento de Física Aplicada, Tesis Doctoral*. 2003, Universidad de Granada: Granada (Spain). p. 268.

87.   Yeung, T., et al., *Lipid signaling and the modulation of surface charge during phagocytosis.* Immunol Rev, **2007**. 219: p. 17-36.

88.   http://lipidlibrary.aocs.org/.

89.   Farhood, H., et al., *The role of dioleoyl phosphatidylethanolamine in cationic liposome mediated gene transfer.* Biochim Biophys Acta, **1995**. 1235(2): p. 289-295.

90.   Radler, J.O., et al., *Structure and interfacial aspects of self-assembled cationic lipid-DNA gene carrier complexes.* Langmuir, **1998**. 14(15): p. 4272-4283.

91.   Xu, Y., et al., *Physicochemical characterization and purification of cationic lipoplexes.* Biophys J, **1999**. 77(1): p. 341-353.

92.   Eastman, S.J., et al., *Biophysical characterization of cationic lipid: DNA complexes.* Biochim Biophys Acta, **1997**. 1325(1): p. 41-62.

93.   Gustafsson, J., et al., *Complexes between cationic liposomes and DNA visualized by cryo-TEM.* Biochim Biophys Acta, **1995**. 1235(2): p. 305-312.

94. Dias, R.S., et al., *Compaction and decompaction of DNA in the presence of catanionic amphiphile mixtures.* Journal of Physical Chemistry B, **2002**. 106(48): p. 12608-12612.

95. Martin-Molina, A., et al., *Effect of surface charge on colloidal charge reversal.* J Phys Chem B, **2009**. 113(19): p. 6834-6839.

96. Quesada-Perez, M., et al., *Electrophoretic mobility of model colloids and overcharging: theory and experiment.* Molecular Physics, **2002**. 100(18): p. 3029-3039.

97. Quesada-Perez, M., et al., *Overcharging in colloids: beyond the Poisson-Boltzmann approach.* Chemphyschem, **2003**. 4(3): p. 234-248.

98. Nguyen, T.T., et al., *Complexation of a polyelectrolyte with oppositely charged spherical macroions: Giant inversion of charge.* Journal of Chemical Physics, **2001**. 114(13): p. 5905-5916.

99. Nguyen, T.T., et al., *Complexation of DNA with positive spheres: Phase diagram of charge inversion and reentrant condensation.* Journal of Chemical Physics, **2001**. 115(15): p. 7298-7308.

100. Sennato, S., et al., *On the phase diagram of reentrant condensation in polyelectrolyte-liposome complexation.* J Chem Phys, **2004**. 121(10): p. 4936-4940.

101. Martin-Molina, A., et al., *Electrophoretic mobility and primitive models: Surface charge density effect.* Journal of Physical Chemistry B, **2002**. 106(27): p. 6881-6886.

102. Marcus, Y., *Ion Solvation.* 1985, Chichester (UK): John Wiley and Sons.

103. Israelachvili, J., *Intermolecular and Surface Forces*, ed. Second. 1992, London: Academic Press.

104. Grosberg, A.Y., et al., *Colloquium: The physics of charge inversion in chemical and biological systems.* Reviews of Modern Physics, **2002**. 74(2): p. 329-345.

105. Levin, Y., *Electrostatic correlations: from plasma to biology.* Reports on Progress in Physics, **2002**. 65(11): p. 1577-1632.

106. Besteman, K., et al., *Charge inversion accompanies DNA condensation by multivalent ions.* Nature Physics, **2007**. 3(9): p. 641-644.

107. Pandit, S.A., et al., *Molecular dynamics simulation of dipalmitoylphosphatidylserine bilayer with Na+ counterions.* Biophys J, **2002**. 82(4): p. 1818-1827.

108. Besteman, K., et al., *Influence of charged surfaces on the morphology of DNA condensed with multivalent ions.* Biopolymers, **2007**. 87(2-3): p. 141-148.

109. Vijayanathan, V., et al., *DNA condensation by polyamines: a laser light scattering study of structural effects.* Biochemistry, **2001**. 40(45): p. 13644-13651.

110. Roldan-Vargas, S., et al., *Aggregation of liposomes induced by calcium: a structural and kinetic study.* Phys Rev E Stat Nonlin Soft Matter Phys, **2007**. 75(2 Pt 1): p. 021912.

111. Roldan-Vargas, S., et al., *Growth of lipid vesicle structures: from surface fractals to mass fractals.* Phys Rev E Stat Nonlin Soft Matter Phys, **2008**. 78(1 Pt 1): p. 010902.

112. Roldan-Vargas, S., et al., *Surface fractals in liposome aggregation.* Phys Rev E Stat Nonlin Soft Matter Phys, **2009**. 79(1 Pt 1): p. 011905.

113. Martin-Molina, A., et al., *Electric double layers with electrolyte mixtures: Integral equations theories and simulations.* Journal of Physical Chemistry B, **2006**. 110(3): p. 1326-1331.

114. Quesada-Perez, M., et al., *Simulation of electric double layers undergoing charge inversion: Mixtures of mono- and multivalent ions.* Langmuir, **2005**. 21(20): p. 9231-9237.

115. Bentz, J., et al., *Membrane-Fusion - Kinetics and Mechanisms.* Colloids and Surfaces, **1988**. 30(1-2): p. 65-112.

116. Ohki, S., et al., *A mechanism for ion-induced lipid vesicle fusion.* Colloids and Surfaces B-Biointerfaces, **2000**. 18(2): p. 83-97.

117. Roux, M., et al., *Ca2+, Mg2+, Li+, Na+, and K+ distributions in the headgroup region of binary membranes of phosphatidylcholine and phosphatidylserine as seen by deuterium NMR.* Biochemistry, **1990**. 29(30): p. 7077-7089.

118. Portis, A., et al., *Studies on the mechanism of membrane fusion: evidence for an intermembrane Ca2+-phospholipid complex, synergism with Mg2+, and inhibition by spectrin.* Biochemistry, **1979**. 18(5): p. 780-790.

119. Ventura, A.C., et al., *Simple data-driven models of intracellular calcium dynamics with predictive power.* Phys Rev E Stat Nonlin Soft Matter Phys, **2006**. 74(1 Pt 1): p. 011917.

120. Mansilla-Olivares, A., *[Calcium, the atom triggering life and cellular function].* Cir Cir, **2004**. 72(2): p. 139-151.

CAPÍTULO 5

ANEXO DE LOS ARTÍCULOS PUBLICADOS

A THEORETICAL AND EXPERIMENTAL APPROACH TO THE COMPACTATION PROCESS OF DNA BY DIOCTADECYLDIMETHYLAMMONIUM BROMIDE/ZWITTERIONIC MIXED LIPOSOMES

Alberto Rodríguez-Pulido,[†] Alberto Martín-Molina,[‡]
César Rodríguez-Beas,[‡] Oscar Llorca,[§] Emilio Aicart[†]
and Elena Junquera[†]

[†]*Grupo de Química Coloidal y Supramolecular, Departamento de Química Física I, Facultad de Ciencias Químicas, Universidad Complutense de Madrid, 28040-Madrid, Spain.*[‡]*Grupo de Física de Fluidos y Biocoloides, Departamento de Física Aplicada, Facultad de Ciencias, Universidad de Granada 18071- Granada, Spain.*[§]*Centro de Investigaciones Biológicas, CSIC, Ramiro de Maeztu 9, 28040-Madrid, Spain.*

Abstract

The compaction of DNA by cationic liposomes constituted by a mixture of a cationic lipid, dioctadecyldimethylammoniumbromide (DODAB) and a zwitterionic lipid, the 1,2-dioleoyl-sn-glycero-3-phosphatidylethanolamine (DOPE) or the 1,2-dilauroyl-*sn*-glycero-3-phosphocholine (DLPC), has been evaluated by means of experimental studies (electrophoretic mobility, conductometry, cryogenic electron transmission microscopy or cryo-TEM and fluorescence spectroscopy) as well as theoretical calculations. This information reveals that DODAB/DOPE and DODAB/DLPC liposomes are mostly spherical and unilamellar, with a mean diameter of around 70 and 61 nm, respectively, a bilayer thickness of 4.5 nm and gel-to-fluid transition temperatures, T_m, of around 19 and 28 ºC, respectively. Their positively charged surfaces efficiently compact the negatively charged DNA by means of a strong entropically driven surface interaction that yields DODAB/DOPE-DNA and DODAB/DLPC-DNA lipoplexes as confirmed by zeta potential and ethidium bromide fluorescence intercalation assays. These experiments have permitted as well the evaluation of the different microenvironments of varying polarity of DNA helix, liposomes and/or lipoplexes. DODAB/DOPE-DNA and DODAB/DLPC-DNA lipoplexes have been characterized by isoneutrality ratios, $(L/D)_\phi$, of around 4.7 and 4.8, respectively, a more fluid membrane than that of the parent liposomes and T_m around 24 and 28 ºC, respectively, as revealed by fluorescence anisotropy. Cryo-TEM micrographs reveal a rich scenario of nanostructures and morphologies, from unilamellar

DNA-coated liposomes to multilamellar lipoplexes passing through cluster-like structures. Phase diagrams (aggregation and re-entrant condensation phenomena), calculated by means of a phenomenological theory, have confirmed the experimental concentration domains and the isoneutrality conditions. The influence of helper lipid in the compaction process, as well as the optimum choice among those herein chosen, has been analyzed.

1. Introduction

Although viral based DNA carriers constitute nowadays the most common method for gene delivery, there has been in the last decade an increasing research in developing nonviral vectors.[1-8] Particularly, cationic liposomes have shown potential application as transfer vectors, due to their easily production and low toxicity.[4,5,9-12] The transmission efficiency of DNA using cationic liposomes (CL) varies so much depending on the kind of liposome, the presence of helper lipid, the lipid/DNA ratio, or the cells targeted,[4,6,13] although an universal behavior can be obtained when liposomes characteristics are compared with respect to charge density.[14,15] From those previous studies, it is clear that the interaction between cationic liposomes and DNA, when forming the complex named lipoplex, plays an important role, and for that reason a currently renovated area of research is focused on improving the understanding of this interaction, from both experimental and theoretically points of view.[6,13] In fact, it is expected that a physicochemical characterization of the process can shed light

on the formation of these complexes, and, accordingly, on transfection mechanisms.

It is well known that the presence of both a cationic and a neutral helper lipids, forming a mixed liposome, may improve the efficiency of transfection.[4,6,13] In fact, the choice of the helper is very important because, depending on it, the transfection efficiency can be increased or unaffected.[16] We recently reported[17,18] a series of experimental studies of DNA compaction with mixed liposomes constituted by a cationic lipid and a zwitterionic helper lipid of the phosphatidylethanolamine family (DOPE). The results revealed mainly two features: a) a strong surface electrostatic interaction drives the formation of lipoplexes and; b) lipoplexes showed, in the vicinity of the isoneutrality, a clear tendency to form cluster-type structures not well understood. With the aim of sheding light to these and others points related to lipoplexes, we report in this work a deeper study involving lipoplexes formed by DNA with the cationic lipid DODAB (a dialkyldimethylammonium cationic lipid with two 18C saturated hydrocarbon tails), in the presence of two helper zwitterionic lipids, DOPE and/or DLPC. DOPE is a helper lipid with a single olefinic unsaturation on the *cis* configuration at the 9 position in the two 18C hydrocarbon chains, while DLPC, of the phosphatidylcholine family, presents full saturation in the two 12C hydrocarbon chains. Both (mostly DOPE) are frequently used for *in vitro* and *in vivo* transfection, because they increases the elasticity of the liposome bilayer and promotes the fusion of lipoplexes with the cell membrane, which results in an increase of the transfection efficiency of DNA into

the cells.[4,15,19-26] One of the objectives of this work is to analyze from an experimental point of view, as well as to predict from a theoretical standpoint, the influence that the presence of those helper lipids has in the compaction process and in the behavior of the DODAB-DNA lipoplexes, trying, if possible, to elucidate which one shows potentially better capabilities as a helper lipid. The results will confirm from a physicochemical standpoint, what is usually accepted by biochemists in transfection studies, i.e., DOPE is a better helper lipid than DLPC.

To carry on this study, the lipoplexes have been characterized by means of a wide variety of experimental techniques. Electrochemical methods, such as conductometry and zeta potential, are a powerful tool to analyze the electrostatic forces within the bulk solution and on the surface of the liposomes and/or the lipoplexes,[4,24,27-31] respectively. Fluorescence spectroscopy is used to check the cationic liposome-DNA interaction, by means of fluorescence intercalating assays, and the fluidity of the lipidic bilayer of liposomes in the absence and presence of DNA, by means of fluorescence anisotropy.[24,30,32-42] Cryogenic transmission electron microscopy (cryo-TEM) is widely used to get information about the shape, size, and morphology of the lipoplexes.[19,23,24,43-49] Two important novelties have been incorporated in this work to extend the type of experiments of previous studies: i) a complete fluorescence anisotropy study as a function, of both temperature and lipoplex composition, that will allow for carefully analyzing of the effect of bilayer fluidity on the lipoplex, which, in turn, is seems to be a key on transfection efficacy and; ii) a complete

image processing protocol to optimize the cryo-TEM micrographs with the aim of having a deeper insight on the structure and morphology of lipoplexes, in some lipid/DNA composition ratio forming clusters. This image analysis has allowed us for finding a rich scenario of structures and morphologies not seen before in this kind of studies.

In addition, the compaction process of DNA by the cationic liposomes has been also analyzed from a theoretical point of view. For that purpose, a phenomenological theory recently developed for the interaction among liposomes and polyelectrolytes[50,51] has been used to build the phase diagrams of the lipoplexes studied in this work, including the charge inversion and re-entrant condensation processes among the lipoplexes. These phase diagrams contain information about the liposome and DNA concentration necessary to have either anionic or cationic isolated lipoplexes or also clusters of lipoplexes. By predicting them, we will know the optimum values of DNA and liposome concentrations for an efficient transfection from a physicochemical stand point. The theoretical predictions regarding the concentration domains of the aggregated and disaggregated lipoplexes have been checked against the experimental results obtained in cryo-TEM experiments; in this sense, a new limit concentration has been defined to explain the presence of cluster domains in coexistence with isolated cationic lipoplexes, at lipid concentrations higher than those ones predicted by the model. Also, theoretical isoneutrality conditions, determined with the phenomenological model, are consistent with those experimentally obtained in this work.

2. Experimental section

A. Materials. Cationic lipid (DODAB) and zwitterionic lipids (DOPE and DLPC), with purities greater than 99 % mass, were from Avanti Polar Lipids. Sodium salt of calf thymus DNA, with less than 5 % of protein, the fluorescent probes, i.e. ethidium bromide (EtBr), 1,6-diphenyl-1,3,5-hexatriene (DPH) and the components of HEPES buffer were from Sigma-Aldrich. All of them were used without further purification. Solutions were prepared with deionized water (Super Q Millipore, conductivity lower than 18 μS cm^{-1}), by mass, and, unless otherwise stated, all were buffered at pH=7.4 by using HEPES 40 mM, ionic strength = 15.3 mM, at 298.15 K.

B. Preparation of mixed liposomes, DNA and lipoplexes. Dry films of mixed lipids, prepared by dissolving appropriate amounts of DODAB (L^+) and DOPE or DLPC (L^0) (1:1 L^+/L^0) in chloroform followed by evaporation of the solvent, were hydrated in HEPES, using a protocol previously described in detail.[17] This procedure yields a polydisperse population of multilamellar vesicles,[52-54] which were transformed to large unilamelar vesicles (with a reduction on the polydispersity) by a sequential extrusion procedure previously explained,[17,55-58] which consists in 5 extrussions through 400 nm pore size, 5 passes through 200 nm pore size and 10 passes through 100 nm pore size polycarbonate membranes.

A stock solution of DNA (0.100 mg/mL = 1.18x10^{-4} M base pair) was prepared by dissolving an appropriate amount of the solid in HEPES two days before the mixing with liposomes. DNA

concentrations (expressed in mM base-pairs) were determined by absorbance at 260 nm.[10,59,60] A A_{260}/A_{280} ratio of 1.90 and a negligible absorbance at 320 nm[25,53,58-60] reveal that the contamination of the DNA by the presence of a certain percentage of proteins is negligible. Agarose gel electrophoresis experiments show that the DNA used herein consists of around 2700 bp fragments on average.

Equal volumes of DNA and DODAB/DOPE or DODAB/DLPC liposome extruded solutions were mixed by adding DNA over liposome, as usually done in these studies,[17,22,24] following an optimized protocol widely explained elsewhere. Concentrations of both solutions were controlled to fit the final desired L/D ratio, defined as:

$$L/D = \frac{L^+ + L^0}{D} \tag{1}$$

where L and D are the total lipid and DNA masses. Once the addition was concluded, the solution was maintained under agitation during 10 minutes to favour the formation of lipoplexes.

C. Zeta potential and conductometry. A laser Doppler electrophoresis (LDE) technique previously described,[61] was used to measure electrophoretic mobilities. Temperature was controlled at (298.15 ± 0.01 K). Each electrophoretic mobility data is taken as an average over 10 independent measurements. DNA concentration was kept constant at around 0.05 mg/mL and the total lipid concentration

was varied to cover an L/D ratio range from around 1 to 15. Electrophoretic mobility for liposome solutions in the absence of DNA ($L/D = \infty$) were also measured.

Conductivity data were collected at 298.15 K ($\pm$ 1 mK) with a Hewlett-Packard 4263A LCR Meter. The whole equipment, the preparation of mixtures and the fully computerized procedure was widely described previously.[62,63] This highly accurate method permits to obtain the specific conductivity, κ, with a reproducibility better than 0.03%. The conductivity measurements were made as a function of total lipid concentration at constant DNA concentration of 0.050 mg/mL, thus varying L/D ratio from 0 to 10.

D. Cryo-TEM. Transmission electron microscopy experiments under liquid nitrogen temperatures (cryo-TEM) were run on samples of DODAB/DOPE and DODAB/DLPC liposomes in the absence and presence of DNA at different L/D ratios below and above the isoneutrality ratio, $(L/D)_\phi$. All the samples were prepared and vitrified according to the method fully described earlier,[64,65] and the experimental protocol was widely explained elsewhere.[17] Observations were conducted at a JEOL 1230 microscope operated at 100 kV. Micrographs were recorded on Kodak SO-163 film at zero degrees tilt and a nominal magnification of 30000X. Selected micrographs were digitalized in a Dimage Scan Multi Pro scanner (Minolta) at 600 dpi, corresponding to a final sampling of 1.4 nm/pixel at the specimen. 500×500 pixel square images were extracted from these micrographs using the boxer command found in

the EMAN software for image processing[18] and low pass filtered to remove high frequency noise. These images were then saved as .png files with EMAN and visualised with "ImageJ" (Image processing and analysis in Java). Images were analysed using some of the tools in "ImageJ" by drawing a line through a desired section of the images and plotting its profile.

E. Fluorescence spectroscopy. Steady state fluorescence experiments were carried out as described earlier,[17,66] using a stirred cuvet holder whose temperature was kept constant ($\pm$ 0.01 K) with a recirculating water circuit. Two types of experiments were done: (a) EtBr intercalation assays to analyze the type of interaction that takes place between the cationic liposomes and DNA, and (b) anisotropy measurements with DPH probe to evaluate the fluidity of the lipidic bilayer, in the absence and presence of the DNA.

Fluorescence emission spectra of EtBr in the 530-700 nm region were recorded with excitation at 520 nm.[17] Probe concentration was kept constant at [EtBr] = 6.34 μM in all the cases. The emission of an EtBr/DNA solution (DNA:EtBr molar ratio is bigger than 6:1 and [DNA] = 0.025 mg/mL) was registered at increasing [L], thus covering from L/D = 0 to 8. In all the cases, excitation and emission band slits were fixed at 2.5 and 5.0 nm, respectively, and scan rate was selected at 240 nm/min. Fluorescence spectra were corrected from the background intensities of the buffer solution.

Fluorescence anisotropy was measured by using the DPH probe included in DODAB/DOPE or DODAB/DLPC liposomes to yield a

molar ratio of probe to lipid of 1:200, following a procedure widely explained in a previous work.[67] DNA (0.051 mg/mL) was added to the labelled liposomes to yield the desired L/D ratios of lipid and DNA (covering from $L/D = 0$ to around 8). Fluorescence intensities of the emitted light with the excitation and the emission polarized following the modes: vertical-vertical (I_{VV}) vertical-horizontal (I_{VH}) horizontal-horizontal (I_{HH}) and horizontal-vertical (I_{HV}) were measured by exciting DPH at 360 nm and recording its fluorescence emission at 430 nm. The slit widths were 2.5 nm for both the excitation and the emission. Fluorescence anisotropy, r, was calculated by using:[33]

$$r = \frac{I_{VV} - GI_{VH}}{I_{VV} + 2GI_{VH}} \tag{2}$$

where $G(=I_{HV}/I_{HH})$ is the instrument grating factor, estimated as an averaged of 10 measurements for each solution, thus correcting optical and electronic differences in the parallel and perpendicular channels. The influence of the light scattering of samples in anisotropy values was also evaluated and considered with the corresponding blank solutions. Each anisotropy value is an average over 36 experimental independent measurements.

3. Theoretical background

The complexation of liposomes (particles) and DNA (polyion) in aqueous solution is has been also studied from a theoretical point of view, using the formalism derived by Sennato *et al.*,[50] which is in turn

based on the complexation theory recently developed by Nguyen and Shklovskii.[68,69] This theory describes the complexation of a long flexible polyelectrolyte with oppositely charged spherical particles such as liposomes or micelles,[68] particularized to account for the complexation of a single negative molecule of DNA with a total charge, $-q$, and contour length, l, with uniformly charged positive spheres with charge Q and radius a.[50] According to the resulting phase diagrams, authors found that complexes experience aggregation and disaggregation (also known as condensation and re-entrant condensation) as a function of the spheres-DNA ratio; in particular, for a given concentration of DNA and growing concentration of liposomes, the theory predicts that the resulting lipoplexes experience aggregation at some critical concentration, S_a, below the isoneutrality point, and remain in this aggregated (or condensed) state up to another concentration, S_d, above the isoneutrality point, where the lipoplexes undergo charge inversion, the inverted positive charge of the lipoplex becoming so large that the aggregates or clusters of lipoplexes disaggregate. Such charge inversion process induced by DNA on cationic liposomes can be experimentally measured by means of electrophoresis, as will be shown later.

The theory predicts that for a given concentration of DNA polyions, P, the state of the system can be described in terms of the DNA concentration in the limit of negligible liposome concentrations, P_0, i.e. DNA concentration in equilibrium with lipoplexes. The resulting phase diagram is given by the following set of equations that can be solved in terms of two parameters: P_0 and E_0, last one related

to the energy gained per complex normalized by the number of DNA polyions, N_i, necessary to neutralize the liposome charge ($N_i = Q/q$).

$$S_a \frac{Q}{q}\left(1 + \sqrt{\frac{2C|E_0|}{qQ}}\right) = P - P_0 \exp\left(\sqrt{\frac{2qQ|E_0|}{C(k_B T)^2}}\right) \qquad (3)$$

$$S_d \frac{Q}{q}\left(1 - \sqrt{\frac{2C|E_0|}{qQ}}\right) = P - P_0 \exp\left(-\sqrt{\frac{2qQ|E_0|}{C(k_B T)^2}}\right) \qquad (4)$$

where $C = 4\pi\varepsilon_0\varepsilon a$ is the electrical capacitance (with ε_0 and ε being the vacuum and relative permittivity, respectively). Here, the theory is able to calculate the two boundaries liposome concentrations S_a and S_d, where DNA-liposome complexes begin to aggregate (or condense) forming large aggregates or clusters and where these clusters disaggregate (re-entrant condensation), respectively. In addition, the theory allows predicting the isoelectric point, where the aggregates are almost neutrally charged. If the liposome concentration at the electroneutrality condition is denoted as S_ϕ, this parameter can be calculated in terms of terms of the phenomenological parameter P_0 as follows[50,69]

$$S_\phi = \frac{P - P_0}{N_i} \qquad (5)$$

4. Results and discussion

It is known that the efficiency of cationic colloidal nanoaggregates as DNA vectors and the characteristic properties of the lipoplexes depend very much of several factors that may modulate the transfection process, i.e. the isoneutrality ratio, the type of non-covalent intermolecular forces governing the DNA-liposome interaction, the size, structure and morphology of liposomes and lipoplexes, and the fluidity of liposome bilayer in the presence of DNA. The foregoing sections present the most relevant experimental and theoretical results obtained in this work regarding all the abovementioned factors.

A. Isoneutrality ratio. If n^+ and n^- stand for the number of moles of positive and negative charges, coming from cationic lipid and DNA, respectively, M_{L^+} is the molar mass of cationic lipid and $\overline{M}_{bp}$ is the average molar mass per base pair, the lipoplex charge ratio (*CR*) is given by:

$$CR = \frac{n_+}{n_-} = \frac{L^+ / M_{L^+}}{2D / \overline{M}_{bp}} = \frac{L^+}{D} \frac{\overline{M}_{bp}}{2M_{L^+}} = \left(\frac{L - L^0}{D} \right) \frac{\overline{M}_{bp}}{2M_{L^+}}$$

(6)

The *isoneutrality ratio*, $(L/D)_\phi$, is characteristic of each lipoplex and can be defined as the *L/D* ratio at which *CR* equals 1. Considering M_L^+ (for DODAB) and M_L^0 (for DOPE and DLPC neutral lipids), and that L^+ and L^0 are in 1:1 molar relation in the liposome, the isoneutrality ratio, $(L/D)_{\phi,calc}$, calculated from eq 6, is 4.2 for

DODAB/DOPE-DNA and 3.9 for DODAB/DLPC-DNA lipoplexes. $(L/D)_\phi$ can be determined from different experimental properties. Among all, electrophoretic mobility and magnitudes related with it, such as the zeta potential, ζ, and the surface charge density enclosed by the shear plane, σ_ζ, are often used to obtain $(L/D)_\phi$ since all of them show an inversion of sign at this particular L/D. Eqs (7-8)[70,71] are normally used to determine ζ and σ_ζ from electrophoretic experiments (Table 1 of Supplementary Information collects electrokinetic data):

$$\zeta = \frac{3\eta}{2\varepsilon_0 \varepsilon_r f\left(\kappa_D a\right)} \mu_e \tag{7}$$

$$\sigma_\zeta = \frac{2\varepsilon_0 \varepsilon_r \kappa_D k_B T}{ze} \sinh\left(\frac{ze\zeta}{2k_B T}\right) \tag{8}$$

In these equations η is the viscosity of water, z the ion valence, and $f(\kappa_D a)$ the Henry function, that depends on the reciprocal Debye length, κ_D, and the hydrodynamic particle radius, a. For medium-to-large particles in a medium of moderate ionic strength ($a \gg \kappa_D^{-1}$), Smoluchowski limit is usually applied ($f(\kappa_D a) = 1.5$) to estimate the Henry function.[70,71] Figure 1 shows zeta potential values vs. L/D ratio for the lipoplexes studied in this work. Similar graphs can be drawn with either μ_e or σ_ζ and have been omitted. As previously found for other lipoplexes and surfoplexes,[4,17,18,24,30,52,67,72] the experimental data

fit to a sigmoidal curve that divides the L/D axis in three different zeta potential regions: (i) a region where lipoplexes show a net negative and almost constant zeta potential; (ii) a region where the inversion of zeta potential sign takes place, pointing to a typical surface liposome-DNA interaction, mainly electrostatically driven; and (iii) a region of net positive zeta potentials that tend to the value for the pure liposomes. $(L/D)_{\phi,exp,\zeta}$ ratios have been calculated from the L/D value at which zeta potential is zero, $(L/D)_{\phi,exp,\zeta} = 4.8$ for DODAB/DOPE-DNA and 4.6 for DODAB/DLPC-DNA lipoplexes, slightly higher than calculated values. Table 1 resumes both experimental and calculated $(L/D)_{\phi}$ values determined in this work.
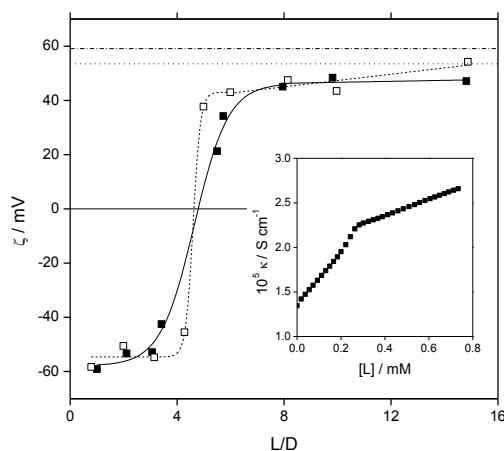

Figure 1. Electrochemical study: the main figure shows the values of zeta potential (ζ) of DODAB/DOPE/DNA (solid squares) and DODAB/DLPC/DNA (empty squares) lipoplexes at different L/D ratios in aqueous buffered medium at 298.15 K. DODAB:DOPE and DODAB:DLPC ratios are 1:1; [DNA] = (0.050 ± 0.001) mg/mL. Solid line: sigmoidal fit of experimental values. Dot and dashed lines correspond to the ζ values for DODAB:DOPE ($\zeta = (53 \pm 2)$ mV) and DODAB:DLPC ($\zeta = (59 \pm 2)$ mV) liposomes in the absence of DNA ($L/D = \infty$).

Errors are estimated to be around 3%. The inset shows the specific conductivity, κ, as a function of total lipid concentration, in the presence of DNA at constant concentration (= 0.050 mg/mL) in aqueous medium at 298.15 K.

Conductivity data may also inform about the isoneutrality ratio. Figure 1 (inset) shows the plot of specific conductivity of the aqueous solutions of DNA at constant concentration, as a function of total lipid concentration, [L], for DODAB/DOPE-DNA lipoplexes, as an example. The reason for carrying on conductivity studies in aqueous solutions is that the buffered medium (HEPES) used in the other experiments herein reported yields such a high conductivity ($\sim 10^{-3}$ S cm^{-1}) that masks all the changes assignable to the formation of lipoplexes (around 100 times lower). The clear change on the positive slope of the property at [L] = 0.27 mM, corresponding to $(L/D)_{\phi,exp,\kappa}$ = 3.8, can be attributed to the *isoneutrality ratio*. Below the isoneutrality, the electrostatic interaction between the positive charges facing outward from the liposome surface and the negative charges of DNA, i.e. the lipoplex formation, provokes a release of counterions, Na$^+$ from DNA and Br$^-$ from liposomes, justifying the increase observed in conductivity. Above the isoneutrality (all DNA is complexed), the increase in conductivity (but with a smaller slope) can be only due to the addition of liposomes that partially dissociate (L$^+$ and Br$^-$ counterions), but do not associate with DNA. Similar behavior has been recently found for cationic and catanionic vesicles or micelles binding DNA.[17,18,67,72] The $(L/D)_{\phi,exp,\kappa}$ value thus obtained is slightly lower than that one obtained from zeta potential sigmoidal plots, this feature being attributed to the different ionic strength used

in both experiments. In any case, both are in reasonable good agreement with those ones calculated from eq 6.

Table 1: Experimental, $(L/D)_{\phi,exp}$, Calculated, $(L/D)_{\phi,calc}$, and Theoretical, $(L/D)_{\phi,theo}$, Values of the isoneutrality Ratio, Obtained from the Experimental Methods Reported in This Work, Eq 9, and the Aggergation-Disaggregation Theory (eq 8), respectively.

lipoplex	Calculated $(L/D)_{\phi,calc}$	LDE $(L/D)_{\phi,exp,\xi}$	Conductometry $(L/D)_{\phi,exp,\kappa}$	Fluorescence EtBr intercalation $(L/D)_{\phi,exp,fl}$	Aggregation-disaggregation Theory $(L/D)_{\phi,theo}$
DODAB/ DOPE-DNA	4.2	4.7	3.8[a]	4.7	5.0
DODAB/ DLPC-DNA	3.9	4.7	–	4.8	4.6
DSTAP/ DOPE-DNA	4.7	5.6	3.6[a]	5.4	5.6

[a] Experimental done in aqueous nonbuffered solution, [b] reference 17.

B. DNA-Cationic liposomes interaction. In the previous section, the electrostatic character of the interaction that takes place between the positively charged surface of the liposome and the negatively charged DNA helix has been shown. It is also known that electrostatics plays an important role as well in various steps of the transfection process, although the interaction is entropically driven due to the release of counterions (cations from the DNA surface and anions from the cationic liposome surface).[23,45] EtBr intercalation assays are very often used to confirm and characterize this surface electrostatic interaction. EtBr is an aromatic planar cationic fluorophore whose fluorescence intensity clearly increases when it is intercalated between base pairs of double-stranded DNA.[16,73-76] In the

presence of cationic liposomes, DNA is compacted to form the lipoplex, the EtBr probe is moved from the DNA helix to the bulk solvent and its fluorescence intensity decreases.[24,32-35] Thus, a decrease in the probe emission intensity can be used as a way to asses DNA-liposome compaction. Figure 2 shows the fluorescence of EtBr, at constant DNA concentration, at different L/D ratios for DODAB/DLPC-DNA lipoplexes, from below to above the $(L/D)_\phi$ ratio. A similar graph (omitted for the sake of conciseness) can be drawn for DODAB/DOPE-DNA lipoplexes.
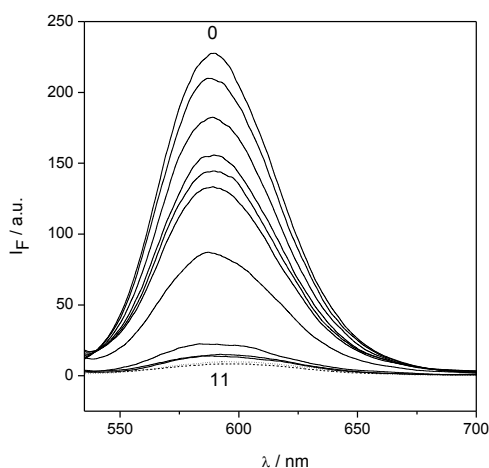

Figure 2. Emission fluorescence spectra of EtBr in the presence of DODAB/DLPC-DNA lipoplexes at different L/D ratios: 0, $L/D = 0$; 1, $L/D = 1.0$; 2, $L/D = 2.1$; 3, $L/D = 3.2$; 4, $L/D = 3.6$; 5, $L/D = 4.2$; 6, $L/D = 4.7$; 7, $L/D = 5.2$; 8, $L/D = 5.7$; 9, $L/D = 6.2$; 10, dotted line, shows the emission fluorescence spectra of EtBr in the absence of liposomes and lipoplexes; and 11, dashed line, shows an example of the emission fluorescence spectra of EtBr only in presence of liposomes (L/D = ∞) at $[L] = 0.180$ mg/mL. Medium: aqueous HEPES 40 mM, pH = 7.4. DODAB:DLPC ratio is 1:1; DNA:EtBr ratio is 6:1; [DNA] = 0.025 mg/mL.

Also included in the figure is the EtBr fluorescence in the absence of DNA and also in the absence of liposomes. The maximum emission intensity, found at $\lambda = 588$ nm, is plotted as a function of L/D in Figure 3, for both lipoplexes. Several features can be remarked in these figures: (i) the emission of EtBr in the presence of liposomes is comparable to that in the bulk, indicating that the probe does not interact with the cationic liposomes, as also found for other lipoplexes and surfoplexes;[17,18,24,32,34,35,67] (ii) probe emission shows clear changes when DNA is present, gradually decreasing with L/D down to a constant intensity (at $L/D \approx 5$), comparable to that one found in the absence of DNA and even in the absence of liposomes. This behaviour confirms that DNA-liposome interaction is stronger than that between EtBr and DNA, the probe being displaced by the addition of lipid from the DNA base pair hydrophobic microenvironment towards the bulk, where its quantum fluorescence yield falls down; (iii) the above commented trend permit to calculate the isoneutrality ratios on Figure 3; $(L/D)_{\phi,exp,fl}$ is 4.7 for DODAB/DOPE-DNA and 4.8 for DODAB/DLPC-DNA lipoplexes. Both values are in very good agreement with those obtained from electrochemical properties, and also with those calculated from eq 6. EtBr may be immersed within two different microenvironments in the presence of DNA (the helix interior, more hydrophobic, and the buffered bulk, more polar), while in the absence of DNA it remains in only one microenvironment, the bulk, giving that probe and liposome does not interact. Accordingly, one would expect to see this transition, from two microenvironments

at L/D = 0 to one microenvironment, when EtBr is totally displaced from DNA interior towards the bulk, i.e. at L/D > $(L/D)_\phi$.
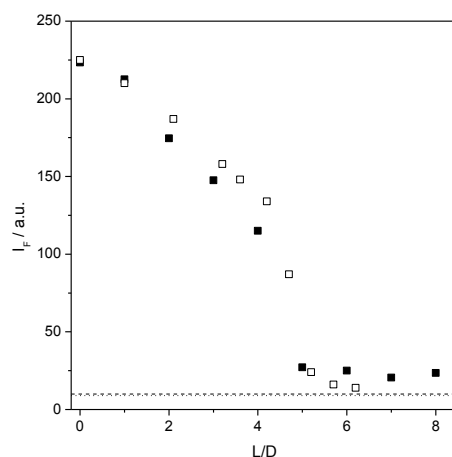

Figure 3. Emission fluorescence intensity of EtBr at 588 nm in the presence of DODAB/DOPE-DNA, ▪, or DODAB/DLPC-DNA, □, lipoplexes as a function of *L/D* ratio. Medium: aqueous HEPES 40 mM, pH = 7.4. DODAB:DOPE ratio is 1:1; DNA:EtBr ratio is 6:1; [DNA] = 0.025 mg/mL. Dashed lines: emission fluorescence intensity of EtBr in the presence of DODAB/DOPE-DNA ([*L*] = 0.075 mg/mL). Dotted line: emission fluorescence intensity of EtBr in the presence of DODAB/DLPC liposomes ([*L*] = 0.180 mg/mL).

A deconvolution procedure widely explained in a previous work[17] has been applied to confirm it. Thus, all the experimental $\pi \rightarrow \pi^*$ emission bands of Figure 2 (and those for DODAB/DOPE-DNA system, not shown) have been deconvoluted into overlapping gaussian curves with a non-linear least-squares multi-peaks fitting procedure, each of which being attributed to the $\pi \rightarrow \pi^*$ emission of the probe immersed within different microenvironments, characterized by its hydrophobicity, microviscosity, rigidity and/or solvation features. Figure 4 shows a resume of the deconvolution process into the best

119

components (one or two gaussians) at a selection of the *L/D* ratios for DODAB/DLPC-DNA lipoplexes, as an example (see Figure 1 of Suppl. Information for more examples).
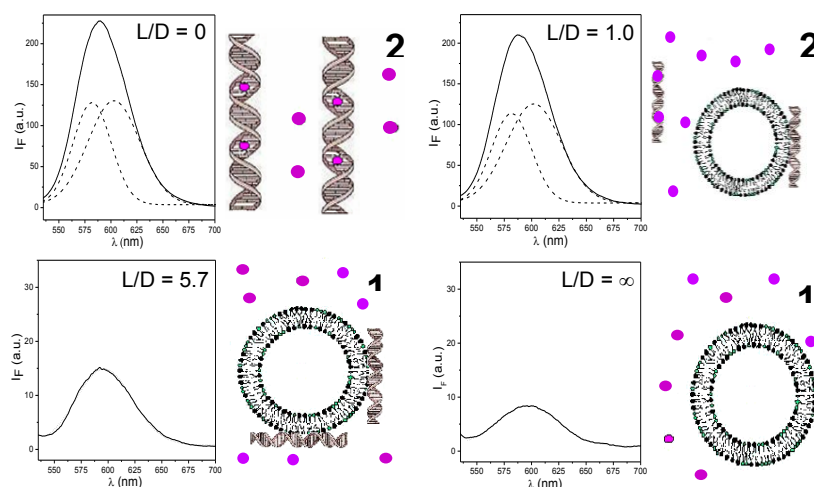

Figure 4. Emission fluorescence spectra of EtBr in the presence of DODAB/DLPC-DNA lipoplexes at a selection of *L/D* ratios, together with their deconvolutions into 1 or 2 gaussian components: *L/D* = 0, only DNA; *L/D* = 1.0, below $(L/D)_\phi$; *L/D* = 5.7, above $(L/D)_\phi$; *L/D* = ∞, only DODAB/DLPC liposomes. Solid line: experimental spectra. Dash line: gaussian components. Dot line in 2 gaussian cases: total sum of gaussian components. Medium: aqueous HEPES 40 mM, pH = 7.4. DODAB/DLPC ratio is 1:1. A schematic diagram with the microenvironments where the probe (coloured circle) is housed is included.

The information recorded in Figure 4 (and Tables 2-3 on Suppl. Information) confirms the abovementioned features: (i) at *L/D* = ∞ (in the absence of DNA) and just in the solvent (absence of DNA and liposomes), the best fit corresponds to the one-gaussian fit, centered at $\lambda = (597 \pm 1)$ nm, since only one microenvironment, the bulk, is

expected in these cases; (ii) however, at $L/D = 0$, the best choice corresponds to the two-gaussians option, confirming that in the absence of liposome but in the presence of DNA, EtBr is partitioned between two microenvironments, the DNA helix interior, at $\lambda_1 = (581 \pm 2)$ nm, and the bulk, at $\lambda_2 = (599 \pm 4)$ nm; and (iii) at (L/D) ratios within the lipoplex formation range, the two-gaussian fit is applied at $(L/D) < (L/D)_\phi$, while only one gaussian is found at $(L/D) > (L/D)_\phi$; EtBr, initially within the DNA helix, is displaced to the aqueous bulk when the lipoplex is formed, confirming that EtBr-DNA interaction is weaker than the electrostatic liposome-DNA interaction. Moreover, Figure 5, that shows a plot of the areas of the gaussians above commented as a function of the L/D ratio, is consistent with this reasoning: A_1 (blue shifted gaussian, helix interior) decreases while A_2 (red shifted gaussian, bulk) increases with (L/D) confirming that the probe content decreases inside the helix and increases in the bulk as long as the lipoplex is formed. It can be observed that A_1 is lower (and A_2 is higher) for DODAB/DOPE-DNA than for DODAB/DLPC-DNA lipoplexes; i.e. it seems that DODAB/DOPE displaces EtBr from inside DNA helix more effectively than DODAB/DLPC does, which would be indicating that the compaction of DNA by DODAB/DOPE cationic liposomes is stronger than that one with DODAB/DLPC. The phosphathydilcholine (PC) headgroup is strongly hydrated and, in addition, its three methyl groups sterically hinders the electrostatic interaction of negatively charged phosphate residues of DNA and the positive charges of DODAB. In other words, the more efficient coulombic interaction of the weakly hydrated $-NH_3^+$ moiety of the

phosphathydilethanolamine (PE) headgroup with DNA, in conjunction with the tendency to form inverted hexagonal phases by this lipid,[11,77] justifies the enhanced transfection shown by cationic liposomes containing PE headgroup.
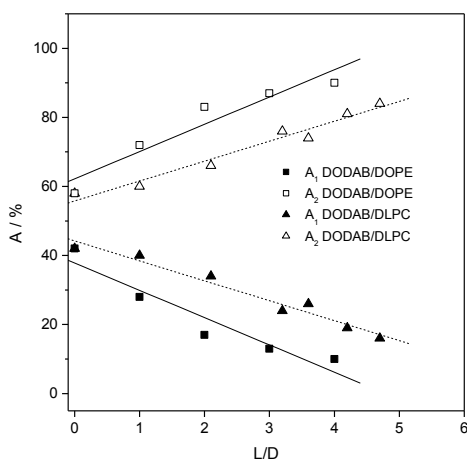

Figure 5. Plot of the areas (in terms of % of the total area) of gaussian bands as a function of L/D ratios for DODAB/DOPE-DNA (solid, A_1, and open, A_2, squares) and DODAB/DLPC-DNA lipoplexes (solid, A_1, and open, A_2, triangles).

C. Structure, size and morphology of liposomes and lipoplexes. Different factors, such as the type of cationic lipid (L^+), type of helper neutral lipid (L^0), L^+:L^0 and L/D ratios, concentration, etc. are responsible of the optimum structure for a lipoplex. Lipoplex structure, size and morphology are known to be key factors on transfection efficiency.[8] In this section, DODAB/DOPE and DODAB/DLPC liposomes, in the absence and in the presence of DNA, are studied from this point of view, by means of cryo-TEM

experiments. Figure 6a-b shows two cryo-TEM micrographs among those taken for pure liposomes. These images reveal that DODAB/DOPE and DODAB/DLPC liposomes are spherical and essentially unilamellar, an average diameter of (70 ± 6) nm and (61 ± 10) nm, respectively, and a bilayer thickness of (4.5 ± 0.5) nm, both parameters averaged over the structures found in all the micrographs (not only over those shown herein).
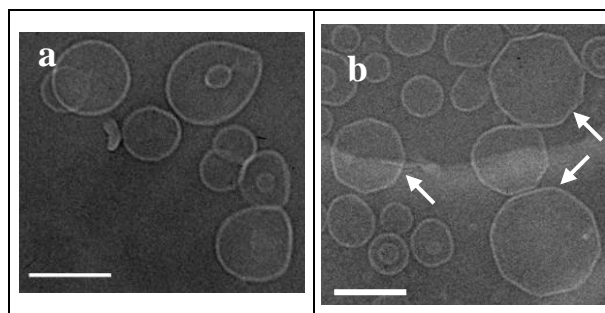

Figure 6. Details extracted from the original cryo-TEM micrographs of liposomes in the absence of DNA, i.e. at $L/D = \infty$: (a) DODAB/DOPE (1:1); and (b) DODAB/DLPC (1:1). Scale bar: 100 nm.

Although DODAB/DLPC liposomes show a slightly smaller size than DODAB/DOPE, it can be concluded that, within the experimental error, the different length of both helper lipids does not seem to affect very much the size of the mixed liposome, mainly determined by the larger lipid, DODAB in this case. In the case of DODAB/DLPC, faceted structures, usually related with the fact that the lipid membrane is not completely in the fluid state at the sample preparation conditions, are also found (arrows on Figure 6b). Cryo-TEM experiments were also run on lipoplex samples at (L/D) ratios

below and above $(L/D)_\phi$. Figures 7-9 show a gallery of selected micrographs of DODAB/DOPE-DNA and DODAB/DLPC-DNA lipoplexes with negative (i.e. $L/D < (L/D)_\phi$, Figure 7) and positive (i.e. $L/D > (L/D)_\phi$, Figures 8 and 9) net charge, respectively. It is common to both situations that liposome structure, size, and morphology change in the presence of DNA.
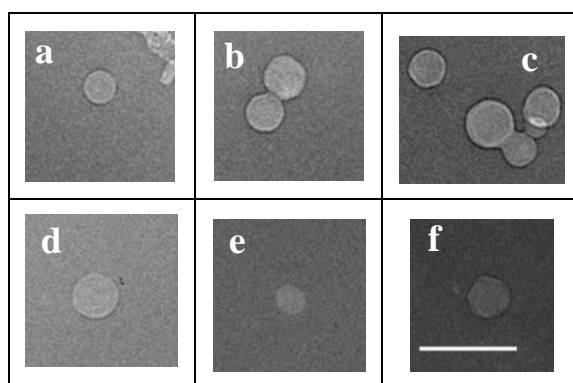

Figure 7. Details extracted from the original cryo-TEM micrographs of (a-c) DODAB/DOPE-DNA lipoplexes (DODAB:DOPE = 1:1) and (d-f) DODAB/DLPC-DNA lipoplexes (DODAB:DLPC = 1:1), at $L/D < (L/D)_\phi$. Scale bar: 100 nm.

Additionally, clear differences are also found among lipoplexes with an excess of DNA (Figure 7) and lipoplexes with an excess of lipid (Figures 8 and 9). Thus, in the former case, lipoplex structures are mostly roughly spherical, as liposomes, but with smaller diameters (~ 40 nm for DODAB/DOPE-DNA and ~ 30 nm for DODAB/DLPC-DNA lipoplexes), indicating that liposomes are disrupted in the presence of DNA to form smaller structures, irrespectively of the type of helper lipid. Similar behavior has been previously reported by our

group for DSTAP/DOPE-DNA lipoplexes.[17] Compared with the micrographs of Figure 6, it can be clearly seen as well that lipoplexes are more condensed than liposomes, with a clear accumulation of density on the surface. Note that the neat characteristic contrast between the line representing the lipidic bilayer and the interior of the liposomes (Figure 6), has been lost in most cases in Figure 7. This increase of density on the surface of the spherical liposomes confirm that DNA is compacted at the surface of liposomes by means of a strong electrostatic interaction, as corroborated by zeta potential and fluorescence results.

However, as can be seen in the micrographs of Figures 8 and 9 (and many others, omitted for the sake of conciseness), lipoplexes at L/D above electroneutrality show, together with the increase of density on the surface of liposomes above commented, a rich distribution of complex structures, including unilamellar DNA-coated liposomes, multilamellar lipoplexes and also cluster-like structures. It is also evident in Figure 8 that, in opposition to what has been found below the electroneutrality, the unilamellar DNA-coated DODAB/DOPE liposomes show diameters comparable to that of liposomes in the absence of DNA. However, in the case of DODAB/DLPC-DNA lipoplexes (Figure 9, micrographs on right side), a certain percentage of original liposomes have been disrupted to form smaller lipoplexes, as majority found below the electroneutrality.
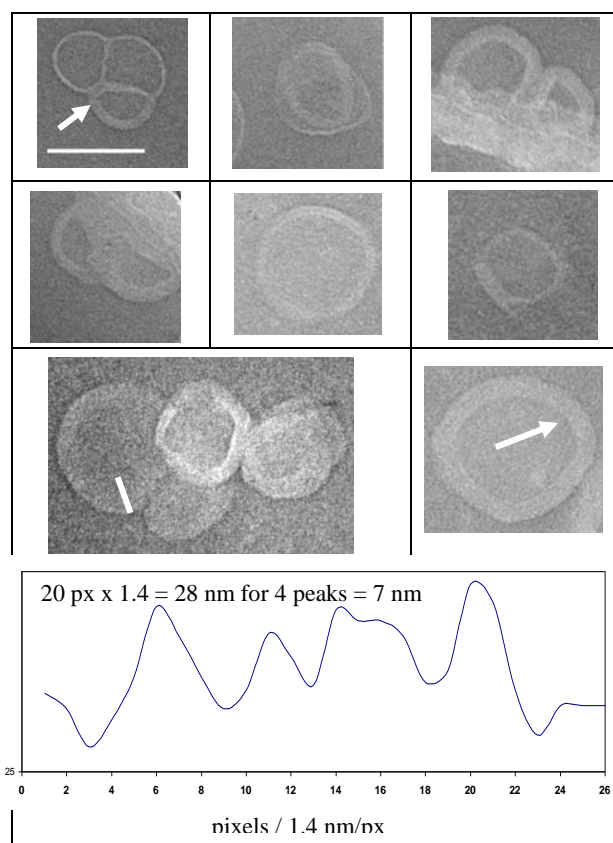
Figure 8. Details extracted from the original cryo-TEM micrographs of DODAB/DOPE-DNA lipoplexes (DODAB:DOPE = 1:1), at $L/D > (L/D)_\phi$. Scale bar: 100 nm. Down: Plot of the grey level vs. distance along a straight line across the 2D image (see white line).

As can be seen in Figures 8 and 9, a certain percentage of the structures retain the unilamelar lipidic bilayer coated with a monolayer of DNA, but most of the nanostructures show a clear thickening of the wall. This fact indicates the presence of multilamellar complexes, constituted by a series of lipidic bilayers with DNA superficially compacted between them. Two different

126

mechanisms have been proposed[45,59,78] to explain the formation of these multilamellar complexes from one DNA-coated liposome: (i) lipoplexes may rupture and envelop a lipoplex-host, as can be seen in Figure 9 (asterisks); and/or (ii) flattened lipoplexes stack to a template lipoplex to form the DNA adsorbed bilayers, as can be seen for example on Figure 9 (arrows).
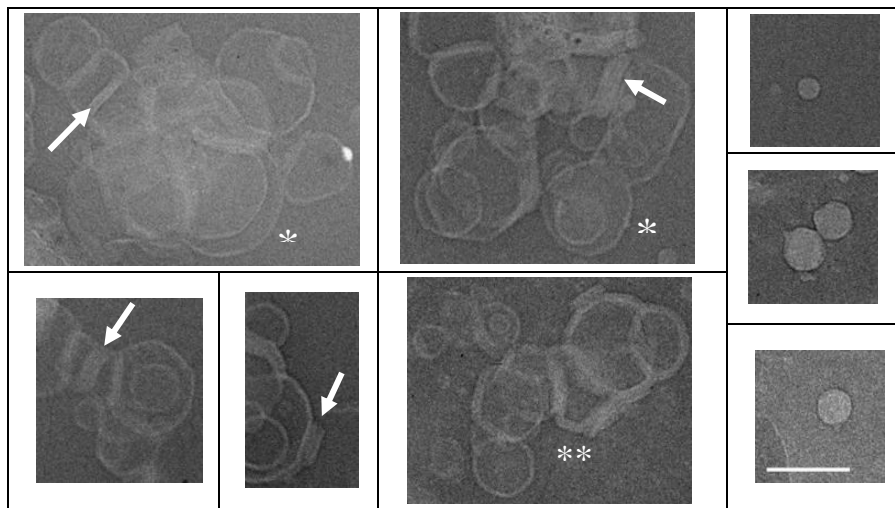

Figure 9. Details extracted from the original cryo-TEM micrographs of DODAB/DLPC-DNA lipoplexes at $L/D > (L/D)_\phi$. (DODAB:DLPC = 1:1). Scale bar: 100 nmFIGURE 9.

Some of those micrographs where clear thickening of the walls is observed were chosen to analyze the presence of possible patterns of periodicity that would confirm the formation of multilamellar structures above commented, and, if so, to study the regular arrangement of the multilamellae (Figure 8 for DODAB/DOPE-DNA). These selected micrographs were analyzed with the image

processing protocol explained in the Experimental Section. Thus, a collection of lines were drawn (see line in Figure 8 on the left bottom micrograph, as an example), and the grey levels along these lines were plotted using the "plot profile" tool in ImageJ (see Figures 2 and 3 in Suppl. Information for more examples). The maximum and minimum levels of density of all the images studied revealed a clear pattern and the distance between repetitions were estimated by measuring the number of pixels between maximums. As can be seen in Figure 8 (down) a complex profile with several peaks and a wider dimension, indicate the presence of several layers. An averaged value of (7.3 ± 0.3 nm) has been determined for the interlamellar spacing of both DODAB/DOPE-DNA and DODAB/DLPC-DNA lipoplexes (not shown), consistent with the fact that DNA helix is effectively sandwiched and aligned between each two bilayers (~ 4.5 nm/bilayer + ~ 2.5 nm/DNA helix). Similar results, obtained either with SAXS or EM experiments, are reported in the literature for other lipoplexes.[19,32,79,80] This tendency to form multilamellar structures are justified by the packing parameters of DOPE and DLPC.[11,77]

Also evident in the micrographs of Figures 8 and 9 (mostly 9, DODAB/DLPC-DNA lipoplexes) is the formation of clusters (or aggregates) of lipoplexes. It seems that the presence of the biopolymer induces liposome aggregation to form cluster like structures, where the liposomes are deformed at the surface of contact with adjacent liposomes, without rupture. This deformation could be pointing to the flexibility of DODAB/DOPE or DODAB/DLPC, but it could also be indicating that DNA-liposome interaction is quite asymmetric. The

formation of lipoplex, by adsorption and compaction of DNA at the outer positive-charged surface of the liposome provokes a reduction of the effective headgroup size of the cationic lipids and, accordingly, an asymmetry in packing pressure,[78] given that positive charges are partially compensated on only one side of the bilayer. As a consequence, the membrane is destabilized, thus promoting lipoplexes fusion and/or aggregation, as also reported by other lipoplex systems.[78,81] Additionally, the flexibility of the lipidic bilayer in the presence of DNA is quite evident in the micrographs shown in Figure 9 (double asterisk), where several folded multilayer can be seen.

D. Bilayer fluidity and stability. Flexibility is a key factor on the morphology of lipoplexes and, mostly, on the formation of clusters. Furthermore, it is known that fluidity is an important biophysical parameter that affects the stability of liposomes and lipoplexes, and, accordingly, the transfection efficiency.[36,82,83] Among other properties, fluorescence anisotropy, r, serves as a measurement of membrane fluidity. Thus, as long as membrane becomes more fluid, the degree of rotation of an excited fluorophore placed within will increase, and, accordingly, anisotropy decreases. Figure 10 shows anisotropy values of the non polar DPH fluorophore buried in the lipidic bilayer of DODAB/DOPE and DODAB/DLPC liposomes as a function of temperature. There can be found in the literature two different types of anisotropy vs. T profiles:[41] (i) anisotropy drops from high anisotropy level to a lower level within a small temperature range, showing a clear phase transition; and (ii) a rather monotonous decrease, followed

by a smaller and less distinct reduction of anisotropy. Profile type (i) is usually found in cationic liposomes and their corresponding lipoplexes, with some exceptions, while profile type (ii) is typical for mixtures of cationic liposomes with DOPE or cholesterol, as helper lipids, and their lipoplexes.[41] As can be seen in Figure 10, DODAB/DOPE liposomes show a typical profile type (ii), while DODAB/DLPC liposomes present a clear sigmoidal trend that reveals a neat gel-to-fluid transition, i.e. profile type (i). Thus, until recently, it was thought that the inclusion of helper lipids had a very striking effect on anisotropy profiles, abolishing a clear transition at a transition temperature, T_m, but we have demonstrated in this work that it is not the presence or absence of helper lipid but the type of helper lipid what controls the anisotropy profile, whether sigmoidal or a monotonous decreament. As could be expected, the fluidity of the liposome bilayer increases (anisotropy decreases) with increasing temperature in both cases. Values of T_m have been determined from the intersection of two straight lines for DODAB/DOPE, $T_m = (18.9 \pm 0.5)$ ºC, and from the inflexion point of the sigmoidal curve for DODAB/DLPC, $T_m = (27.9 \pm 0.2)$ ºC. These results are consistent with what could be roughly estimated for a 1:1 mixture of DODAB (T_m around 55 ºC), and DOPE or DLPC (T_m around -16 ºC to 0 ºC and -2 to 5 ºC, respectively). It is well-known that the inclusion of DOPE increases liposome stability, due in part to its low T_m, reducing T_m of the mixture below room temperature, and also to its structure, a typical cone-shaped molecule with a known tendency to form hexagonal phases.[11,77]
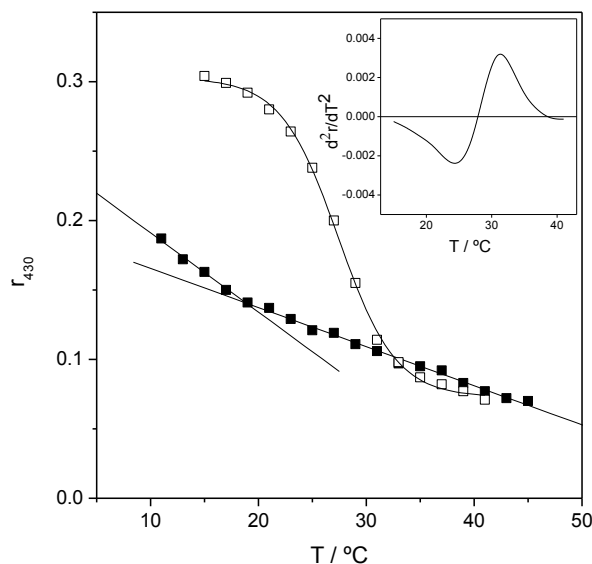
Figure 10. Fluorescence anisotropy at 430 nm (r_{430}) of DPH as a function of temperature for DODAB/DOPE (solid squares) and DODAB/DLPC (empty squares) liposomes. Medium: aqueous HEPES 40 mM, pH = 7.4. Errors by light scattering are less than 3%. The inset shows the second derivative of anisotropy (d^2r/dT^2) as a function of temperature for DODAB/DLPC data, for T_m determination.

Similarly, although DLPC does not usually provoke the formation of hexagonal phases, it also reduces T_m of the lipid mixture, and, accordingly, it could be useful as a potentially efficient helper and fusogenic lipid in transfection studies. Additionally, it can be concluded that DODAB/DOPE bilayer is clearly more fluid than DODAB/DLPC bilayer at $T < T_m$, this effect tending to cancel with increasing temperature; at $T > 30$ °C, both bilayers show comparable fluidity.

Figures 11 and 12 show the anisotropy of the lipoplexes studied in this work as a function of temperature. As can be seen in these figures, DODAB/DOPE-DNA and DODAB/DLPC-DNA lipoplexes

131

show typical profiles (ii) and (i), respectively. These evidences reveal that the presence of the polyelectrolyte does not modify the anisotropy vs. T profiles. Thus, helper lipids of the PEs family and/or cholesterol induce profile type (ii), while helper lipids of the PCs family yield a profile type (i). Table 2 resumes T_m values for the liposomes and lipoplexes studied in this work; it seems that the presence of DNA increases T_m of DODAB/DOPE liposomes, while almost no effect is observed in the case of DODAB/DLPC liposomes ($T_m \approx 27$ °C). In both cases, L/D ratio seems to have a negligible effect on the T_m value. The influence of L/D ratio on the fluidity of the lipidic membrane is shown on the inset of Figure 11 for DODA/DOPE-DNA lipoplexes. Several features can be remarked in the figure: (i) the trend of both curves, quite similar, suffers a clear change at L/D around 4.5, due to the isoneutrality, although there is not enough experimental information to determine with precision $(L/D)_\phi$ in this case; (ii) three zones can be distinguished, irrespectively of the temperature: r slightly increases at $L/D < (L/D)_\phi$, it clearly decreases when reaching $(L/D)_\phi$ and again increases at $L/D > (L/D)_\phi$ tending to the value found for DODAB/DOPE liposomes; and (iii) DODAB/DOPE-DNA lipoplexes are more flexible structures (lower anisotropy) than liposomes at temperatures below T_m, while the fluidity of the membrane seems to be almost the same on average with and without DNA at temperatures above T_m. The interaction of the positively charged head groups with the polyanion DNA could lead to a less tightly packed organization, increasing the distance between the lipid molecules in the membrane and thus favouring lateral diffusion of the

132

lipids in the bilayer. Similar conclusions can be extracted for DODAB/DLPC-DNA lipoplexes (Figure 12, inset).
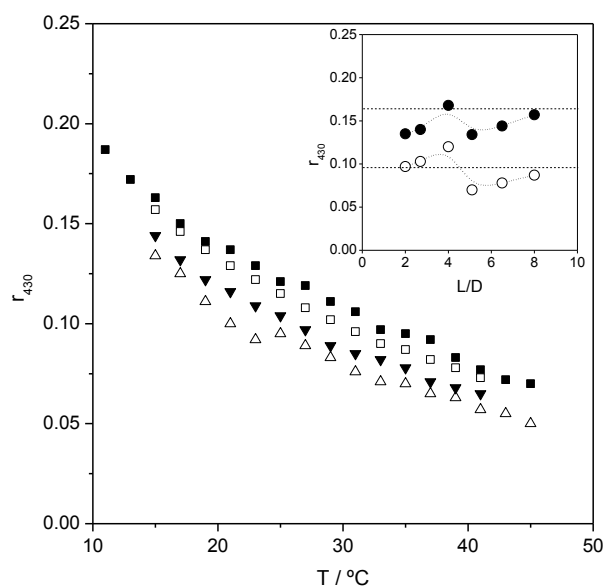

Figure 11. Fluorescence anisotropy at 430 nm (r_{430}) of DPH as a function of temperature for DODAB/DOPE liposomes in the absence (solid squares) and in the presence of DNA at various *L/D* ratios: empty up triangles, 5.0; solid down triangles, 6.5; and empty squares, 8.0. [DNA] = 0.050 mg/mL. Medium: aqueous HEPES 40 mM, pH = 7.4. Errors by light scattering are less than 3%. The inset shows r_{430} of DPH as a function of *L/D* ratio at two temperatures, T: solid circles, 15 °C (below T_m); and empty circles, 35 °C (above T_m). Dotted lines show anisotropy values for DODAB/DOPE liposomes in the absence of DNA.

The increase on the fluidity of the membrane by DNA association due to lipid packing changes has been also reported by NMR experiments.[84,85] Furthermore, it can be concluded that DODAB/DLPC-DNA membrane is less flexible than that one of DODAB/DOPE-DNA, at $T < T_m$, but these differences decrease with temperature, to be null at $T > T_m$, as also found for liposomes in the

absence of DNA. These evidences are also corroborated by cryo-TEM results that show faceted structures in Figure 6 (arrows).
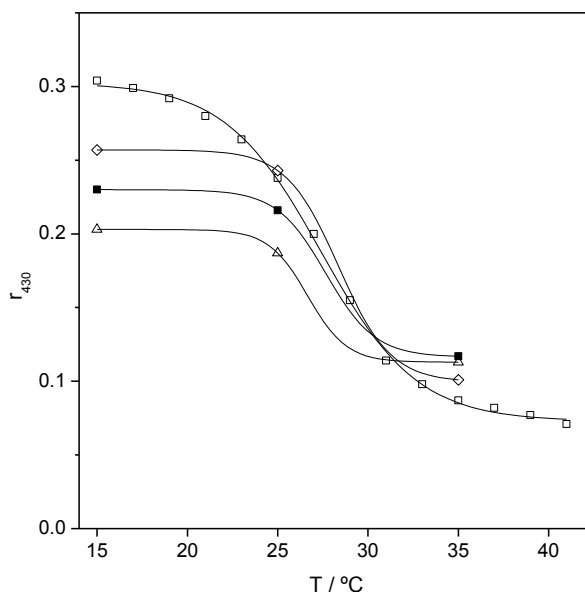

Figure 12. Fluorescence anisotropy at 430 nm (r_{430}) of DPH as a function of temperature for DODAB/DLPC liposomes in the absence (empty squares) and in the presence of DNA at various *L/D* ratios: empty up triangles, 2.8; solid squares, 5.1; and empty diamonds, 8.5. [DNA] = 0.051 mg/mL. Medium: aqueous HEPES 40 mM, pH = 7.4. Errors by light scattering are less than 3%. The inset shows r_{430} of DPH as a function of *L/D* ratio at two temperatures, T: solid down triangles, 15 °C (below T_m); and empty down triangles, 35 °C (above T_m). Dotted lines show anisotropy values for DODAB/DLPC liposomes in the absence of DNA.

Furthermore, lipofection efficiency is strongly correlated with stability, which is known to be quite influenced by membrane fluidity of lipoplexes. In the solid gel-like phase, the cationic lipid aggregates are not flexible enough to allow for efficient DNA interaction. At this respect, anisotropy measurements represent a very helpful tool to

characterize the potential efficacy of transfection process. Anisotropy levels of more than 0.2 are normally related with unstable liposomes and lipoplexes, while when phase transition to the fluid state is completed at smaller r, liposomes are supposed to be stable.[41] Considering the influence of the T_m on the fluidity and stability of lipoplex membrane, it should be emphasized the importance of the choice of the cationic and/or helper lipids based on T_m for optimal DNA transfection.

TABLE 2: Gel-to-fluid phase transition temperaturesfor
DODAB/DOPE-DNA and DODAB/DLPC-DNA lipoplexes
at various L/D ratios, including thecorresponding liposomes, i.e. $L/D = \infty$.

LIPOPLEX	L/D	T_m (ºC)
DODAB/DOPE-DNA[a]	∞[c]	18.9
	5.0	23.6
	6.5	24.1
	8.0	24.8
DODAB/DLPC-DNA[b]	∞[d]	27.9
	2.8	26.7
	5.1	27.7
	8.5	28.4

[a]Intersecting lines method. Precision of ± 0.5 ºC
[b]Inflexion point method. Precision of ± 0.2 ºC
[c]DODAB/DOPE liposome
[d]DODAB/DLPC liposome

Thus, it can be concluded that the conditions contributing to a better efficacy on lipofection process would be: (i) working at $T > T_m$; regarding the lipoplexes studied in this work, a temperature of 35 - 37

ºC (roughly the body temperature) would be adequate; (ii) DOPE helper lipid shows better properties than DLPC at $T < T_m$ (it is known that the introduction of unsaturation in the hydrocarbon chains of the lipids enhances the transfection capacities) but both would work more or less the same at 35 ºC (above T_m); and (iii) a marked effect of L/D ratio on the fluidity of the membrane has not been found, but, keeping in mind that only above $(L/D)_\phi$ the net charge of the lipoplex is favorably positive, it would be better to work at $L/D > (L/D)_\phi$.

F. Phase diagrams: Aggregation-disaggregation phenomena. Cryo-TEM micrographs have shown that DODAB/DOPE and DODAB/DLPC liposomes tend to form clusters of lipoplexes in the presence of DNA, within a certain concentration domain. Similar results were found by our group for other lipoplexes consisting of DOPE as helper lipid and other cationic lipids.[17,18] It is thus interesting to know and predict the concentrations of both liposome and polyelectrolyte at which this aggregation phenomena takes place, and, once the clusters are formed, their possible disaggregation into free lipoplexes. The aggregation-disaggregation model (or condensation/re-entrant condensation), explained in the theoretical background section, has then been applied for the first time to predict the phase diagrams of the lipoplexes studied in this work. Calculations for DSTAP/DOPE-DNA lipoplex, whose experimental characterization has been already reported by our group,[17] has been also included with the aim of analyzing the effect of changing the type of cationic lipid. Table 3 displays the input data required to solve eqs

3-4, in order to calculate the free parameters P_0 and E_0 for the three lipoplex systems, as well as the results obtained (last four lines). In particular, P is the DNA concentration used in the electrophoresis experiments, a is the average lipoplex radius estimated from cryo-TEM micrographs, q value is based on the 2700 bp fragments on average obtained from agarose gel electrophoresis experiments, Q is calculated from the surface area of the liposome and the estimated area for the headgroup of the lipid,[86] and the values of $S_a(P)$ and $S_d(P)$ are obtained from electrophoresis experiments (L/D = 3.3 and 6.0 for DODAB/DOPE-DNA; L/D = 4.3 and 4.9 for DODAB/DLPC-DNA; and L/D = 5.2 and 6 for DSTAP/DOPE-DNA). Although Nguyen and Shklovskii,[68,69] and Sennato *et al.*[50] claim that P_0 and E_0 are phenomenological parameters and it is difficult to assign them a real meaning on the basis of a microscopic theory, the results on Table 3 appear reasonable considering that the energy E_0 and P_0 are related to the strength of liposome-DNA binding and DNA concentration in equilibrium with the lipoplexes, respectively. Accordingly, taking into account that most of DNA molecules are forming complexes with liposomes, the total energy required for the complexes are formed (normalized by the thermal energy, k_BT) is much lower than 1, in agreement with the spontaneous complexation of DNA by liposomes observed in the experiments. It is also remarkable that the theory predicts very small and similar E_0 values for the three systems, which could be indicating that a change on liposome composition, either on the helper zwitterionic lipid (phosphathydilcholine vs. phosphathydilethanolamine) or on the cationic lipid (DODAB vs.

TABLE 3: Input parameters on the aggregation-disaggregation theory and results obtained (last four lines) for DODAB/DOPE-DNA, DODAB/DLPC-DNA and DSTAP/DOPE-DNA lipoplexes.

Parameter[a]	DODAB/DOPE-DNA	DODAB/DLPC-DNA	DSTAB/DOPE-DNA[b]
a / nm	35.0	30.5	38.5
10^{16} C / $(C^4\ J^{-2}\ m^{-1})$	3.056	2.663	3.361
Φ / (lipids/liposome)	42400	28400	48000
Q / (C/e)	12200	8350	13700
q / (C/e)	5400	5400	5400
10^{-15} P / (DNA segments/L)	17.16	17.16	17.16
10^{-15} $S_a(P)$ / (liposomes/L)	3.41	7.28	4.51
10^{-15} $S_d(P)$ / (liposomes/L)	6.20	8.29	5.20
10^{29} E_0 / (J)	0.46	4.65	5.05
10^8 E_0/kT	0.11	1.13	1.23
10^{-15} P_0 / (DNA segments/L)	5.46	5.06	4.76
10^{-15} $S_\phi(P)$ / (liposomes/L)	5.15	7.79	4.89

[a]a, liposome radius; C, liposome capacitance; Φ, number of lipids per liposome; Q, liposome charge; q, charge of DNA segment; P, DNA concentration; $S_a(P)$, liposome concentration at aggregation; $S_d(P)$, liposome concentration at disaggregation; E_0, DNA-liposome interaction energy; P_0, DNA concentration in equilibrium with lipoplexes; and $S_\phi(P)$, liposome concentration at isoneutrality

[b]Ref. 17

DSTAP), does not affect appreciably the interaction energy between DNA and liposomes. On the other hand, $P_0 << P$ in all cases, which agrees with the previous assumption consisting in that most of the DNA molecules are forming complexes.

Figure 13 shows the theoretical phase diagram for DODAB/DOPE-DNA lipoplexes (similar diagrams obtained for the other two lipoplexes are omitted for the sake of conciseness). The theory allows to predict the boundary values $S_a(P)$ and $S_d(P)$, for any value of DNA concentration, as well as the electroneutrality curves $S_\phi(P)$ (eq 5) at which the lipoplex charge inverts the sign. Assuming a constant value for E_0 and P_0, it is predicted that for $S < S_a(P)$, the complexes are stable due to the negative charge provided by the compacted DNA. As S increases, complexes experience aggregation and large aggregates or clusters of lipoplexes are formed. In this region of the diagram (between $S_a(P)$ and $S_d(P)$), the isoelectric point of the complexes $S_\phi(P)$ is reached and the electrophoretic mobility is expected to be zero. However, at this point the theory predicts that complexes attract more liposomes than those required to neutralize the negative charge.[68,69] As a result, if the $S > S_\phi(P)$, the systems undergo charge inversion. Finally, for $S > S_d(P)$, clusters tend to dissolve giving rise to a stable system formed by positively charged lipoplexes. The figure includes schematic drawings that try to illustrate the different type of lipoplexes predicted by the aggregation-disaggregation theory: (1) free lipoplexes in an excess of polyelectrolyte (net negative charge) at $S < S_a(P)$; (2) clusters of lipoplexes, at $S_a(P) < S < S_d(P)$; and (3) free lipoplexes in an excess of liposomes (net positive charge), at $S > S_d(P)$.
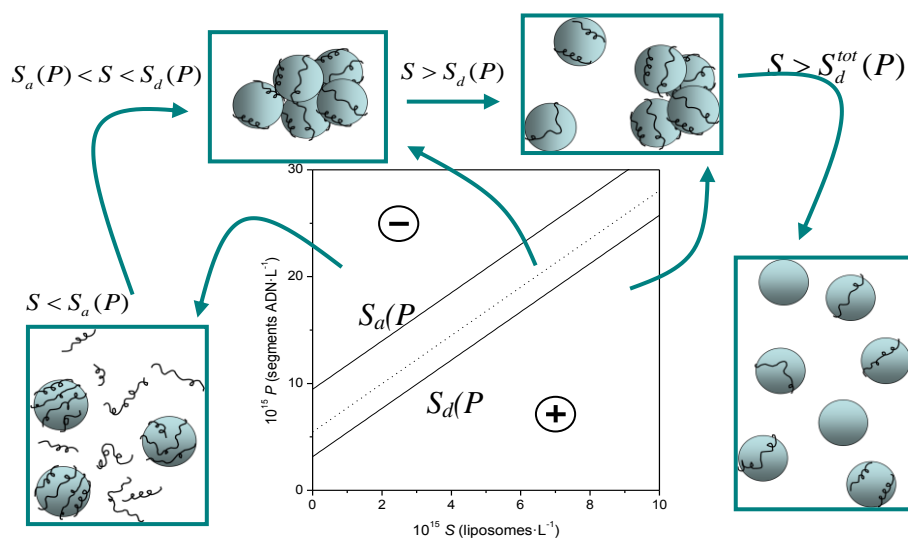
Figure 13. Phase diagram for DODAB/DOPE-DNA lipoplexes, according with aggregation-disaggregation theory (condensation/re-entrant condensation). Solid lines are $S_a(P)$ and $S_d(P)$, while dotted line is $S_\phi(P)$. Boxes are illustrative sketches: (1) isolated lipoplexes with net negative charge; (2) clusters of lipoplexes with net charge around or equal to zero (isoneutrality); and (3) isolated lipoplexes with net positive charge. Combining theory and cryo-TEM evidences, box (3') stands for clusters of lipoplexes in coexistence with isolated lipoplexes with net positive charge.

These results are mostly in good concordance with those ones obtained by cryo-TEM experiments. Thus, the micrographs taken below the isoneutrality (Figure 7) show isolated lipoplexes, as predicted by theory, but those ones above isoneutrality (Figure 9) show not only free lipoplexes (micrographs on right side), predicted as well by theory, but also clusters of lipoplexes in coexistence, with a wide variety of morphologies. It seems that the clusters formed at $S_a(P) < S < S_d(P)$ according to theory, persist at $S > S_d(P)$, according to the experiments. The persistence of aggregation of lipoplexes out of

the theoretical limits can be due, from our point of view, to the fact that $S_d(P)$ is, in fact, a minimum concentration for the clusters to disaggregate. In other words, it marks the beginning of the disaggregation (re-entrant condensation) phenomena, the minimum concentration from which there will be a liposome concentration range within clusters of lipoplexes and isolated lipoplexes coexist. This concentration range is that one studied on cryo-TEM experiments. It is possible and expectable that if S increases, a concentration that we call $S_d^{tot}(P)$ will be reached, from which all clusters of lipoplexes will disaggregate; however, the concentration range $S > S_d^{tot}(P)$ has not been analyzed from an experimental point of view in this work. A similar situation was described for mixed micellar systems,[87,88] constituted by cationic surfactants of one and two hydrocarbon chains; as long as total surfactant concentration increases in this kind of colloidal systems, a series of transition occurs: from free monomers to mixed vesicles, at the critical mixed vesicle concentration (*cvc**), from mixed vesicles to a mixture of mixed vesicles and mixed micelles in coexistence, at the critical mixed micelle concentration (*cmc**), and, finally, from this mixture to only mixed micelles at the total mixed micelle concentration (cmc_{tot}^{*}). This model came to complete the well-known three-stage model of Lichtenberg,[89,90] that only considered the global transition from mixed vesicles to mixed micelles at an unique *cmc**. Transferring this approach to the present case, it can be concluded that there is a transition from free lipoplexes with net negative charge to clusters of

lipoplexes at $S_a(P)$; another from these clusters to a mixture of them and isolated lipoplexes in coexistence (coming from partial cluster disaggregation), at $S_d(P)$; and, finally, from this mixture to only isolated lipoplexes with net positive charge, at $S_d^{tot}(P)$. Figure 13 also includes a drawing (see box 3') illustrating, together with boxes 1-3, the whole picture of transitions, those predicted by theory in conjunction with those either experimentally seen or proposed in this work, as an hypothesis. Of course, there can be another concomitant reason to explain why theory and experiment seems to disagree at $S > S_d(P)$: the own limitations of the models proposed by both Nguyen *et al*. and Sennato *et al*. The formers assumed that there is an interaction between small liposomes and big polyanions, while the other ones based their development in the interaction between liposomes that are much bigger than the polyanion. Considering the mean radius of DODAB/DOPE, DODAB/DLPC and DSTAP/DOPE liposomes (Table 3) it can be deduced by means of a simple calculation that the perimeters of the liposomes are smaller than the total contour length of the DNA herein used. As a consequence, DNA may surround the liposome surface around 4 or 5 turns, indicating that, although within Sennato's assumptions, the difference on the sizes of DNA and liposomes is not as high as assumed by the theory.

Figure 14 shows $S_a(P)$ and $S_d(P)$ boundary lines for the three lipoplexes studied, for comparison. It can be observed that for a given DNA concentration (draw an imaginary horizontal line) the boundary lines are shifted toward higher liposome concentrations in the order
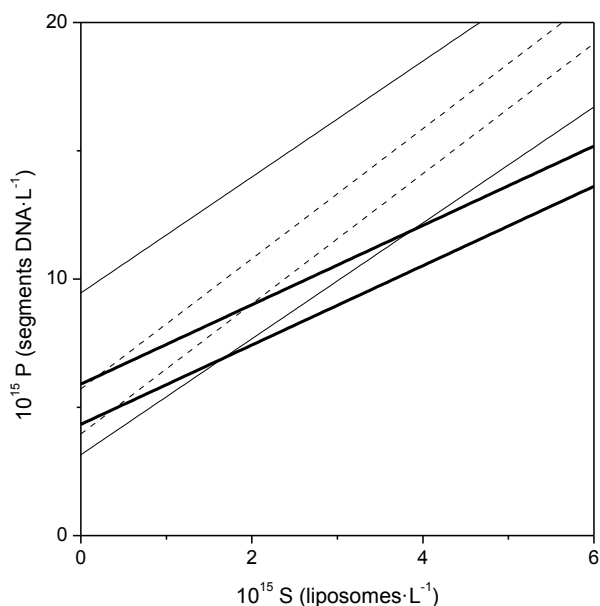
DODAB/DOPE–DNA < DSTAP/DOPE–DNA < DODAB/DLPC–
DNA.

Figure 14. Boundary concentration lines, $S_a(P)$ (up) and $S_d(P)$ (down), for DODAB/DOPE-DNA (thin solid lines), DSTAP/DOPE-DNA (dashed lines) and DODAB/DLPC-DNA (thick solid lines) lipoplexes, according with the aggregation-disaggregation theory.

This feature is in agreement with the fact that the bare charge of DODAB/DLPC is smaller than those ones estimated for DODAB/DOPE and DSTAP/DOPE. Consequently, those lipoplexes constituted by DOPE as a helper lipid require a lower number of liposomes to induce charge inversion, feature that may be quite advantageous since they may be less cytotoxic. The effect is even more pronounced if the cationic lipid is DODAB. These results,

consistent with those ones obtained with anisotropy experiments, point to DODAB/DOPE–DNA and DSTAP/DOPE–DNA (mainly the first one) as the gene transfer vehicles potentially most efficient (among those studied in this work). Accordingly, the efficiency of DOPE as a fusogenic lipid and as a gene transfer agent is widely documented on the literature related with gene therapy.[8,23-26,91,92]

Finally, as commented above, the theory also predicts the liposome concentration at the isoneutrality, $S_\phi(P)$. This concentration can be expressed in terms of mass ratio, $(L/D)_{\phi,theo}$, by means of:

$$\left(L/D\right)_{\phi,theo} = \frac{S_\phi(P)\Phi}{2P\overline{\Lambda}}\left(\frac{M_{L^+} + M_{L^0}}{M_{bp}}\right) \qquad (9)$$

where $\overline{\Lambda}$ is the average number of base pairs per DNA segment ($= 2700$ bp, agarose gel electrophoresis experiment) and Φ is the number of lipids per liposome (Table 3), calculated considering a lipidic bilayer with a thickness of $\sim$ 4.5 nm, polar headgroups with average surfaces of around 0.63, 0.70 and 0.68 nm^2 for DODAB/DOPE, DODAB/DLPC and DSTAP/DOPE liposomes, respectively,[86] and liposome surface areas of the spherical liposomes calculated by using the diameters found in cryo-TEM experiments. The values thus obtained (eq 9) for theoretical isoneutrality ratios are 5.0, 4.6 and 5.6 for the lipoplexes formed by DNA with DODAB/DOPE, DODAB/DLPC and DSTAP/DOPE liposomes,

respectively. It is remarkable the good concordance among theoretical, calculated (eq 6), and experimental results reported ere or previously determined in our laboratory[17] (see Table 1).

5. Conclusions

Experimental and theoretical studies prove that DODAB/DOPE and DODAB/DLPC cationic liposomes condense and compact DNA by means of a strong entropically driven interaction. The results reveal that the coulombic interaction of the weakly hydrated $-NH_3^+$ moiety of the PE headgroup with DNA, is more efficient than that one with the PC headgroup, since its three methyl groups are strongly hydrated and sterically hinders the electrostatic interaction of negatively charged phosphate residues of DNA and the sterically less shielded positive charges of DODAB. The isoneutrality of these lipoplexes, determined by zeta potential and EtBr intercalation assays, and also calculated, is reached when the lipid mass is around 4.7 times the DNA mass in both cases. DODAB/DOPE and DODAB/DLPC liposomes are mainly spherical and unilamellar with diameter of around 70 and 61 nm, respectively, a bilayer thickness of 4.5 nm and gel-to-fluid transition temperatures, T_m of 18.9 and 27.9 ºC, respectively. The presence of insaturations in the hydrophobic chains of the lipids fluidifies the membrane. These lipoplexes present a broad distribution of different morphologies as revealed by the cryo-TEM micrographs, from DNA-coated unilamellar lipoplexes, clusters of liposomes-DNA mediated, lipoplex nanostructures with thickened, flattened and deformed walls, and also multilamellar lipoplexes. The periodicity in these

multilamellar structures has been determined by digitizing and image processing techniques as being around 7 nm, indicating that DNA helixes are effectively sandwiched and aligned between cationic lipidid bilayers. Fluorescence anisotropy experiments have shown that DODAB/DOPE-DNA and DODAB/DLPC-DNA membranes are more fluid than those ones of the parent liposomes. Considering the importance of fluidity of the lipidic bilayer on the efficiency of the transfection process, and that a net positive charge on the lipoplex also favours its interaction with the negatively charged cellular membrane, it can be concluded that DODAB/DOPE-DNA and DODAB/DLPC-DNA lipoplexes are potentially efficient on transfecting cells when the mass of lipid is around 4-5 times that of DNA. The aggregation-disaggregation model has predicted the isoneutrality of both lipoplexes in very good concordance with experimental results. The model also predicts the aggregation of lipoplexes to form clusters, seen in cryo-TEM micrographs; however, to combine experimental and theoretical conclusions, a liposome concentration named $S_d^{tot}(P)$ has been proposed as the threshold concentration for the disaggregation or re-entrant condensation of these clusters. The theory also points to DODAB/DOPE as the most convenient liposome, among those studied in this work, to efficiently compact and transfer DNA. To conclude, all these factors, charge density of liposomes and lipoplexes, their structure, size and morphology, affinity of DNA-liposome interaction, and the fluidity of liposomes and lipoplexes membranes are closely related to the compaction of DNA, and, accordingly, they are key parameters on the transfection efficiency,

although *in vitro* and *in vivo* transfection essays would be necessary and welcomed to confirm all these findings.

Supporting Information Available: This section includes three tables with electrophoretic (Table S1) and fluorescente spectroscopic data (Tables S2 and S3), and three figures with the fluorescente deconvolutions (Fig. S1) and cryo-TEM images and analyzes (Figs. S2 and S3). This material is available free of charge via the Internet at http://pubs.acs.org.

References and Notes

(1) Felgner, J. H.; Gadek, T. R.; Holm, M.; Roman, R.; Chan, H. W.; Wenz, M.; Northrop, J. P.; Ringold, G. M.; Danielsen, M. *Proc. Nat. Acad. Sci., U.S.A.* **1987**, *84*, 7413.

(2) Felgner, P. L.; Heller, M. J.; Lehn, J. M.; Behr, J.-P.; Szoka, F. C. *Artificial Self-Assembling Systems for Gene Delivery*; American Chemical Society: Washington, DC, 1996.

(3) Mahato, R. I.; Kim, S. W. *Pharmaceutical Perspectives of Nucleic Acid-Base Therapeutics*; Taylor and Francis: London, 2002.

(4) Lasic, D. D. *Liposomes in Gen Delivery*; CRC Press: Boca Raton, FL, 1997.

(5) Ewert, K.; Slack, N. L.; Ahmad, A.; Evans, H. M.; Lin, A. J.; Samuel, C. E.; Safinya, C. R. *Curr. Med. Chem.* **2004**, *11*, 133.

(6) Lonez, C.; Vandenbranden, M.; Ruysschaert, J. M. *Progress in Lipid Research* **2008**, *47*, 340.

(7) Ma, B. C.; Zhang, S. B.; Jiang, H. M.; Zhao, B. D.; Lv, H. T. *J. Control. Release* **2007**, *123*, 184.

(8) Safinya, C. R.; Ewert, K.; Ahmad, A.; Evans, H. M.; Raviv, U.; Needleman, D. J.; Lin, A. J.; Slack, N. L.; George, C.; Samuel, C. E. *Phil. Trans. Royal Soc. A: Math. Phys. Eng. Sci.* **2006**, *364*, 2573.

(9) Kennedy, M. T.; Pozharski, E. V.; Rakhmanova, V. A.; MacDonald, R. C. *Biophys. J.* **2000**, *78*, 1620.

(10) Pozharski, E.; MacDonald, R. C. *Biophys. J.* **2003**, *85*, 3969.

(11) Rädler, J. O.; Koltover, I.; Salditt, T.; Safinya, C. R. *Science* **1997**, *275*, 810.

(12) Caracciolo, G.; Pozzi, D.; Caminiti, R.; Marchini, C.; Montani, M.; Amici, A.; Amenitsch, H. *J. Phys. Chem. B* **2008**, *112*, 11298.

(13) Dias, R. S.; Lindman, B. *DNA Interaction with Polymers and Surfactants*; Wiley & Sons: Hoboken, 2008.

(14) Ahmad, A.; Evans, H. M.; Ewert, K.; George, C. X.; Samuel, C. E.; Safinya, C. R. *J. Gene Medicine* **2005**, *7*, 739.

(15) Lin, A. J.; Slack, N. L.; Ahmad, A.; George, C. X.; Samuel, C. E.; Safinya, C. R. *Biophys. J.* **2003**, *84*, 3307.

(16) Farhood, H.; Serbina, N.; Huang, L. *Biochim. Biophys. Acta* **1995**, *1235*, 289.

(17) Rodriguez-Pulido, A.; Aicart, E.; Llorca, O.; Junquera, E. *J. Phys. Chem. B* **2008**, *112*, 2187.

(18) Rodriguez-Pulido, A.; Ortega, F.; Llorca, O.; Aicart, E.; Junquera, E. *J. Phys. Chem. B* **2008**, *112*, 12555.

(19) Lasic, D. D.; H., S.; Stuart, M. A. C.; R., P.; Frederik, P. *J. Am. Chem. Soc.* **1997**, *119*, 832.

(20) Barreleiro, P. C. A.; Olofsson, G.; Brown, W.; Edwards, K.; Bonassi, N. M.; Feitosa, E. *Langmuir* **2002**, *18*, 1024.

(21) Feitosa, E.; Alves, F. R.; Niemiec, A.; Oliveira, M.; Castanheira, E. M. S.; Baptista, A. L. F. *Langmuir* **2006**, *22*, 3579.

(22) Salvati, A.; Ciani, L.; Ristori, S.; Martini, G.; Masi, A.; Arcangeli, A. *Biophys. Chem.* **2006**, *121*, 21.

(23) Gustafsson, J.; Arvidson, G.; Karlsson, G.; Almgren, M. *Biochim. Biophys. Acta* **1995**, *1235*, 305.

(24) Xu, Y. H.; Hui, S. W.; Frederik, P.; Szoka, F. C. *Biophys. J.* **1999**, *77*, 341.

(25) Hirsch-Lerner, D.; Zhang, M.; Eliyahu, H.; Ferrari, M. E.; Wheeler, C. J.; Barenholz, Y. *Biochim. Biophys. Acta* **2005**, *1714*, 71.

(26) Zuidam, N. J.; Barenholz, Y. *Biochim. Biophys. Acta* **1998**, *1368*, 115.

(27) Janoff, A. S. *Liposomes: Rational Design*; Marcel Dekker: New York, 1999.

(28) Rosoff, M. *Vesicles*; Marcel Dekker: New York, 1996.

(29) Rädler, J. O.; Koltover, I.; Jamieson, A.; Salditt, T.; Safinya, C. R. *Langmuir* **1998**, *14*, 4272.

(30) Birchall, J. C.; Kellaway, I. W.; Mills, S. N. *Int. J. Pharm.* **1999**, *183*, 195.

(31) Lobo, B. C.; Rogers, S. A.; Choosakoonkriang, S.; Smith, J. G.; Koe, G. S.; Middaugh, C. R. *J. Pharm. Sci.* **2001**, *91*, 454.

(32) Eastman, S. J.; Siegel, C.; Tousignant, J.; Smith, A. E.; Cheng, S. H.; Scheule, R. K. *Biochim. Biophys. Acta* **1997**, *1325*, 41.

(33) Lakowicz, J. R. *Principles of Fluorescence Spectroscopy*; Kluwer Acad./Plenum: New York, 1999.

(34) MacDonald, R. C.; Ashley, G. W.; Shida, M. M.; Rakhmanova, V. A.; Tarahovsky, Y. S.; Pantazatos, D. P.; Kennedy, M. T.; Pozharski, E. V.; Baker, K. A.; Jones, R. D.; Rosenzweig, H. S.; Choi, K. L.; Qiu, R.; McIntosh, T. J. *Biophys. J.* **1999**, *77*, 2612.

(35) Tarahovsky, Y. S.; Koynova, R.; MacDonald, R. C. *Biophys. J.* **2004**, *87*, 1054.

(36) Bhattacharya, S.; Mandal, S. S. *Biochemistry* **1998**, *37*, 7764.

(37) Geall, A. J.; Eaton, M. A. W.; Baker, T.; Catterall, C.; Blagbrough, I. S. *FEBS Lett.* **1999**, *459*, 337.

(38) Borenstain, V.; Barenholz, Y. *Chem. Phys. Lipids* **1993**, *64*, 117.

(39) Hirsch-Lerner, D.; Barenholz, Y. *Biochim. Biophys. Acta* **1998**, *1370*, 17.

(40) Lentz, B. R.; Moore, B. M.; Barrow, D. A. *Biophys. J.* **1979**, *25*, 489.

(41) Regelin, A. E.; Fankhaenel, S.; Gurtesch, L.; Prinz, C.; von Kiedrowski, G.; Massing, U. *Biochim. Biophys. Acta* **2000**, *1464*, 151.

(42) Ryhänen, S. J.; Säily, M. J.; Paukku, T.; Borocci, S.; Mancini, G.; Holopainen, J. M.; Kinnunen, P. K. *Biophys. J.* **2003**, *84*, 578.

(43) Alfredsson, V. *Curr. Opin. Colloid Interface Sci.* **2005**, *10*, 269.

(44) Dias, R. S.; Lindman, B.; Miguel, M. G. *J. Phys. Chem. B* **2002**, *106*, 12600.

(45) Huebner, S.; Battersby, B. J.; Grimm, R.; Cevc, G. *Biophys. J.* **1999**, *76*, 3158.

(46) Mel'nikova, Y. S.; Mel'nikov, S. M.; Lofroth, J. E. *Biophys. Chem.* **1999**, *81*, 125.

(47) Scarzello, M.; Chupin, V.; Wagenaar, A.; Stuart, M. C. A.; Engberts, J. B. F. N.; Hulst, R. *Biophys. J.* **2005**, *88*, 2104.

(48) Silvander, M.; Edwards, K. *Anal. Biochem.* **1996**, *242*, 40.

(49) Smisterova, J.; Wagenaar, A.; Stuart, M. C. A.; Polushkin, E.; Brinke, G.; Hulst, R.; Engberts, J. B. F. N.; Hoekstra, D. *J. Biol. Chem.* **2001**, *276*, 47615.

(50) Sennato, S.; Bordi, F.; Cametti, C. *J. Chem. Phys.* **2004**, *121*, 4936.

(51) Sennato, S.; Bordi, F.; Cametti, C.; Di Biasio, A.; Diociaiuti, A. *Colloids Surf. A* **2005**, *270-271*, 138.

(52) Ciani, L.; Ristori, S.; Calamai, L.; Martini, G. *Biochim. Biophys. Acta* **2004**, *1664*, 70.

(53) Gonçalves, E.; Debs, R. J.; Heath, T. D. *Biophys. J.* **2004**, *86*, 1554.

(54) Hsu, W. L.; Chen, H. L.; Liou, W.; Lin, H. K.; Liu, W. L. *Langmuir* **2005**, *21*, 9426.

(55) Clamme, J. P.; Bernachi, S.; Vuilleumier, C.; Duportail, G.; Mély, Y. *Biochim. Biophys. Acta* **2000**, *1467*, 347.

(56) Even-Chen, S.; Barenholz, Y. *Biochim. Biophys. Acta* **2000**, *1509*, 176.

(57) Lleres, D.; Dauty, E.; Behr, J. P.; Mély, Y.; Duportail, G. *Chem. Phys. Lipids* **2001**, *111*, 59.

(58) Zuidam, N. J.; Hirsch-Lemer, D.; Margulies, S.; Barenholz, Y. *Biochim. Biophys. Acta* **1999**, *1419*, 207.

(59) Barreleiro, P. C. A.; Lindman, B. *J. Phys. Chem. B* **2003**, *107*, 6208.

(60) Mel'nikov, S. M.; Lindman, B. *Langmuir* **1999**, *15*, 1923.

(61) Junquera, E.; Arranz, R.; Aicart, E. *Langmuir* **2004**, *20*, 6619.

(62) Junquera, E.; Aicart, E. *Rev. Sci. Instrum.* **1994**, *65*, 2672.

(63) Junquera, E.; Aicart, E. *Int. J. Pharm.* **1999**, *176*, 169.

(64) Dubochet, J.; Adrian, M.; Chang, J. J.; Homo, J. C.; Lepault, J.; McDowall, A. W.; Schultz, P. *Q. Rev. Biophys.* **1988**, *21*, 129.

(65) Torreira, E.; Jha, S.; Lopez-Blanco, J. R.; Arias-Palomo, E.; Chacon, P.; C., C.; Ayora, S.; Dutta, A.; Llorca, O. *Structure* **2008**, *16*, 1511.

(66) Junquera, E.; Peña, L.; Aicart, E. *Langmuir* **1997**, *13*, 219.

(67) Rodriguez-Pulido, A.; Aicart, E.; Junquera, E. *Langmuir* **2009**, *25*, 4402.

(68) Nguyen, T. T.; Shklovskii, B. I. *J. Chem. Phys.* **2001**, *114*, 5905.

(69) Nguyen, T. T.; Shklovskii, B. I. *J. Chem. Phys.* **2001**, *115*, 7298.

(70) Delgado, A. V. *Interfacial Electrokinetics and Electrophoresis*; Marcel Dekker: New York, 2002; Vol. 106.

(71) Ohshima, H.; Furusawa, K. *Electrical Phenomena at Interfaces. Fundamentals, Measurements, and Applications*; Marcel Dekker: New York, 1998.

(72) Lobo, B. C.; Davis, A.; Koe, G.; Smith, J. G.; Middaugh, C. R. *Arch. Biochem. Biophys.* **2001**, *386*, 95.

(73) Congiu, A.; Pozzi, D.; Esposito, C.; Castellano, C.; Mossa, G. *Colloids Surf. B* **2004**, *36*, 43.

(74) Esposito, C.; Generosi, J.; Mossa, G.; Masotti, A.; Castellano, A. C. *Colloids Surf. B* **2006**, *53*, 187.

(75) Tarahovsky, Y. S.; Rakhmanova, V. A.; Epand, R. M.; MacDonald, R. C. *Biophys. J.* **2002**, *82*, 264.

(76) Caplen, N. J.; Alton, E. W.; Middleton, P. G.; Dorin, J. R.; Stevenson, B. J.; Gao, X.; Durham, S. R.; Jeffrey, P. K.; Hodson, M. E. *Nature Med.* **1995**, *1*, 39.

(77) Koltover, I.; Salditt, T.; Rädler, J. O.; Safinya, C. R. *Science* **1998**, *281*, 78.

(78) Keller, M.; Jorgensen, M. R.; Perouzel, E.; Miller, A. D. *Biochemistry* **2003**, *42*, 6067.

(79) Dias, R.; Antunes, F.; Miguel, M.; Lindman, S.; Lindman, B. *Braz. J. Med. Biol. Res.* **2002**, *35*, 509.

(80) Rosa, M.; Moran, M. D.; Miguel, M. D.; Lindman, B. *Colloids Surf. A* **2007**, *301*, 361.

(81) Boffi, F.; Bonincontro, A.; Bordi, F.; Bultrini, E.; Cametti, C.; Congiu-Castellano, A.; De Luca, F.; Risuleo, G. *Phys. Chem. Chem. Phys.* **2002**, *4*, 2708.

(82) Aljaberi, A.; Spelios, M.; Kearns, M.; Selvi, B.; Savva, M. *Colloids Surf. B* **2007**, *57*, 108.

(83) Zantl, R.; Baicu, L.; Artzner, F.; Sprenger, I.; Rapp, G.; Rädler, J. O. *J. Phys. Chem. B* **1999**, *103*, 10300.

(84) Leal, C.; Topgaard, D.; Martin, R. W.; Wennerstrom, H. *J. Phys. Chem. B* **2004**, *108*, 15392.

(85) Leal, C.; Sandstrom, D.; Nevsten, P.; Topgaard, D. *Biochim. Biophys. Acta* **2008**, *1778*, 214.

(86) Wiethoff, C. M.; Gill, M. L.; Koe, G. S.; Koe, J. G.; Middaugh, C. R. *J. Biol. Chem.* **2002**, *277*, 44980.

(87) del Burgo, P.; Aicart, E.; Junquera, E. *Colloids Surf. A* **2007**, *292*, 165.

(88) Junquera, E.; del Burgo, P.; Boskovic, J.; Aicart, E. *Langmuir* **2005**, *21*, 7143.

(89) Lichtenberg, D. *Biochim. Biophys. Acta* **1985**, *821*, 470.

(90) Lichtenberg, D.; Robson, R. J.; Dennis, E. A. *Biochim. Biophys. Acta* **1983**, *737*, 285.

(91) de Lima, M. C. P.; Simoes, S.; Pires, P.; Faneca, H.; Duzgunes, N. *Adv. Drug. Delivery Rev.* **2001**, *47*, 277.

151

(92) Hui, S. W.; Langner, M.; Zhao, Y.-L.; Ross, P.; Hurley, E.; Chan, K. *Biophys. J.* **1996**, *71*, 590.

EFFECT OF SURFACE CHARGE ON
COLLOIDAL CHARGE REVERSAL

A. Martin-Molina,[†] C. Rodríguez-Beas,[†] R. Hidalgo-Álvares[†] and M. Quesada-Pérez[‡]

[†]*Grupo de Física de Fluidos y Biocoloides, Facultad de Ciencias, Universidad de Granada, Campus de Fuentenueva, sn, 18071, Granada, Spain*

[‡]*Departamtento de Física, Escuela Politécnica Supérior de Linares, Universidad de Jaén, 23700 Linares, Jaén, Spain*

Abstract

The objective of this research work is to understand the effect of the surface charge density on the charge reversal phenomenon. To this end, we use experimental results and computer simulations. In particular, we measure the electrophoretic mobility of latex particles (macroions) in the presence of a multivalent electrolyte. We have focused on the electrolyte concentration range at which a reversal in the electrophoretic mobility is expected to happen. In particular, the role of the surface charge on the charge reversal process is looked into from several latexes with the same functional group but different surface charge densities. Although the mechanism responsible for the colloidal charge reversal is still a controversial issue, it is proved that ionic correlations are behind the appearance of such phenomenon (especially near the macroion surface). This conclusion can be inferred from a great variety of theoretical models. According to them, one of the factors that determine the charge reversal is the surface charge density of the macroions. However, this feature has been rarely analyzed in experiments. Our results appear therefore as a demanded survey to test the validity of the theoretical predictions. Moreover, we have also performed Monte Carlo simulations that take the ion size into account. The correlation found between experiments and simulations is fairly good. The combination of these techniques provides new insight into the colloidal charge reversal phenomena showing the effect of surface charge.

Introduction

Although considerable effort has been done in the last decades with the aim of comprehending how ions adsorb onto charged interfaces, the mechanism of such ion *condensation* is still under investigation.[1-4] The resulting structure of ions around a charged macroion is termed electric double layer (EDL). Obviously, this ionic distribution plays an important role in the stability and electrokinetic of electrostatically stabilized colloidal dispersions. This is the case for instance of DNA molecules dispersed in biological solutions. The basic model of planar EDL was developed by Gouy and Chapman (GC) more than ninety years ago. This classical model is in turn based on the Poisson-Boltzmann (PB) equation, which neglects the ion size. According to the GC model, the colloidal particles are smooth and uniformly charged planes immersed in a dielectric continuum comprised of mobile ions. Although this rudimentary description of a double layer is a very simple model to represent any real colloidal system, it may be reasonable when the electrolyte (mostly monovalent) concentration and the surface charge are low enough. However, the model fails if these conditions do not hold. For instance, in the presence of multivalent electrolyte, the colloid charge can become overcompensated and its effective charge is reverted. This phenomenon is called *charge reversal* (CR). Although in the literature the term charge reversal is also called *overcharging* or *charge inversion*,[3-5] some authors have recently defined these concepts elucidating the differences between them.[6] Accordingly, we will use

155

the term charge reversal along this work. From a theoretical point of view, the PB equation is not able to predict CR if the so-called *specific interactions* are not considered. On the contrary, a vast number of theories such as integral equations,[3,6-10] field-theoretic approaches,[11,12] one component plasma models (OCP)[1,2,13] have been put forward to describe this effect. All these theories have in common that they consider the correlations between ions as the responsible of the CR. Accordingly this phenomenon is expected to occur for highly charged macroions in the presence of multivalent ions. This feature is also predicted by computer simulations, which are frequently used to study the validity of the theoretical models.[14-28] In contrast to the enormous theoretical and simulations research works, CR has been scarcely studied from an experimental viewpoint. The lack of experimental studies is generally due to the technical difficulties found in dispersion with high concentrations of multivalent ions. Nevertheless, CR can be studied by means of electrophoresis experiments, where a reversed in the electrophoretic mobility (μ_e) is reported for charged colloids in a solution that contained multivalent ions.[29-38] AFM experiments performed by Besteman at al. have also provided very interesting results of CR,[39,40,41] and the survey on the different origins of charge inversion for phospholipids performed by Vaknin et al.[42,43] must be mentioned as well.

Although some technical aspects make difficult to perform systematic studies of CR (as stated above), the effect of the surface charge density on CR has already been previously studied in a preliminary paper.[31] However, the experimental systems employed

therein were diverse types of latexes, whose charge depended on the pH because their functional groups were weak acids. Given that some authors claim that the CR process occurred in this kind of systems can be due to chemical interactions between ions and the macroion surface groups (i. e. *specific adsorption*)[29], CR could not be unequivocally attributed to ion correlations appearing at high surface charge densities and neglected by the PB approach. In order to overcome this deficiency, we intend to study several latexes with the same strong acid surface groups but different surface charge density. Thus, differences in the mobility reversal of these systems can be clearly attributed to changes in ionic correlations with varying the surface charge density. Furthermore, in the previous work, the experimental data were analyzed with the integral equation theory termed hyper-netted-chain/mean-spherical approximation (HNC/MSA). However, Monte Carlo (MC) simulations have recently proved that the HNC/MSA theory can fail in the description of experimental data at high multivalent electrolyte concentration and/or high surface charge density,[21,24,38] which might lead to imprecise conclusions. Accordingly, our new experimental results are compared with MC simulations rather than with such theoretical predictions. In short, two aspects of the previous work on the surface charge effect are therefore improved in this survey: i) the experimental systems (replacing weak-acid latexes by a set of strong-acid latexes with different surface charge densities); ii) and the theoretical description of the electric double layer (replacing the integral equation approach by MC computations). The remainder of the work is organized as follows. In

the next section, some technical details of simulations are outlined. Next, the samples used for this study and the experimental technique are presented. Subsequently, the results are shown and discussed and some conclusions are finally highlighted.

Theoretical Background

In the MC simulations performed in this work, the planar EDL is described by a primitive model (PM) of electrolyte in which the plane wall is assumed to be smooth and uniformly charged whereas the ions are treated as charged hard spheres immersed in a dielectric continuum. The calculations have been carried out by using the Metropolis algorithm applied to a canonical ensemble for a collection of N ions confined in a rectangular prism (or cell) of dimensions $W \times W \times L$. The impenetrable charged wall is located at $z=0$ whereas at $z=L$ another impenetrable wall without charge is placed whereas periodic boundary conditions were used in the lateral directions (x and y). The cell contains the ionic mixture corresponding to the bulk electrolyte solution together with an excess of counterions neutralizing the surface charge. The interaction energy between mobile ions is given by

$$u(\vec{r}_{ij}) = \frac{Z_i Z_j e^2}{4\pi\varepsilon_0 \varepsilon_r r_{ij}} \qquad r_{ij} > d$$

$$u(\vec{r}_{ij}) = \infty \qquad r_{ij} < d$$

(1)

where d is the hydrated ion diameter, Z_i is the valence of ion i, e is the elementary charge, ε_0 is the permittivity of free space, ε_r (=78.5) the relative permittivity of the solvent (corresponding to water at a temperature of 298 K), $\vec{r}_{ij}$ is the relative position vector and $r_{ij} = \left| \vec{r}_{ij} \right|$ is the distance between ions i and j, whereas the interaction energy of ion i with the charged wall is

$$u(\vec{r}_i) = \frac{\sigma_0 Z_i e z_i}{2\varepsilon_0 \varepsilon_r} \tag{2}$$

where z_i is the z-coordinate of particle i, and σ_0 is the surface charge density of the charged wall.

The number of ions in each simulation was fixed, checking that the cell size was always large enough. Likewise, the systems were always thermalized before collecting data for averaging and the acceptance ratio was kept between 0.4 and 0.6.

Due to the long range of the electrostatic interactions, the energy must be evaluated very carefully. In these simulations, we have applied the so-called *external potential method* (EPM), in which each mobile ion is allowed to interact with the others in the MC cell according to the usual minimum image convention.[14,15,44] The remaining part (all charges outside the cell) is considered in the evaluation energy through an external potential, $\psi_{ext}(z)$. This function is calculated assuming that the ionic distribution profiles outside the cell are identical to those inside. Thus the external potential must be

updated during the simulation using the current ion profiles and is given by

$$\psi_{ext}(z) = \frac{1}{4\pi\varepsilon_0\varepsilon_r} \int_0^L \int_{\pm W/2}^{\pm\infty} \int_{\pm W/2}^{\pm\infty} \frac{\rho(z')}{\sqrt{(x')^2 + (y')^2 + (z'-z)^2}} dx'dy'dz' \quad (3)$$

where $\rho(z')$ is the charge density at z' (both outside and inside the cell). The integration over x' and y' can be performed analytically, whereas the integration over z' must be carried out numerically since the function $\rho(z')$ is tabulated. This is equivalent to considering the electrostatic potential generated by a set of infinite sheets of thickness dz' and surface charge density $\rho(z')dz'$ from which the central square 'hole' (of dimensions $W \times W$) is removed. The electrostatic potential of an *entire* infinite sheet can be calculated as in equation 5, whereas the electrostatic potential of the square hole removed from its center, which must be subtracted, can be calculated using the integral appearing in equation 16 of ref. 44. In a previous work,[21] the energy was also calculated by following an alternative method to the EPM, originally developed by Lekner for systems with 2D symmetries that has recently been improved by Sperb.[45,46] However, no significant differences were found in comparing with the EPM.

Having computed the local ion concentrations, the diffuse potential can be calculated from

$$\psi_d \equiv \psi(a) = \frac{e}{\varepsilon_r\varepsilon_0} \int_a^\infty (a - z)\sum_j Z_j\rho_j(z)dz \quad (4)$$

where $a=d/2$ is the hydrated ion radius and $\rho_j(z)$ is the local density of j-ions at a distance z from the charged surface ($j=1,2$ for counterions and coions, respectively). The integral appearing in equation 4 should be evaluated over an infinite interval, but this is not feasible in practice because computer simulations are always carried out in a box with a finite length (L). In order to take this aspect into account, it is usual to choose a cut-off distance (L_c) admitting that, theoretically, the contribution to such an integral is negligible (for $z > L_c$) if

$$\sum_{j=1,2} Z_j \rho_j(z) = 0$$. This is the condition of local electroneutrality, which can always be fulfilled far enough from the charged surface (in the solution bulk). Due to the term $(a-z)$, however, the fluctuations of $\sum_{j=1,2} Z_j \rho_j(z)$ (computed from simulations) could be considerably amplified, contributing appreciably to the integral of equation 7. To avoid this undesirable contribution L_c must not be too large. In our runs, we took $L_c = 0.5L$, and chose values for L trying to guarantee the electroneutrality condition at $0.5L$. The diffuse potential and its statistical error were computed by collecting many averages of ψ_d (according to equation 7) during the runs.

Experimental Section

As mentioned before, this research work is focused in the study of similar latexes that only differ in the surface charge density. The main properties of the systems are displayed in Table 1. The first two

systems (L1 and L2) were prepared by a two stage 'shot growth' emulsion polymerization process in absence of emulsifiers and subsequently, accordingly two styrene/sodium styrene sulfonate copolymers were obtained. The details of synthesis method are described in ref 47. In order to study similar systems with different surface charge, two other sulfonate latexes (L3 and L4) were provided by Ikerlat Polymers S.L. Table 1 shows the diameter and surface charge density of the latexes.

Table I: Particle diameter and surface charge density of the latexes.

Latex	Diameter (nm)	σ_0 (C m^{-2})
L1	186±6	-0.04
L2	85±1	-0.08
L3	507±5	-0.12
L4	505±6	-0.46

The particle sizes were obtained by photon correlation spectroscopy (PCS) whereas conductimetric and potenciometric titrations were used to determine the surface charge density. These experiments were performed with Crison instruments (pH-meter and conductimeter), at 25ºC in a stirred vessel flushed with nitrogen. Titration agents were NaOH and HCl (these titration techniques are illustrated in refs 31,32,48. As can be seen, the four latexes present different particle size and well differentiated values of σ_0, ranging from -0.04 Cm^{-2} (L1) to -0.46 Cm^{-2} (L4). Previous experiments show that differences in the particle size such as those found in these

systems do not involve changes in the electrophoresis data.[33] In contrast, differences in the surface charge allows us to study its effect in the electrophoretic behavior within one order of magnitude. In particular, μ_e is measured as a function of $La(NO_3)_3$. According to previous studies, this multivalent electrolyte enhances the CR process for salt concentrations that can be used straightforward in our electrophoresis experiments.[33-36,38]

The electrophoretic mobility measurements were performed by using a *ZetaPALS* instrument (Brookhaven, USA), which is based on the principles of phase analysis light scattering (PALS). The setup is especially useful at high ionic strengths and non-polar media, where mobilities are usually low. The PALS is able to measure values of μ_e at least two orders of magnitudes lower than traditional light scattering methods based on the shifted frequency spectrum (spectral analysis). Both techniques have in common the analysis of a mixing of scattered light from a suspension of colloidal particles moving in an electric field, with light directly from the source (reference beam light). The frequency of the scattered light is shifted by the Doppler Effect and its superposition with the *unshifted* reference one, leads to a beating at a frequency that depends on the speed of the particles. The problem arises when the particle velocity is low. For those cases, spectral analysis is not able to generate a complete cycle of the detected signal. However, phase analysis takes place over many cycles of the respective waveforms since the optical phase of the scattered light is characterized by means of the so-called the *amplitude-weighted phase difference* (AWPD) function instead of a simple correlation treatment.

163

This function improves the statistic behavior because the detected signal fluctuates in amplitude due to the relative movements of particles and concentration fluctuations. For a complete discussion of the PALS method and AWPD treatment, we refer the reader to refs 49 and 50.

Results and Discussion

In order to study the effect of charge, let us first evaluate the electrophoretic mobility for the four different latexes as a function of the salt concentration. In this way, changes in the electrokinetic behavior of the systems will be univocally related to differences of the surface charge densities. In particular, figure 1 shows μ_e as a function of the concentration of $La(NO_3)_3$. The most remarkable feature in these data is that CR is observed only for the two most charged latexes (L3 and L4). Before discussing this experimental finding in detail, let us outline some general aspects found in the figure. As can be seen, we may distinguish four features of the electrophoretic mobility as a function of electrolyte concentration: i) For salt concentrations smaller than 0.02 M, the magnitude of μ_e decreases (in all cases) as the electrolyte concentration increases. ii) Above 0.02 M, latexes L3 and L4 present mobility reversal, whereas the electrophoretic mobility measured for latexes L1 and L2 tends to be zero at high salt concentrations. iii) The latex of the greatest surface charge density, σ_0 = -0.46 Cm^{-2}, has an electrokinetic behavior quite similar to that found for σ_0 = -0.12 Cm^{-2}. iv) Once the reversal is reached, the inverted electrophoretic mobility seems to reach a saturation value.
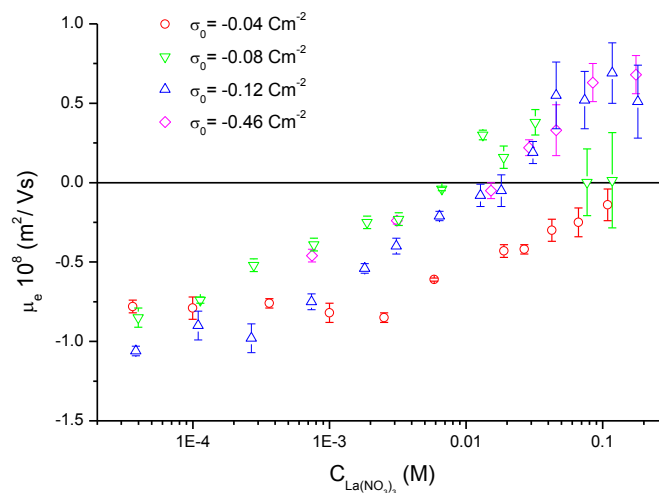
Figure 1: Experimental results: Electrophoretic mobility as a function of the concentration of $La(NO_3)_3$ for the four latexes shown in table 1.

From the two former observations, it is clearly deduced that the occurrence of CR depends fundamentally on the surface charge density. Only when the σ_0 is large enough (-0.12 Cm^{-2}, in this case), the sign of the mobility changes and remains positive. At this point it should be stressed that we admit that a mobility reversal is reached when all the measures at high salt concentrations exhibit a clear reversal in their sign. This criterion is used to distinguish from those cases, such as latex L2, where positive and negatives values of μ_e are observed. In general, alternating values (positive and negative) in the mobility indicates that the system is not stable under these conditions.

Accordingly, the fact that a clear CR is only found for elevated values of σ_0 and for high concentrations of $La(NO_3)_3$, implies that only the most charged systems could be electrostatically stabilized under this situation. This feature is apparently logical from a classical

point of view: the more surface charge, the more stable system. However, the surprising point is that under these conditions, the more charged systems are stable as a consequence of an effective surface charge that is positive. This aspect is not considered in the framework of classical EDL theories where an increasing of the ionic strength always results in electrostatic destabilization. Accordingly, our results suggest that colloidal systems with elevated surface charge densities can be electrically stabilized by the presence of high concentrations of multivalent electrolytes. When this situation occurs, the role of counterions and coions are exchanged as compared to their role at low salt concentration. This feature is predicted by many theoretical models as well as simulations, where the ionic profiles calculated exhibit non-monotonic behaviors (see for instance Figures 10-12 in ref 21). Therein, CR is justified in terms of ion-ion correlations, which become more important as the colloidal surface charge, valence and concentrations of counterions increase. As can be seen, such predictions are confirmed by our experiments. Furthermore, our measurements are also consistent with the theoretical predictions obtained by Pianegonda et al.[13] as well as with the simulations of Diehl and Levin.[51,52] In their OCP theory, the formers proved that the CR can take place if σ_0 is larger than a critical surface charge density (σ_c).[13] This feature is also predicted by MC simulations performed by Diehl and Levin. These authors calculated the ζ-potential as a function of σ_0 for a high concentration of 3:1 electrolyte (with and without 1:1 salt) in order to predict σ_c.[51,52] Moreover, in their most recent work, the authors show how σ_c strongly depends on the ionic size and on the

166

electrolyte concentration of multivalent electrolyte. Although their results qualitatively agree with our experiments, there are slight quantitative discrepancies. For instance, they predict that a reversal in the ζ-potential for surface charge densities larger than 0.05 Cm^{-2} when the 3:1 salt concentration is 0.1 M (see figure 1 in ref 52). A similar value for σ_c is predicted by the OCP theory of Pianegonda *et al.*[13]. However, according to our results, the mobility reversal is not expected to happen under these conditions. We think that there are two explanations for such apparent disagreement. On one hand, Diehl and Levin calculated the ζ-potential at a distance of one ionic diameter from the surface (instead of an ionic radius). On the other hand, the ion size used in their simulations was 0.3 nm whereas in the case of Pianegonda *et al.* the ion diameter was 0.4 nm. In both cases, the ion size is smaller than that expected for hydrated trivalent cations.[53,54] Accordingly, if these parameters (distance at which ζ-potential is calculated and the ion size) are modified, the agreement with our electrophoretic measurements could enhance.

Concerning the third aspect previously summarized, above $\sigma_0 = -0.12$ Cm^{-2} no differences are appreciated in systems more charged. This finding is also predicted by recent EDL theories and simulations. For instance MC simulations and the HNC/MSA predict this saturation effect in the electrokinetic potential as the surface charge density increases. Moreover, in some cases, the potential decreases when the surface charge is large enough (see Figure 14 in ref 21). Consequently, the data shown in Figure 1 provide an experimental

confirmation of some of the most relevant findings predicted theoretically.

In relation to the fourth characteristic of Figure 1, the idea of saturation in the CR is experimentally confirmed. Although this experimental feature had been previously reported by electrophoresis, it is still a controversial issue given that some theoretical approaches do not predict such saturation effect.[38]

To deepen into the understanding of the effect of the surface charge effect in the occurrence of CR, we have used MC simulations to calculate the diffuse potential as a function of the electrolyte concentration for several values of σ_0. The diffuse potential is intimately related to the ζ-potential, which is an essential quantity to characterize electrokinetic phenomena. In general, the conversion of the electrophoretic mobility into ζ-potential for colloidal particles is not a trivial matter because it involves a rather complex hydrodynamical problem. However, if the electrokinetic radius is large enough, the ζ-potential can be straightforwardly obtained from the Helmholtz – Smoluchowski (HS) approximation:

$$\mu_e = \frac{\varepsilon_0 \varepsilon_r \zeta}{\eta} \tag{5}$$

where η is the viscosity. The electrokinetic potential is often equated to the diffuse potential ($\zeta = \psi_d$). The most compelling argument for making this choice is the experimental evidence that colloidal interaction correlate well with theories if the diffuse layer is chosen as

the characterizing parameter.[55,56] Accordingly, under our experimental conditions we can assume that there is a lineal relationship between μ_e and ψ_d (i.e. equation 5).

Concerning the widely known approximation $\zeta \approx \psi_d$, it should also be mentioned that it is equivalent to assuming that the shear plane is located at one ionic radius from the surface. However, as commented above, Diehl and Levin suggest that the shear plane should rather be located at one ionic diameter.[51] This innovative idea presents two advantages (as compared to classical location of the shear plane): i) It takes the thermal fluctuations into account; ii) It overcomes the problems derived from the strong variation of the mean electrostatic potential over a length of one ionic diameter. However, the authors of this paper also admit that this definition is far from intuitive and should be checked by more detailed molecular dynamics simulations, including the explicit solvent.

Figure 2 shows the diffuse potential as a function of the concentration of $La(NO_3)_3$ for values of σ_0 in the range [-0.02 and -0.16] Cm^{-2}. As in previous works, an ion diameter of 0.90 nm obtained from the literature was chosen in the calculations for all the species.[53,54] As can be seen, the behavior of ψ_d is quite similar to that found for μ_e in Figure 1. A clear reversal is observed for σ_0 larger than -0.12 Cm^{-2} (in magnitude). Moreover, the electrolyte concentrations at which $\psi_d = 0$ and $\mu_e = 0$ are practically the same. In both cases it takes places at a concentration of $La(NO_3)_3 = 0.02$ M. In general, the experimental findings obtained from Figure 1, are confirmed by the

simulations. Even the ambiguous behavior found for the latex L2 is corroborated by the simulations. In Figure 1, it can be seen how this latex seems to undergo a mobility reversal but μ_e remains around zero above 0.02 M. This feature is qualitatively captured by simulations in Figure 2, where we can see how a very slight reversal for the highest salt concentration in the case of $\sigma_0 = -0.08$ Cm^{-2}.
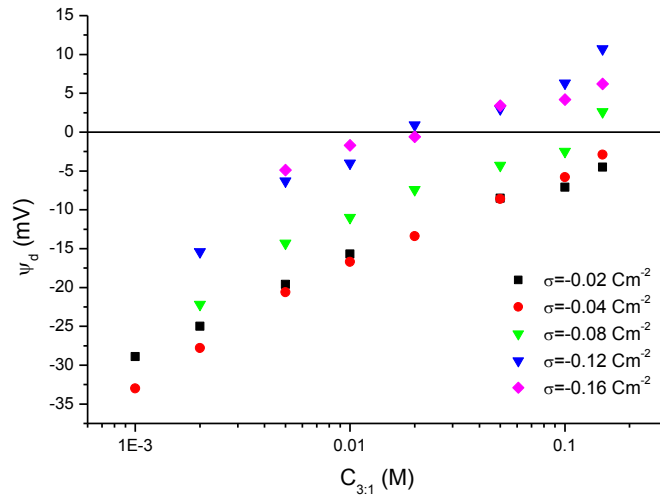

Figure 2: Diffuse potential calculated by MC simulations as a function of the concentration of 3:1 electrolyte for five different values of σ_0. A value of d=0.90 nm was chosen for the calculations.

In order to improve the comparison between figures 1 and 2, a double y-graph is shown as figure 3. Herein, we have selected two opposite situations in relation to the reversal point. In particular, we have plotted both the electrophoretic mobility (left axis) and diffuse potential (right axis) as a function of the surface charge density for two electrolyte concentrations.
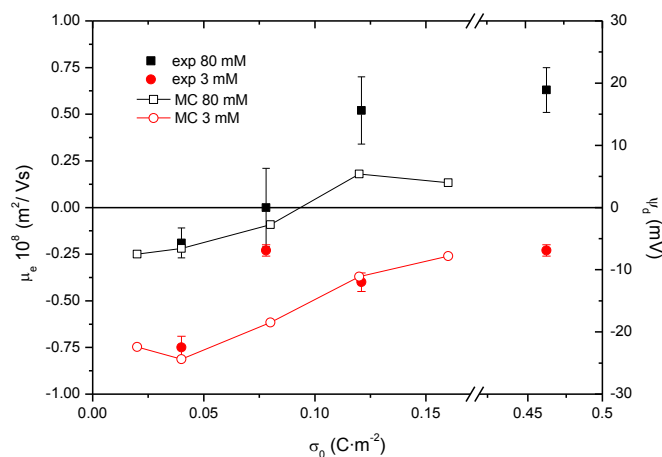
Figure 3: Comparison between experiments and simulations for two particular cases: low and high 3:1 salt concentrations. Symbols stand for μ_e measurements (solid circles and squares for 3 and 80 mM, respectively) whereas lines with symbols correspond to diffuse potentials predicted by simulations (open circles and squares for 3 and 80 mM, respectively).

On one hand, we have chosen a low salt concentration of 0.003 M at which CR never takes place. On the other, the situation at $La(NO_3)_3 = 0.08$ M is also shown. In this case, a CR clearly occurs for high surface charge densities. From this figure, significant features can be deduced. Firstly, the diffuse potential calculated by MC simulations and electrophoretic mobility experimentally measured exhibit a similar behavior as a function of the surface charge density. Also, these results confirm the fact that CR is propitiated when the multivalent electrolyte concentration and the surface charge density are large enough. Finally, the results also confirm that the CR reaches a saturation value for elevated salt concentration and high surface charge densities. These findings are very important towards the

understanding of CR and provide an original quantification of the role played by the surface charge.

Conclusions

We have investigated the role of the surface charge density in the colloidal charge reversal by a double experimental and simulation study that provides unique insight into this phenomenon. In particular we have studied four latexes of similar functional groups, but different surface charge densities. Furthermore, a model of EDL based on a PM of electrolyte has been analyzed by MC simulations. Accordingly, we have studied the variation of the experimental mobility and the diffuse potential calculated from simulations, as a function of $La(NO_3)_3$ concentration. In both cases we have found similar tendencies. The CR is reached for σ_0 above 0.12 C m^{-2} and electrolyte concentrations larger than 0.02 M. This finding corroborates some of the theoretical predictions addressed by sophisticated EDL models that have not been properly tested from an experimental point of view. In this sense, our experiments and simulations also confirm that once CR takes place, it saturates. In other words, values of μ_e and ψ_d reach a saturation situation when the surface charge density and multivalent electrolyte concentration are large enough.

Acknowledgments

References

(1) Levin, Y. *Rep. Prog. Phys.* 2002, *65*, 1577.

(2) Grosberg, A. Y.; Nguyen, T. T.; Shklovskii B. I. *Rev. Modern Phys.* 2002, *74*, 329.

(3) Quesada-Pérez, M.; González-Tovar, E.; Martín-Molina, A.; Lozada-Cassou, M.; Hidalgo-Álvarez, R. *ChemPhysChem*. 2003, *4*, 234.

(4) Lyklema, J., *Colloids Surf. A* 2006, *291*, 3.

(5) Lenz, O.; Holm, C. *Eur. Phys. J. E* 2008, *26*, 191.

(6) Jiménez-Ángeles, F.; Lozada-Cassou, M. *J. Phys. Chem. B* 2004, *108*, 7286.

(7) Lozada-Cassou, M.; Saavedra-Barrera, R.; Henderson, D. *J. Chem. Phys.* 1982, 77, 5150.

(8) González-Tovar, E.; Lozada-Cassou, M. *J. Phys. Chem.* 1989, 93, 3761.

(9) Kjellander, R. *Ber. Bunsenges. Phys. Chem.* 1996, 100, 894.

(10) Greberg, H.; Kjellander, R. *J. Chem. Phys.* 1998, 108, 2940.

(11) Netz, R.R.; Orland, H. *Eur. Phys. J. E* 2000, *1*, 67.

(12) Moreira, A. G.; Netz, R. R. *Eur. Phys. J. E* 2002. *8*. 33.

(13) Pianegonda, S.; Barbosa, M. C.; Levin, Y. *Europhys. Lett.* 2005, *71*, 831.

(14) van Megen, W.; Snook, I. *J. Chem. Phys*. 1980. *73*. 4656.

(15) Torrie, G. M.; Valleau, J. P. *J. Chem. Phys.* 1982. *86*. 3251.

(16) Mier-y-Teran L.; Suh S. H.; White H. S.; Davis H. T. *J. Chem. Phys.* 1990, 92, 5087.

(17) Degrève, L.; Lozada-Cassou, M.; Sánchez, E.; González-Tovar, E. *J. Chem. Phys.* 1993. *98*. 8905.

(18) Boda, D.; Fawcett, W. R.; Henderson, D.; Sokolowski, S. *J. Chem. Phys.* 2002, 116, 7170.

(19) Bhuiyan, B.; Outhwaite C. W. *Phys. Chem. Chem. Phys.* 2004, 6, 3467.

(20) Valiskó, M; Henderson, D.; Boda, D. *J. Phys. Chem. B* 2004. *108*. 16548.

(21) Quesada-Pérez, M.; Martín-Molina, A.; Hidalgo-Álvarez, R. *J. Chem. Phys.* 2004. *121*. 8618.

(22) Quesada-Pérez, M.; Martín-Molina, A; Hidalgo-Álvarez, R. *Langmuir* 2005, *21*, 9231.

(23) Henderson, D.; Gillespie, D.; Nagy, T.; Boda, D. *J. Chem. Phys.* 2005, *122*, 084504.

(24) Martín-Molina, A.; Quesada-Pérez, M.; Hidalgo-Álvarez, R. *J. Phys. Chem. B* 2006, *110*, 1326.

(25) Martín-Molina, A.; Maroto-Centeno, A.; Hidalgo-Álvarez, R.; Quesada-Pérez, M. *J. Chem. Phys.* 2006, *125*, 144906.

(26) Madurga, S.; Martín-Molina, A.; Vilaseca, E.; Mas, F.; Quesada-Pérez, M. *J. Chem. Phys.* 2007, *126*, 234703.

(27) Faraudo, J.; Travesset, A. *J. Phys. Chem. C* 2007, *111*, 987.

(28) Ibarra-Armenta, J. G.; Martín-Molina, A.; Quesada-Pérez, M. *Phys. Chem. Chem. Phys.* 2009, *11*, 309.

(29) Ottewill, R. H.; Shaw, J. N. *J. Colloid Interface Sci.* 1968, *26,* 110.

(30) Elimelech, M.; O'Melia, C. R. *Colloid Surf.* 1990, 44, 165.

(31) Martín-Molina, A.; Quesada-Pérez, M.; Galisteo-González, F.; Hidalgo-Álvarez, R. *J. Phys. Chem. B* 2002, *106*, 6881.

(32) Quesada-Pérez, M.; Martín-Molina, A.; Galisteo-González, F.; Hidalgo-Álvarez, R. *Mol. Phys.* 2002, *100*, 3029.

(33) Martín-Molina, A.; Quesada-Pérez, M.; Galisteo-González, F.; Hidalgo-Álvarez, R. *J. Chem. Phys.* 2003, 118, 4183.

(34) Martín-Molina, A.; Quesada-Pérez, M.; Galisteo-González, F.; Hidalgo-Álvarez, R. *Colloid Surf. A* 2003, *222*, 155.

(35) Martín-Molina, A.; Quesada-Pérez, M.; Galisteo-González, F.; Hidalgo-Álvarez, R. *J. Phys. Condens. Matter* 2003. *15*. S3475.

(36) Quesada-Pérez, M.; González-Tovar, E.; Martín-Molina, A.; Lozada-Cassou, M.; Hidalgo-Álvarez, R. *Colloid Surf. A* 2005, *267*, 24.

(37) Lyklema, J.; Golub, T. *Croat. Chem. Acta* 2007, *80*, 303.

(38) Martín-Molina, A.; Maroto-Centeno, A.; Hidalgo-Álvarez, R.; Quesada-Pérez, M. *Colloid Surf. A* 2008, *319*, 103.

(39) Besteman, K.; Zevenbergen, M. A. G.; Heering, H. A.; Lemay, S.G. *Phys. Rev. Lett.* 2004, 93, 170802.

(40) Besteman, K.; Zevenbergen, M. A. G.; Lemay, S.G. 2005 *Phys. Rev. E* 72 061501

(41) Besteman, K.; van Eijk, K.; Lemay, S. G. *Nature Physics* 2007, *3*, 641.

(42) Vaknin, D.; Kruger, P.; Losche, M. *Phys. Rev. Lett.* 2003, *90*, 178102.

(43) Pittler, J.; Bu, W.; Vaknin, D.; Travesset, A.; McGillivray, D.J.; Lösche, M. *Phys. Rev. Lett.* 2006, *97*, 046102.

(44) Jönsson, B.; Wenneström, H.; Halle, B. *J. Phys. Chem.* 1980. *84*. 2179.

(45) Lekner, J. *Phys. A* 1991. *176*. 485.

(46) Sperb, R. *Mol. Simul.* 1998. *20*. 179.

(47) De Las Nieves, F. J.; Daniels, E. S.; El-Aasser, M. S. *Colloids Surf.* 1991, *60*, 107.

(48) Bastos, D.; De Las Nieves, F. J. *Colloid Polym. Sci.* 1993, *271*, 870.

(49) Miller, J. F.; Schätzel, K.; Vincent, B. *J. Colloid Interface Sci.* 1991, 143, 532.

(50) Mcneil-Watson, F.; Tscharnuter, W.; Miller, J. F. *Colloid Surf. A* 1998, 140, 53.

(51) Diehl, A; Levin, Y. *J. Chem. Phys.* 2006. *125*. 054902.

(52) Diehl, A; Levin, Y. *J. Chem. Phys.* 2008. *129*. 124506.

(53) Marcus, Y. *Ion Solvation*, John Wiley and Sons, Chichester, 1985.

(54) Israelachvili, J. *Intermolecular And Surface Forces (2nd Ed.)*; Academic Press: London, 1992.

(55) Lyklema, J. *Solid/liquid dispersions,* Academic Press: London, 1987.

(56) Elimelech, M.; Gregory, J.; Jia, X.; Williams, R. *Particle Deposition & Aggregation. Measurement, Modelling and Simulation*, Butterwoth Heinemann, Amsterdam, 1995.
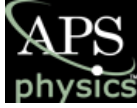
CHARGE REVERSAL IN ANIONIC LIPOSOMES:
EXPERIMENTAL DEMOSTRATION AND
MOLECULAR ORIGIN

A.Martin-Molina,[1] C. Rodríguez-Beas[1] and J. Faraudo[2]

[1]*Grupo de Física de Fluidos y Biocoloides, Dept. de Física Aplicada Universidad de Granada, 18071, Granada, Spain*
[2]*Institut de Ciència de Materials de Barcelona (ICMAB-CSIC), Campus de la UAB, E-08193 Bellaterra, Spain*

Abstract

We present experimental and simulation evidence for a new mechanism of charge reversal operating only for ions capable to penetrate into soft interfaces. It is based on the preferential solvation of counterions by amphiphilic molecules and hydration water rather than by bulk water. This mechanism does not require high surface charge densities and it is not affected by the addition of 1:1 salt. This behavior is opposite to that observed in systems as diverse as microfluidic channels or latex colloids. The robustness of the mechanism to physiological amounts of 1:1 salt suggests a significant impact in processes involving ion-amphiphile interaction in salty water (typical e.g. of biophysics).

The interaction of interfaces with electrolyte is of key importance in determining physico-chemical properties and functionality of systems as diverse as macromolecules, colloids, membranes or microfluidic devices [1]. The case in which the counterions are multivalent is attracting a great deal of experimental and theoretical interest due to their ability to induce complex and rich new phenomena [2-4]. A paradigmatic example is the charge reversal phenomenon (also known as overcharging or charge inversion) in which counterions are attracted to a charged interface in excess of its own bare charge [2,5]. The driving force for this counterintuitive phenomenon is still subject to debate [5,6], but there is strong evidence supporting the view that ion-ion correlations play a major role [2]. Calculations including ion-ion correlations are consistent with the concentrations of multivalent counterions required to obtain charge inversion in DNA [7], silica nanochannels [8], latex colloids [9] and calcium silicate hydrate nanoparticles [10]. According to the ion-ion correlation mechanism, charge reversal shows two outsanding features. First, it is found only for highly charged surfaces [2,11] and secondly, the effect is strongly weakened after addition of background 1:1 electrolyte [12] (as demonstrated both by experiments [8,13] and computer simulations [14,15]).

A common feature in all these previous experimental examples of charge reversal is that ions are able to accumulate at the solid/liquid interface but being always restricted to be in the water phase (i.e. they are unable to penetrate into the solid phase). The situation is different in the case of interfaces such as those found in Langmuir monolayers,

membranes, liposomes and nanoparticles or colloids functionalized with surfactants. Experimental techniques [16-18], reveal that in these cases, small ions are able to penetrate to the nonaqueous side of the interface. As a consequence, the phenomenology of ionic interactions observed in these systems highly depends on the structural or chemical details of the system [19-21], so current models of charge reversal (based on general features of ion-ion correlations) cannot be applied [6]. Our objective in this Letter is to identify (by combining electrophoretic measurements and MD simulatons) a different mechanism for charge reversal in these systems (soft interfaces). As we will see, this mechanism is clearly distinguishable from ion-ion correlations since it is robust to physiological concentrations of added background 1:1 electrolyte and it does not require high surface charge.

The experimental systems considered in this work will be liposomes based either on anionic phosphatidylserine (PS$^-$) or zwitterionic phosphatidylcoline (PC) lipids (see the chemical formula in Fig. 1). Both lipids are extremely important in industrial applications (drug delivery systems, nanoreactors,...) and biophysics [22]. They are the most abundant lipids of the plasma membrane, giving rise to the major contribution to its surface potential [23].

Let us first discuss our experimental and simulation results for PS$^-$ liposomes (the preparation of the liposomes is described in full detail in the accompanying EPAPS material [24]). The electrophoretic mobility of the liposomes at 25ºC was measured with a *ZetaPALS* apparatus (Brookhaven Instruments, USA) as a function of La(NO$_3$)$_3$ concentration both in absence of background electrolyte and with 100

mM of added $NaNO_3$. All experiments were made at pH = 5.4 so the PS^- molecule had a total charge of $-e$ (PS^- has three charged groups with pKa = 1, 3.6 and 9.8) and La cations had $+3e$ charge since they are not significantly hydrolyzed (La has a hydrolysis constant K_H of $\log_{10} K_H \approx 8.6$ [25]).

We observe (see Fig.1) that in both cases electrophoretic mobility reverses its sign at $[La(NO_3)_3] \approx 10^{-4}$ M, i.e., charge reversal is observed at low concentrations of trivalent counterions. The effect of the 1:1 salt is typical of an indifferent electrolyte (see curve I of Fig. 6.8 of Ref. [26]): it reduces the absolute value of the mobility leaving the point of zero mobility unaltered.
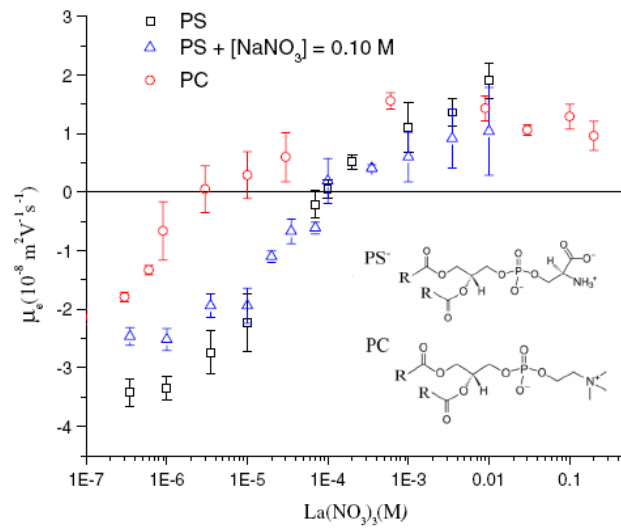

FIG. 1 Electrophoretic mobility μ_e of PS^- and PC liposomes as a function of $[La(NO_3)_3]$. Squares correspond to PS^- (no background electrolyte), triangles to PS^- with 100 mM of $NaNO_3$ as a background electrolyte and circles correspond to PC (no background electrolyte). Inset: Chemical structures of the PS^- and PC lipids.

This result is opposite to that obtained for negatively charged latex microspheres [11,13], which are a classical model system for colloidal behavior. Charge reversal is observed at $[La(NO_3)_3]$ between 10–20 mM in absence of background electrolyte. After addition of $[NaNO_3] = 0.1$ M, a completely different behavior is observed. For $[La(NO_3)_3] < 20$ mM, the mobility is higher than that observed in absence of background electrolyte, and strongly decreases (being essentially zero) for larger $La(NO_3)_3$ concentrations (no charge reversal can be identified). This behavior observed for latexes, is typically expected for charge reversal induced by the ion-ion correlation mechanism mentioned above, as demonstrated by Monte Carlo simulations [14,15]. In the ion-ion correlation mechanism, the condensation of trivalent cations at the negative latex interface is weakened by the added 1:1 electrolyte thereby producing a larger mobility. It is clear that in this case, the 1:1 electrolyte plays a very active role not being the simple screening of interfacial charge found in our PS$^-$ liposomes.

It has to be noted that the extremely low value for the charge reversal concentration obtained in Fig. 1 can be attributed to the high valency of La^{3+}. In previous systematic electrophoresis experiments of PS$^-$ considering salts of different divalent cations [27] it was found that the point of zero mobility was very difficult to attain and charge reversal was barely noticeable for concentrations larger than 0.1M (with only slight differences between different cations following the sequence $Ba^{2+} > Ca^{2+} > Mg^{2+}$). Since these experiments were done using background electrolyte ([NaCl] = 100 mM), we have repeated

182

the experiments in absence of added 1:1 salt, obtaining essentially the same results [28].

In order to obtain a molecular picture of the cation-PS$^-$ interaction, we have performed all-atomic molecular dynamics simulations (MD) in the NPT ensemble of a fully hydrated phosphatidylserine (PS$^-$) bilayer in contact with La^{3+} neutralizing counterions. Our simulation box contains 14700 atoms from a membrane with 128 PS$^-$ molecules distributed in two leaflets (as in previous simulations, see [29]), 2624 water molecules and enough counterions to ensure charge neutrality (42 La^{3+} and 2 Na$^+$). As a model for the La^{3+} ion, we employed the force field developed in [30] which reproduces correctly the hydration structure and free energy of the cation. All other technical details concerning molecular models, force fields, algorithms, parameters and equilibration procedure are the same as reported in previous simulations of hydrated PS membranes [29] except otherwise stated. Our production run was of 10 ns preceded by an equilibration run of 4 ns. The simulations were performed using the *DLPOLY2* package [31] running in parallel using 64 PowerPC processors during 376 hours.

The main results are as follows. We have obtained a mean area per phospholipid of $a_p = 55.4$ Å^2, in agreement with the results obtained in [29] with Na$^+$ as the counterion. The La^{3+} cations, uniformly distributed in the initial configuration (before the equilibration run), are observed to condense to the negatively charged bilayer membrane, i.e., all La^{3+} counterions contain at least one oxygen atom from PS molecules in their first coordination shell,

implying binding to the bilayer. In Fig. 2 we show the distribution of electronegative atoms (oxygen atoms from lipid molecules and water molecules) around adsorbed La^{3+} ions.

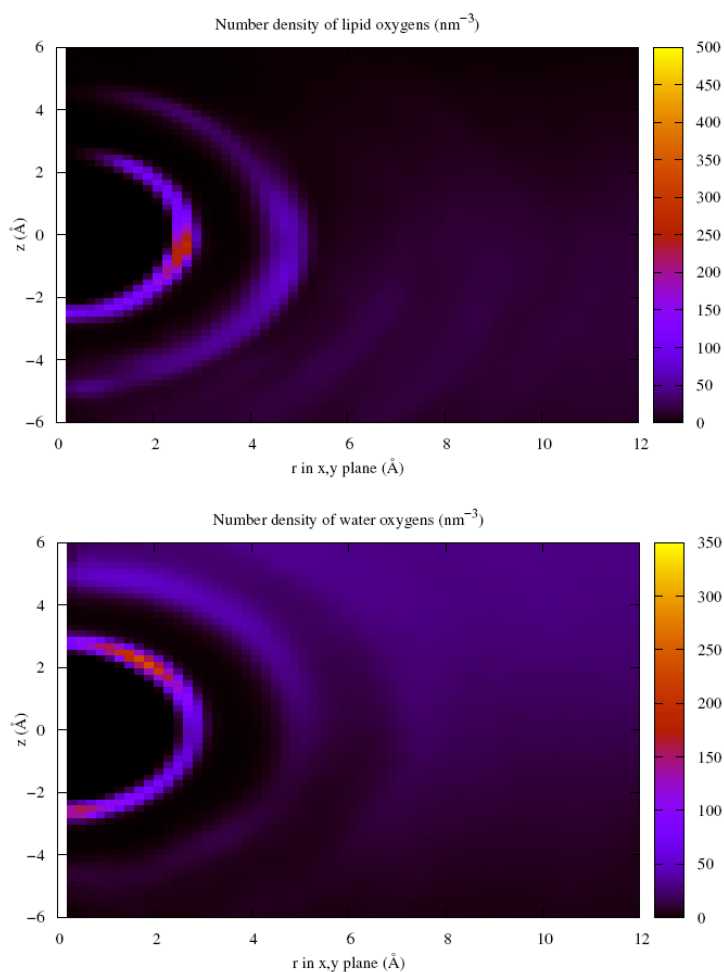**FIG. 2** Structure of the interface near adsorbed La^{3+} counterions from MD simulations. (a) Particle density (atoms/nm^3) of oxygen atoms from PS$^-$ molecules around adsorbed La^{3+} cations. The cylindrical coordinates r, z centered at the adsorbed ions are defined so that z is negative towards the membrane interior and positive towards the bulk water; (b) Same as (a) but for oxygen atoms from water molecules.

Note the nearly isotropic distribution of oxygen atoms from either PS or water molecules around La^{3+}, although there is a slight tendency of finding more lipid oxygens towards the membrane interior and more water oxygens towards the aqueous region. Integration of the density distributions up to the first minimum gives the average coordination numbers. On average, the first coordination shell of La^{3+} contains 4.95 ± 0.01 oxygen atoms from phospholipids. These oxygen atoms come from 2 or 3 phosphate groups from different PS^- molecules. Also, the first coordination shell of La^{3+} contains an average of 4.17 ± 0.01 oxygen atoms from water molecules (for La^{3+} in bulk TIP3P water the coordination number is 10 [30]). In Figure 3 we show several density profiles averaged over the *xy* plane as a function of *z*. The distributions for both La^{3+} cations and oxygen atoms from PS have very similar shapes, with a peak at 2 nm from the center of the bilayer and a thickness of ~ 1 nm. The cations are typically embedded by oxygen atoms from lipids, as can be seen in the snapshot shown as an inset in Fig. 3. This region containing La^{3+} and lipid headgroups is substantially hydrated, with interfacial water with a density about half the density of bulk water (see Fig. 3). Overall, the results shown in Figs. 2 and 3 (also see additional figures in the EPAPS material [24]) demonstrate that La^{3+} cations are incorporated deep inside the hydrophilic region containing the headgroups and interfacial water. This prediction of MD simulations can in principle be tested by surface sensitive anomalous x-ray experiments, which allow the identification of the environment of ions at interfaces [32].
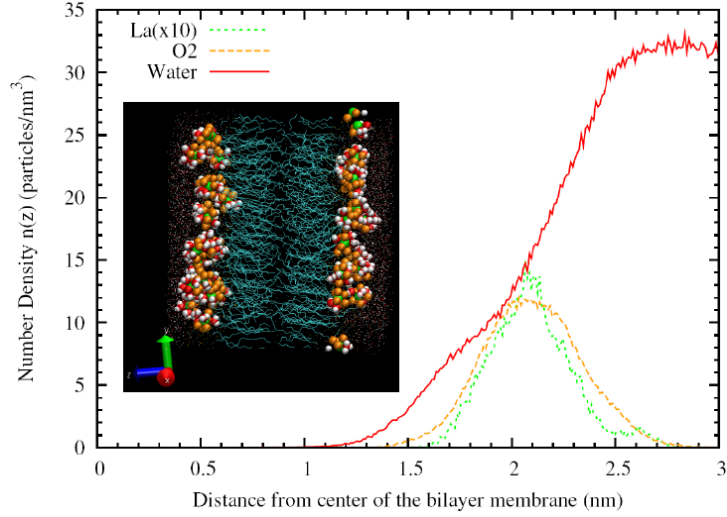
FIG. 3 Average density profile of different species as a function of the z coordinate (perpendicular to the membrane) obtained from MD simulations. Solid line: water density (molecules/nm^3), dashed line: oxygen atoms of O2 type from PS$^-$ molecules (atoms/nm^3), dotted line: number density of La^{3+} cations (ions/nm^3) multiplied by a factor 10 for clarity. Inset: snapshot from MD simulations showing the oxygen lipids, La ions and hydration water and the other atoms as lines.

Our simulation results can be interpreted in physico-chemical terms by saying that small metal ions are preferentially solvated by oxygen atoms from lipids and interfacial water rather than bulk water, thereby penetrating inside the region containing the interfacial charges. The free energy involved in this preferential solvation can be estimated as follows. At the point of zero electrophoretic mobility, the charge of the liposomes is balanced by multivalent counterions of charge q_c distributed across a layer of thickness δz (see Fig. 3) with a typical concentration $\approx e/(q_c a_p dz)$. Outside the membrane, there is an approximately uniform concentration c_0 of counterions (recall that we are considering the zero mobility point), so the free energy difference

per adsorbed La^{3+} ion is $\Delta\mu = k_B T ln[c_0 \backslash dz a_p q_c/e] \approx -9k_B T$ (we used q_c = 3+e, δz = 1 nm and $c_0 \approx 10^{-4}$ M = 6x10^{-3} ions/nm^3).

In view of our simulation results, we can understand why in our case the addition of 1:1 salt does not change the charge inversion concentration. The competition for binding between ions is controlled by the respective free energy of interaction The interaction between Na$^+$ and PS$^-$ has been extensively analyzed by different experimental methods (electrokinetics, NMR,...), giving an association constant of K = 0.6 M^{-1} [27,33] which corresponds to a free energy per ion of μ = $-k_B T \backslash ln(55.5K) \approx -3.5k_B T$, much smaller than that of the La^{3+}-PS$^-$ interaction.

In order to corroborate our interpretation for the charge inversion mechanism, it is relevant to consider the interaction of La^{3+} with phosphatidylserine (PC) lipids whose chemical structure is very similar to the PS$^-$ structure (see Fig. 1) but is zwitterionic instead of anionic, which means that it has no net charge but it has a substantial dipolar moment which generates a significant surface potential in membranes [22]. Calorimetric measurements [34] give a free energy around $\Delta G = -12k_B T$ for the interaction of La^{3+} with PC, which is even larger than our estimate for the interaction of La^{3+} with PS$^-$. Consequently, we would expect to observe an inversion of electrophoretic mobility even at smaller La^{3+} concentrations than in the previous PS$^-$ case. This expectation is confirmed by our measurements (see Fig. 1); in this case electrophoretic mobility

reverses its sign at the extremely low concentration $[La(NO_3)_3] \approx 3$ μM.

Again, experiments with PC liposomes demonstrate that the effect is strongly dependent on the valency of the ions. Titration calorimetry gives $\Delta G \approx -6.5 K_B T$ for the PC-Ca^{2+} interaction [34], much lower than that obtained for La^{3+}. Interestingly, measurements show that the (favorable) entropic contributions to ΔG are almost equal in Ca^{2+} and La^{3+} being the difference in the enthalpy. Electrophoretic results are also in line with these thermodynamic results. For example, previous results [35] show reversal of electrophoretic mobility of PC for Ca(NO$_3$)$_2$ concentrations between 0.01 mM − 0.1 mM. Our own results [28] give inversion of electrophoretic mobility at $\approx$ 0.6 mM and 2 mM concentrations of Ca(NO$_3$)$_2$ and Mg(NO$_3$)$_2$ respectively.

In conclusion, in this Letter, we provide electrophoresis measurements demonstrating charge reversal in anionic liposomes at low concentrations of trivalent cations. The driving force for this effect is shown to be not related to the surface charge and not weakened by monovalent salt. Hence, we show that the charge inversion is also possible in presence of physiological amounts of monovalent salt, usual in biophysical systems and in biotechnological applications [36]. Comparison of our MD simulation results and experiments allow us to identify the underlying mechanism as a preferential solvation of counterions by amphiphilic molecules and hydration water. It can be conclude that, under appropriate conditions, solvent mediated effects (hydration in the case of small metal ions as discussed here or hydrophobic interactions in the case of solutions

containing organic ions [37]) are strong to govern the electrostatic of soft interactions.

References

[1] *Electrostatic Effects in Soft Matter and Biophysics*, edited by C. Holm, P. Kékicheff and R. Podgornik, NATO Science Series Vol. 46, (Springer, Berlin, 2001).

[2] A.Y. Grosberg, T.T. Nguyen and B.I. Shklovskii, *Rev. Mod. Phys.* **74**, 329 (2002); Y. Levin, *Rep. Prog. Phys.* **65**, 1577 (2002).

[3] Y. S. Jho et al., *Phys. Rev. Lett.* **101**, 188101 (2008); H. Boroudjerdi et al., *Phys. Rep.* **416**, 129 (2005).

[4] H. Greberg and R. Kjellander, *J. Chem. Phys.* **108**, 2940 (1998).

[5] J. Lyklema, *Adv. Colloid Interface Sci.*, **147-148**, 205 (2009); J. Lyklema, *Colloids Surf. A*, **291**, 3 (2006).

[6] J. Faraudo and A. Travesset, *J. Phys. Chem. C* **111**, 987 (2007).

[7] K. Besteman, K. van Eijk and S. Lemay, *Nature Phys.* **3**, 641 (2007).

[8] F. H. van der Heyden et al., *Phys. Rev. Lett.* **96**, 224502 (2006).

[9] A. Martín-Molina et al. *Colloids and Surfaces A*, **319**, 103 (2008).

[10] C. Labbez, B. Jönsson, M. Skarba, M. Borkovec, *Langmuir* **25**, 7209 (2009).

[11] A. Martín-Molina et al. J. Phys. Chem. B **113**, 6834 (2009).

[12] S. Pianegonda, M. C. Barbosa and Y. Levin, *Europhys. Lett.* **71**, 831 (2005).

[13] A. Martín-Molina et al. *J. Phys. Condens. Matter* **15**, S3475 (2003).

[14] A. Martín-Molina, M. Quesada-Pérez and R. Hidalgo-Álvarez, *Langmuir* **21**, 9231 (2005); A. Martín-Molina, M. Quesada-Pérez and R. Hidalgo-Álvarez, *J. Phys. Chem. B* **110**, 1326 (2006).

[15] O. Lenz and C. Holm, *Eur. Phys. J. E* **26**, 191 (2008).

[16] M. Petersheim and J. Sun, *Biophys. J.* **55**, 631 (1989); J. Bentz et al. *Biophys. J.* **53**, 593 (1988); M.M. Hammoudah et al., *Biochim. Biophys. Acta, Biomembr.* **645**, 102 (1981).

[17] M. Sovago, G. W. H. Wurpel, M. Smits, M. Müller and M. Bonn, *J. Am. Chem. Soc.* **129**, 11079–11084 (2007).

[18] T.Ohki, M. Harada and T. Okada, *J. Chem. Phys. B* **110**, 15486 (2006).

[19] S. Kundu and D. Langevin, *Colloids Surf. A* **325**, 81 (2008); E. Le Calvez et al., *Langmuir* **17**, 670 (2001).

[20] J. Pitler et al. *Phys. Rev. Lett.* **97**, 46102 (2006).

[21] J. Faraudo and A. Travesset, *Biophys. J.* **92**, 2806 (2007).

[22] The lipid library, http://www.lipidlibrary.co.uk.

[23] T. Yeung and S. Grinstein, *Immunol. Rev.* **219,** 17 (2007).

[24] See supplementary material at http://www.link.aps.org/ supplemental/10.1103/PhysRewLett.104.168103.

[25] J. Lyklema and T. Golub, *Croatica Chemica Acta* **80**, 303 (2007).

[26] R.J. Hunter, *Zeta Potential in Colloid Science* (Academic Press, USA, 1988), 3rd ed..

[27] S. McLaughlin et al., *J. Gen. Physiol.* **77**, 445 (1981).

[28] A. Martín-Molina et al. (to be pulished).

[29] S. A. Pandit and M.L. Berkowitz, *Biophys. J.* **82**, 1818 (2002).

[30] F.C.J.M. van Veggel and D.N. Reinhoudt, *Chem. Eur. J.* **5**, 90 (1999).

[31] W. Smith, *Mol. Simul.* **32**, 933 (2006).

[32] W. Bu, P.J. Ryan and D. Vaknin, *J. Synchrotron Radiat.* **13**, 459 (2006).

[33] R. Kurland et al. *Biochim. Biophys. Acta, Biomembr.* **551**, 137 (1979); M. Eisenberg et al., *Biochemistry* **18**, 5213 (1979).

[34] R. Lehrmann and J. Seeling, *Biochim. Biophys. Acta, Biomembr.* **1189,** 89 (1994).

[35] J. Sabin et al., *Langmuir* **21,** 10968 (2005).

[36] Y. Kim and W. Sung, *Phys. Rev. Lett.* **91**, 118101 (2003).

[37] A. Martín-Molina et al., *Soft Matter* **5,** 1350 (2009).

EFFECT OF CALCIUM AND MAGNESIUM ON
PHOSPHATIDYLSERINE MEMBRANES:
EXPERIMENTAL AND ALL–ATOMIC SIMULATIONS

A. Martin-Molina,[*] C. Rodríguez-Beas[*] and J. Faraudo[†]

[*]*Grupo de Física de Fluidos y Biocoloides, Departamento de Física Aplicada Universidad de Granada, 18071, Granada, Spain*
[†]*Institut de Ciència de Materials de Barcelona (ICMAB-CSIC), Campus de la UAB, E-08193 Bellaterra, Spain*

ABSTRACT It is known that PS$^-$ lipids have very similar affinity for Ca^{2+} and Mg^{2+} cations. This finding is reported by means of electrokinetic and stability experiments. However, in spite of this similar affinity, experimental evidence shows that the presence of Ca^{2+} or Mg^{2+} induces very different aggregation behavior for PS$^-$ liposomes as characterized by their fractal dimensions. Also, turbidity measurements confirm substantial differences in aggregation behavior depending on the presence of Ca^{2+} or Mg^{2+} cations. These puzzling results suggest that, although both cations have similar affinity for the PS$^-$ lipids, they induce substantial structural differences in lipid bilayers containing each of these cations. In other words, these cations have strong ionic specific effects in the structure of PS$^-$ membranes. This interpretation is supported by all-atomic Molecular Dynamic simulations, which show that Ca^{2+} and Mg^{2+} cations have different binding sites and induce different membrane hydration. We show that both ions are incorporated deep into the hydrophilic region of the membrane, but the positioning and configuration of both cations at the membrane is different; absorbed Ca^{2+} cations present a peak at a distance about 2 nm from the centre of the lipid bilayer, and their most probable binding configuration involves 2 oxygen atoms from each of the charged moieties of the PS molecule (phosphate and carboxyl groups). On the contrary, the distribution of absorbed Mg^{2+} cations has two different peaks, located a few Å before and after the Ca^{2+} peak. The most probable configurations (corresponding to these two peaks) involve binding to two oxygen atoms from carboxyl groups

192

(the most superficial binding peak) or two oxygen atoms from phosphate groups (the most internal peak). Moreover, simulations also show differences in the hydration structure of the membrane; we obtain a hydration of 7.5 and 9 water molecules per lipid in the simulations with Ca^{2+} and Mg^{2+} respectively.

INTRODUCTION

The interaction between metal cations, particularly Ca^{2+}, and lipids plays an essential role in the structure and function of biological membranes. In order to study this interaction, phospholipids liposomes (or vesicles) have been widely used as models of biological membranes (Ekerdt and Papahadjopoulos, 1982; Nir et al., 1983; Wilschut and Hoekstra, 1986; Papahadjopoulos et al., 1990; Cevc, 1990; Lasic and Papahadjopoulos, 1998; Ohki and Ohshima, 1999; Binder and Zschörnig, 2002). For instance, it has been shown that multivalent cations could mediate membrane fusion by interacting with negatively charged phospholipids (Bentz and Ellens, 1988; Ohki and Arnold, 2000; Tanaka and Yamazaki, 2004; Schultz et al., 2009). Since phosphatidylserine is the most abundant negatively charged lipid in cell membranes, cation-induced fusion of phospholipid liposomes composed of pure bovine brain phosphatidylserine (PS⁻) has been extensively studied. In particular, special attention has been paid to the ability of Ca^{2+} or Mg^{2+} to induce aggregation and fusion of liposomes made of only PS⁻ or mixtures of PS⁻ with other phospholipids (Ekerdt and Papahadjopoulos, 1982; Wilschut and Hoekstra, 1986; Lasic and Papahadjopoulos, 1998; Ohki and

Ohshima, 1999; Portis et al., 1979; Wilschut et al., 1980; Duzgunes et al., 1981; Duzgunes and Ohki, 1981; McLaughlin et al, 1981; Ohki, 1982; Silvius and Gagne, 1984; Bentz et al., 1985; Casal et al., 1987). In most of these works (and studies cited therein), aggregation of PS^- vesicles induced by Ca^{2+} and Mg^{2+} appears as a prerequisite for fusion of PS^- membranes. Moreover, such aggregation and fusion processes seem to be intimately related to the capability of these cations to bind to phospholipid headgroups and form dehydrated intermembrane complexes. In this sense, the effectiveness of Ca^{2+} and Mg^{2+} in inducing membrane aggregation and fusion has been correlated to their respective binding constants. To this end, procedures based on a modified version of the classical Derjaguin-Landau-Verwey-Overbeek colloidal stability theory (DLVO theory) have been used to interpret these stability results (Ekerdt and Papahadjopoulos, 1982; Wilschut and Hoekstra, 1986; Lasic and Papahadjopoulos, 1998; Ohki and Ohshima, 1999; Portis et al., 1979; Wilschut et al., 1980; Duzgunes et al., 1981; Duzgunes and Ohki, 1981; McLaughlin et al, 1981; Ohki, 1982; Silvius and Gagne, 1984; Bentz et al., 1985; Casal et al., 1987) whereas analyses using mass action models have been applied to the description of fusion (Ohki and Ohshima, 1999; Bentz et al., 1988). In the case of divalent cations (such as Ca^{2+}), more sophisticated approaches beyond the Poisson-Boltzmann electrostatics embedded in classical DLVO theory have been proposed to take into account electrostatic and binding effects in membrane fusion (Marcelja, 1992).

In any case, recent studies (Róldan-Vargas et al., 2007; Róldan-Vargas et al., 2008; Róldan-Vargas et al., 2009) show that the

different effect of Ca^{2+} and Mg^{2+} in membranes is more profound than a simple numerical difference in binding constants (which are anyway of the same order of magnitude). In these studies, the aggregation processes of PS^- vesicles induced by of Ca^{2+} and Mg^{2+} was examined by both, static and dynamic light scattering techniques. In this way, not only the kinetics of aggregation of PS^- liposomes induced by Ca^{2+} and Mg^{2+} was studied, but also the structure of the resulting clusters. Accordingly, the ability of these cations to bind to PS^- membranes as well as other factors involved in the destabilization of these liposomes was studied. In particular, the kinetic exponents of the aggregating curves as well as the fractal dimensions of the resulting clusters were reported. Surprisingly, the morphology of the aggregates depended strongly on the divalent cation used to induce aggregation; PS^- aggregates formed by Ca^{2+} were branched structures whereas dense structures were observed for PS^- clusters induced by Mg^{2+}. Also, FT-IR measurements clearly show that PS^- membranes have different hydration in the presence of Ca^{2+} or Mg^{2+}. In fact, the different structures of the aggregates were rationalized in terms of an ion-specific short range interaction depending on the different degrees of hydration of PS^- liposomes in the presence of these divalent cations. At this point, it is interesting to recall that the difference in hydration of PS^- lipids in the presence of Ca^{2+} or Mg^{2+} could be related to the binding thermodynamics of these ions. Calorimetric measurements (Sinn et al., 2006; Lehrmann and Seelig, 1994) show that the binding of Ca^{2+}, Mg^{2+} and La^{3+} cations to PS^- is endothermic and entropy driven. The dominant entropic contribution is likely coming from the

195

liberation of solvating water molecules from lipid headgroups. Hence their different binding constants may be related to their different dehydration ability.

These reported differences also suggest the possibility of different binding modes or binding sites for Ca^{2+} and Mg^{2+} with PS^- lipids. A first insight is given by NMR studies, which allow a comparison of the relative distribution of membrane bound cations within the three dimensional space associated with the lipid-solution interface. It has been shown (Roux and Bloom, 1990) that both Ca^{2+} and Mg^{2+} are deeply buried into the membrane (more buried than monovalent cations) and the results also suggest different binding locations for these ions. Also, it has been suggested (Portis et al., 1979) that Ca^{2+} binds to the carboxyl group of PS^- lipids inducing a "trans" lipid complex while Mg^{2+} favors a "cis" geometry. These different conformational effects on the lipid bilayers induced by Ca^{2+} and Mg^{2+} can be responsible of the dissimilar aggregation and fusion of PS^- bilayers in the presence of these cations. However, other experimental studies (Schultz et al., 2009) (based on infrared spectroscopy in PC-PS mixtures) conclude that Mg^{2+} binds to PS in a fashion similar to that of Ca^{2+}.

In the case of Ca^{2+}, it seems clear (Feigenson, 1986) that the most probable stoichiometry is 2 PS^- lipids per bound Ca^{2+}. In addition, NMR studies (Roux and Bloom, 1990) show the existence of at least two different binding sites. Early infrared spectroscopic studies (Dluhy et al., 1983) show the formation of a strong Ca^{2+}-PO_4^- complex

although a combination of MD simulations with magic angle spinning (MAS) and solid-state NMR measurements (Boettcher et al., 2011) favor a binding of Ca^{2+} to carboxyl in the PS headgroup. Also, this latter work shows that Ca^{2+} induced the formation of microdomains of PS in mixtures containing PC and PS lipids (Boettcher et al., 2011). In fact, Ca^{2+} induces rapid demixing in PS-PC mixtures (Silvius and Gagne, 1984; Ross et al., 2001). In the case of Mg^{2+}, Schultz *et al.* (2009) have shown experimentally the formation of cation-PS microclusters in membranes made of mixtures of PC and PS^- lipids but quite interestingly, Mg^{2+} does not induce phase separation Schultz et al., 2009).

Summing up all these accumulated evidences, it seems clear that Ca^{2+} and Mg^{2+} have slightly different affinities for PS^- lipids, but they induce different phenomena. As we mentioned above, Ca^{2+} and Mg^{2+} induce different structures of PS^- aggregates and different clustering and mixing behavior of PS^- with PC. These observed effects suggest the possibility of substantial differences in the atomistic details of the binding of Ca^{2+} and Mg^{2+} cations in membranes. Our objective in this work is to understand in more depth the interaction of Ca^{2+} and Mg^{2+} with PS^- lipids. We provide new experiments and all-atomic Molecular dynamics (MD) simulations concerning the interaction between PS^- lipids with Ca^{2+} and Mg^{2+}. Our experiments are aimed at emphasizing the similitude and differences between the interaction of Ca^{2+} and Mg^{2+} with PS^- lipids and the focus of the simulations is at understanding the atomistic details of the cation − lipid interaction (such as the location of binding sites for the ions, identification of the

chemical groups involved in the binding and hydration effects both in lipids and cations).

MATERIALS AND METHODS

Phosphatidylserine liposomes

The phosphatidylserine (PS⁻) liposomes were prepared as follows. The lipids (3-sn-Phosphatidyl-L-serine from bovine brain) with purities greater than 99 % mass were obtained from Avanti PolarLipids (Alabama, USA). This kind of lipids has been chosen in agreement with previous experimental works in which similar lipids were used to prepare the corresponding liposomes of PS⁻ (Róldan-Vargas et al., 2007; Róldan-Vargas et al., 2008; Róldan-Vargas et al., 2009). Accordingly, the experimental results obtained in the present work will be directly comparable to those found in the cited references. The phospholipids at the proportions indicated below were dissolved in a mixture (2:1, volume ratio) of chloroform and methanol in a round-bottom flask and dried in a rotary evaporator at low pressure at 40^0C to form a thin film on the flask. The film was hydrated with deionized water (conductivity lower than 18 μS cm^{-1}, MilliQ-Millipore, USA) to give a lipid concentration of 30mM. A polydisperse population of multilamellar vesicles were formed by constant vortexing for 4 min on a vortex mixer and sonication in a Transonic Digitals bath sonifier (Elma, Germany) for 10 min. Multilamellar vesicles were transformed to large unilamellar vesicles (with a reduction on the polydispersity) by a sequential extrusion

procedure (Extruder device form Lipex Biomembranes, Canada). The suspension was then filtered by polycarbonate membrane filters of variable pore size under nitrogen pressures of up to 55×10^5 Nm^{-2} (Hope et al., 1985) by following three steps: first, three consecutive extrusions through a 0.8 μm pore diameter filter and three other consecutive extrusions through two stacked 0.4 μm membranes. The resulting lipid suspension was finally extruded fifteen consecutive times through two stacked 0.2 μm filter. After preparation, a nitrogen stream was passed to displace the air, and liposomes were stored at 4-7 ^{0}C.

Electrophoretic mobility

The instrument *ZetaPALS* (Brookhaven, USA), based on the principles of phase analysis light scattering (PALS), was used to measure electrophoretic mobilities (μ_e). The setup is especially useful at high ionic strengths and non-polar media, where mobilities are usually low. Under this situation, a phase analysis is employed instead of the traditional spectral analysis based on the shifted frequency spectrum. Both techniques have in common the analysis of a mixing of scattered light from a suspension of colloidal particles moving in an electric field, with light directly from the source (reference beam light). The scattered light is frequency shifted by the Doppler Effect and its superposition with the *unshifted* reference one, leads to a beating at a frequency dependent on the speed of the particles. When the particle velocity is low, the spectral analysis is not able to generate

a complete cycle of the detected signal. However, phase analysis takes place over many cycles of the respective waveforms since the optical phase of the scattered light is characterized by means of the so-called the *amplitude-weighted phase difference* (AWPD) function instead of a simple correlation treatment. This function improves the statistic behavior because the detected signal fluctuates in amplitude due to the relative movements of particles and concentration fluctuations. For a complete discussion of the PALS method and AWPD treatment, we refer the reader to ref (Tscharnuter, 2001).

Lastly, electrophoretic mobility measurements were performed at 25 ºC and pH=5.5. The particle concentration (ρ_p) was 1.4 x 10^9 particle·mL^{-1}. We chose this value after plotting the corresponding μ_e vs. ρ_p curves. The electrolyte used to perform experiments were $Ca(NO_3)_2$ and $Mg(NO_3)_2$.

Stability ratio

To study the stability of the liposome suspensions, stability measurements were carried out at pH 5.5 and the ionic strength was adjusted between 0.1 mM and 300 mM by the addition of $Ca(NO_3)_2$ and $Mg(NO_3)_2$. Determinations of Fuchs stability ratio W (or stability factor) were performed by spectrophotometric monitoring. This magnitude is a criterion for the stability of the colloidal system: $W = k_r / k_s$ where the rate constant k_r describes rapid coagulation and k_s is the rate constant for the slow coagulation regime. Thus, the inverse of the stability ratio provides a measure of the effectiveness of collisions

leading to coagulation. In this work, the stability ratio was obtained experimentally from the rate constant of coagulation of the liposomes by measuring the dispersed light with a commercial spectrophotometer (Bio-rad680, microplatereader). Information on the kinetics-aggregation constants of dimer formation can be directly derived from the initial slopes of the absorbance vs. time curves (dAbs/dt) (Miraballes-Martinez et al., 2001). Accordingly, plotting W as a function of the electrolyte concentration in a double-logarithmic scale becomes useful to estimate the critical coagulation concentration (CCC) which is defined as the minimum concentration of electrolyte required to induce coagulation (W=1). The CCC value is therefore related to destabilization processes (*i. e.* low CCC means low stability).

Turbidity Measurements

Turbidity of the vesicle suspensions as a function of Ca^{2+} and Mg^{2+} concentrations at 400 nm of wave length was studied by using a commercial spectrophotometer (Thermo/Milton Roy Spectronic Genesys 5^{TM}, USA). The volume fraction of vesicles samples was 0.1%, and the ion concentrations were raised step by step by adding small amounts of its concentrated salt solutions. The change of absorbance at 400 nm (ΔA_{400}) was measured 2 minutes after changing the ion concentration. The procedure was repeated until the absorbance no longer changed. All experiments were performed at

room temperature and each reported data point is the average of six measurements.

Kinetic aggregation and structural properties of aggregates

Kinetic aggregations experiments of PS liposomes induced by divalent cations and the subsequent structural analysis of resulting aggregates were carried out in previous work (Roldán-Vargas et al., 2007; Roldán-Vargas et al., 2008). Therein the calcium and magnesium-induced aggregation of the liposomes was studied by means of static and dynamic light scattering techniques. By so doing, kinetic exponents of the aggregating curves and fractal dimensions of the resulting clusters were reported. The whole experimental procedure is described in detail in the above cited references.

Molecular dynamics (MD) Simulations

In order to obtain a molecular picture of the cation-PS$^-$ interaction, we have performed all-atomic molecular dynamics simulations (MD) in the NPT ensemble of a fully hydrated phosphatidylserine (PS$^-$) bilayer in contact with neutralizing divalent counterions (Ca^{2+} or Mg^{2+}). Our simulation box contains 14720 atoms from a membrane with 128 PS$^-$ molecules distributed in two leaflets (as in previous simulations, see (Pandit and Berkowitz, 2002; Martín-Molina et al., 2010), 2624 water molecules and 64 divalent counterions to ensure charge neutrality (Ca^{2+} or Mg^{2+} depending on

202

the simulation). The model and force field employed for describing the PS⁻ molecules was the one developed in (Pandit and Berkowitz, 2002). The force field is based on a united atom description modified to include explicitly the hydrogen atoms of the NH_3^+ group. Partial atomic charges and bond, angle and dihedral parameters were derived from *ab initio* calculations and are given in Fig. 2 and Table 1 of Ref. (Pandit and Berkowitz, 2002). Water was modeled using the standard TIP3P model. In modeling the ions, we employed the Lennard-Jones parameters developed for several ions in (Aqvist, 1990), which were compatible with the TIP3P model of water. All Lennard-Jones interactions between atoms were cut-off at a distance of 1.5 nm. This large cut-off was employed to avoid any possible spurious effects due to truncation of Lennard-Jones interactions, recently reported in the literature (Bonthuis, 2010), although they result in larger computational costs. Long range electrostatic interactions were computed using the Ewald summation method with a precision of 10^{-4} with periodic conditions along all three directions. All simulations correspond to a temperature of 350 K as in previous simulation studies (Pandit and Berkowitz, 2001; López Casales et al., 1996), which is well above the main transition temperature (330K), so we can be sure that our simulated bilayer is in the liquid crystalline state. In real experiments at ambient temperature PS⁻ lipids are assumed to be in the liquid crystalline state because the mixture of PS⁻ lipids with different hydrocarbon tails prevents crystallization. Also, the use of the same temperature (350K) employed in previous simulations of PS lipids with other cations (Pandit and Berkowitz, 2001; López Casales et al.,

1996) facilitates comparison with previous results. The temperature was maintained constant by using a Nosé-Hoover thermostat, with a relaxation constant of 0.5 ps. Our simulations were also performed under a pressure of 1 atm maintained by a Nosé-Hoover isotropic barostat with a relaxation constant of 0.5 ps. All simulations were performed using the DLPOLY2.19 package (Forester and Smith, 2007). The equations of motion were solved using the Verlet leapfrog algorithm with a time step of 2 fs. On average, the cost of a simulation time step is about 0.23 s with the code running in parallel using 64 PowerPC processors. The protocols employed for generating initial configurations, equilibration and production runs were identical to those employed in our previous study of the same lipid bilayer in the presence of La^{3+} (Martín-Molina et al., 2010). The values of quantities of interest such as the area per lipid or the number of adsorbed cations were typically stabilized after 1-2 ns of simulation as in previous works (Pandit and Berkowitz, 2002; Martín-Molina et al., 2010). Hence, we decided to perform production runs of 10 ns preceded by equilibration runs of 4 ns. Visualisation and representation of the resulting trajectories was performed using the VMD software (Humphrey et al., 1996).

RESULTS AND DISCUSSION

Electrokinetic and Stability Characterization

First of all, we performed electrokinetic measurements in order to characterize the affinity of our PS⁻liposomes for Mg^{2+} and Ca^{2+}. In

previous works (Portis et al., 1979; McLaughlin et al., 1981; Ohki, 1982), it was found that the affinity of PS$^-$ liposomes for Ca^{2+} is only slightly greater than the affinity for Mg^{2+}. This concept is confirmed by our electrokinetic results shown in Fig. 1. In this figure, we show the electrophoretic mobility of PS$^-$ liposomes as a function of the salt concentration for Mg(NO$_3$)$_2$ and Ca(NO$_3$)$_2$. As can be seen, very similar electrokinetic behaviors are obtained for the two salts. In both cases, the magnitude of the electrokinetic mobility decreases with increasing the electrolyte concentration and a feeble inversion in the mobility appears at very high salt concentrations (around 60 mM for Ca^{2+} and 100 mM for Mg^{2+}).
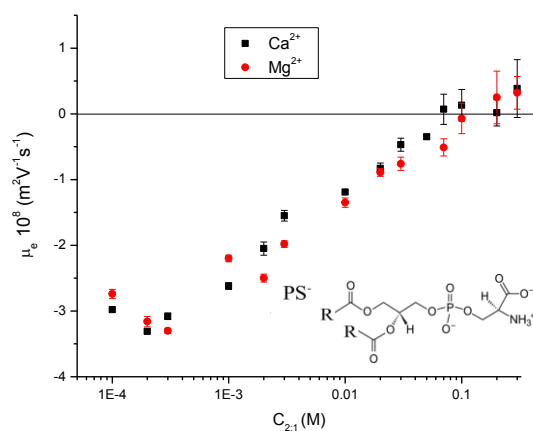

FIGURE 1 Electrophoretic mobility of PS$^-$ liposomes as a function of Ca(NO$_3$)$_2$ and Mg(NO$_3$)$_2$. Squares and circles stand for Ca(NO$_3$)$_2$ and Mg(NO$_3$)$_2$, respectively. Inset: Molecular structure of PS$^-$ lipids.

Let us remark that the value of the concentration of charge inversion is a valuable quantitative measure of the affinity of ions for

interfaces which can be obtained directly from experiments without any theoretical assumption (in contrast with quantities such as binding constants, which require the *a priori* formulation of a theoretical model (Tatulian, 1995)). Our results give a slightly larger affinity of PS^- for Ca^{2+} than for Mg^{2+}, in agreement with previous studies. For example, classical results (Portis et al., 1979) based on equilibrium dialysis experiments give estimations for the charge inversion concentrations of 60 mM and 100 mM respectively, which coincide with our own results. Classical electrophoretic mobility measurements by McLaughlin made in the presence of 0.1 M of NaCl give similar but slightly larger results; in that case the estimated charge inversion concentrations were 83 mM for Ca^{2+} and 125 mM for Mg^{2+} (McLaughlin et al., 1981). Hence, we can conclude that the affinity of PS^- lipids for Mg^{2+} and Ca^{2+} is very similar, with charge inversion concentrations (and hence affinities) differing only in a factor about $1.5 - 1.7$ between these two cations.

In Fig. 2 we show the stability rate of PS^- liposomes as a function of the salt concentration for the same electrolytes employed in electrokinetic measurements ($Mg(NO_3)_2$ and $Ca(NO_3)_2$). Again, very similar results are obtained for the two electrolytes, although small differences in the values of CCC are found. In particular we estimate a CCC around 10 mM for $Mg(NO_3)_2$ and 8 mM for $Ca(NO_3)_2$. Hence, we need to employ slightly larger concentrations of Mg^{2+} (as compared to Ca^{2+}) to induce aggregation of liposomes. These results indicate a higher affinity of PS^- for Ca^{2+} than for Mg^{2+}, in line with the electrokinetic results. Also, these results are in agreement with the

prevailing concept that larger concentrations of Mg^{2+} (as compared with Ca^{2+}) are required to induce fusion of membranes containing PS^- (Schultz et al., 2009).
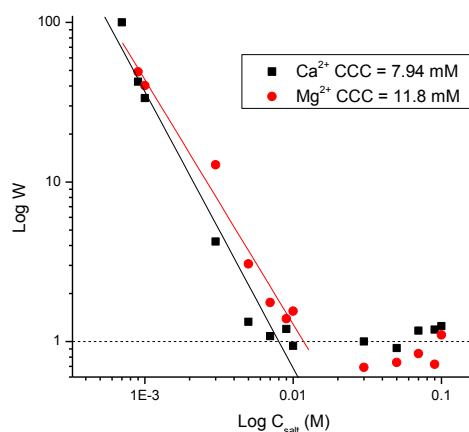

FIGURE 2 Stability ratio of PS^- liposomes as a function of $Ca(NO_3)_2$ and $Mg(NO_3)_2$. Determination of the experimental critical coagulation concentration (CCC). Squares and circles stand for $Ca(NO_3)_2$ and $Mg(NO_3)_2$, respectively.

Experimental aggregation of liposomes induced by Ca^{2+} and Mg^{2+}

The aggregation process of liposomes induced by $Mg(NO_3)_2$ and $Ca(NO_3)_2$ has been characterized by turbidity measurements as those performed by Ohki et al. in 1982. By following the prescriptions given in the cited reference, we have measured the absorbance obtained 2 min after changing each ion concentration. Our results, presented in Fig. 3, extend the range measured in the original reference toward higher salt concentrations in order to better illustrate the differences between observed Ca^{2+} and Mg^{2+}. In general, we can see that in both cases the absorbance increases with the electrolyte concentration,

indicating liposome aggregation. Absorbance increases until a maximum plateau is reached. However, clear differences are observed between measurements made in the presence of Ca^{2+} or Mg^{2+}. The Mg^{2+} curve is clearly shifted to higher salt concentrations and therefore less concentration of Ca^{2+} is required to induce aggregation, in agreement with our previous CCC estimation. Fig. 3 also shows that the plateau of absorbance reached for Ca^{2+} is noticeably larger than that observed for Mg^{2+}. This observation suggests that the volume corresponding to the PS^- aggregates induced by Ca^{2+} is larger than that corresponding to clusters induced by Mg^{2+}.

FIGURE 3 Relative absorbance at 400nm of wave length of PS^- liposomes as a function of $Ca(NO_3)_2$ and $Mg(NO_3)_2$. Turbidity at 2 min after the addition of the 2:1 electrolyte is plotted. Squares and circles stand for $Ca(NO_3)_2$ and $Mg(NO_3)_2$, respectively.

It is interesting to analyze the results of our turbidity measurements (Fig. 3) in view of the kinetic and structural parameters obtained for this system in previous work (Roldán-Vargas et al., 2007; Roldán-

Vargas et al., 2008). Therein, the fractal dimensions of the structures resulting from aggregating liposomes (d_f) were calculated by means of static light scattering experiments (SLS). The results for a representative divalent salt concentration of 5 mM (corresponding to the plateau in absorbance observed in Fig. 3) are given in Table 1. The d_f values reported for the resulting clusters indicate substantial differences in the morphology of the aggregates induced by Ca^{2+} and Mg^{2+}.

TABLE 1 Experimental Kinetic Exponents and Fractal Dimensions for PS$^-$ liposomes in the presence of 5mM of $Ca(NO_3)_2$ and $Mg(NO_3)_2$. Data obtained from references (Roldán-Vargas et al., 2007; Roldán-Vargas et al., 2008).

Electrolyte (5 mM)	α	d_f
$Ca(NO_3)_2$	-0.54 ± 0.02	1.75 ± 0.06
$Mg(NO_3)_2$	-0.35 ± 0.02	3.46 ± 0.08

Historically, two limiting regimes have been identified in colloidal aggregation: a rapid diffusion-limited cluster aggregation (DLCA) and a slow reaction-limited cluster aggregation (RLCA). Salt-induced aggregation of electrically stabilized bare colloidal particles aggregating at low and high electrolyte concentrations, are examples of these limiting regimes. In the case of Ca^{2+}, the fractal dimension of 1.75 reported in Table 1 is the well-established value for the DLCA regime; it means that at 5mM the liposomes have reached such a regime and form ramified open structures (classical mass-fractal structures) (Roldán-Vargas et al., 2007). In contrast, a singular surface- to mass-fractal transition is reported for the case of clusters induced by Mg^{2+} giving rise to values of d_f higher than 1.75 as the

cation concentration increases. In particular, for a $Mg(NO_3)_2$ concentration of 5 mM, the value of d_f reported for PS^- liposomes is 3.46 (see Table 1). Such high value implies that dense cluster morphologies are observed for PS^- aggregates induced by Mg^{2+}. These dense structures were interpreted in terms of the ability of Mg^{2+} to allow internal restructuring of the lipid bilayers (Roldán-Vargas et al., 2008). This difference in the structure of the aggregates justifies the different absorbance reported in Fig. 3 for this concentration (5 mM).

Given the fact that the structures of the aggregates of liposomes induced in the presence of Ca^{2+} and Mg^{2+} are different, it is natural to think that the kinetic process leading to these structures is also different. In fact, the kinetics of aggregation was also followed in these experiments by employing the dynamic light scattering (DLS) technique. The variation of the translational diffusion coefficients of liposomes as a function of the time was measured for different concentrations of Ca^{2+} and Mg^{2+} and its exponential decrease with time was characterized by a kinetic exponent (α) shown in Table 1. Since α quantifies how fast the kinetic aggregation of PS^- liposomes occurs, we can deduce that the aggregation of PS^- induced by Ca^{2+} is faster than in the case of Mg^{2+}. In other words, the formation of denser structures by Mg^{2+} proceeds more slowly than the formation of the branched structures induced by Ca^{2+}. All together, the evidence discussed here shows that, although the affinity of PS^- for Ca^{2+} or Mg^{2+} are similar, the interaction of these ions with lipids give raise to different structures indicating the possibility of substantial differences

at the molecular scale organization of the PS$^-$ bilayer after incorporation of Ca^{2+} or Mg^{2+}.

Results of Molecular dynamics (MD) Simulations

Our MD simulations allow us to obtain an atomistic picture of the interaction between PS$^-$ lipids and Mg^{2+} or Ca^{2+} cations. In both cases, the divalent counterions are observed to condense to the negatively charged bilayer membrane, i.e., all cations contain at least one oxygen atom from PS$^-$ molecules in their first coordination shell (this is the usual definition for binding in MD simulations). In all cases, the oxygen atoms from PS$^-$ lipids are of O2 type. In the employed force field (Pandit and Berkowitz, 2002), the oxygen atoms assigned to the O2 type are the two oxygen atoms coming from the carboxylic moiety and the two oxygen atoms coming from the phosphate moiety which are bonded to phosphorus atoms but not to carbon atoms (see the structure of PS lipids in the inset of Fig. 1). Hence, the more internal oxygen atoms of the lipid molecule are not observed to be involved in ion binding.

The fact that cations are incorporated into the membrane influences the area per lipid of the membrane. Previous simulations of PS$^-$ bilayers with Na$^+$ counterions (Pandit and Berkowitz, 2002) reported an area per lipid about 53.7 ± 0.1 Å^2. Our simulations give a larger area per lipid: 55.55 ± 0.01 Å^2 for simulations with Ca^{2+} and 55.30 ± 0.01 Å^2 for simulations with Mg^{2+}. In our previous simulations with La^{3+} (Martín-Molina et al., 2010), we obtained an area per lipid of

55.41$\pm$0.01 Å^2. Hence, the area per lipid is almost identical for Ca^{2+}, Mg^{2+} and La^{3+} but it is slightly larger than that obtained with Na$^+$.

Interestingly, our simulations show that both Ca^{2+} and Mg^{2+} are incorporated deep into the hydrophilic region of the membrane but the positioning of both cations at the membrane is different. In Fig. 4, we show the density profiles averaged over the xy plane as a function of z. In both cases, the cations are typically embedded by oxygen atoms of the O2 type from lipids, as can be seen in the snapshots shown as insets in Fig. 4. The distribution of O2 atoms (responsible for the cation binding) is identical for simulations containing Ca^{2+} or Mg^{2+} cations. However, the distribution of cations is different in each case. In the case of Ca^{2+}, the cations and O2 atoms have very similar distributions, with a peak at a distance around 2 nm from the centre of the bilayer membrane. In the case of Mg^{2+}, the distribution of cations has two distinct peaks, located at z values of 1.8 nm and 2.2 nm (i.e. a few angstroms before and after the peak of the O2 distribution). These results are consistent with NMR results (Jena, 2008) which indicate that both cations are deeply buried in the hydrophilic region of the membrane with a slightly larger tendency of Mg^{2+} to be found in more superficial regions. Apart from the density profiles of cations, the different hydration of absorbed Ca^{2+} or Mg^{2+} cations as well as the hydration of lipid molecules are also included in Fig. 4. In bulk electrolyte, both Ca^{2+} and Mg^{2+} cations have around 6 water molecules in their first coordination shell. After absorption at the lipid membrane, these cations become partially dehydrated. On average, the

first coordination shell of absorbed Ca^{2+} cations contains 4.2 oxygen atoms from lipids and 2.8 oxygen atoms from water molecules.
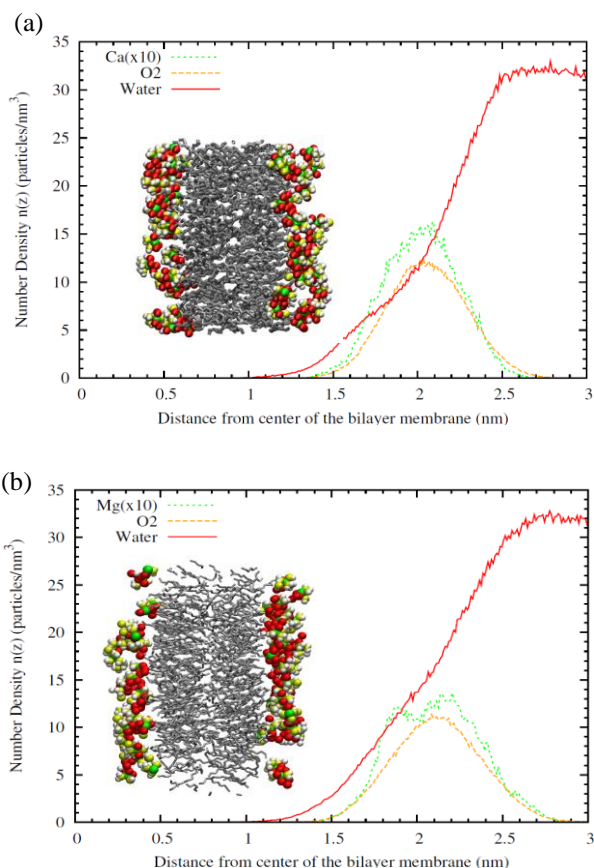

FIGURE 4 Average density profile of different species as a function of the z coordinate (perpendicular to the membrane) obtained from MD simulations. Solid line: water density (molecules/nm^3), dashed line: oxygen atoms of O2 type from lipid molecules (atoms/nm^3), dotted line: number density of divalent cations (ions/nm^3) multiplied by a factor of 10 for clarity. (a) simulations with Ca^{2+} and (b) simulations with Mg^{2+}. Inset: snapshot from MD simulations showing the divalent cations (green ball) and the oxygen lipids (ball) and water molecules inside the first coordination shell of cations. For helping interpretation of the figure we also show schematically the hydrocarbon tails as lines.

In the case of Mg^{2+}, we obtain 2.7 oxygen atoms from lipids and 3 oxygen atoms from water molecules. Hence, these cations retain around half of their inner hydration water. In the case of the Ca^{2+} cations, their first coordination shell is slightly expanded by absorption since it replaces 3 oxygen atoms from water by about 4 oxygen atoms from lipids. In the case of Mg^{2+}, 3 oxygen atoms from water are replaced by about 3 oxygen atoms from lipids.

Concerning the hydration of the lipids, we have computed the number of water molecules near the carbonyl ester group of the PS^- lipids since the (relative) hydration of this group of the lipid can be observed experimentally (Roldán-Vargas et al., 2008). We obtain a hydration of 7.5 water molecules per lipid in the simulations with Ca^{2+} and 9 water molecules per lipid in the case of Mg^{2+} simulations.

These differences in the hydration behavior can be also observed from the differences in the density profiles of water inside the hydrophilic region of the bilayer. In order to facilitate this comparison, we have plotted the density profiles of water shown in Fig. 4a and Fig. 4b in a single plot (Fig. 5) and also we have added the results for La^{3+} obtained in a previous work (Martín-Molina et al., 2010). As seen in Fig. 5, there is depletion in the water density profile in the region with z between 1.6 nm and 2.3 nm for the simulations with Ca^{2+}, a feature which is not observed for Mg^{2+}. Hence, our MD results point out the larger capability of Ca^{2+} to dehydrate the PS^- membrane whereas an intermediate value of hydration between Ca^{2+} and Mg^{2+} cases was obtained for La^{3+}. Hence, the dehydration efficiency of these cations

follows the sequence $Ca^{2+} > La^{3+} > Mg^{2+}$ which is coincident with the sequence of sizes for these cations. These results are also consistent with calorimetric experimental results (Sinn et al., 2006) which were interpreted as indicating a larger dehydration of the PS lipids due to Ca^{2+} as compared with Mg^{2+}. In addition, the origin of the dissimilar morphology experimentally found for PS⁻ liposome aggregates induced by Ca^{2+} and Mg^{2+} (see Table 1) was attributed to a different degree of hydration of liposomes in the presence of these divalent cations. This interpretation was supported by the analysis of Fourier-transform infrared spectroscopy (FTIR) spectra (Roldán-Vargas, 2009). Therein, FTIR measurements indicated that, under equal concentrations, liposomes are more hydrated in the presence of $MgCl_2$ than in the presence of $CaCl_2$, as observed in our simulations. This feature agrees also with another study in which the destabilization of the lipid bilayers induced by Ca^{2+} (required for the membrane fusion), is related to its ability to dehydrate the lipid membrane (Jena, 2008).
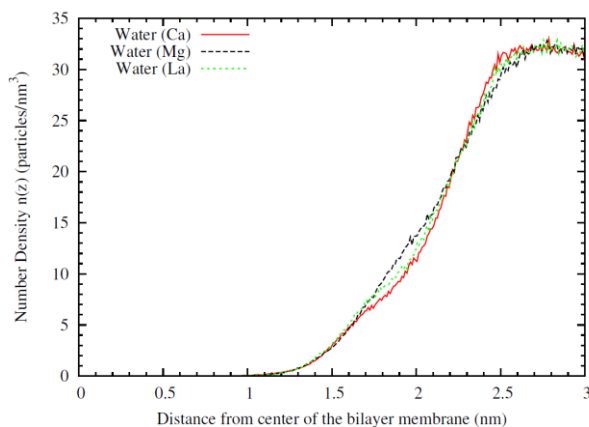

FIGURE 5 Hydration profiles of PS⁻ bilayers in the presence of Ca^{2+}, Mg^{2+} and La^{3+}. Data obtained from Fig. 4 for Ca^{2+} and Mg^{2+} and reference (38) for La^{3+}.

Our simulations also show that the organization of the cations within the lipid bilayer is different for Ca^{2+} and Mg^{2+}. In order to characterize in detail the binding of cations to lipids, we have computed the number of oxygen atoms and its origin for all observed binding events. A histogram with the results is shown in Fig. 6a and illustrative snapshots of the most probable binding modes are shown in Fig. 6b. In the case of Ca^{2+}, the most probable case corresponds to binding to 2 oxygen atoms from phosphate and 2 from carboxyl (see Fig. 6a). This binding mode involves two PS⁻ lipids and it is illustrated in the snapshot of Fig. 6b. This finding is consistent with the experimental expectation (Feigenson, 1986) of a dominant 2:1 binding ratio for PS lipids and bound Ca^{2+} ions. Also, this finding emphasizes that both phosphate and carboxyl moieties are relevant in the binding process, reconciling in a way the findings obtained from different experimental techniques (Dlughy et al., 1983; Boettcher et al., 2011). Other configurations also contribute significantly, and in general they tend to have more oxygen atoms from the carboxyl moiety than from phosphate. The average corresponds to 1.8 oxygen atoms from phosphate and 2.4 from carboxyl moieties. This gives a total of 4.2 oxygen atoms from lipids on the average first coordination shell of absorbed Ca^{2+} cations. Interestingly, the distribution of binding modes shows significant differences between Ca^{2+} and Mg^{2+}. In the case of Mg^{2+}, the peak of the distribution is not clearly defined, with several different configurations being important (see Fig. 6a). The two most probable cases correspond to binding involving 2 oxygen atoms from a single moiety (either phosphate or carboxyl) and involve two lipid
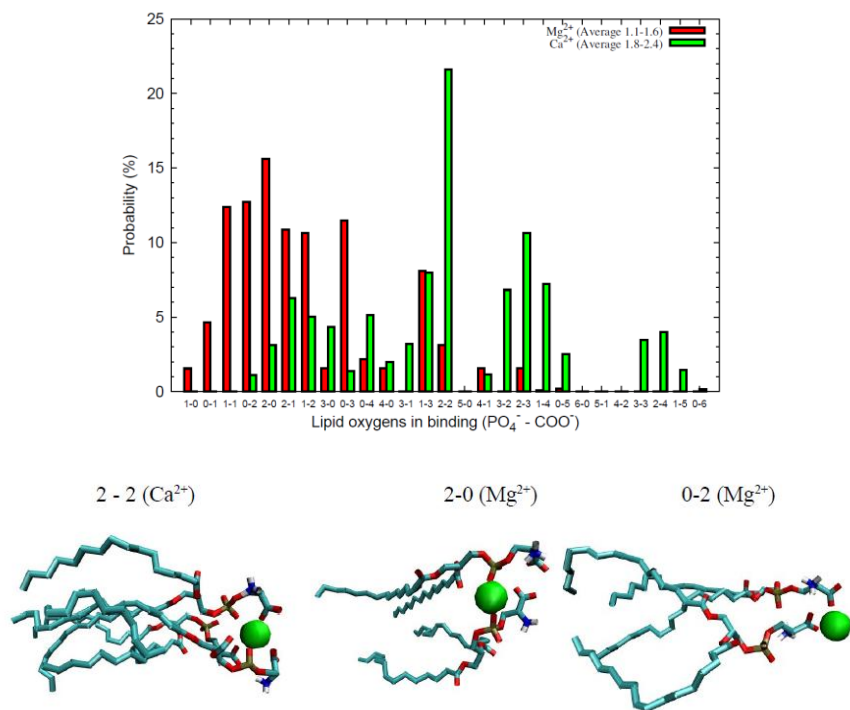
FIGURE 6. Different binding modes of Ca^{2+} and Mg^{2+} as observed in MD simulations. (a) Histogram showing the probability of different binding modes involving PO_4^- or COO^- groups of PS^- lipids. The first number indicates the number of oxygen atoms from PO_4^- and the second the number of oxygen atoms from COO^-. The most probable configurations for each cation are indicated with arrows. Snapshots of these configurations are shown in (b). The snapshots were made using the VMD program. Green balls correspond to divalent cations and the color codes for lipid atoms are the following: red O2 oxygen, pink OS oxygen atoms, ochre P, cyan C from carboxyl group, blue N, white hydrogen atoms in amine group, grey C in the hydrocarbon tails (other atoms not shown).

molecules, as illustrated in the snapshot of Fig. 6b. The binding mode involving 2 phosphate oxygen atoms implies a deeper penetration of

the Mg^{2+} cation inside the membrane, whereas the binding to 2 oxygen atoms from carboxyl implies a more superficial or external location of bound Mg^{2+} cations.

The different location of the cation in these two binding modes can be correlated with the two peaks appearing in the density profile of Mg^{2+} in Fig. 4b, appearing at a distance about 1.8 nm and 2.2 nm from the centre of the bilayer. Other configurations also contribute in addition to these two most probable cases, and the average binding for Mg^{2+} corresponds to 1.1 oxygen atoms form phosphate and 1.6 oxygen atoms from carboxyl. In this case, the total number of oxygen atoms on the average coordination shell of an absorbed Mg^{2+} cation is 2.7.

CONCLUSIONS

In this work we provide new experiments concerning the interaction between PS^- liposomes in the presence of Ca^{2+} and Mg^{2+}. Similar electrokinetic and stability behavior of PS^- liposomes in the presence of Ca^{2+} and Mg^{2+} is found. However, aggregation experiments show specific ionic effects: different aggregation kinetic and morphologies for aggregates of PS^- induced by Ca^{2+} and Mg^{2+} are observed. In order to explain these experimental findings, an analysis of the interaction between PS^- phospholipids and Ca^{2+} and Mg^{2+} is done by means of all-atomic MD simulations. Our MD results show subtle but important differences at the molecular level in the way that cations (Ca^{2+} or Mg^{2+}) interact with the bilayer. Both cations are

incorporated deeply in the hydrophilic region of the membrane. Adsorbed Ca^{2+} cations tend to be bound to 2 PS$^-$ headgroups in a binding mode which involves both the carboxylic and phosphate moieties of the lipid headgroup. On the other hand, binding of Mg^{2+} involves typically 2 lipids through their phosphate or carboxylic moieties. As a consequence, the distribution of Mg^{2+} cations inside the membrane peaks at two different locations, one of them more superficial and the other one more profound than the most probable location found for the Ca^{2+} cation. Interestingly, these different binding modes induce different hydration of the membrane containing Ca^{2+} or Mg^{2+} absorbed cations. Simulations show that the dehydration efficiency of cations follows the sequence $Ca^{2+} > La^{3+} > Mg^{2+}$ which is coincident with the sequence of sizes for these cations. In view of the structural differences (different lipid-cation organization as well as different hydration content) it is natural to expect a different liposome-liposome interaction and aggregation behavior depending on the cation present in the membrane. Our main conclusion is that the similar affinities of Ca^{2+} or Mg^{2+} cations to PS$^-$ lipids involve different molecular arrangements which become evident only when studying the liposome-liposome interaction and aggregation behavior.

REFERENCES

Aqvist, J. 1990. Ion Water Interaction Potentials Derived From Free-Energy Perturbation Simulations. *J. Phys. Chem.* 94:8021-8024.

Bentz, J., and H. Ellens. 1988. Membrane-Fusion - Kinetics And Mechanisms. *Col. Surf.* 30:65-112.

Bentz, J., N. Duzgunes, and S. Nir. 1985. Temperature-Dependence Of Divalent-Cation Induced Fusion Of Phosphatidylserine Liposomes - Evaluation Of The Kinetic Rate Constants. *Biochemistry* 24:1064-1072.

Bentz, J., S. Nir, and D. G. Covell. 1988. Mass-Action Kinetics Of Virus-Cell Aggregation And Fusion. *Biophys. J.* 54:449-462.

Binder, H., and O. Zschörnig. 2002. The effect of metal cations on the phase behavior and hydration characteristics of phospholipid membranes. *Chem. Phys. Lipids* 115:39-61.

Boettcher, J. M., R. L. Davis-Harrison, M. C. Clay, A. J. Nieuwkoop, Y. Z. Ohkubo, E. Tajkhorshid, J. H. Morrissey, and C. M. Rienstra. 2011. Atomic View of Calcium-Induced Clustering of Phosphatidylserine in Mixed Lipid Bilayers. *Biochemistry* 50:2264-2273.

Bonthuis, D. J., K. Falk, C. N. Kaplan, D. Horinek, A. N. Berker, L. Bocquet, and R. R. Netz. 2010. Comment on "Pumping of Confined Water in Carbon Nanotubes by Rotation-Translation Coupling". *Phys. Rev. Lett.* 105:209401.

Casal, H. L., H. H. Mantsch, and H. Hauser. 1987. Infrared Studies Of Fully Hydrated Saturated Phosphatidylserine Bilayers - Effect Of Li+ And Ca-2+. *Biochemistry* 26:4408-4416.

Cevc, G. 1990. Membrane Electrostatics. *Biochim. Biophys. Acta* 1031:311-382.

Duzgunes, N., S. Nir, J. Wilschut, J. Bentz, C. Newton, A. Portis, and D. Papahadjopoulos. 1981. Calcium-Induced And Magnesium-Induced Fusion Of

Mixed Phosphatidylserine-Phosphatidylcholine Vesicles - Effect Of Ion Binding. *J. Membr. Biol.* 59:115-125.

Duzgunes, N., and S. Ohki. 1981. Fusion Of Small Unilamellar Liposomes With Phospholipid Planar Bilayer-Membranes And Large Single-Bilayer Vesicles. *Biochim. Biophys. Acta* 640:734-747.

Dluhy, R. A., D. G. Cameron, H. H. Mantsch, and R. Mendelsohn. 1983. Fourier-Transform Infrared Spectroscopic Studies Of The Effect Of Calcium-Ions On Phosphatidylserine. *Biochemistry* 22:6318-6325.

Ekerdt, R., and D. Papahadjopoulos. 1982. Intermembrane Contact Affects Calcium-Binding To Phospholipid-Vesicles. *Proc. Nat. Acad. Sci* 79:2273-2277.

Feigenson, G. W. 1986. On The Nature Of Calcium-Ion Binding Between Phosphatidylserine Lamellae. *Biochemistry* 25:5819-5825.

Forester, T. R., and W. Smith. 2007. DLPOLY Package of Molecular Simulations v2.19. CCLRC, Daresbury Laboratory, Cheshire, UK. Available at www.ccp5.ac.uk/DL_POLY/.

Hope, M. J., M. B. Bally, G. Webb, and P. R. Cullis. 1985. Production of large unilamellar vesicles by a rapid extrusion procedure. Characterization of size distribution, trapped volume and ability to maintain a membrane potential. *Biochim. Biophys. Acta* 812:55-65.

Humphrey, W., A. Dalke, and K. Schulten. 1996. VMD: Visual molecular dynamics. *J. Mol. Graphics* 14:33-38, 27-28.

Jena, B. P. 2008. Understanding Membrane Fusion: Combining Experimental and Simulation Studies Methods in Cell Biology. In Methods in Nano Cell Biology. B. P. Jena, editor. Academic Press, New York. 183.

Lehrmann, R., and J. Seelig. 1994. Adsorption Of Ca2+ And La3+ To Bilayer-Membranes - Measurement Of The Adsorption Enthalpy And Binding Constant With Titration Calorimetry. *Biochim. Biophys. Acta-Biomembranes* 1189:89-95.

López Cascales, J. J., H. J. C. Berendsen, and J. García de la Torre. 1996. Molecular Dynamics Simulation of Water between Two Charged Layers of Dipalmitoylphosphatidylserine. *J. Phys. Chem.* 100:8621-8627.

Marcelja, S. 1992. Electrostatics Of Membrane Adhesion. Biophys. J. 61:1117-1121.

Martín-Molina, A., C. Rodríguez-Beas, and J. Faraudo. 2010. Charge reversal in anionic liposomes: Experimental demonstration and molecular origin. *Phys. Rev. Lett.* 104: 168103.

McLaughlin, S., N. Mulrine, and T. Gresalfi. 1981. Adsorption of divalent cations to bilayer membranes containing phosphatidylserine. *J. Gen. Physiol.* 77:445-473.

Miraballes-Martinez, I., A. Martin-Molina, F. Galisteo-Gonzlez, and J. Forcada. 2001. Synthesis of amino-functionalized latex particles by a multistep method. *J. Pol. Sci.* 39:2929-2936.

Nir, S., N. Duzgunes, and J. Bentz. 1983. Binding Of Mono-Valent Cations To Phosphatidylserine And Modulation Of Ca-2+-Induced And Mg-2+-Induced Vesicle Fusion. *Biochim. Biophys. Acta* 735:160-172.

Ohki, S., and H. Ohshima. 1999. Interaction and aggregation of lipid vesicles (DLVO theory versus modified DLVO theory). *Col. Surf. B* 14:27-45.

Ohki, S., and K. Arnold. 2000. A mechanism for ion-induced lipid vesicle fusion. *Col. Surf. B* 18:83-97.

Ohki, S. 1982. A Mechanism Of Divalent Ion-Induced Phosphatidylserine Membrane-Fusion. *Biochim. Biophys. Acta* 689:1-11.

Pandit, S. A., and M. L. Berkowitz. 2002. Molecular dynamics simulation of dipalmitoylphosphatidylserine bilayer with Na+ counterions. *Biophys. J.* 82:1818-1827.

Papahadjopoulos, D., S. Nir, and N. Duzgunes. 1990. Molecular Mechanisms Of Calcium-Induced Membrane-Fusion. *J. Bioenerg. Biomembr.* 22:157-179.

Portis, A., C. Newton, W. Pangborn, and D. Papahadjopoulos. 1979. Studies on the mechanism of membrane fusion: evidence for an intermembrane calcium(2+) ion-phospholipid complex, synergism with magnesium(2+) ion, and inhibition by spectrin. *Biochemistry* 18:780-790.

Roldan-Vargas, S., R. Barnadas-Rodriguez, A. Martin-Molina, M. Quesada-Perez, J. Estelrich, and J. Callejas-Fernandez. 2008. Growth of lipid vesicle structures: From surface fractals to mass fractals. *Phys. Rev.* E 78:010902.

Roldan-Vargas, S., R. Barnadas-Rodriguez, M. Quesada-Perez, J. Estelrich, and J. Callejas-Fernandez. 2009. Surface fractals in liposome aggregation. *Phys. Rev.* E 79:011905.

Roux, M., and M. Bloom. 1990. Calcium, magnesium, lithium, sodium, and potassium distributions in the headgroup region of binary membranes of phosphatidylcholine and phosphatidylserine as seen by deuterium NMR. *Biochemistry* 29:7077-7089.

Ross, M., C. Steinem, H. J. Galla, and A. Janshoff. 2001. Visualization of chemical and physical properties of calcium-induced domains in DPPC/DPPS Langmuir-Blodgett layers. *Langmuir* 17:2437-2445.

Roux, M., and M. Bloom. 1991. Calcium-Binding By Phosphatidylserine Headgroups - Deuterium Nmr-Study. *Biophys. J.* 60:38-44.

Schultz, Z. D., I. M. Pazos, F. K. McNeil-Watson, E. N. Lewis, and I. W. Levin. 2009. Magnesium-Induced Lipid Bilayer Microdomain Reorganizations: Implications for Membrane Fusion. *J. Phys. Chem. B* 113:9932-9941.

Silvius, J. R., and J. Gagne. 1984. Lipid Phase-Behavior And Calcium-Induced Fusion Of Phosphatidylethanolamine-Phosphatidylserine Vesicles - Calorimetric And Fusion Studies. *Biochemistry* 23:3232-3240.

Sinn, C. G., M. Antonietti, and R. Dimova. 2006. Binding of calcium to phosphatidylcholine-phosphatidylserine membranes. *Colloids Surf. Physicochem. Eng. Aspects* 282-283:410-419.

Tanaka, T., and M. Yamazaki. 2004. Membrane Fusion of Giant Unilamellar Vesicles of Neutral Phospholipid Membranes Induced by La3+. *Langmuir* 20:5160-5164.

Tatulian, S. A. 1995. Evaluation Of Divalent-Cation Binding To Phosphatidylserine Membranes By An Analysis Of Concentration-Dependence Of Surface-Potential. *J. Colloid Interface Sci.* 175:131-137.

Tscharnuter, W. W. 2001. Mobility measurements by phase analysis. *Appl. Opt.* 40:3995-4003.

Wilschut, J., and D. Hoekstra. 1986. Membrane-Fusion - Lipid Vesicles As A Model System. *Chem. Phys. Lipids* 40:145-166.

Wilschut, J., N. Duzgunes, R. Fraley, and D. Papahadjopoulos. 1980. Studies On The Mechanism Of Membrane-Fusion - Kinetics Of Calcium-Ion Induced Fusion Of Phosphatidylserine Vesicles Followed By A New Assay For Mixing Of Aqueous Vesicle Contents. *Biochemistry* 19:6011-6021.

INTERACTION BETWEEN DNA AND MIXTURES OF ANIONIC/ZWITTERIONIC PHOSPHOLIPIDS MEDIATED BY CALCIUM

C. Rodríguez-Beas, G. Luque-Caballero, G. Bresezinski[†],
Miguel A. Cabrerizo-Vílchez, Julia Maldonado-Valderrama,
and A. Martín-Molina

Grupo de Física de Fluidos y Biocoloides, Dept. de Física Aplicada
Universidad de Granada, 18071, Granada, Spain
[†]*Max Planck Institute of Colloids and Interfaces, 14476 Golm/*
Potsdam, Germany

Abstract

Cationic liposomes have been widely investigated as nonviral gene delivery vectors due to their properties and easy DNA compaction, in spite of the cytotoxicity caused by their positive charge. In contrast, anionic liposomes, which show lower cytotoxicity, have been less studied due to their reduced ability to condensate DNA. In this work, we analyze the complexation of anionic liposomes with DNA mediated by Ca^{2+} cations. A mixture of anionic (DOPS) and zwitterionic (DOPC) lipids with linear DNA is used in order to probe the effectiveness of Ca^{2+} in the formation of the complexes. Electrophoretic mobility measurements reveal that the ternary system (liposomes/Ca^{2+}/DNA) acquires a higher electrokinetic charge than those corresponding to pure liposomes or DNA. Compression isotherms of DOPS/DOPC monolayers present also an increase of the lipid molecular area and of the Gibbs elasticity of the lipids/Ca^{2+}/DNA monolayers, compared to those of lipids/Ca^{2+} and lipids/DNA. Moreover, IRRA-spectra showed an increase of the phosphate asymmetric and symmetric bands of the lipid monolayer with Ca^{2+} and DNA respect to lipids/Ca^{2+} and lipids/DNA. On the basis of the analysis of the electrokinetic and interfacial results, it can be concluded that the DNA is incorporated into the DOPS/DOPC lipids forming anionic complexes only in the presence of the Ca^{2+}. This is an important contribution towards the better understanding of anionic lipoplexes.

Introduction

The evolution of gene–based drugs represents a new class of therapy that has the potential to prevent, correct or modulate the human gene disorder in both inherited and acquired diseases as: cancer, cystic fibrosis, hemophilia, neuromuscular disorder and others [1]. Liposomes have been investigated since 1970's as drug carriers to enhance the delivery of therapeutic agents [2-3]. Particularly, the complexation of cationic liposomes with DNA (cationic lipoplexes) has been studied as principal delivery vectors. But, despite their easy formation, cationic lipoplexes have some limitations. For instance, studies have shown that they cause cytotoxicity in both, *in vitro* and *in vivo* [4-5]. Consequently, recent investigations revealed the complexation of anionic liposomes with DNA (anionic lipoplexes) as an alternative to classical cationic lipoplexes due to their lower cytotoxicity [6-8]. In order to link anionic lipids (ALs) and DNA, both with negative net charge, divalent cations, such as (Ca^{2+}), have been used [7-9].

As a result of the above mentioned, the research of anionic lipoplexes has vertiginously grown on gene therapy, but there are still many open questions. In fact, recent studies have shown that the genetic transference of these systems is intimately related to their physical, chemical and biological properties [10-11]. Patil et al. studied the complexation of anionic/zwitterionic liposomes of DOPG/DOPE (dioleoylphosphatidylglycerol/dioleoylphosphatidyl-ethanolamine, respectively) with a plasmid DNA, mediated by Ca^{2+} [7,9]. According to them, biophysical studies of anionic lipoplexes can be used to identify formulation conditions and electrochemical properties for optimal

transfections. In addition, Srinivasan et al. [12] and Khiati et al. [8] studied the complexation of anionic lipoplexes with DNA mediated by divalent cations, concluding that the anionic lipoplexes exhibit high transfection efficacy. Srinivasan et al. also compared the transfection efficiency of anionic lipoplexes with cationic lipoplexes concluding that it was similar or higher, but the cellular toxicity was meaningfully less when anionic liposomes were used. [12] Liang et al. carried out also experiments with anionic lipoplexes by using different divalent cations at diverse concentrations [6]. According to them, the structural phase of the resulting anionic lipoplexes depends on the lipidic membrane charge density and the type/concentration of the cations.

Although phospholipid bilayers have been used as a model of biological membranes for many years [13-15], Langmuir monolayers are an interesting alternative to study the lipid bilayers. In particular they are easier to manipulate and also mimic the biomembrane properties [16-18]. Lipid monolayers present a rich polymorphism that can be analyzed at different length scales and with a variety of techniques [19]. The fluidity of monolayers can be controlled with the temperature, the nature of the lipids, the compression barrier of the trough, etc. In particular, it is accepted that the lipid monolayer at surface pressures ≥ 30 mN/m is directly related to the effective lateral pressure of the bilayers [17,20]. Hence, Langmuir monolayer at the air−water interface offers a clear advantage over bilayers for the evaluation and comparison of interfacial models of ion binding in order to study specific ionic effects. Moreover, the Gibbs elasticity of the monolayers plays an important role in the understanding the lipid

biomembranes [21-22]. Elastic membrane parameters such as bending rigidity and stretching modulus, tend to increase in the presence of Ca^{2+}. These features were attributed to the bridging effect of the Ca^{2+} to the anionic lipid head [23]. Furthermore, molecular vibrations studies of the surface pressure lipid monolayers carried out with IRRAS, give information about the conformation, orientation and reorientation of the lipid chains, and the changes of these properties can be detected with the interaction of the lipid headgroups with particles as divalent cations and DNA [24], proteins [25] and also with lipid mixtures [26].

The study of interactions of DNA with lipid monolayers in the presence of Ca^{2+} offers an interesting insight of the electrostatic interaction process of ALs and DNA mediated by divalent cations. To this purpose, two specific phospholipids were used: anionic 1,2-dioleoyl-*sn*-glycero-3-phosphoserine (DOPS) and zwitterionic 1,2-dioleoyl-*sn*-glycero-3-phospho-choline (DOPC). This sort of phospholipids with monounsaturated lateral chains were chosen because have specific interest in gene therapy applications owing to the presence of double bonds in the hydrophobic part of the phospholipid, which has been proved to enhance the transfection efficiency of lipoplexes [27]. The complexation was carried out using calf thymus DNA (CT–DNA), mediated by divalent Ca^{2+}. To our knowledge, these types of mixtures have not been previously reported in the literature. The objective of this work is twofold: On the one hand, we aim to characterize the electrokinetic behavior of DOPS/DOPC liposomes and CT–DNA complexes in the presence of Ca^2. On the other hand, we performed an interfacial characterization

of DOPS/DOPC monolayers in the presence of Ca^{2+} and/or CT–DNA in the aqueous subphase, obtaining isotherms, elasticities and IRRA spectra. The combination of these experimental approaches offers a new perception of the interaction between the ALs and DNA which in turn, becomes decisive to understand the behavior of the resulting complexes. The information obtained can be crucial towards the application of anionic lipoplexes in gene therapy.

Materials and Methods

DNA from calf thymus (CT–DNA) (95% of purity) used in this work whereas the lipids were: anionic 1,2-dioleoyl-*sn*-glycero-3-phospho-L-serine sodium salt (DOPS) and zwitterionic 1,2-dioleoyl-*sn*-glycero-3-phosphocholine (DOPC). All of them were purchased from Sigma-Aldrich. Calcium nitrate ($Ca(NO_3)_2$) was acquired from Scharlau Chemie S.A. containing 99% of purity. HEPES buffer (4-(2-hydroxyethyl) piperazine-1-ethanesulfonic acid and its sodium salt) was purchased from Sigma-Aldrich. Reagent grade Chloroform and methanol were acquired from Scharlau Chemie S.A. (Spain). Milli-Q ultrapure water, with resistivity lower than 18 MΩ·cm was used for buffer preparation. All solutions were prepared in buffer 40 mM HEPES (pH = 7.4) at 298 K.

Preparation of liposomes and DNA

Dry films of mixed lipids were prepared by dissolving 0.0406 g and 0.0394 g of DOPS and DOPC (1:1M) respectively, in 10 ml of

chloroform/methanol (3:1v). The solvent was evaporated under vacuum by rotary evaporation for at least 2 h and then passed through a steady stream of nitrogen gas (N_2). The dry films were hydrated in 40 mM HEPES (pH = 7.4) for 4 h, using a protocol previously described in detail in [28]. This hydration was carried out above the transition temperature (T_m) of both lipids. Alternating cycles of vigorous sonication and hydration were used to help the homogenization of solution and the total time of sonication remained under 5 min. Finally, small unilamellar vesicles were formed by using the extrusion technique [29-30], which consists in 5 passes through 800 nm then 5 passes through 200 nm pore size polycarbonate membranes. The extrusion was carried out using a Thermobarrel Lipex Extruder (Northern Lipids Inc., Canada), with 10 ml of capacity, that uses a N_2 current under pressure to force the solution through the membrane. The final liposome solution was stored in the fridge at 4–7ºC. The monodispersity of the sample was tested before each experiment by photon correlation spectroscopy (PCS), obtaining a mean particle size of 144 ± 14 nm and mean polydispersity of 0.28 ± 0.15.

A stock solution (2.5 mg/ml) of CT–DNA was prepared by dissolving solid DNA in 40 mM HEPES, pH = 7.4 on the day before the measurements and kept in the fridge at 4–7°C. Dilutions from this stock were prepared just before use.

Preparation of complexes

A liposome concentration of 5×10^{-4} M was used and kept constant for all the experiments. First, Ca^{2+} was added to the negatively charged liposomes within a range of concentration from 10^{-6} to 0.2 M. The liposomes with Ca^{2+} were kept incubated for 5 min at room temperature, after magnetic stirring, to ensure a good interaction. Then, the DNA was added to get the lipoplexes, using two different DNA concentrations of 0.0295 and 1.25 mg/ml. The additions were performed at the speed of 0.2 ml/min, with continuous and constant magnetic stirring to get a better distribution in the solution as it is described in a previous work [31]. Magnetic stirring was stopped at least 5 minutes before each measurement.

Electrophoretic mobility studies

The electrophoretic mobility (μ_e) measurements were performed by using two experimental techniques. Namely, a ZetaPALS instrument Brookhaven (USA), based on the principles of Phase Analysis Light Scattering (PALS) technique [32-33] and Zetasizer Nano series, Malvern instruments (UK), which combines Electrophoresis and Laser Doppler Velocimetry (LDV) [34]. The electrophoretic mobility of liposomes and complexes were taken as the average over at least three measurements for each sample. Liposomes concentration was 5×10^{-4} M and two concentrations of DNA were used in the complexes (0.0295 and 1.25 mg/ml). The concentration of Ca^{2+} was varied from 10^{-6} to 0.2 M. The measurements were carried out at room temperature. The experiments were performed with at least three independent samples.

Surface compression isotherms studies

The surface compression isotherms, pressure (π) – area (A), were carried out with a KSV, Biolin Scientific Oy (Finland), Langmuir trough of total volume 180 ml, equipped with paper Wilhelmy plates pressure measuring system. Firstly, the absence of surface–active contaminants in the HEPES solution was verified by recording the π–A compression of the buffer solution and assuring values of $\pi < 0.1$ mN/m. Then, 14 μl of phospholipids solved in chloroform with a concentration of 1.3×10^{-3} M were spread on the surface of HEPES solution. After an evaporation time of 30 min, the monolayer was compressed with a velocity of 7.5 cm^2/min. The addition of Ca^{2+} or DNA to the subphase was carried out after the lipid deposition and evaporation, by injection and dispersion of stock solutions 0.3 M Ca^{2+} and DNA 0.25 mg/ml from behind of the trough barriers using a syringe. In the case of the experiments with both Ca^{2+} and DNA in the subphase, they were sequentially added, in this order, at intervals of 30 min. All the π–A isotherms were recorded and analyzed by using computer software provided by KSV. The reproducibility of the π–A isotherms was tested by repeating three times each experiment.

Infrared Reflection–Absorption Spectroscopy (IRRAS) studies

IRRAS measurements were performed using an IFS 66 FT–IR spectrometer from Bruker (Ettlingen, Germany) equipped with a nitrogen cooled MCT (mercury cadmium telluride) detector. The spectrometer is coupled to a Langmuir–film trough (R&K, Potsdam,

Germany) placed in an external air–water reflection unit (XA–511, Bruker). A KRS–5–wire–grid polarizer is used to polarize the IR beam perpendicular to the incidence plane (s–polarized) and it is then focused on the water surface of the Langmuir trough. The incidence angle with respect to the surface normal was set to 40° and the reflected radiation was collected and measured at the same angle. The setup consisted of two troughs connected by little pipes to ensure the same liquid height and it is placed inside of a hermetically sealed compartment. The both troughs have a total volume of 120 ml and the surface pressure was measured by a filter paper Wilhemy plate system.

Firstly, the absence of surface–active contaminants in the buffer was verified by recording the π–A compression isotherm and assuring values of $\pi < 0.1$ mN/m. Then, 50 μl of 5.4×10^{-4} M of DOPS/DOPC solution were spread on the water surface in one trough (sample), whereas the other (reference) is filled with the pure subphase. 1 h was given for the equilibration and water vapor saturation and then the monolayer was compressed at the rate of 9 cm^2/min. Once the surface pressure (π) reached the values of 5 or 30 mN/m, the barrier motion was programmed to keep the pressure constant during IRRAS acquisition time. In order to eliminate the interference due to water vapour, measurements were performed by switching between the two troughs at regular intervals using a trough shuttle system. IRRAS data are reported in terms of reflectance–absorbance (R–A) vs. wavenumber. R–A is defined as $-log(R/R_0)$, where R is the reflectivity

of the film−covered surface and R_0 is the reflectivity of the bare subphase. The spectra were recorded with a spectral resolution of 8 cm^{-1}, a scanner speed of 20 kHz, accumulated using 400 scans and shifted to zero at 1157 cm^{-1}.

Results and Discussion

Electrophoretic mobility

Electrophoretic mobility measurements were carried out in order to study the interaction of DOPS/DOPC liposomes and DNA, mediated by Ca^{2+}. To this end, the following results are shown in Figure 1: *i)* First, the effect of Ca^{2+} on the electrophoretic mobility of DOPS/DOPC liposomes is reported, *ii)* then, electrophoretic mobility of DNA in the presence of Ca^{2+} is also measured, *iii)* finally, the effect of the Ca^{2+} on the electrophoretic mobility of the binary system liposome/DNA is studied. Liposome concentration was fixed to 5x10^{-4} M in all cases and the concentration of Ca^{2+} was varied from 10^{-6} to 0.2 M. In the case of DNA, two concentrations were used. First, a concentration of 0.0295 mg/ml was chosen (Figure 1A) in agreement with the DNA concentration used in a previous work in which the complexation of DNA by cationic liposomes was studied [31]. Then, since the electrophoretic mobility of DNA depends on its concentration, a higher DNA concentration of 1.25 mg/ml was also tested (Figure 1B). Accordingly, the electrophoretic mobility of the DOPS/DOPC liposomes in the presence of Ca^{2+} is discussed in first place. As can be seen in Figure 1, the absolute value of the mobility of

liposomes tends in general to decrease as the concentration of Ca^{2+} increases. For the lower concentrations of Ca^{2+}, the value of the μ_e of the liposomes remains constant being its value similar to that measured for liposomes in bulk $(-5.0 \pm 0.7) \times 10^{-8} m^2 V^{-1} s^{-1}$.
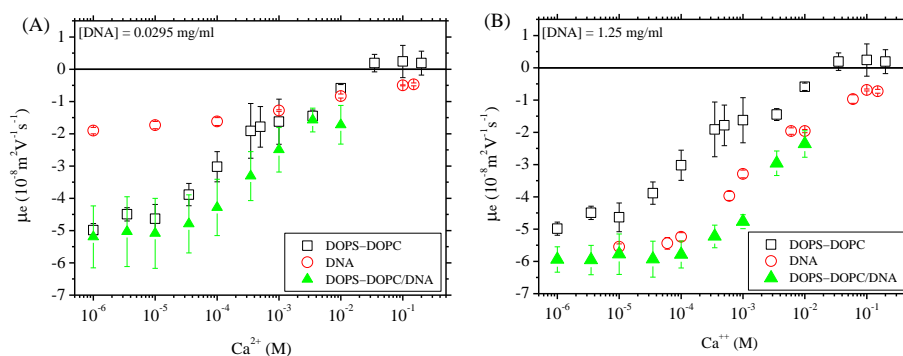

Figure 1.- Electrophoretic mobility of liposomes, DNA and lipoplexes as a function of Ca^{2+} concentration. Effect of the DNA and Ca^{2+} concentrations on the electrokinetic behaviour of liposomes $(5 \times 10^{-4} M)$.

For higher Ca^{2+} concentrations, $|\mu_e|$ decreases with the electrolyte concentration until the isoelectric point is reached in the system (*i.e.* $\mu_e = 0$). This behavior is common for charged colloids which are immersed in electrolyte solutions, where ions screen the electrostatic interaction due to the surface charge of the particles. In our case, DOPS/DOPC liposomes are negatively charged and they become unstable for concentrations of Ca^{2+} above 10^{-2} M. At this point, aggregation of liposomes is expected to happen and hence, μ_e tends to be null. Similar results are found for liposomes made of pure phosphatidylserine (PS) lipids and mixtures of phosphatidylcoline

236

(PC) and PS lipids [35-36] and for combinations of other anionic lipids [37]. Apart from the screening effect of the Ca^{2+} on anionic liposomes, Sinn et al. show that Ca^{2+} tends to bind to the polar head of the PS and PC lipids by following a process entropycally driven, related to liberation of water molecules from the hydration shells of the ion and the lipid headgroups [38].

Consider now the electrophoretic mobility of DNA in the presence of Ca^{2+}. First, the lower concentration of DNA (0.0295 mg/ml) is discussed (Figure 1A). It can be seen that, as in the case of the liposomes, the electrophoretic mobility of DNA tends to decrease as the concentration of Ca^{2+} increases. For low concentrations of Ca^{2+}, μ_e remains constant being its value similar to that measured for DNA in bulk $(-1.98 \pm 0.19) \times 10^{-8} m^2 V^{-1} s^{-1}$. Then, $|\mu_e|$ gradually decreases as the concentration of Ca^{2+} increases and an aggregation of DNA molecules is expected to take place. Figure 1B shows a completely similar behavior encountered for the mobility of a higher concentration of DNA (1.25 mg/ml). For concentrations of Ca^{2+} within the range of $[10^{-6} - 10^{-4}]$ M, μ_e remains comparable to that of DNA in the absence of Ca^{2+}: $(-5.4 \pm 0.3) \times 10^{-8} m^2 V^{-1} s^{-1}$. Above a concentration of Ca^{2+} of 10^{-4} M, we find a rapid decrease of $|\mu_e|$ as the concentration of electrolyte increases further. As in the case of anionic lipids, metal cations have a tendency to bind the phosphate groups of DNA. As a consequence, electric repulsion between DNA molecules (and intramolecular repulsion) is reduced and they tend to aggregate. Duguid et al. have studied this aggregation by means of laser Raman spectroscopy for CT–DNA/Ca^{2+} and also different divalent metal ions

[39]. Moreover, aggregations of DNA were also reported with melted CT–DNA/Ca^{2+} and other divalent metal ions by differential scanning calorimetry and optical densitometry [40].

Once the electrokinetic behavior of liposomes and DNA have been independently analyzed, the effect of the Ca^{2+} on the electrophoretic mobility of the binary system DOPC–DOPS/DNA is analyzed for the two concentrations of DNA: 0.0295 mg/ml (Figure 1A) and 1.25 mg/ml (Figure 1B). In both cases, $|\mu_e|$ tends to decrease as the concentration of Ca^{2+} increases in the system. The main difference is found at low concentrations of Ca^{2+}. That is, for the lowest concentration of DNA (Figure 1A), the $|\mu_e|$ of the mixture tends to the value of pure DOPS/DOPC liposomes. Differently, for the highest concentration of DNA (Figure 1B), the $|\mu_e|$ tends to the value of pure DNA.

Nevertheless, in both cases, the electrophoretic mobility of the system DOPS–DOPC/DNA is in general more electronegative than the μ_e of pure liposomes and pure DNA. In other words, $|\mu_e|$ curves of liposomes/DNA appear below those of the pure systems for the two concentrations of DNA studied (Figures 1A and 1B). Hence, in general, it can be concluded that at low concentrations of Ca^{2+}, the electrophoretic mobility of DOPS–DOPC/DNA tends to that of the most electronegative system; i.e., liposomes, in Figure 1A and DNA, in Figure 1B. At any rate, the resulting complex liposome/Ca^{2+}/DNA presents a higher electrokinetic charge for higher concentrations of Ca^{2+}. Then, the question is: does this finding demonstrates the

formation of anionic lipoplexes mediated by Ca^{2+}? Let us first suppose that lipoplexes were not obtained. Then, since different negatively charged colloids (DNA and liposomes) are electrostatically repelled to each other, they would give rise to different electrophoretic behaviors. At the same time, because the electrokinetic device assumes that the experimental sample is monodisperse, it would provide an average value for μ_e. Accordingly, if no complexes were formed, the μ_e of the mixture should be always comprised between the μ_e of pure DNA and that of pure liposomes. However, this is not the case as can be seen in Figures 1A and 1B where the electrophoretic mobility of the DOPC–DOPS/Ca^{2+}/DNA exhibit $|\mu_e|$ values higher than those reported by the DNA and the liposomes in the presence of Ca^{2+}. This higher value could indicate that Ca^{2+} is acting as a bridge between the liposomes and the DNA implying that anionic complexes with new electrokinetic properties are being formed. Precisely, this is the idea used to explain the formation of anionic lipoplexes mediated by multivalent cations found in the literature such as those made of DOPG/DOPE liposomes and a plasmid DNA in the presence of Ca^{2+} [9,12]. Anionic lipoplexes obtained from other type of lipids and divalent cations are also reported [6,8].

In our case, the complexation of DNA with DOPS/DOPC mediated by Ca^{2+} cannot be directly inferred from electrokinetic measurements. However, it provided evidence of a certain interaction of DNA with DOPS/DOPC liposomes in the presence of Ca^{2+}. In order to further understand the nature of this interaction, interfacial techniques were

applied to study the interaction of DNA with DOPS/DOPC monolayers in the presence (and in the absence) of Ca^{2+}.

Surface pressure isotherms

Surface pressure measurements in the form of surface pressure−area (π−A) isotherms were carried out in order to further study the interaction of DOPS/DOPC liposomes and DNA mediated by Ca^{2+}. To this end, the following results are shown in Figure 2: *i)* First, the π−A isotherm of a DOPS/DOPC monolayer is reported, *ii)* then, the π−A isotherm of this monolayer in the presence of Ca^{2+} in the subphase is also measured, *iii)* likewise, the effect of the addition of DNA in the subphase on the DOPS/DOPC isotherms is also recorded and *iv)* finally, the effect of both Ca^{2+} and DNA, on the π−A isotherm of the lipids is studied. The spread amount of lipids was fixed to 14 μl of concentration 1.3×10^{-3} M. The DNA concentration added into the subphase was 0.0295 mg/ml while two different concentrations of Ca^{2+} were used in order to reproduce the electrophoretic mobility conditions and to test the effect of two extreme concentrations of Ca^{2+}. This concentration range of divalent electrolytes is suggested by Liang et al. in their study of anionic lipoplexes [6].

Figure 2 shows that all isotherms exhibits a progressive increase of the surface pressure (π) during the compression. That is, in all cases a continuous phase transition between the phases gaseous (G) and liquid−expanded (LE) is recorded as the surface area decreases. Table

1 summarizes the values of the limiting area per molecule (A_0) and the collapse pressure (π_c) of the monolayers, when the lipids are in the LE phase. A_0 was calculated from the extrapolated molecular area at $\pi = 0$ of the LE phase.
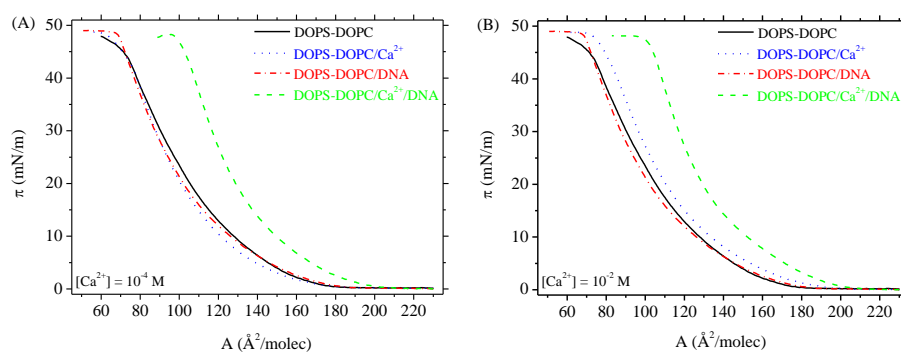

Figure 2.- π–A compression isotherms at the air–water interface of DOPS/DOPC, spread on the surface of buffer 40 mM HEPES at pH = 7.4. Effect of the addition of 0.0295 mg/ml DNA and Ca^{2+}.

Let us first discuss the isotherm of DOPS/DOPC lipids on buffer, which is plotted in figures 2A and 2B. As can be seen, the surface pressure begins to increase at large molecular areas (approximately 180 Å^2/molecule). The expansion of the polar head, provoked by the mixture of phospholipids, causes that the onset for the increase of surface pressure occurs at large areas per molecule, compared with those of separated lipids (graphs not shown). The surface pressure increases progressively until a buckle point around $\pi = 45$ mN/m and reaching the collapse pressure (π_c) at 48 ± 2 mN/m (Table 1). The limiting reached area (A_0) per molecule is 122 ± 8 Å^2/molecule. The isotherm shape and π_c value are similar to others found in the

241

literature for similar systems; for example, the isotherm of the lipid mixture: zwitterionic dioleoyl-*sn*-glycerol-3-ethyphosphocholine (EDOPC) and anionic DOPG [41]. Interestingly, in the isotherms of DOPS/DOPC there is a slight bend appearing just before collapse (Figure 2). Baoukina et al. showed isotherms of mixtures of DPPC and POPG (palmitoylphosphatidylglycerol), which reach a bend point before the collapse. They proposed the formation of a bilayer and then a vesicle in the bulk as possible evolution [42]. Also monolayer compression beyond the collapse can form trilayers composed by a bilayer and a monolayer with the tails oriented to the air [26]. However, this effect is less noticeable in our case as can be seen in Figure 2.

Table 1. – Limiting molecular area $(A_0)^a$, collapse pressure (π_c) and maximum Gibbs elasticity (ε_{max}) of the monolayer values, in presence of Ca^{2+} and/or DNA.

Isotherms	A_0^b (Å^2/molecule)	π_c^b (mN/m)	ε_{max}^b (mN/m)
DOPS−DOPC	122 ± 8	48 ± 2	72 ± 4
DOPS−DOPC/Ca^{2+}(10^{-4} M)	118 ± 14	48 ± 2	90 ± 1
DOPS−DOPC/Ca^{2+}(10^{-2} M)	132 ± 11	48 ± 1	88 ± 4
DOPS−DOPC/DNA	123 ± 3	49 ± 1	79 ± 5
DOPS−DOPC/Ca^{2+}(10^{-4} M)/DNA	146 ± 6	47 ± 1	127 ± 3
DOPS−DOPC/Ca^{2+}(10^{-2} M)/DNA	164 ± 5	47 ± 1	137 ± 1

[a] Calculated from the extrapolated molecular area at $\pi = 0$ of the LE phase.
[b] Mean ± SD correspond to three independent experiments.

Now, we consider the effect on the DOPS/DOPC π–A isotherms of the addition of Ca^{2+} into the subphase. First, the lowest concentration of Ca^{2+} (10^{-4} M) is discussed (Figure 2A). The isotherm has a general behavior which is similar to that of pure lipids on buffer, i.e., both isotherms practically overlap. The π of the isotherm begins to increase at around 180 $\mathring{A}^2$/molecule, until reaching the collapse at π_c 48 $\pm$ 2 mN/m (Table 1), ascending the buckle point approximately at the same π_c value. This could suggest that for higher pressures, where the lipids are closer, the binding of the Ca^{2+} is enhanced due to the high local concentrations of negative charge from lipids. Hauser et al. in their studies with PS and PI (phosphatidylinositol) lipids showed that at the collapse pressure the binding of the Ca^{2+} with the lipids is related with the excess of the negative charge and large independent of the chemical nature of the lipids [43]. The effect of a higher concentration of Ca^{2+} (10^{-2} M) on the π–A isotherm of lipids is shown in figure 2B. It can be seen that the whole isotherm is slightly shifted to higher molecular areas by increasing the electrolyte concentration. Nevertheless, the surface pressure passes through the buckle point and the π_c remains similar to that found for the lowest concentration of Ca^{2+} (Table 1). A small difference is also present in the limiting area per molecule reached. Accordingly, the presence of higher concentration of Ca^{2+} provides a higher molecular area of the DOPS/DOPC isotherm (Table 1). Ross et al. observed a similar slight shift, of the monolayer composed of DPPC/DPPS, to larger molecular areas in the presence of Ca^{2+} [44]. They attributed this increase in the area to the formation of hydrated Ca^{2+}/DPPS complexes.

243

Nevertheless, various reports carried out with PS and Ca^{2+} conclude that the binding of the Ca^{2+} to the PS head group induce a dehydration of the lipid/Ca^{2+} complex [45]. Martin–Molina et al. also confirmed that the Ca^{2+} influences in the area per lipid of the PS membrane [46]. Moreover, the effect caused by higher Ca^{2+} concentration, increasing the area (A_0) per molecule in the monolayer, agrees with the electrophoretic mobility results. After seeing the effect of the Ca^{2+} on the monolayer of DOPS/DOPC, we also analyzed in Figure 2 the effect of DNA on the lipid monolayer, first, in the absence of Ca^{2+}. DNA was added into the subphase prior to compression of the monolayer of lipids once this was stable at the surface. The π–A isotherm practically overlaps the curve corresponding to pure lipids, reaching an area A_0 of 123 $Å^2$/molecule. The surface pressure at the collapse point is slightly higher (Table 1) and the bend prior to collapse which appeared for pure lipids disappears in the presence of DNA as happened also in the presence of Ca^{2+}. Anyway, the DNA does not seem to cause an effect on the monolayer in the absence of Ca^{2+}. Our result agrees with the reported work by Gromelski et al. who used the IRRAS technique to study the effect of CT-DNA on DMPE (dimyristoylphospahtidylethanolamine) monolayers in the presence and in the absence of Mg^{2+}. Therein, the authors showed that the DNA did not bind to the DMPE monolayers in the absence of this divalent cation [24].

Finally, and following a similar procedure than that used in the electrophoretic mobility measurements, the effect of the Ca^{2+} and

DNA together on the monolayers is analyzed after analyzing the effect of Ca^{2+} and DNA on the π–isotherms of DOPC/DOPS separately. Figures 2A and 2B show the effect of addition of DNA for both concentrations of Ca^{2+} (10^{-4} M and 10^{-2} M, respectively). Regardless of the concentration of Ca^{2+}, the isotherms of DOPS/DOPC in the presence of DNA and Ca^{2+} appear clearly more expanded than all the rest. Interestingly, this expansion is even higher for the higher concentration of Ca^{2+} (Table 1). This could be provoked by the strong ion pair formed between the Ca^{2+} and phosphate groups of the lipids, as explained above. However, the π_c remains similar to that of the other systems with a value of 47 ± 1 mN/m (Table 1). The results shown in Figure 2 correlate with those obtained for the electrophoretic mobility measurements in Figure 1. As discussed above, the Ca^{2+} would act as a bridge between lipids and DNA. Similar conclusions are reported in the literature with analogous systems. For instance, Gromelski et al. carried out experiments with DMPE and CT–DNA in the presence of divalent cations [24]. They concluded that the change in the isotherms at the lower pressures and larger areas is the result of penetration of the DNA into the DMPE lipid monolayer. Also, theoretical models predict the interaction of DNA with zwitterionic phospholipids mediated by divalent cations [15]. Logically, this effect is enhanced for the case of mixtures of anionic/zwitterionic lipids. As discussed above, the Ca^{2+} firstly binds to the anionic lipids, then once all the phosphate groups of the anionic lipid are occupied, the Ca^{2+} starts to binds to the zwitterionic lipids [38]. In other words, the negative charges of the anionic lipid are the main responsible of a stronger

attraction of the Ca^{2+} ions. Thus, the increased area A_0 of our results in the ternary system could confirm the crucial role of Ca^{2+} in the interaction between lipids and DNA. This effect is also recorded in isotherms of the ternary system 2POPC:PS/Ca^{2+}/CT–DNA [47]. In summary, the high molecular areas obtained, indicate the effectiveness of Ca^{2+} in promoting the interaction of lipids and DNA. The presence of Ca^{2+} promotes the binding between DNA and lipids, and the presence of higher concentration of Ca^{2+} provides more binding sites, hence providing a further increase of the area per molecule.

To gain further information on the influence of the Ca^{2+} on the surface properties of the lipids in the presence of DNA, information of the packing density of the monolayers was obtained by looking into the calculated Gibbs elasticity (ε_0) of the monolayers.

Monolayer elasticity

Figure 3 shows the Gibbs elasticity (ε_0) of the DOPS/DOPC monolayers as a function of the surface pressure (π). This was calculated from the surface pressure–area isotherms in Figure 2, using the following equation [22,48],

$$\varepsilon_0 = -A \ (d\pi/dA)$$

where A is the area per molecule and π is the corresponding surface pressure. ε_0 represents the rheological quantity related to the monolayer rigidity and to its capability to store elastic energy. These results are discussed by following the same systematic procedure than that used for the isotherms measurements. Therefore, first the

elasticity of the monolayer of the DOPS/DOPC is analyzed. Then, the separately effect of Ca^{2+} and DNA on the monolayer of lipids is discussed. Finally, the effect of Ca^{2+} and DNA at the same time on the DOPS/DOPC monolayer is analyzed for the same two concentrations of Ca^{2+} used before.
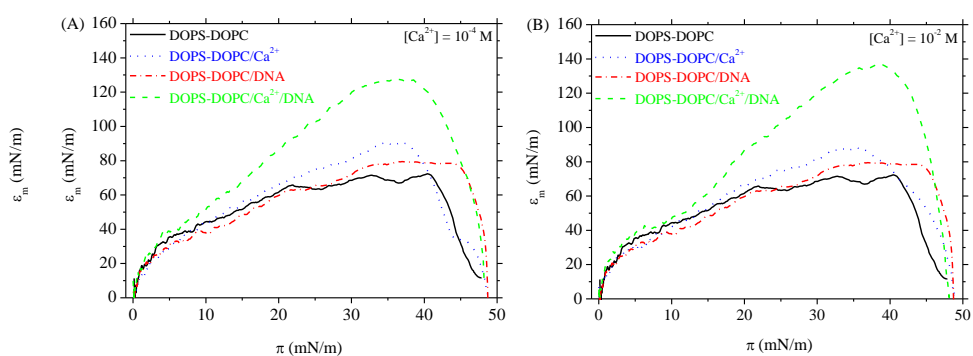

Figure 3.- Monolayer elasticity (ε_m) calculated from the surface pressure−area isotherms with $-A(d\pi/dA)$. With Ca^{2+} 10^{-4} M (A) and 10^{-2} M (B).

In general, the curve of the Gibbs elasticity versus surface pressure (Figure 3), begins with a characteristic value of ε_0 of around 20 mN/m, for surface pressures close to zero (corresponding to the transition phase between G and LE in all cases). Then the elasticity of the monolayer increases with the compression until a maximum value is reached, just before the collapse. The numerical values of the elasticity of the layer at this maximum give an idea of the rigidity of the monolayers (see Table 1).

In the case of pure lipids, the elasticity shows a plateau located at a π of 22 mN/m (Table 1), and then increases until reaching the maximum Gibbs elasticity (ε_{max}) of 72 mN/m, which holds until collapse, being characteristic of the LE state of the monolayer (Figure 3). Similar behavior of the elasticity was reported for the pure DOPC on different subphases [49-50].

The addition of Ca^{2+} causes slight changes in the Gibbs elasticity of the DOPC/DOPS mixture. Hence, the lower concentration of Ca^{2+}, 10^{-4} M (Figure 3A), provides a small increase of ε_{max} in comparison with that obtained for pure lipids (Table 1). For a higher concentration of Ca^{2+} of 10^{-2} M (Figure 3B), the elasticity of the monolayer is also higher. However, this increase is less noticeable than that recorded due to a lower concentration of Ca^{2+}. The addition of Ca^{2+} causes an increase of the lipid monolayer elasticity; when the Ca^{2+} concentration increases, there is a slight decrease of the elasticity because the increased area per molecule in the monolayer, i.e., the monolayer is less compact. To our knowledge, comparable results of elasticity of these lipids in interaction with Ca^{2+} have been not reported in the literature. Similar behavior in the increase of the area per molecule and compressibility is reported for hemoglobin (Hb) in interaction with potassium chloride (KCl) ions by Mahato et al. [51]. The authors suggested that the increase of the compressibility may be due the unfolding and/or partial squeezing out of the Hb preceding the full collapse caused by KCl.

The effect of DNA on the elasticity of the DOPS/DOPC monolayer is also plotted in Figure 3. As a general trend, the elasticity of the monolayer appears similar to that of lipids alone and with Ca^{2+}. This agrees with the similarities recorded in the $\pi-A$ isotherms in Figure 2. Figure 3 shows that how the elasticity reaches a plateau that remains until the monolayer collapses at a value of 79 mN/m. This effect was also observed in the absence of DNA (see Table 1). Interestingly, the plateau extends over a wider range of surface pressures and also finishes more abruptly. This could be related to the disappearance of the bend in Figure 2 and the indication of the higher stability of the monolayer of lipids in the presence of DNA. Anyhow, the presence of DNA does not affect the elasticity of the lipid monolayer in the absence of Ca^{2+} and therefore there is no indication of structural changes induced in the lipid monolayer. To our knowledge, monolayer elasticities of these types of lipids and DNA have not been reported yet in the literature.

Finally, the presence of Ca^{2+} and DNA at the same time in the aqueous subphase of the lipid monolayer is analyzed. Figure 3 shows the effect of two previously selected concentrations of Ca^{2+} on the monolayers: 10^{-4} M (A) and 10^{-2} M (B). In both cases, the addition of Ca^{2+} and DNA has a very noticeable effect on the Gibbs elasticity of the monolayer as compared to those of the components separately (Figure 3). The elasticity no longer reaches a plateau but the value increases importantly until reaching a maximum value which is much higher than that attained for the previous systems (Table 1). In other

words, DOPS–DOPC/Ca^{2+}/DNA monolayers yield higher Gibbs elasticities compared with the monolayers formed by a single or two components. Moreover, this maximum increases as the concentration of Ca^{2+} increases in the system (Figures 3A and 3B). This feature suggests that the DNA affects the structural properties of the lipid in the presence of Ca^{2+}. This fact importantly correlates with the π–A isotherms and the electrophoretic mobility, but also importantly provides structural information of the interaction. The increment of the elasticity of the lipid monolayer is probably due to the interaction with DNA molecules mediated by Ca^{2+}. Another important observation is that the elasticity of the monolayers practically remains equal for surface pressures below 5 mN/m and only above this surface pressure, some differences in the elasticity behavior appear due to the presence of Ca^{2+} and DNA. This is a fascinating finding which could suggest that the binding of DNA to the lipids is not only mediated by Ca^{2+} but also requires a minimum surface coverage. Furthermore, the maximum appears displaced towards higher values of surface pressure for the highest concentration of Ca^{2+} used. This could be due to the higher presence of binding sites in the monolayer which allows the interaction to take place at higher concentration of lipids. In the literature, it is known that properties of the monolayers at surface pressure ~ 35 mN/m can be extrapolated with the free tension properties of lipid bilayers [17-18], that mimic the biomembrane properties [17,52]. Accordingly, these results could resemble the case of lipid bilayers when they form liposomes.

IRRAS

IRRA spectra were performed in order to gain further insight into the interaction between DNA and DOPS/DOPC monolayers mediated by Ca^{2+}. To this end, the following IRRA spectra were registered: *i)* firstly, lipids monolayer on buffer, *ii)* then, lipids monolayer in the presence of Ca^{2+}, *iii)* lipid monolayer in the presence of DNA, *iv)* finally, the lipid monolayer in the presence of Ca^{2+} and DNA together. The concentration of Ca^{2+} used was 10^{-2} M, considering the effects caused in the isotherms, and the concentration of DNA was the same used for the isotherms (0.0295 mg/ml). IRRA spectra provide information about vibration of groups of all the molecules located at or close to the air−solution interface [53]. Therefore, both the phospholipid monolayer and the molecules interacting with their headgroups can contribute to the measured spectra.

As can be seen in Figure 4, the main differences between the spectra recorded on the different subphases were located in the phosphate band region (1300 − 1000 cm^{-1}). Phosphate asymmetric and symmetric stretching bands ($\nu_{as}(PO_2^-)$ and $\nu_s(PO_2^-)$, respectively) were assigned according to Blume [54]. Let us first describe the spectrum registered on the bare buffer. $\nu_{as}(PO_2^-)$ and $\nu_s(PO_2^-)$ appear at 1220 and 1088 cm^{-1}, respectively. Asymmetric and symmetric CH_2 stretching bands ($\nu_{as}(CH_2)$ and $\nu_s(CH_2)$) were registered at 2925 and 2855 cm^{-1}, respectively. These values did not change depending on the subphase compositions used in this work and they match the characteristic values for the LE phase of the lipid monolayer [55] at the

surface pressure of 30 mN/m, in good agreement with the $\pi-A$ isotherms (Figure 2). They also agree with the already published PM-IRRAS measurements reported by Vié et al [56] for this system.
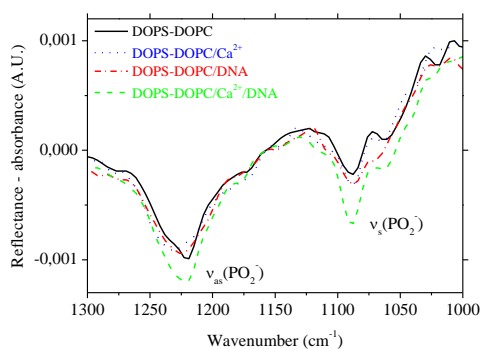

Figure 4.- IRRAS of DOPC/DOPS monolayers at a surface pressure of 30 mN/m on different subphases consisting on Ca^{2+} 10^{-2} M and 0.0295 mg/ml DNA on 40 mM HEPES at pH = 7.4.

Then, we performed the IRRA spectrum at the same conditions with Ca^{2+} and we observed that the phosphate stretching bands are similar in intensity respect to the ones recorded on the pure buffer. Differently, the $\nu_{as}(PO_2^-)$ center of gravity $COG(\nu_{as}(PO_2^-))$ displayed a shift to higher wavenumbers, with respect to the one recorded on the pure buffer, in the presence of Ca^{2+} in the subphase. Similarly, Flach et al. [57] reported a shift for the equimolecular mixture of DPPC/DPPS with 5 mM Ca^{2+} added to the subphase. Since the $COG(\nu_{as}(PO_2^-))$ increases to higher wavenumbers with the hydration degree [45], this shift in the presence of Ca^{2+} and other divalent cations has already been explained in terms of the dehydration of phosphate non-esterified

252

oxygens due to the interaction with the cations [58] and this matches with the previously commented results of limiting molecular areas (table 1).

The IRRA spectrum in the presence of the DNA is also plotted in figure 4. In this case, the phosphate stretching bands are similar to the ones measured on the pure buffer, so we can deduct that there is not any detectable binding of the DNA to the monolayer in the absence of Ca^{2+} cations in the subphase.

Following the procedure already mentioned in the previous sections, we now analyze the IRRA spectrum of the phospholipid monolayer in the presence of both the Ca^{2+} and the DNA at the same time. Interestingly, only when Ca^{2+} cations and DNA are present together in the subphase a significant intensity increase of these two bands was observed. This finding indicates that DNA binds to the phospholipid monolayer only in the presence of Ca^{2+}. This result is in a good agreement with the already described $\pi-A$ isotherms (Figure 2), which were shifted towards larger molecular areas only when both DNA and Ca^{2+} were added together into the subphase. This observation agrees with the Gibbs elasticity and the electrophoretic mobility measurements as well. It is also remarkable that the presence of Ca^{2+} and DNA together in the subphase produced a $\nu_{as}(PO_2^-)$ band with the same center of gravity as the one measured on the pure buffer for DOPS/DOPC monolayers. Therefore, this indicates that the water molecules should interact with both, DNA and lipid phosphate groups, in the ternary system monolayer/Ca^{2+}/DNA.

Similar results of phosphate band amplification were previously described by Brezesinski and Gromelski for DMPE zwitterionic monolayers using Ca^{2+} or Mg^{2+} cations to mediate the electrostatic interaction among the phospholipids and DNA [59]. The reason of this increase could be the contribution of DNA phosphate groups that bound to the monolayer under these specific conditions or a change in the phospholipid phosphate group vibrational transition moment (orientation of the headgroup) in respect of the interface plane [60]. Unfortunately, a quantification of each contribution on the increase of the phosphate stretching band intensity is not easy. At any rate, IRRAS measurements qualitatively confirm that DNA binding to the DOPS/DOPC monolayer is mediated by Ca^{2+} cations.

Moreover, we can obtain additional information from the comparison between the IRRA spectra and the surface elasticity measurements. As can be observed in figure 3, the presence of only the LE phase is established for the monolayers on the subphases with the pure buffer, only Ca^{2+} and only DNA. However, for the subphase with both Ca^{2+} and DNA the elasticity increase above 100 mN/m, which is a reference value for a liquid-condensed (LC) phase [61]. Taking into account that there is no change in the IRRAS wavelength of the CH_2 asymmetric and symmetric stretching bands respect to the other subphases, we can deduct that these high values of surface elasticity are not due to a change in the order of phospholipid hydrophobic chains, but they could be due to the change in the interface composition as a result of the DNA binding to the phospholipid monolayer mediated by the Ca^{2+}.

Conclusions

In this work, we have used different experimental techniques to provide evidences of the complexation of the CT–DNA with DOPS/DOPC lipids, mediated by Ca^{2+}. To our knowledge, these types of mixtures have not been previously reported in the literature. The higher absolute value of the electrophoretic mobility of the ternary system (liposomes/Ca^{2+}/DNA), compared with those of pure liposomes and the pure DNA in the presence of Ca^{2+} appears as the first indication of a possible complexation of the liposomes with the DNA, which is mediated by Ca^{2+}. Subsequently, Langmuir monolayers provide new evidences of molecular interactions at the surface between the lipids and the DNA only in the presence of Ca^{2+}. Namely, the higher molecular area and elasticity of the isotherms composed by the lipids/Ca^{2+}/DNA, compared with those monolayers of lipids/Ca^{2+} and lipids/DNA, suggest that the DNA "sticks" to the lipid monolayer. Interestingly, this displacement is even higher for the higher concentration of Ca^{2+}. A remarkable finding is that the value of the elasticity of all monolayers practically remains equal in all the systems analized for surface pressures below 5 mN/m. This suggests that the interaction of Ca^{2+} with the lipids and the DNA requires a minimal surface coverage of the monolayer. In addition, the lipid/Ca^{2+}/DNA monolayers reached their maximum values of elasticity at surface pressures of about 35 mN/m, which are equivalent to the lateral pressure of a biomembrane bilayers. Therefore, these results should allow modeling the bilayer of the liposomes. According to IRRA spectra, the increased phosphate asymmetric and symmetric

stretching bands, of the monolayer composed of lipids/Ca^{2+}/DNA (with respect to the monolayers of lipids/Ca^{2+} and lipids/DNA) confirms the interaction of the lipids with the DNA in presence of Ca^{2+}. An interesting observation from the asymmetric band was deduced from the lipid/Ca^{2+}/DNA monolayer: this band matches with the same center of gravity of that of pure buffer, indicating that the water molecules should interact with both, lipid and DNA phosphate groups.

In summary, the results obtained from the different experimental techniques, provide valuable information of the interactions of the complexes formed by the anionic lipids, Ca^{2+} and DNA. Although more studies are still needed to fully understand these types of complexes and to use them as nonviral delivery vectors, this work extends the comprehension of the anionic lipoplexes, in order to be used in gene therapy in the near future.

References

(1)   Lasic, D. D. *handbook of Biological Physics*; Elsevier: London, 1995; Vol. 1.

(2)   Gregoriadis, G.; Ryman, B. E. *Biochem J* **1971**, *124*, 58P.

(3)   Gregoriadis, G. *Nature* **1978**, *275*, 695.

(4)   Filion, M. C.; Phillips, N. C. *International Journal of Pharmaceutics* **1998**, *162*, 159.

(5)   Lv, H.; Zhang, S.; Wang, B.; Cui, S.; Yan, J. *J Control Release* **2006**, *114*, 100.

(6)   Liang, H.; Harries, D.; Wong, G. C. *Proc Natl Acad Sci U S A* **2005**, *102*, 11173.

(7)   Patil, S. D.; Rhodes, D. G.; Burgess, D. J. *AAPS J* **2004**, *6*, e29.

(8)   Khiati, S.; Pierre, N.; Andriamanarivo, S.; Grinstaff, M. W.; Arazam, N.; Nallet, F.; Navailles, L.; Barthelemy, P. *Bioconjug Chem* **2009**, *20*, 1765.

(9)   Patil, S. D.; Rhodes, D. G.; Burgess, D. J. *Biochim Biophys Acta* **2005**, *1711*, 1.

(10)   Alberola, A. P.; Radler, J. O. *Biomaterials* **2009**, *30*, 3766.

(11)   Bonacucina, G.; Cespi, M.; Misici-Falzi, M.; Palmieri, G. F. *J Pharm Sci* **2009**, *98*, 1.

(12)   Srinivasan, C.; Burgess, D. J. *J Control Release* **2009**, *136*, 62.

(13)   Radler, J. O.; Koltover, I.; Salditt, T.; Safinya, C. R. *Science* **1997**, *275*, 810.

(14)   Reviakine, I.; Simon, A.; Brisson, A. *Langmuir* **2000**, *16*, 1473.

(15)   Mengistu, D. H.; Bohinc, K.; May, S. *J Phys Chem B* **2009**, *113*, 12277.

(16)   Jahnig, F. *Biophys J* **1984**, *46*, 687.

(17)   Marsh, D. *Biochim Biophys Acta* **1996**, *1286*, 183.

(18)   Wydro, P.; Hac-Wydro, K. *J Phys Chem B* **2007**, *111*, 2495.

(19)   Brezesinski, G.; Mohwald, H. *Advances in Colloid and Interface Science* **2003**, *100*, 563.

(20)   Feng, S. *Langmuir* **1999**, *15*, 998.

(21)   Smaby, J. M.; Momsen, M. M.; Brockman, H. L.; Brown, R. E. *Biophys J* **1997**, *73*, 1492.

(22)   Montanha, E. A.; Pavinatto, F. J.; Caseli, L.; Kaczmarek, O.; Liebscher, J.; Huster, D.; Oliveira, O. N., Jr. *Colloids Surf B Biointerfaces* **2010**, *77*, 161.

(23)   Huster, D.; Arnold, K.; Gawrisch, K. *Biophysical Journal* **2000**, *78*, 3011.

(24)   Gromelski, S.; Brezesinski, G. *Physical Chemistry Chemical Physics* **2004**, *6*, 5551.

(25)   Gericke, A.; Flach, C. R.; Mendelsohn, R. *Biophys J* **1997**, *73*, 492.

(26)   Saccani, J.; Castano, S.; Beaurain, F.; Laguerre, M.; Desbat, B. *Langmuir* **2004**, *20*, 9190.

(27)   Koynova, R.; Tenchov, B.; Wang, L.; Macdonald, R. C. *Mol Pharm* **2009**, *6*, 951.

(28)   Rodriguez-Pulido, A.; Ortega, F.; Llorca, O.; Aicart, E.; Junquera, E. *J Phys Chem B* **2008**, *112*, 12555.

(29)   Lleres, D.; Dauty, E.; Behr, J. P.; Mely, Y.; Duportail, G. *Chem Phys Lipids* **2001**, *111*, 59.

(30)   Zuidam, N. J.; Hirsch-Lerner, D.; Margulies, S.; Barenholz, Y. *Biochim Biophys Acta* **1999**, *1419*, 207.

(31)   Rodriguez-Pulido, A.; Martin-Molina, A.; Rodriguez-Beas, C.; Llorca, O.; Aicart, E.; Junquera, E. *J Phys Chem B* **2009**, *113*, 15648.

(32)   Martin-Molina, A.; Rodriguez-Beas, C.; Hidalgo-Alvarez, R.; Quesada-Perez, M. *J Phys Chem B* **2009**, *113*, 6834.

(33)   McNeil-Watson, F.; Tscharnuter, W.; Miller, J. *Colloids and Surfaces a-Physicochemical and Engineering Aspects* **1998**, *140*, 53.

(34)   Jachimska, B.; Wasilewska, M.; Adamczyk, Z. *Langmuir* **2008**, *24*, 6866.

(35)   Roldan-Vargas, S.; Martin-Molina, A.; Quesada-Perez, M.; Barnadas-Rodriguez, R.; Estelrich, J.; Callejas-Fernandez, J. *Phys Rev E Stat Nonlin Soft Matter Phys* **2007**, *75*, 021912.

(36)   Mclaughlin, S.; Mulrine, N.; Gresalfi, T.; Vaio, G.; Mclaughlin, A. *Journal of General Physiology* **1981**, *77*, 445.

(37)   Huster, D.; Arnold, K.; Gawrisch, K. *Biophys J* **2000**, *78*, 3011.

(38)   Sinn, C. G.; Antonietti, M.; Dimova, R. *Colloids and Surfaces a-Physicochemical and Engineering Aspects* **2006**, *282*, 410.

(39)   Duguid, J.; Bloomfield, V. A.; Benevides, J.; Thomas, G. J., Jr. *Biophys J* **1993**, *65*, 1916.

(40)   Duguid, J. G.; Bloomfield, V. A. *Biophys J* **1995**, *69*, 2642.

(41)   MacDonald, R. C.; Gorbonos, A.; Mornsen, M. M.; Brockman, H. L. *Langmuir* **2006**, *22*, 2770.

(42)   Baoukina, S.; Monticelli, L.; Amrein, M.; Tieleman, D. P. *Biophys J* **2007**, *93*, 3775.

(43)   Hauser, H.; Chapman, D.; Dawson, R. M. *Biochim Biophys Acta* **1969**, *183*, 320.

(44)   Ross, M.; Steinem, C.; Galla, H. J.; Janshoff, A. *Langmuir* **2001**, *17*, 2437.

(45)   Dluhy, R. A.; Cameron, D. G.; Mantsch, H. H.; Mendelsohn, R. *Biochemistry* **1983**, *22*, 6318.

(46)   Martín-Molina, A.; Rodríguez-Beas, C.; Faraudo, J. *Biophyscal Journal.* **2012**, *DOI:10.1016/j.bpj.2012.03.009*.

(47)   Frantescu, A.; Tonsing, K.; Neumann, E. *Bioelectrochemistry* **2006**, *68*, 158.

(48)   Sakamoto, N.; Sakai, K.; Takagi, K. *Physical Review E* **1997**, *56*, 1838.

(49)   Lucero, A.; Rodriguez Nino, M. R.; Gunning, A. P.; Morris, V. J.; Wilde, P. J.; Rodriguez Patino, J. M. *J Phys Chem B* **2008**, *112*, 7651.

(50)   Rodriguez Nino, M. R.; Caro, A. L.; Rodriguez Patino, J. M. *Colloids Surf B Biointerfaces* **2009**, *69*, 15.

(51)   Mahato, M.; Pal, P.; Kamilya, T.; Sarkar, R.; Chaudhuri, A.; Talapatra, G. B. *Phys Chem Chem Phys* **2010**, *12*, 12997.

(52)   Smaby, J. M.; Momsen, M.; Kulkarni, V. S.; Brown, R. E. *Biochemistry* **1996**, *35*, 5696.

(53)   Dittrich, M.; Bottcher, M.; Oliveira, J. S. L.; Dobner, B.; Mohwald, H.; Brezesinski, G. *Soft Matter* **2011**, *7*, 10162.

(54)   Blume, A. *Current Opinion in Colloid & Interface Science* **1996**, *1*, 431.

(55)   Mendelsohn R.; CR., F. *The Handbook of Vibrational Spectroscopy* **2002**, *2*, 1028.

(56)   Vie, V.; Legardinier, S.; Chieze, L.; Le Bihan, O.; Qin, Y.; Sarkis, J.; Hubert, J. F.; Renault, A.; Desbat, B.; Le Rumeur, E. *Biochim Biophys Acta* **2010**, *1798*, 1503.

(57)   Flach, C. R.; Brauner, J. W.; Mendelsohn, R. *Biophys J* **1993**, *65*, 1994.

(58)   Binder, H.; Zschornig, O. *Chem Phys Lipids* **2002**, *115*, 39.

(59)   Gromelski, S.; Brezesinski, G. *Langmuir* **2006**, *22*, 6293.

(60)   Mendelsohn, R.; Mao, G.; Flach, C. R. *Biochim Biophys Acta* **2010**, *1798*, 788.

(61)   Toimil, P.; Prieto, G.; Minones, J., Jr.; Sarmiento, F. *Phys Chem Chem Phys* **2010**, *12*, 13323.

APÉNDICE A

MATERIAL UTILIZADO Y PREPARACIÓN
DE LIPOSOMAS Y LIPOPLEJOS

A continuación se describen algunas características técnicas y fisicoquímicas de los lípidos, el tampón y los cationes multivalentes, así como de los procesos de formación de los liposomas, y lipoplejos utilizados en este estudio:

A.1. Lípidos

Lípido catiónico *Bromuro de Dioctadecildimetilamonio (DODAB)* de dos cadenas saturadas de 18 carbonos cada una, Fig. A.1 (utilizado en el artículo 1).
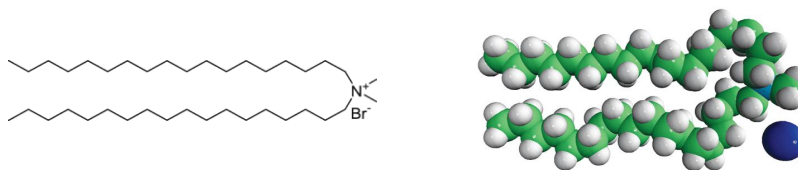

Fig. A.1. Estructura química del lípido DODAB.
[Fuente:http://www.avantilipids.com]

Lípido zwitteriónico *1,2-dilauroil-sn-glicero-3-fosfatidilcolina (DLPC)* de dos cadenas saturadas de 12 carbonos cada una, Fig. A.2 (utilizado en el artículo 1).
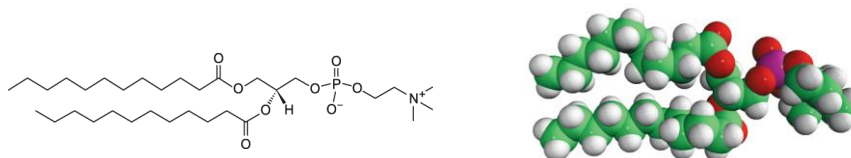
Fig. A.2. Estructura química del lípido DLPC.
[Fuente:http://www.avantilipids.com]

Lípido zwitteriónico *1,2-dioleoil-sn-glicero-3-fosfatidiletanolamina (DOPE)* de dos cadenas insaturadas de 18 carbonos cada una, Fig. A.3 (utilizado en el artículo 1).
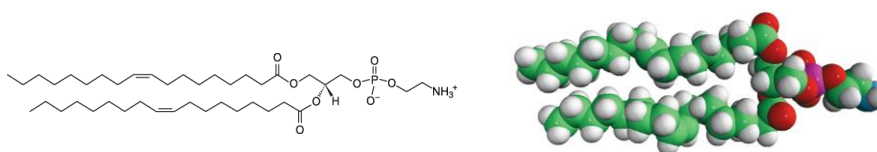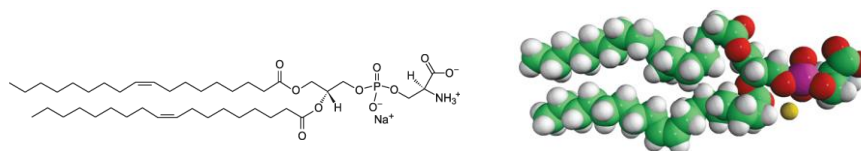

Fig. A.3. Estructura química del lípido DOPE.
[Fuente:http://www.avantilipids.com]

Lípido aniónico *1,2-dioleoil-sn-glicero-3-fosfatidilserina (DOPS)* de dos cadenas insaturadas de 18 carbonos cada una, Fig. A.4 (utilizado en los artículos 3, 4 y 5).

Fig. A.4. Estructura química del lípido DOPS.
[Fuente:http://www.avantilipids.com]

Lípido zwitteriónico *1,2-dioleoil-sn-glycero-3-fosfatidilcolina (DOPC)* de doble cadena insaturadas de 18 carbonos cada una, Fig. A.5 (utilizado en los artículos 3 y 5).
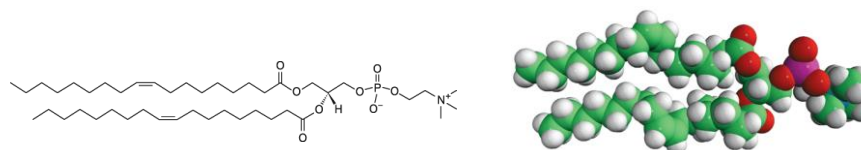

Fig. A.5. Estructura química del lípido DOPC.
[Fuente:http://www.avantilipids.com]

La Tabla A.1 muestra los valores del peso molecular (PM) y de la temperatura de transición (T_m)[8] gel–líquido de los lípidos anteriores.

Tabla A.1. Peso molecular y temperatura de transición de los lípidos.

Lípido	PM (g/mol)	T_m (ºC)
DODAB	630.97	45
DLPC	621.83	−1
DOPE	744.034	−16
DOPS	810.025	−11
DOPC	786.13	−20

_____

[8]La *T_m* es la temperatura de transición en la que los lípidos pasan de su estado de gel (sólido) a un estado líquido, es decir, las cadenas hidrófobas de los lípidos pasan de un estado rígido a ser más flexibles.

A.2. Tampón

Ácido (*Sulfónato de 4-(2-Hidroxietil)-1-Piperacina*) (HEPES) es un agente químico, orgánico y zwitteriónico que se utiliza como tampón, usado para mantener las soluciones a pH fisiológico (pH=7.4). El HEPES contiene ambos grupos iónicos; positivos y negativos, donde los grupos secundarios y terciarios de aminas proveen de carga positiva y los grupos sulfónico y ácido carboxílico proveen de carga negativa. En el HEPES, como el agua, la disociación iónica decrece con la temperatura. La Fig. A.6 muestra el equilibrio del HEPES en disolución. El tampón de HEPES se utilizó en los artículos 1 y 5.
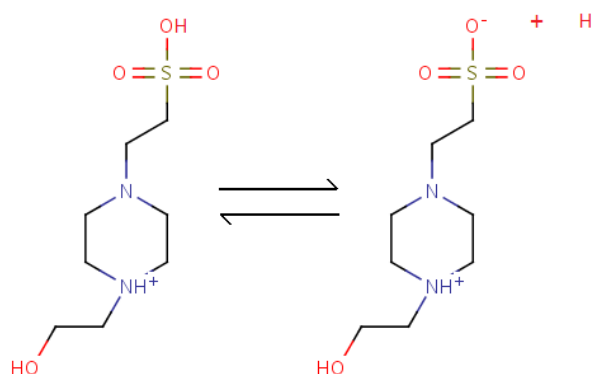

Fig. A.6. Estructura química y equilibrio del HEPES/HEPES⁻ (ácido/base) en disolución.

A.3. Cationes Multivalentes

Como sal trivalente se utilizó el Nitrato de Lantano ($La(NO_3)_3$). El La^{3+} es un ion comúnmente utilizado en estudios de interacción de sistemas aniónicos por su habilidad de invertir la carga de las moléculas.

Además, es un elemento químico metálico que tiene diferentes usos comerciales, como la fabricación de vidrios ópticos especiales y de pantallas intensificadoras de las unidades de rayos X. El lantano se utilizó en los artículos 2 y 3.

El electrolito divalente Nitrato de Calcio ($Ca(NO_3)_2$). Se usó porque el calcio favorece a la transfección. El calcio es un ión que aparece como un mensajero intracelular. Puede ingresar a las células a través de los canales insertados en la membrana plasmática o membrana celular. Una vez dentro del citoplasma, el calcio puede difundir o unirse a estructuras móviles o inmóviles que pueden atraparlo por un tiempo y luego liberarlo nuevamente. Estas estructuras, como las proteínas, se denominan *tampones*, y tienen la capacidad de almacenar el calcio y controlar su concentración intracelular, protegiendo así a la célula [119-120]. El catión de calcio se utilizó en los artículos 4 y 5.

El electrolito de Nitrato de Magnesio ($Mg(NO_3)_2$) se usó porque el magnesio es esencial para todas las células vivas ya que contiene una función estabilizadora de la estructura de las cadenas del ADN y ARN. La mayoría del magnesio está dentro de la célula. Mientras que el hierro es el átomo central de la hemoglobina, el magnesio es el núcleo central de la molécula de clorofila (las clorofilas son un grupo de pigmentos (material que cambia de color la luz que refleja como resultado de la absorción selectiva del color) que se encuentran en diversas células eucariotas y algunas procariotas). En general, la mayor parte del magnesio se encuentra en los huesos y sus iones desempeñan un papel

importante en la actividad de muchas coenzimas y en reacciones que dependen del ATF (trifosfato de adenosina – nucleótido fundamental en la obtención de energía celular). El catión de magnesio se utilizó en el artículo 4.

A.4. Preparación de Liposomas

Desde hace años, se vienen desarrollado diversos métodos de preparación de liposomas que han resultado rápidos, fiables y que proporcionan estructuras homogéneas. El tamaño de los liposomas es muy importante para su estabilidad, pues se considera que cuanto más grande es el liposoma, mayor es su estabilidad. Sin embargo, en muchas de las aplicaciones se requieren liposomas de tamaño reducido. En todos nuestros trabajos, la preparación de los liposomas se llevó a cabo en cuatro pasos, siendo uno de ellos la reducción de tamaño.

En la preparación se hace uso de un *rotavapor*, un *extrusor* y un *sonicador*. Cabe señalar que el procedimiento para la producción de liposomas formados por un tipo de lípido, o por la mezcla de dos tipos de lípidos, es el mismo. A continuación se describen estos pasos:

1. *Formación de bicapas:* Se disuelven los lípidos en cloroformo/metanol (3:1 v) para tener una óptima homogenización. Después se elimina el disolvente mediante evaporación al vacío, usando un rotavapor a una temperatura superior a la T_m del lípido con el que se trabaja (Tabla A.1),

durante un tiempo superior a dos horas. De este modo se forma una bicapa o película de lípidos seca de estructura lamelar, Fig. A.7. Después, a la película se le hace pasar un flujo de gas de nitrógeno seco durante varios minutos para asegurar la completa evaporación del disolvente.
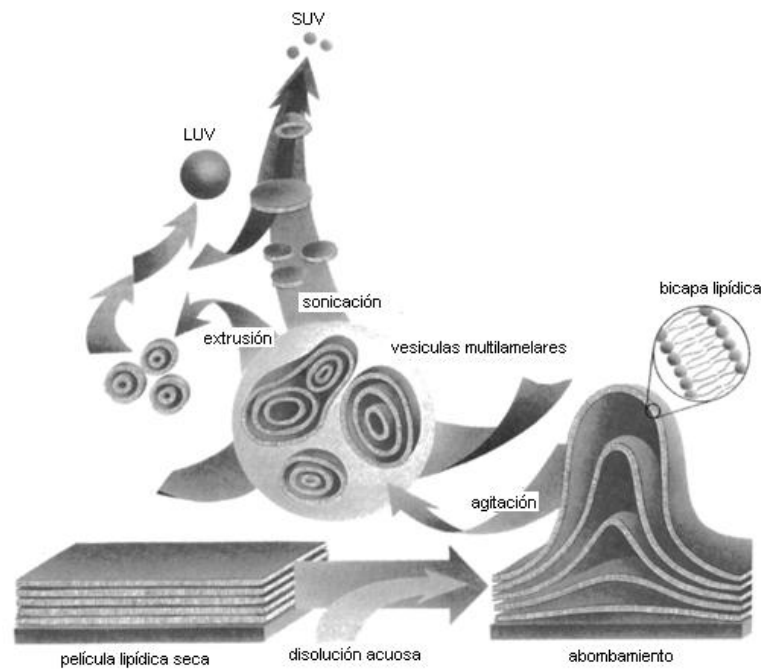

Fig. A.7. Etapas de formación de los liposomas mediante la técnica de extrusión. [Fuente:http://www.etseq.urv.cat/dinamic/catala/places/postdoc_ sullivan2.htm]

2. *Rehidratación:* La película lipídica seca es hidratada con agua ultrapura o con disolución tampón HEPES según sea el caso de estudio, mediante agitación continua en el rotavapor, alternando con pequeños periodos de sonicación (cuya suma no supera los

dos minutos). Durante este tiempo se mantiene una temperatura por encima de la T_m del lípido para evitar rigidez en la película lipídica. En esta etapa se forman liposomas multilamelares grandes (LMG).

3. *Reducción del tamaño y homogenización:* Actualmente existen varios métodos para reducir el tamaño de los liposomas, así como el número de bicapas: *sonicación, extrusión, homogenización,* etc. En este trabajo se utilizo el método de extrusión y sonicación para disminución de tamaño y homogenización de los liposomas multilamelares, para obtener liposomas unilamelares pequeños (LUP), Fig. A.7.

4. *Extrusión:* Los liposomas son forzados a pasar mecánicamente a través de filtros de policarbonato de un tamaño de poro determinado mediante la presión ejercida por el nitrógeno. Para asegurar una homogeneidad de los liposomas, la muestra se hace pasar de manera sucesiva 5 veces por un filtro con tamaño de poro de 800 nm y 5 veces por uno de 200 nm. Al utilizar este método, se forman liposomas unilamelares grandes (LUG) y después LUP, con diámetros en torno a 200 nm y baja polidispersidad.

Los liposomas preparados mediante este protocolo se almacenan a una temperatura entre 4 y 7ºC para su conservación hasta que son utilizados en la formación/caracterización de lipoplejos catiónicos y lipoplejos aniónico.

A.5. Preparación de Lipoplejos

En la preparación de lipoplejos catiónicos (Fig. A.8) se utilizó una concentración fija de ADN, mientras que la concentración de liposomas variaba en un intervalo de concentración dado por la relación de masa de $L/D = 1$ a $L/D = 15$. Recordando que la relación de masa $(L/D) = (L^{+}+L^{0})/D$, con L es la masa total de lípidos en la disolución, L^{+} es la masa del lípido catiónico, L^{0} es la masa del lípido zwitteriónico y D es la masa del ADN. Para distinta concentraciones de liposomas se le añade una concentración fija de ADN de manera muy lenta y gota a gota manteniendo la disolución bajo agitación magnética.
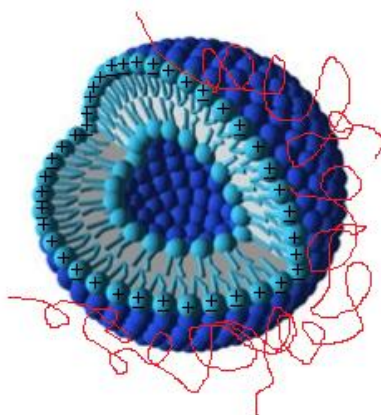

Fig. A.8. Lipoplejos catiónicos, formado por liposomas catiónicos y ADN.

Después, la disolución se deja en reposo alrededor de cinco minutos justo antes de cada medida experimental.

De igual forma, en la preparación de lipoplejos aniónicos se fija una concentración de liposomas (previamente obtenida mediante medidas de movilidad electroforética) y se añaden los cationes y el ADN, Fig. A.9.
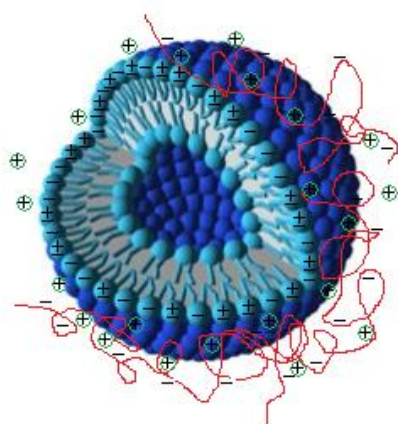

Fig. A.9. Lipoplejo aniónico, formado por liposomas aniónicos/cationes divalentes/ADN.

Primero se añade Ca^{2+} a la disolución de liposomas en pequeñas dosis (gota a gota) y con agitación magnética para favorecer la formación de los complejos. La disolución liposomas/Ca^{2+} se mantiene en reposo durante varios minutos antes de añadir el ADN. Después, a la disolución de liposomas/Ca^{2+} se le añade el ADN, de las misma forma que se añadió el Ca^{2+}, para formar los lipoplejos. De igual manera, la adición del ADN se hizo bajo agitación magnética y de gota en gota. Finalmente, la disolución liposomas/Ca^{2+}/ADN se mantuvo en reposo alrededor de cinco minutos a temperatura ambiente para favorecer la formación de los lipoplejos antes de las medidas experimentales.

Felgner y col. (1987) en su trabajo original se refirieron a los lipoplejos como: *"Pequeños liposomas unilamelares compuestos de DOTMA (dioctadeceniltrimetilamonio) que interactúan espontáneamente con ADN para formar complejos lípido−ADN, atrapando el ADN al 100%. El DOTMA facilita la fusión de los complejos con la membrana plasmática de las células cultivadas, dando como resultado la captación y la expresión del ADN. La técnica es simple, altamente reproducible y efectiva para la expresión transitoria y estable del ADN transferido"*.